

GEOTECHNICAL SITE CHARACTERIZATION THROUGH GEOELECTRICAL IMAGING

A THESIS

*Submitted in partial fulfilment of the
requirements for the award of the degree*

of

DOCTOR OF PHILOSOPHY

in

EARTH SCIENCES

by

PARAM KIRTI RAO GAUTAM



DEPARTMENT OF EARTH SCIENCES
INDIAN INSTITUTE OF TECHNOLOGY ROORKEE
ROORKEE - 247 667 (INDIA)

DECEMBER, 2009

**©INDIAN INSTITUTE OF TECHNOLOGY ROORKEE, ROORKEE- 2009
ALL RIGHTS RESERVED**



INDIAN INSTITUTE OF TECHNOLOGY ROORKEE

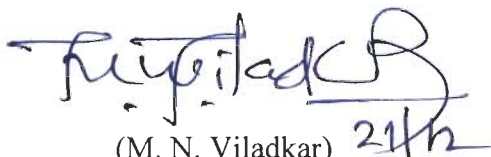
CANDIDATES'S DECLARATION

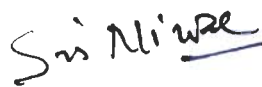
I hereby certify that the work which is being presented in this thesis entitled **GEOTECHNICAL SITE CHARACTERIZATION THROUGH GEOELECTRICAL IMAGING** in partial fulfilment of the requirements for the award of the Degree of Doctor of Philosophy and submitted in the Department of Earth Sciences, Indian Institute of Technology Roorkee, Roorkee is an authentic record of my own work carried out during a period from July 2004 to December 2009 under the supervision of Dr. Rambhatla G. Sastry, Professor, Dr. Sri Niwas, Professor, Department of Earth Sciences and Dr. M. N. Viladkar, Professor, Department of Civil Engineering, Indian Institute of Technology Roorkee, Roorkee, India.

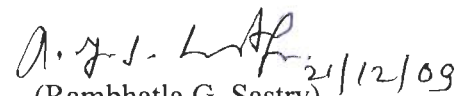
The matter presented in this thesis has not been submitted by me for the award of any other degree of this or any other University / Institute.


(PARAM KIRTI RAO GAUTAM)

This is to certify that the above statement made by the candidate is correct to the best of our knowledge.


(M. N. Viladkar) 21/12
Supervisor


(Sri Niwas)
Supervisor


(Rambhatla G. Sastry) 21/12/09
Supervisor

Date: 21.12.2009

The Ph.D. Viva-Voce Examination of **Mr. Param Kirti Rao Gautam**, Research Scholar, has been held on _____.

Signature of Supervisors

Signature of External Examiner

ABSTRACT

Geophysical methods are increasingly being used for civil engineering related site investigation studies. They are non-invasive, cost-effective with proven spatial resolutions of different scales. While geotechnical tests provide geo-mechanical information on a very refined depth scales but their advantage is offset by their inherent point-wise information attended by drilling, which is costly; Further, in a complex geological settings, the problems get compounded due to excessive drilling budget to fulfill the geotechnical site investigation needs. While geophysical methods are quite effective in subsurface exploration, yet their results can not be directly translated to geotechnical knowledge due to absence of suitable transforms. So, a leveraged approach is needed to yield better quality subsurface information at a much lesser cost. The key problem which still remains to be addressed concerns with the prediction of different formation and geotechnical parameter images of subsurface on the basis of few geotechnical investigations and ample number of geophysical measurements.

A very good coverage of SASW & MASW methods (Park et al., 2005) is available in literature and these methods are routinely used in site testing. However, similar progress has not been made in the application of geo-electrical imaging to geotechnical site characterization. As evident from literature, very meager attention is paid to this important aspect. Recent literature (Gautam et al., 2007; Sudha et al., 2008; Cosenza et al., 2006) shows that efforts are limited to site-specific qualitative correlations between geo-electrical and geotechnical data. However, a preliminary attempt has been initiated by Gautam et al. (2007) to predict the SPT profile using the correlations of geo-electric and geotechnical data (SPT). Even though qualitative correlations are available for shear wave / elastic moduli and SPT (Morgan et al., 2005; Ulugergerli and Uyanik, 2007; Iyisan, 1996), no worthwhile predictive effort has been made to complement the geotechnical tests at a site.

Here, 2-D resistivity and IP image profile data along with projected geotechnical data (Standard Penetration Test, SPT / Direct Cone Penetration Test, DCPT / Static Cone Penetration Test, SCPT) from nearby boreholes have been used for predicting different 2-D

formation and geotechnical parameter sections along the same profile. This prediction method is based on site-specific regression equations describing observed correlations of geo-electrical and geotechnical data and site-independent well established empirical relations of SPT 'N' with different formation and geotechnical parameters.

The designed methodology is applied to geo-electrical and geotechnical data gathered from four sites. Three sites belong to Indo-Gangetic Alluvial Plains of Uttarakhand and fourth site belongs to Delhi Group of rocks in the vicinity of Delhi, India. The achieved results in four case studies demonstrate that the inferred 2-D formation, geotechnical test results and parameter sections along a chosen geo-electric profile describe near surface soil structure in a vivid manner. These may prove to be quite useful to a geotechnical engineer for site investigation studies. Even though the reported results are SPT based, the outlined methodology is quite general enough to deal with any other relevant geotechnical data sets for a comprehensive geotechnical assessment of a site.

In this context, the following remarks need to be mentioned:

- a) The bearing capacity factors based on CPT method is not attempted here. However, earlier outlined procedure for SPT 'N' can easily be extended to CPT method also.
- b) The present procedure is applicable to soil strata only, where conventional geotechnical tests are valid.
- c) The quality of input geo-electric sections affect inferred lithology, formation and geotechnical sections. So, basic data quality of geo-electrical data and attendant processing and inversion schemes has to be very high.
- d) The regression equations that were employed for angle of internal friction, unit weights of soil (dry & saturated), unconfined compressive strength and different bearing capacity factors, have remained constant throughout the study and they are based on current geotechnical literature.
- e) The regression equations for prediction of geotechnically derived sand, clay / shale, lithology, SPT, DCPT, SCPT, porosity and water saturation are site-specific and geo-electrical profile specific.

- f) Here, a pair of boreholes in the vicinity of geo-electric profile is used for arriving at a regression equation. But the procedure remains unaltered if more boreholes are available for this analysis and in such an event, prediction quality improves.
- g) The designed methodology is applied in four case study sites and the results support the efficacy and cost-effectiveness of the approach.
- h) By a careful scrutiny of achieved results suggest that geo-electric imaging could be implemented at pre-investigation stage leading to better location of requisite number of boreholes for carrying out conventional geotechnical field tests. Further, it can be utilized in the next stage to infer 2-D image sections of lithology, formation and geotechnical parameters. Such a scheme optimizes the entire site investigation procedures, minimizing both cost and time and provides quality information to a geotechnical engineer to refine his models.
- i) The designed methodology is very general and it can rope in other scientific inputs also, so that new methodologies can be devised to meet the emerging challenges before a site geotechnical engineer.
- j) It is envisaged that densification of geoelectrical profiles could lead to a 3-D reconstruction of various formation and geotechnical parameter sections in the study region. But traditional geotechnical tests are still needed for better control.
- k) All inferred 2-D sections clearly show that 1-D models often resorted to by geotechnical engineers are far from reality and efforts need to be made to refine their quality or new procedures need to be evolved.

LIST OF PUBLICATIONS

Gautam, P. K., Sastry, R. G., and Mondal, S. K., 2007. The utility of Multi-electrode resistivity data in geotechnical investigations-A case study, 20th Annual Meeting SAGEEP, April 1-5, 2007, Denver, Colorado, 731-737.

Mondal, S. K., Sastry, R. G., Pachauri, A. K., and Gautam, P. K., 2008. High resolution 2D electrical resistivity tomography to characterize active Naitwar Bazar landslide, Garhwal Himalaya, India, Current Science, VOL. 94, No.7, 871-875.

Sastry, R. G., Mondal, S. K., Gautam, P. K., and Pachauri, A. K., 2008. Integrated geophysical approach for mapping an active landslide in Himalaya: a case study, "Energy security: Exploration, Exploitation & Economics", M/S SPG, ONGCL at Hyderabad, Jan. 13-16, 2008.

Sastry, R. G., Mondal, S. K., Gautam, P. K., and Pachauri, A. K., 2007. Integrated geophysical approach for mapping an active landslide in Himalaya: a case study, 20th Annual Meeting SAGEEP, April 1-5, 2007, Denver, Colorado, 248-254.

Mondal, S. K., Sastry, R. G., Gautam, P. K., and Pachauri, A. K., 2007. High resolution resistivity imaging of Naitwar Bazar landslide, Garhwal Himalaya, India, 20th Annual Meeting SAGEEP, April 1-5, 2007, Denver, Colorado, 629-635.

ACKNOWLEDGEMENTS

On the accomplishment of this thesis, I would like to take this opportunity to extend my deepest sense of gratitude and words of appreciation toward those, who dedicated their today for my tomorrow. I deem it a proud privilege and feel immense pleasure to acknowledge all those who are directly or indirectly involved.

*First of all, I consider myself fortunate and greatly privileged to have worked under the supervision and guidance of **Dr. Rambhatla G. Sastry**, Professor, Department of Earth Sciences, IIT Roorkee. Words are inadequate in the available lexicon to avouch the excellent supervision, cooperation, constructive discussions and suggestions given by him. His dedication to research, meticulous planning, counsel and unreserved help served as a beacon light throughout my research work. With deep sense of gratitude, I thank him for his unflinching and invaluable inspirations, the introspective guidance and active persuasion throughout my research study. His professional expertise, ideas and passions in science exceptionally inspire and enrich my growth as a student and a researcher. Throughout my research work, he has been a pillar of strength which I knew I could lean upon for support anytime, be it academic or personal matters. Some words of acknowledgement will never substitute for the knowledge I have acquired from him. It is a fact that without his effort, expertise, consistent help, persuasion and motivation this thesis could never have been completed.*

*I take this opportunity to express my sincere gratitude to **Dr. Sri Niwas**, Professor, Department of Earth Sciences, IIT Roorkee. I feel indebted to him for his constant motivation and support in various ways throughout my study period. My research work benefited from his critical advices, ideas and suggestions. As one of the supervisors, his involvement in the administrative matters helped and supported me. Due to his support and interest, I could carry out my field work for my Ph.D thesis. His admirable co-operation and encouraging words are greatly acknowledged.*

*I express my heartfelt thanks to **Dr. M. N. Viladkar**, Professor, Department of Civil, IIT Roorkee for having readily consented to take me as his student and for providing critical comments and valuable suggestions at every stage and constant encouragement during the entire research work. He has been instrumental in seeing to*

the completion of the work that goes into this thesis, through his gentle persuasion and encouragement. I am also very thankful for his guidance theoretically as well as in the field work, apart from the invaluable time to go through my thesis and making helpful suggestions. I enjoyed complete academic freedom under his guidance and enjoyed working with him.

*I extend sincere thanks to **Prof. V. N. Singh**, former Head and **Prof. R. P. Gupta**, present Head, Department of Earth Sciences, for providing all the infrastructural facilities and the nice working environment for successful completion of this thesis. I am thankful to the entire staff of the Department, especially Nairji and Sarbeshji for their support and cooperation.*

I would also like to thank the Ministry of Human Resources Development (MHRD) for providing me fellowship, which enabled me to complete this research study comfortably.

*My sincere thanks are due to members of the Departmental Research Committee (DRC), **Prof. A. K. Pachauri** and **Prof. P. K. Gupta**, Department of Earth Sciences and **Prof. Mahendra Singh**, Department of Civil Engineering for their valuable suggestions and comments through out the research programme.*

*I am deeply grateful to **Dr. B. R. Arora**, former Director and **Dr. A. K. Dubey**, present Director, Wadia Institute of Himalayan Geology (WIHG), Dehradun for giving me permission and required facilities to complete my Ph. D. work after joining as Scientist, WIHG, Dehradun.*

*I am profoundly thankful to **Shri V.C. Flura**, Assistant Engineer, Central Public Works Department (CPWD), Roorkee, Uttarakhand, India for providing the informative data of the study area, without which the completion of this thesis would not have been possible.*

At this moment, it is a great pleasure for me to acknowledge the immense help and encouragement rendered by my friends at the various stages, especially Dr. Suman Kumar Mondal. I thank my seniors, juniors, classmates and friends, especially, Dr. Ramesh, Dr. Krishna Kumar, Mr. Lekh Raj, Dr. Aman Pal, Asish Gaur, Anil, Rupesh, Santram, for their love, supports and companionship during this difficult effort.


Due to them my stay in Roorkee for my research work will always remain a good memory for me.

*I would also like to acknowledge my thanks to my Geophysics Group Head, **Dr. V. M. Chaubey**, my senior and scientist (WIHG), **Dr. P. K. Mukherjee**, as well as my colleagues at WIHG, Dehradun, namely, Dr. Ajay Paul, Mr. Gautam Rawat, Mr. Naresh K., Dr. Narendra Meena, Dr. Khayingshing Luirei, Dr. Dilip Yadav, Dr. Devajit Hazarika and for their support and encouragement. My special thanks go to Dr. Swapnamita Choudhury for her kind co-operation, suggestions and help, especially during the last stages of my thesis work.*

*The continuous inspiration, encouragement and affection received from my sisters, **Prakash Vati Gautam**, **Shama Gautam** and my elder brother **Manohar Kirti Rao Gautam** shall be remembered always. Especially, my brother has played a very vital role in my whole life. I have no words to expressing his real contribution. My vocabulary utterly fails in expressing my accolade to my revered parents, **Shri Tulsi Ram and Smt. Hardaie Devi**, because of whom I am what I am today. I deeply express my gratitude to my sister-in-law, Mrs. Seema Devi Meena who has not only provided me with moral support but also took care of my meals in Dehradun. My regards go to each and every family member for their trust and love for me. Last but not the least, I heartily thank my well-wisher **Anuradha Aditya** for instilling in me patience and strength to remain focused and boosted up my moral spirits during the period of study.*

Finally, I would like to thank everybody who was important to the successful realization of thesis, as well as expressing my apology for the faux pas in the hostel and Department. I hope those who have extended their good wishes for my successful completion kindly pardon me if I have failed to mention their names in this acknowledgement. I extend best wishes to one and all.

*I.I.T. Roorkee
December, 2009*


(P.K.R. Gautam)

CONTENTS

<i>Title</i>	<i>Page No.</i>
CANDIDATE'S DECLARATION	
ABSTRACT	iii
LIST OF PUBLICATIONS	vii
ACKNOWLEDGEMENT	ix
CONTENTS	xiii
LIST OF FIGURES	xix
LIST OF TABLES	xxxv
LIST OF PLATES	xxxix
CHAPTER 1: INTRODUCTION	1-4
1.1 PREAMBLE	1
1.2 ROLE OF GEOPHYSICAL METHODS	2
1.3 NOVELTY OF THE WORK	3
1.4 PRACTICAL UTILITY	3
1.5 THESIS LAYOUT	4
CHAPTER 2: LITERATURE REVIEW	5-11
2.1 GENERAL	5
2.2 REVIEW OF LITERATURE	5
2.2.1 Geophysical Efforts	6
2.2.2 Correlation of Geophysical and Geotechnical Test Data	8
2.3 GAPS IN STATE OF ART	10
2.4 OBJECTIVES OF THESIS	11
CHAPTER 3: GEOELECTRICAL IMAGING	13-29
3.1 INTRODUCTION	13
3.2 2-D - ELECTRICAL RESISTIVITY TOMOGRAPHY (ERT)	14
3.2.1 Basics of DC Resistivity Method	15

3.3	INDUCED POLARIZATION METHOD	17
3.3.1	IP Sources	17
3.3.2	Methods of Measurement of IP Effect	18
3.3.2.1	Time domain	19
3.4	2-D - MULTI-ELECTRODE GEOELECTRICAL SURVEYS	20
3.4.1	Instrument and Measurement Procedure	20
3.4.2	Selection of Array	21
3.4.3	Wenner-Schlumberger Array	21
3.4.4	Display of Pseudo-section Plots	22
3.5	THEORITICAL ASPECTS OF RESISTIVITY AND IP IMAGING	23
3.5.1	Frechlet Derivative for a Homogeneous Half-Space	24
3.5.2	Inversion Algorithm	27
3.6	SHALY SAND ANALYSIS USING IP	28
3.7	PROCEDURE FOLLOWED IN THIS WORK	29
	CHAPTER 4: GEOTECHNICAL PARAMETERS AND SITE TESTING	31-56
4.1	GENERAL	31
4.2	CLASIFICATION OF SOILS AND INDEX PROPERTIES OF SOILS	32
4.3	ESTIMATION OF SHEAR STRENGTH PARAMETERS	34
4.4	SITE EXPLORATION AND GEOTECHNICAL TESTS	35
4.4.1	Standard Penetration Test (SPT)	35
4.4.1.1	Corrections to the observed SPT values	37
4.4.1.2	SPT values related to relative density of cohesionless soils	37
4.4.1.3	SPT values related to consistency of clay soil	38
4.4.2	Dynamic Cone Penetration Test (DCPT)	40
4.4.3	Static Cone Penetration Test (SCPT)	41
4.4.4	Plate Load Test (PLT)	43
4.5	LABORATORY TESTS	45
4.6	BEARING CAPACITY	47
4.6.1	Shallow Foundation	47

4.7	THE GENERAL BEARING CAPACITY EQUATION	48
4.8	ULTIMATE BEARING CAPACITY OF FOOTINGS BASED ON SPT 'N'	52
4.9	DEEP FOUNDATION	52
4.10	REGRESSION ANALYSIS	54
4.10.1	Inferring Prediction Equation for Angle of Internal Friction from SPT	54
4.10.2	Prediction Equation for Unit Weight of Soil from Porosity / Water Saturation	54
4.10.3	Prediction Equation for Unconfined Compressive Strength from SPT 'N'	54
4.10.4	Prediction Equations for Terzaghi's General Bearing Capacity and Ultimate Bearing Capacity Factors (Strip Footings)	55
4.10.5	Prediction Equation for N_q Factor (Piles) Based on Shear Angle in Case of Deep Sub-Soil Investigations	55
4.11	REMARKS	55
	CHAPTER 5: METHEDOLOGY	57-63
5.1	GENERAL	57
5.2	BASIC STEPS	58
5.3	BROAD DETAILS OF PROPOSED METHODOLOGY	58
5.3.1	Development of Regression Equations	58
5.3.2	Validation of Respective Regression Equations Referred to a Pair of Boreholes on the Profile	59
5.3.3	Development of Regression Equations for Geotechnical Parameters	59
5.3.4	Generation of 2-D Geotechnical Parameter Sections	59
5.3.5	Prediction of 3-D Geotechnical Parameter Volumes	59
5.4	DETAILED PROCEDURE	60
5.4.1	Correlation of Normalized ERT, IPI, Ficles and SPT versus Depth Plots	60

5.4.2	Inferring Prediction Equations for ERT / IPI / Ficles versus SPT, DCPT and SCPT	60
5.4.3	Inferring Prediction Equations for ERT / IPI / Ficles versus Geotechnical Sand, Clay / Shale, Lithology, Water Saturation and Porosity	61
5.4.4	Use of Regression Equations for Obtaining 2-D Sections of SPT, DCPT and SCPT	61
5.4.5	Use of Regression Equations for Obtaining 2-D Sections of Angle of Internal Friction, Porosity, Water Saturation and Unconfined Compressive Strength	61
5.4.6	Use of Regression Equations for Terzaghi's Bearing Capacity and Ultimate Bearing Capacity 2-D Sections for Strip Footings from Angle of Internal Friction	61
5.4.7	Use of Regression Equation for N_q Factor 2-D Sections Based on Friction Angle in Case of Deep Sub-soil (Piles) Investigations	62
5.5	REMARKS	62
CHAPTER 6: GEOTECHNICAL CASE STUDIES-I		65-141
6.1	GENERAL	65
6.2	GEOLOGY OF THE STUDY REGION	65
6.3	SITE LOCATION MAPS	66
6.4	GEOELECTRICAL AND GEOTECHNICAL DATA ACQUISITION	66
6.5	REGRESSION EQUATIONS FOR SPT AND SCPT	71
6.5.1	Regression Equation for SPT	71
6.5.2	Regression Equation for SCPT	71
6.6	REGRESSION EQUATIONS FOR SAND, CLAY, LITHOLOGY, POROSITY AND WATER SATURATION	72

6.7	REGRESSION EQUATIONS FOR UNIT WEIGHT OF SOIL (DRY & SATURATED), UNCONFINED COMPRESSIVE STRENGTH, q_u , INTERNAL FRICTION ANGLE, ϕ AND BEARING CAPACITY FACTORS (SHALLOW AND DEEP INVESTIGATIONS)	74
6.8	GENERATION OF FORMATION AND GEOTECHNICAL PARAMETER SECTIONS	74
6.8.1	Formation Parameter Sections	74
6.8.2	Geotechnical Parameter Sections (SPT, SCPT)	74
6.8.3	Unconfined Compressive Strength (q_u) and Internal Friction Angle (ϕ) Section	75
6.8.4	Bearing Capacity Sections	75
6.9	RESULTS & DISCUSSION	77
	CHAPTER 7: GEOTECHNICAL CASE STUDIES-II	143-179
7.1	GENERAL	143
7.2	SITE LOCATION MAPS	143
7.3	GEOELECTRICAL AND GEOTECHNICAL DATA ACQUISITION	143
7.4	REGRESSION EQUATIONS FOR FORMATION AND SITE GEOTECHNICAL TESTS	144
7.5	PREDICTED 2-D SECTIONS FOR FORMATION AND SITE GEOTECHNICAL TESTS	144
7.6	RESULTS & DISCUSSION	147
	CHAPTER 8: GEOTECHNICAL CASE STUDIES-III	181-219
8.1	GENERAL	181
8.2	SITE LOCATION MAPS	181
8.3	GEOELECTRICAL AND GEOTECHNICAL DATA ACQUISITION	181
8.4	REGRESSION EQUATIONS FOR FORMATION AND SITE GEOTECHNICAL TESTS	182

8.5	REGRESSION EQUATIONS FOR UNIT WEIGHT OF SOIL (DRY & SATURATED), UNCONFINED COMPRESSIVE STRENGTH, q_u , INTERNAL FRICTION ANGLE, ϕ AND BEARING CAPACITY FACTORS (SHALLOW AND DEEP INVESTIGATIONS)	182
8.6	INFERRED 2-D SECTIONS OF FORMATION PARAMETERS	183
8.7	GENERATION OF GEOTECHNICAL PARAMETER SECTIONS	185
8.8	RESULTS & DISCUSSION	185
CHAPTER 9: GEOTECHNICAL CASE STUDIES-IV		221-261
9.1	GENERAL	221
9.2	SITE LOCATION MAPS	221
9.3	GEOLOGY OF THE STUDY REGION	221
9.4	GEOELECTRICAL AND GEOTECHNICAL DATA ACQUISITION	222
9.5	REGRESSION EQUATIONS FOR FORMATION AND SITE GEOTECHNICAL TESTS	223
9.6	PREDICTED 2-D SECTIONS OF FORMATION AND SITE GEOTECHNICAL PARAMETERS	223
9.7	PREDICTED 2-D GEOTECHNICAL PARAMETER SECTIONS	223
9.8	RESULTS & DISCUSSION	226
CHAPTER 10: SUMMARY AND CONCLUSIONS		263-267
10.1	GENERAL	263
10.2	SUMMARY OF THE WORK DONE	264
10.3	CONCLUSION	265
10.4	FURTHER PERSPECTIVES	267
APPENDIX-A		269-278
REFERENCES		279-293

LIST OF FIGURES

<i>Figure No.</i>	<i>Figure Caption</i>	<i>Page No.</i>
3.1	Schlumberger Electrode Arrangements	17
3.2	Induced Polarization Decay Curve	18
3.3	Arrangement of Electrodes for 2-D Geoelectrical Survey and Sequence of Measurements Used to Build up a Pseudo-section (Loke and Barker, 1995)	22
3.4	Comparison of (i) Electrode Arrangement and (ii) Pseudo-section data Pattern for the Wenner and Wenner-Schlumberger Configurations	23
3.5	Rectangular Block of Finite Dimension, C and P are the Current and Potential Electrode Respectively	26
3.6	Arrangement of the blocks used in a model together with data points in the pseudo-section.	28
4.1	Graphical Representation of Mohr-Coulomb Equation.	34
4.2	Static Cone Penetration Equipment and Cone Assembly	41
4.3	Terzaghi's Bearing Capacity Factors for General Shear Failure (Murthy, 2008)	50
4.4	Terzaghi's Bearing Capacity Factors for Mixed State of Local and General Shear Failures in Sand (Murthy, 2008)	50
4.5	Bearing Capacity Factors for Circular Deep Foundations (Murthy, 2008)	53
6.1a	Location Map of Proposed Library Site, IIT Roorkee, Roorkee, India	68
b	Map Showing the Location of ERT, IPI and Geotechnical Site Investigations	69
c	Geological (Soil-Geomorphic) Map of the Study Region	70
6.2a	Resistivity Image (ERT) Along Profile A-B. The Resistivity (ohm-m) and Depth Scales are Logarithmic	80

b	IP Image (IPI) Along Profile A-B. The IP Chargeability (m Sec) and Depth Scales are Logarithmic	80
6.3a	Borehole Data at Location B-1. The Projected Borehole Position Coincides with Electrode, EL-16 of profile A-B	81
b	Borehole Data at Location B-3. The Projected Borehole Position Coincides with Electrode, EL-24 of profile A-B	82
6.4a	Plot of SPT N-Values versus Resistivity, IP and Fictitious Resistivity (EL-16) at Borehole Location- B-1 of Profile A-B	83
b	Plot of SPT N-Values versus Resistivity, IP and Fictitious Resistivity (EL-24) at Borehole Location- B-3 of Profile A-B	83
c	Plot of SPT N-Values versus Resistivity at Borehole Location- B-1	84
d	Plot of Observed versus Computed SPT Through Resistivity at Borehole Location- B-1	84
e	Plot of SPT versus Resistivity at Borehole Location- B-3	85
f	Plot of Observed versus Computed SPT Through Resistivity at Borehole Location- B-3	85
g	Plot of SPT N-Values versus IP at Borehole Location- B-1	86
h	Plot of Observed versus Computed SPT Through IP at Borehole Location- B-1	86
i	Plot of SPT N-Values versus IP at Borehole Location- B-3	87
j	Plot of Observed versus Computed SPT Through IP at Borehole Location- B-3	87
6.5a	SCPT-1 Data. The Corresponding Electrode Position is EL-16 of Profile A-B	88
b	SCPT-2 Data. The Corresponding Electrode Position is EL-29 of Profile A-B	88
6.6a	Plot of Observed SCPT-1, Resistivity, IP and Fictitious Resistivity at the Electrode Location- EL-16 of Profile A-B	89
b	Plot of Observed SCPT-2, Resistivity, IP and Fictitious Resistivity at the Electrode Location- EL-29 of Profile A-B	89
c	Plot of SCPT-1 versus IP at EL -16	90

d	Plot of Observed versus Computed SCPT-1 at EL-16 Using IP	90
e	Plot of SCPT-2 versus IP at EL-29	91
f	Plot of Observed versus Computed SCPT-2 at EL-29 Using IP	91
g	Regression of SCPT-1 with Normalized Resistivity	92
h	Comparison of Observed SCPT-1 and Computed One Using Resistivity	92
i	Regression of Normalized Resistivity with SCPT-2 of Profile A-B	93
j	Comparison of Observed SCPT-2 with Computed One Using Resistivity	93
6.7a	Plot of Geotechnical Sand, Resistivity, IP and Fictitious Resistivity at Borehole Location- B-1 (Electrode Location - EL-16) of Profile A-B	94
b	Plot of Geotechnical Sand, Resistivity, IP and Fictitious Resistivity at Borehole Location- B-3 (Electrode Location - EL-24) of Profile A-B	94
c	Plot of Geotechnical versus Computed Sand at Borehole Location- B-1 Using IP	95
d	Plot of Geotechnical versus Computed Sand at Borehole Location- B-3 Using IP	95
e	Comparison of Observed and Predicted Geotechnical Sand Through Resistivity at the Borehole Location-B-1	96
f	Comparison of Observed versus Computed Geotechnical Sand Through Resistivity at Borehole Location-B-3	96
g	Plot of Geotechnical Shale, Resistivity, IP and Fictitious Resistivity at Borehole Location- B-1 (Electrode Location- EL-16) of Profile A-B	97
h	Plot of Geotechnical Shale, Resistivity, IP and Fictitious Resistivity at Borehole Location- B-3 (Electrode Location- EL-24) of Profile A-B	97
i	Comparison of Observed and Computed Shale Through Resistivity at Borehole Location- B1	98
j	Comparison of Observed and Computed Shale Through Resistivity at Borehole Location-B-3	98
k	Plot of Geotechnical versus Computed Shale at Borehole Location- B-1 Using IP	99

1	Plot of Geotechnical versus Computed Shale at Borehole Location- B-3 Using IP	99
6.8a	Plot of Observed Lithology, Resistivity, IP and Fictitious Resistivity at Borehole Location- B-1 (Electrode Location- EL-16) of Profile A-B	100
b	Plot of Lithology, Resistivity, IP and Fictitious Resistivity at Borehole Location- B-3 (Electrode Location- EL-24) of Profile A-B	100
c	Plot of Observed versus Computed Lithology Through IP at Borehole Location- B-1	101
d	Plot of Observed versus Computed Lithology Through IP at Borehole Location- B-3	101
e	Comparison of Observed and Computed Lithology Through Resistivity at Borehole Location- B-1	102
f	Comparison of Observed and Computed Lithology Through Resistivity at Borehole Location- B-3	102
g	Inferred Lithology Section from Geotechnical and Resistivity Data Along Profile A-B, Library Site, IITR	103
6.9a	Plot of Observed Porosity, Resistivity, IP and Fictitious Resistivity at Borehole Location- B-1 (Electrode Location- EL-16) of Profile A-B	104
b	Plot of Observed Porosity, Resistivity, IP and Fictitious Resistivity at Borehole Location- B-3 (Electrode Location- EL-24) of Profile A-B	104
c	Plot of Observed Porosity versus Computed Porosity at Borehole Location- B-1 Using IP	105
d	Plot of Observed versus Computed Porosity at Borehole Location- B-3 Using IP	105
e	Comparison of Observed and Computed Porosity Through Resistivity at Borehole Location- B-1	106
f	Comparison of Observed and Computed Porosity Through Resistivity at Borehole Location- B-3	106
g	Predicted Porosity (%) Section from Resistivity and Borehole Data Along Profile A-B, Library Site, IITR	107

6.10a	Plot of Water Saturation (S_w) versus Resistivity, IP and Fictitious Resistivity at Borehole Location- B-1 (Electrode Location- EL-16) of Profile A-B	108
b	Plot of Water Saturation (S_w) versus Resistivity, IP and Fictitious Resistivity at Borehole Location- B-3 (Electrode Location- EL-24) of Profile A-B	108
c	Plot of Observed versus Computed S_w at Borehole Location- B-1 Using IP	109
d	Plot of Observed versus Computed S_w at Borehole Location- B-3 Using IP	109
e	Comparison of Observed and Computed S_w at Borehole Location- B-1 Using Resistivity	110
f	Comparison of Observed versus Computed S_w at Borehole Location- B-3 Using Resistivity	110
g	Predicted Water Saturation (%) Section from Resistivity and Borehole Data Along Profile A-B, Library Site, IITR	111
6.11a	IP Derived Sand (%) Section Along Profile A-B, Library Site, IITR	113
b	Resistivity Derived Sand (%) Section Along Profile A-B, Library Site, IITR	113
6.12a	IP Derived Clay (%) Section Along Profile A-B, Library Site, IITR	115
b	Resistivity Derived Clay (%) Section Along Profile A-B, Library Site, IITR	115
6.13a	Predicted of Sand (%) Section from Geotechnical and IP Data Along Profile A-B, Library Site, IITR	117
b	Predicted Sand (%) Section from Geotechnical and Resistivity Data Along Profile A-B , Library Site, IITR	117
6.14a	Predicted Clay (%) Section from Geotechnical and IP Data Along Profile A-B, Library Site, IITR	119
b	Predicted Clay (%) Section from Geotechnical and Resistivity Data Along Profile A-B, Library Site, IITR	119

6.15a	Predicted SPT Section from IP and Borehole Data Along Profile A-B, Library Site, IITR	121
b	Predicted SPT Section from Resistivity and Borehole Data Along Profile A-B, Library Site, IITR	121
6.16a	Predicted SCPT Section from IP and Borehole Data Along Profile A-B, Library Site, IITR	123
b	Predicted SCPT Section from Resistivity and Borehole Data Along Profile A-B, Library Site, IITR	123
6.17a	Predicted Internal Friction Angle Section from Synthetic SPT Section Using IP Along Profile A-B, Library Site, IITR	125
b	Predicted Internal Friction Angle Section from Synthetic SPT Section Using Resistivity Along Profile A-B, Library Site, IITR	125
6.18a	Predicted Unit Weight (Dry) in kN/m^3 Section from Water Saturation Section (Using IP) Along Profile A-B, Library Site, IITR	127
b	Predicted Unit Weight (Dry) in kN/m^3 Section from Water Saturation (Using Resistivity) Section Along Profile A-B, Library Site, IITR	127
6.19a	Predicted Unit Weight (Saturated) in kN/m^3 Section from Water Saturation (Using IP) Section Along Profile A-B, Library Site, IITR	129
b	Inferred Unit Weight (Saturated) in kN/m^3 Section from Water Saturation (Using Resistivity) Section Along Profile A-B, Library Site, IITR	129
6.20	Predicted Unconfined Compressive Strength, q_u Section from SPT 'N' Section (Using Resistivity) Along Profile A-B, Library Site, IITR	131
6.21	Predicted Bearing Capacity Factor of General Shear Failure, N_c Section from Resistivity Derived Angle of Internal Friction Section Along Profile A-B, Library Site, IITR	131
6.22	Predicted Bearing Capacity Factor of General Shear Failure, N_γ (Vesic) Section from Angle of Internal Friction Section Along Profile A-B, Library Site, IITR	133
6.23	Predicted Bearing Capacity Factor of General Shear Failure, N_q Section from Angle of Internal Friction Along Profile A-B, Library Site, IITR	133

6.24	Predicted Ultimate Bearing Capacity Factor, N_c Section for Strip Footings from Angle of Internal Friction Section Along Profile A-B, Library Site, IITR	135
6.25	Predicted Ultimate Bearing Capacity Factor, N_γ Section for Strip Footings from Angle of Internal Friction Section Along Profile A-B, Library Site, IITR	135
6.26	Predicted Ultimate Bearing Capacity Factor, N_q Section for Strip Footings from Angle of Internal Friction Section Along Profile A-B, Library Site, IITR	137
6.27	Predicted Terzaghi's Bearing Capacity (Peck et al. 1974) N_γ Factor Section from Angle of Internal Friction Section Along Profile A-B, Library Site, IITR	137
6.28	Predicted Terzaghi's Bearing Capacity (Peck et al. 1974) Factor, N_q Section from Angle of Internal Friction Section Along Profile A-B, Library Site, IITR	139
6.29	Predicted N_q Factor (Meyerhof, 1953) Section for Driven Piles from Angle of Internal Friction Section Along Profile A-B, Library Site, IITR	139
6.30	Predicted N_q (Meyerhof, 1953) Factor Section for Bored Piles from Angle of Internal Friction Section Along Profile A-B, Library Site, IITR	141
6.31	Predicted N_q (Vesic) Factor Section for Bored Piles from Angle of Internal Friction Section Along Profile A-B, Library Site, IITR	141
7.1a	Location Map of Proposed Multi-storeyed Structure at E. P. Hostel Site, IIT Roorkee, Roorkee, India	149
b	Map Showing the Location of ERT, IPI and Geotechnical Site Investigations	151
c	Geological Map of the Study Region	152
7.2a	Resistivity Image (ERT) Along Profile A-B. The Resistivity and Depth Scales are Logarithmic	153

b	IP Image (IPI) Along Profile A-B. The IP and Depth Scales are Logarithmic	153
7.3	IP Derived Sand (%) Section Along Profile A-B, E. P. Hostel, IITR	155
7.4	IP Derived Clay (%) Section Along Profile A-B, E. P. Hostel, IITR	155
7.5	Predicted Sand (%) Section from Geotechnical and IP Data Along Profile A-B , E. P. Hostel, IITR	157
7.6	Predicted Clay (%) Section from Geotechnical and IP Data Along Profile A-B, E. P. Hostel, IITR	157
7.7	Predicted Lithology Section from Geotechnical and IP Data Along Profile A-B, E. P. Hostel, IITR	159
7.8	Predicted Porosity (%) Section from IP and Geotechnical Data Along Profile A-B, E. P. Hostel, IITR	159
7.9	Predicted Water Saturation (%) Section from IP and Geotechnical Data Along Profile A-B, E. P. Hostel, IITR	161
7.10a	Borehole Data at Location B-1. The Projected Borehole Position Coincides with Electrode, EL-24 of profile A-B	161
b	Borehole Data at Location B-2. The Projected Borehole Position Coincides with Electrode, EL-29 of profile A-B	163
7.11	Predicted SPT Section from IP and Borehole Data Along Profile A- B, E. P. Hostel, IITR	163
7.12	Comparison of Observed and Predicted SPT ‘N’ through IP at Borehole Location- B-1	164
7.13	Comparison of Observed and Predicted SPT ‘N’ through IP at Borehole Location- B-2	164
7.14a	SCPT-1 Data. The Corresponding Electrode Position is EL-15 of Profile A-B	165
b	SCPT-2 Data. The Corresponding Electrode Position is EL-33 of Profile A-B	165
7.15	Predicted SCPT Section from IP and Borehole Data Along Profile A-B, E. P. Hostel, IITR	166

7.16	Predicted Internal Friction Angle Section from Synthetic SPT Section Using IP Along Profile A-B, E. P Hostel Site , IITR	166
7.17	Predicted Unit weight (Dry) in kN/m^3 Section from Water Saturation Section Using IP Along Profile A-B, E. P Hostel Site , IITR	167
7.18	Predicted Unit Weight (Saturated) in kN/m^3 Section from Water Saturation Section Using IP Along Profile A-B, E. P. Hostel, IITR	167
7.19	Predicted Unconfined Compressive Strength, q_u Section from SPT 'N' Section Using IP Along Profile A-B, E. P. Hostel, IITR	169
7.20	Predicted Bearing Capacity Factor of General Shear Failure, N_c Section from IP Derived Angle of Internal Friction Section Along Profile A-B, E. P. Hostel, IITR	169
7.21	Predicted Bearing Capacity Factor of General Shear Failure, N_γ (Vesic) Section from Angle of Internal Friction Section Along Profile A-B, E. P. Hostel, IITR	171
7.22	Predicted Bearing Capacity Factor of General Shear Failure, N_q Section from Angle of Internal Friction Along Profile A-B, E. P. Hostel, IITR	171
7.23	Predicted Ultimate Bearing Capacity Factor, N_c Section for Strip Footings from Angle of Internal Friction Section Along Profile A-B, E. P. Hostel, IITR	173
7.24	Predicted Ultimate Bearing Capacity Factor, N_γ Section for Strip Footings from Angle of Internal Friction Section Along Profile A-B, E. P. Hostel, IITR	173
7.25	Predicted Ultimate Bearing Capacity Factor, N_q Section for Strip Footings from Angle of Internal Friction Section Along Profile A-B, E. P. Hostel, IITR	175
7.26	Predicted Terzaghi's Bearing Capacity (Peck et al. 1974) Factor, N_γ Section from Angle of Internal Friction Section Along Profile A-B, E. P. Hostel, IITR	175
7.27	Predicted Terzaghi's Bearing Capacity (Peck et al. 1974) Factor, N_q Section from Angle of Internal Friction Section Along Profile A-B, E. P. Hostel, IITR	177

7.28	Predicted N_q Factor (Meyerhof, 1953) Section for Driven Piles from Angle of Internal Friction Section Along Profile A-B, E. P. Hostel, IITR	177
7.29	Predicted N_q (Meyerhof, 1953) Factor Section for Bored Piles from Angle of Internal Friction Section Along Profile A-B, E. P. Hostel, IITR	179
7.30	Predicted N_q (Vesic) Factor Section for Bored Piles from Angle of Internal Friction Section Along Profile A-B, E. P. Hostel, IITR	179
8.1	Location Map of Proposed Structure ACL at Bhagwanpur Site, Uttarakhand, India	187
8.2	Map Showing the Location of ERT, IPI and Geotechnical Site Investigations	189
8.3	Geological Map of the Study Region	190
8.4a	Resistivity Image (ERT) Along Profile A ₃ -B ₃ . The Resistivity (ohm-m) and Depth scales are Logarithmic	191
b	IP Image (IPI) Along Profile A ₃ -B ₃ . The Chargeability (mSec) and Depth Scales are Logarithmic	191
8.5	IP Derived Sand (%) Section Along Profile A ₃ -B ₃ , Bhagwanpur	193
8.6	IP Derived clay (%) Section Along Profile A ₃ -B ₃ , Bhagwanpur	193
8.7	Predicted Sand (%) Section from Geotechnical and IP Data Along Profile A ₃ -B ₃ , Bhagwanpur	195
8.8	Predicted Clay (%) Section from Geotechnical and IP Data Along Profile A ₃ -B ₃ , Bhagwanpur	195
8.9	Predicted Lithology Section from Geotechnical and IP Data Along Profile A ₃ -B ₃ , Bhagawanpur	197
8.10	Predicted porosity (%) Section from IP and Borehole Data Along Profile A ₃ -B ₃ , Bhagawanpur	197
8.11a	Borehole Data at Location B-3. The Projected Borehole Position Coincides with Electrode, EL-60 of profile A ₃ -B ₃	198
b	Borehole Data at Location B-6. The Projected Borehole Position Coincides with Electrode, EL-52 of profile A ₃ -B ₃	199

8.12	Predicted SPT Section from IP and Borehole Data Along Profile A ₃ -B ₃ , Bhagawanpur	200
8.13a	Comparison of Observed and Computed SPT 'N' Through Resistivity at Borehole location- B-3	200
b	Comparison of Observed and Computed SPT 'N' Through IP at Borehole Location- B-3	201
8.14a	Comparison of Observed and Computed SPT 'N' Through Resistivity at Borehole Location- B-6	201
b	Comparison of Observed and Computed SPT 'N' Through IP at Borehole Location- B-6	202
8.15a	DCPT-3 Data. The Corresponding Electrode Position is EL-62 of Profile A ₃ -B ₃	202
b	DCPT-6 Data. The Corresponding Electrode Position is EL-49 of Profile A ₃ -B ₃	202
8.16	Predicted DCPT Section from IP and Borehole Data Along Profile A ₃ -B ₃ , Bhagawanpur	203
8.17	Predicted Internal Friction Angle Section from Synthetic SPT Section Using IP Along Profile A ₃ -B ₃ , Bhagwanpur	205
8.18	Predicted Unit Weight (Dry) in kN/m ³ Section from Porosity Section Using IP along Profile A ₃ -B ₃ , Bhagwanpur	205
8.19	Predicted Unit Weight (Saturated) in kN/m ³ Section from Porosity Section Using IP Along Profile A ₃ -B ₃ , Bhagwanpur	207
8.20	Predicted Unconfined Compressive Strength, q _u Section from SPT 'N' Section Using IP Along Profile A ₃ -B ₃ , Bhagwanpur	207
8.21	Predicted Bearing Capacity Factor of General Shear Failure, N _c Section from IP Derived Angle of Internal Friction Section Along Profile A ₃ -B ₃ , Bhagwanpur	209
8.22	Predicted Bearing Capacity Factor of General Shear Failure, N _γ (Vesic) Section from Angle of Internal Friction Section Along Profile A ₃ -B ₃ , Bhagwanpur	209

8.23	Predicted Bearing Capacity Factor of General Shear Failure, N_q Section from Angle of Internal Friction Along Profile A ₃ -B ₃ , Bhagwanpur	211
8.24	Predicted Ultimate Bearing Capacity Factor, N_c Section for Strip Footings from Angle of Internal Friction Section Along Profile A ₃ -B ₃ , Bhagwanpur	211
8.25	Predicted Ultimate Bearing Capacity Factor, N_γ Section for Strip Footings from Angle of Internal Friction Section Along Profile A ₃ -B ₃ , Bhagwanpur	213
8.26	Predicted Ultimate Bearing Capacity Factor, N_q Section for Strip Footings from Angle of Internal Friction Section Along Profile A ₃ -B ₃ , Bhagwanpur	213
8.27	Predicted Terzaghi's Bearing Capacity (Peck et al. 1974) N_γ Factor Section from Angle of Internal Friction Section Along Profile A ₃ -B ₃ , Bhagawanpur	215
8.28	Predicted Terzaghi's Bearing Capacity (Peck et al. 1974) Factor, N_q Section from Angle of Internal Friction Section Along Profile A ₃ -B ₃ , Bhagawanpur	215
8.29	Predicted N_q Factor (Meyerhof, 1953) for Driven Piles from Angle of Internal Friction Section Along Profile A ₃ -B ₃ , Bhagawanpur	217
8.30	Predicted N_q (Meyerhof, 1953) Factor for Bored Piles from Angle of Internal Friction Section Along Profile A ₃ -B ₃ , Bhagawanpur	217
8.31	Predicted N_q (Vesic) Factor for Bored Piles from Angle of Internal Friction Section Along Profile A ₃ -B ₃ , Bhagawanpur	219
9.1	Location Map of Proposed Construction of BPCL at Piyala Site, Haryana, India	228
9.2	Map Showing the Location of ERT, IPI and Geotechnical Site Investigations	229
9.3	Geological Map of Delhi Supergroup in Haryana Including the Study Region	231

9.4a	Resistivity Image (ERT) Along Profile A ₄ -B ₄ . The Resistivity (Ω -m) and Depth Scales are Logarithmic	233
b	IP image (IPI) Along Profile A ₄ -B ₄ . The Chargeability (mSec) and Depth Scales are Logarithmic	233
9.5	Resistivity Derived Sand (%) Section Along Profile A ₄ -B ₄ , Piyala	235
9.6	Resistivity Derived Clay (%) Section Along Profile A ₄ -B ₄ , Piyala	235
9.7	Predicted Sand (%) Section from Geotechnical and Resistivity Data Along Profile A ₄ -B ₄ , Piyala	237
9.8	Predicted of Clay (%) Section from Geotechnical and Resistivity Data Along Profile A ₄ -B ₄ , Piyala	237
9.9	Predicted Porosity (%) Section from Resistivity and Borehole Data Along Profile A ₄ -B ₄ , Piyala	239
9.10	Predicted Lithology Section from Geotechnical and Resistivity Data Along Profile A ₄ -B ₄ , Piyala	239
9.11a	Borehole Data at Location B-7. The Projected Borehole Position Coincides with Electrode, EL-12 of profile A ₄ -B ₄	240
b	Borehole Data at Location B-8. The Projected Borehole Position Coincides with Electrode, EL-33 of profile A ₄ -B ₄	241
9.12	Predicted SPT Section from Resistivity and Borehole Data Along Profile A ₄ -B ₄ , Piyala	242
9.13a	Comparison of Observed and Predicted SPT 'N' Through Resistivity at Borehole Location- B-7	242
b	Comparison of Observed and Predicted SPT 'N' Through IP at Borehole Location- B-7	243
9.14a	Comparison of Observed and Predicted SPT 'N' Through Resistivity at Borehole Location- B-8	243
b	Comparison of Observed and Predicted SPT 'N' Through IP at Borehole location- B-8	244
9.15a	DCPT-5 Data. The Corresponding Electrode Position is EL-18 of Profile A ₄ -B ₄	244

b	DCPT-7 Data. The Corresponding Electrode Position is EL-25 of Profile A ₄ -B ₄	244
9.16	Predicted DCPT Section from Resistivity and Borehole Data Along Profile A ₄ -B ₄ , Piyala	245
9.17a	SCPT-4 Data. The Corresponding Electrode Position is EL-15 of Profile A ₄ -B ₄	245
b	SCPT-5 Data. The Corresponding Electrode Position is EL-25 of Profile A ₄ -B ₄	245
9.18	Predicted SCPT Section from Resistivity and Borehole Data Along Profile A ₄ -B ₄ , Piyala	247
9.19	Predicted Internal Friction Angle Section from Synthetic SPT Section Using Resistivity Along Profile A ₄ -B ₄ , Piyala	247
9.20	Predicted Unit Weight (Dry) in kN/m ³ from Water Saturation Section Using Resistivity Along Profile A ₄ -B ₄ , Piyala	249
9.21	Predicted Unit Weight (Saturated) in kN/m ³ from Water Saturation Section Using Resistivity Along Profile A ₄ -B ₄ , Piyala	249
9.22	Predicted Unconfined Compressive Strength, q _u from SPT 'N' Section Using Resistivity Along Profile A ₄ -B ₄ , Piyala	251
9.23	Predicted Bearing Capacity Factor of General Shear Failure, N _c Section from Angle of Internal Friction Section Along Profile A ₄ -B ₄ , Piyala	251
9.24	Predicted Bearing Capacity Factor of General Shear Failure, N _γ (Vesic) from Angle of Internal Friction Section Along Profile A ₄ -B ₄ , Piyala	253
9.25	Predicted Bearing Capacity Factor of General Shear Failure N _q , Section from Angle of Internal Friction Section Along Profile A ₄ -B ₄ , Piyala	253
9.26	Predicted Ultimate Bearing Capacity Factor N _c Section for Strip Footings from Angle of Internal Friction Section Along Profile A ₄ -B ₄ , Piyala	255

9.27	Predicted Ultimate Bearing Capacity Factor, N_y Section for Strip Footings from Angle of Internal Friction Section Along Profile A ₄ -B ₄ , Piyala	255
9.28	Predicted Ultimate Bearing Capacity Factor, N_q Section for Strip Footings from Angle of Internal Friction Section Along Profile A ₄ -B ₄ , Piyala	257
9.29	Predicted Terzaghi's Bearing Capacity (Peck et al., 1974) N_y Factor Section from Angle of Internal Friction Section Along Profile A ₄ -B ₄ , Piyala	257
9.30	Predicted Terzaghi's Bearing Capacity (Peck et al., 1974) Factor, N_q Section from Angle of Internal Friction Section Along Profile A ₄ -B ₄ , Piyala	259
9.31	Predicted N_q Factor (Meyerhof, 1953) Section for Driven Piles from Angle of Internal Friction Section Along Profile A ₄ -B ₄ , Piyala	259
9.32	Predicted N_q (Meyerhof, 1953) Factor Section for Bored Piles from Angle of Internal Friction Section Along Profile A ₄ -B ₄ , Piyala	261
9.33	Predicted N_q (Vesic) Factor Section for Bored Piles from Angle of Internal Friction Section Along Profile A ₄ -B ₄ , Piyala	261
A.1a	Regression Equation for Porosity versus Unit Weights of Typical Soils (Dry) in natural state (Murthy, 2008)	273
b	Regression Equation for Porosity versus Unit Weights of Typical Soils (Saturated) in Natural State (Murthy, 2008)	273
c	Regression Equation for Water Saturation versus Unit Weights of Typical Soils (Dry) in Natural State (Murthy, 2008)	273
d	Regression Equation for Porosity versus Unit Weights of Typical Soils (Saturated) in Natural State (Murthy, 2008)	274
A.2	Regression Equation for Unconfined Compressive Strength, q_u versus SPT 'N' for Clay (Murthy, 2008)	274

A.3a	Regression Equation for Bearing Capacity Factor, N_c of Terzaghi for General Shear Failure versus Angle of Internal Friction, ϕ (Murthy, 2008)	275
b	Regression Equation for Bearing Capacity Factor, N_q of Terzaghi for General Shear Failure versus Angle of Internal Friction, ϕ (Murthy, 2008)	275
c	Regression Equation for Bearing Capacity Factor, N_γ of Terzaghi for General Shear Failure versus Angle of Internal Friction, ϕ (Murthy, 2008)	275
A.4a	Regression Equation for Terzaghi's Relationship Between Angle of Internal Friction, ϕ and SPT 'N' (Murthy, 2008)	276
b	Regression Equation for Terzaghi's Bearing Capacity Factor N_q as a Function of Angle of Internal Friction, ϕ (Murthy, 2008)	276
c	Regression Equation for Terzaghi's Bearing Capacity Factor N_γ as a Function of Angle of Internal Friction, ϕ (Murthy, 2008)	276
A.5a	Regression Equation for Bearing Capacity Factor, N_c versus Angle of Internal Friction, ϕ (Murthy, 2008)	277
b	Regression Equation for Bearing Capacity Factor, N_q versus Angle of Internal Friction, ϕ (Murthy, 2008)	277
c	Regression Equation for Bearing Capacity Factor, N_γ (Vesic) versus Angle of Internal Friction, ϕ (Murthy, 2008)	277
A.6a	Regression Equation for Bearing Capacity Factor, N_q (Vesic) for Bored Piles (Deep Soil Investigations) versus ϕ (Murthy, 2008)	278
b	Regression Equation for Bearing Capacity Factor, N_q (Meyerhof, 1953) for Bored Piles (Deep Soil Investigations) versus ϕ (Murthy, 2008)	278
c	Regression Equation for Bearing Capacity Factor, N_q (Meyerhof, 1953) for Driven Piles (Deep Soil Investigations) versus ϕ (Murthy, 2008)	278

LIST OF TABLES

<i>Table No.</i>	<i>Table Caption</i>	<i>Page No.</i>
3.1	Different Geoelectrical Arrays with Corresponding Geometrical Factors (Loke, 1999)	14
3.2	Percentage of Shaliness and Related Lithology (Mondal, 2009)	29
4.1	Nomenclature of Soils According to IS: 1498 (1970)	33
4.2	In-Situ Geotechnical Tests - Summary	39
4.3	Relation of N with Friction Angle (ϕ) and Relative Density, (Murthy, 2008)	40
4.4	Relation between N and Unconfined Compressive Strength, q_u (Murthy, 2008)	40
4.5	Relationship between Relative Density (D_r) of Fine Sand, SPT (N), Static Cone Resistance (q_c) and Angle of Internal Friction (ϕ°) (Murthy, 2008)	42
4.6	Relationship between q_c and N (Murthy, 2008)	43
4.7	Geotechnical Properties and Related Laboratory Tests	46
4.8	Bearing Capacity Factors of Terzaghi (Murthy, 2008)	51
4.9	The Value of N_c , N_q and N_γ Factors of Meyerhof (M), Hansen (H) and Vesic (V) (Murthy, 2008)	51
4.10	Inferred Predictive Equations of Different Geotechnical Parameters from Available Correlations in Literature (Murthy, 2008) for SPT	56
5.1	Resistivity / IP Values versus Lithology as per Geotechnical Soil Classification	63
6.1	Generalized Stratigraphy of the Indo-Gangetic Plain (After Kumar, 2005) Pertinent Study Region	67

6.2	Inferred Regression Equations Based on Borehole and Geoelectrical Depth Profiles Gathered from Respective Geoelectrical Images at Projected Borehole Positions onto Geoelectrical Profile A-B at Library Site, IITR	73
6.3	Details of Illustrations	76
7.1	Inferred Predictive Equations from Cross-correlation of Normalized Plots at Different Geophysical Sites Projected onto Profile A-B at E. P. Hostel, IITR	145
7.2	Predicted 2D Geotechnical Parameter Sections	146
8.1	Inferred Predictive Equations from Cross-correlation of Normalized Plots at Different Geophysical Sites Projected onto Profile A ₃ -B ₃ at Bhagawanpur	183
8.2	Details of Illustrations	184
9.1	Inferred Regression Equations Based on Borehole and Geoelectrical Depth Profiles Gathered from Respective Geoelectrical Images at Projected Borehole Position onto Profile A ₄ -B ₄ at Piyala Site, Haryana	224
9.2	Details of illustrations	225
A.1a	Porosity and Unit Weights of Typical Soils in Natural State (Murthy, 2008)	269
A.1b	Relationship between Water Content (%) and Unit Weights (γ_d, γ_{sat}) (After Murthy, 2008)	269
A.2	Unconfined Compressive Strength, q_u versus SPT 'N' for Clay (Murthy, 2008)	270
A.3	Bearing Capacity Factors of Terzaghi for General Shear Failure (Murthy, 2008) versus Angle of Internal Friction, ϕ	270
A.4a	Terzaghi's Relationship between Internal Angle of Friction, ϕ and SPT 'N' (Murthy, 2008)	270
A.4b	Terzaghi's Bearing Capacity Factor N_q as a Function of Internal Angle of Friction, ϕ (Murthy, 2008)	271

A.4c	Terzaghi's Bearing Capacity Factor N_γ as a Function of Internal Angle of Friction, ϕ (Murthy, 2008)	271
A.5	The Relation of ϕ with Different Bearing Capacity Factors, N_c , N_q and N_γ (Vesic) (Murthy, 2008)	272
A.6	Bearing Capacity Factors (Murthy, 2008) for Piles (Deep Soil Investigations) versus ϕ	272

LIST OF PLATES

<i>Plate No.</i>	<i>Plate Caption</i>	<i>Page No.</i>
3.1	Electrical Restivity Imaging System (IRIS)	20
4.1	Different Standard Sieves	32
4.2	Standard Penetration Test (SPT) in Progress	36
4.3	Standard Penetration Test-Details	37
4.4	Setup and Procedure of Cone Penetration Test (CPT)	42
4.5	Plate load test (PLT)	44
4.6	Sampling from SPT Split Spoon	45

1.1 PREAMBLE

The science of ground engineering is called 'Rock Mechanics' when applied to rocks and called 'Soil Mechanics' when applied to soils and soft rocks. The geotechnical site testing is aimed at assessing the mechanical properties of subsoil towards planning the foundations of structures. However, they are all point-based.

Sampling at discrete points, drilling of holes in the ground and in-situ or laboratory testing refer only to a very small proportion of the volume of soil and rock that will affect construction, can be sampled and tested. Geophysical techniques offer the chance to overcome some of the problems inherent in some conventional ground investigation techniques. Ground between boreholes can be checked to see whether ground conditions at the boreholes are representative of them elsewhere. They can help locate cavities, backfilled mine shafts and dissolution features in carbonate rocks. Geophysicists have very little idea of the constructional constraints with which civil and construction engineers must work.

Major civil engineering structures require a good quality geotechnical soil testing to assess the bearing capacity for planning foundation structures. However, many existing geotechnical site investigations provide point information only. The current practice is geared towards developing 1-D layered earth based geotechnical model(s) based on these point-wise geotechnical data. However, real near surface earth is far from such a simplistic situation. So, to meet this need, civil engineers include a very high factor of safety in their 1-D model parameters.

1.2 ROLE OF GEOPHYSICAL METHODS

Geophysical methods are increasingly being used for civil engineering related site investigation studies. They are non-invasive, cost-effective with proven spatial resolutions of different scales. While geotechnical tests provide geo-mechanical information on a very refined depth scales but their advantage is offset by their inherent point-wise information attended by drilling, which is costly; Further, in a complex geological settings, the problems get compounded due to excessive drilling budget to fulfill the geotechnical site investigation needs.

Generally, geophysical techniques, which are used to estimate seismic velocities in the subsurface focus on the low strain levels that are not large enough to induce significant nonlinear, nonelastic stress-strain behaviour (Luna and Jadi, 2000), which is normally evaluated when addressing liquefaction potential of soils in the shallow subsurface. Soil parameters relevant to seismic ground response (Rechtien, 1996) are density, relative density and void ratio, permeability, shear modulus, water saturation, soil fabric and stress history. Detailed characterization of elastic properties near a major construction site (say a bridge) is useful for a near field dynamic analysis of soil-structure interaction (SSI) effects. The coupled effect of the bridge foundation (piles, piers or abutments) and the soil immediately surrounding these substructure elements is essential for dynamic SSI analysis of these critical bridge structures.

Multi-channel analysis of surface wave method (MASW) and its predecessor, Surface wave analysis method (SASW) have gained wide popularity in assisting a geotechnical site characterization studies as they assess in-situ elastic moduli of near surface soil. SASW and MASW methods are non-invasive and test a large zone of soil. They are particularly suited to soils containing stones and rock debris like glacial tills, residual soils, boulder clay and to fractured and jointed rock, where penetration testing and boreholes cannot be used. Presently, stiffness profiles in soft ground can successfully be obtained up to 10 m. In hard soils / soft rocks profiles to a depth of 50 m can be obtained. The method uses very small strains that are now known to be close to the operational stiffness near real civil engineering structures like foundations, retaining walls and tunnels.

These stiffness profiles correlate well qualitatively with CPT profiles and other borehole logs. However, no alternate cost-effective method from geophysics is available now.

The soil moisture affects both geotechnical parameters and geoelectric parameters (resistivity and chargeability / polarizability). Further, a lot of advances have taken place in geoelectric imaging (Electrical Resistivity Imaging (ERT) and Induced Polarization imaging (IPI)), thanks to Loke and Barker's (1995) algorithm. The current geophysical literature is replete with immense applications of this powerful, non-invasive and cost-effective method (geoelectric imaging).

While geophysical imaging is quite effective in subsurface exploration, yet their results can not be directly translated to geotechnical knowledge due to absence of suitable transforms. So, a leveraged approach is needed to yield better quality subsurface information at a much lesser cost. The key problem, which still remains to be addressed concerns with the prediction of different formation and geotechnical parameter images of subsurface on the basis of few geotechnical investigations and ample number of geoelectric image measurements.

1.3 NOVELTY OF THE WORK

Here, 2-D resistivity and IP image profile data along with projected geotechnical data (Standard Penetration Test, SPT / Dynamic Cone Penetration Test, DCPT / Static Cone Penetration Test, SCPT) from nearby boreholes have been used for predicting different 2-D formation and geotechnical parameter sections along the same profile. This prediction method is based on site-specific regression equations describing actual correlations of geo-electrical and geotechnical data and site-independent well established empirical relations of SPT 'N' with different formation and geotechnical parameters.

1.4 PRACTICAL UTILITY

The designed methodology and results achieved in four case studies demonstrate that the inferred 2-D formation, geotechnical test results and parameter sections along a chosen geo-electric profile describe near surface soil structure in a vivid manner.

These may prove to be quite useful to a geotechnical engineer for site investigation studies. Even though the reported results are SPT based, the outlined methodology is quite general enough to deal with any other relevant geotechnical data sets for a comprehensive geotechnical assessment of a site.

1.5 THESIS LAYOUT

The thesis consists of 10 chapters. Chapter 1 is devoted to introduction, wherein the actuality of the problem is highlighted. Chapter 2 is devoted to literature review pertinent to the thesis topic. Chapter 3 deals with geo-electrical (Resistivity and Induced Polarization) imaging. Chapter 4 is devoted to basic geotechnical site testing, soil mechanics laboratory studies of soil samples and estimation of various geotechnical parameters. In Chapter 5, the methodology has been outlined which is based on both geo-electrical image and site geotechnical test and laboratory data. In Chapters 6-9, application of designed methodology has been illustrated in three case studies pertaining to Indo-Gangetic Alluvial Plains and one belonging to Delhi Super Group of rocks. Results and ensuing discussion are included in those chapters. Chapter 10 is devoted to summary, conclusions and further perspectives.

LITERATURE REVIEW

2.1 GENERAL

Engineering geophysical methods, including geoelectrical methods, were tried by several workers (Sastry and Viladkar, 2004; Giao et al., 2003; Giao et al., 2002; Giao, 2001; Drahor, 2006; Pujari and Nanoti, 2006; Gautam et al., 2007; Mondal et al., 2007; Mondal et al., 2008; Pujari et al., 2007a). Geotechnical characterization and liquefaction potential of sites using surface waves have been undertaken by several workers (Sitharam, 2008; Vipin et al., 2008; Foti, 2000; Hadidi and Gucunski, 2003; Xu and Butt, 2006; Oh et al., 2003; Matthews et al., 2000; Matthews et al., 1996; Jianghai et al., 2002; Jianghai et al., 2000; Joh, 1996). A very good coverage of SASW & MASW methods (Park et al., 2005; Seshunarayan, 2006; Seshunarayan and Sunderrajan, 2004) is available in literature and these methods are routinely used in site testing. However, similar progress has not been made in the application of geo-electrical imaging to geotechnical site characterization. As evident from literature, very meagre attention has been paid to this important aspect (Roth et al., 2002; Roth and Nyquist, 2003). Recent literature (Gautam et al., 2007; Sudha et al., 2009; Cosenza et al., 2006) shows that scientific efforts are limited to site-specific qualitative correlations between geo-electrical and geotechnical data. However, a preliminary attempt has been initiated by Gautam et al., (2007) to predict the SPT profile by using the correlations of geo-electric and geotechnical data (SPT). Even though qualitative correlations are available for shear wave / elastic moduli and SPT (Morgan et al., 2005; Ulugergerli and Uyanik, 2007; Iyisan, 1996), no worthwhile predictive effort has been made to complement the geotechnical tests at a site.

2.2 REVIEW OF LITERATURE

In recent years, several geophysical methods have been proposed, viz., Resistivity cone penetration resistance (RCPT), Seismic Cone penetration resistance, ERT, GPR, MASW and SASW. The basic motive is to complement the traditional geotechnical field

tests and obtain a broad image of subsurface geology, which can strengthen the geotechnical knowledge of the subsurface in a cost-effective and non-invasive manner.

2.2.1 Geophysical Efforts

The soil mechanics pioneers like Terzaghi (1943) and Hvorslev (1949) were interested in the 1940s in using geophysics in the study of machine foundations that are subject to vibrations. According to Durkee et al. (2006), geophysical measurements applied over a broad area can complement the geotechnical sampling methods applied at discrete locations. The geophysical investigations have led to a detailed subsurface geological characterization which led to optimize the tunnelling depth, perform engineering analysis for support of excavation and underpinning and evaluate the stand-up time and tunnelling methods. SASW & MASW methods (Park et al., 2005) are routinely used in site testing for assessment of soil stiffness. Akintorinwa and Adesoji (2009) have utilized VES and CPT for examining the subsoil and electrical properties at a site in Nigeria for installation of electrical switch station facility. Steeples (2005) has summarized the progress of the near surface geophysics. Relation between P-waves / shear waves and elastic parameters has been studied by several workers (Ghosh et al., 2003; Ghose and Drijkoningen, 2000; Cha and Cho, 2007; Inazaki, 2006, 1998).

Cone Resistivity Penetrometer (CRP) has been used by Yoon et al. (2009) for assessing the local behaviour in soft offshore soil and found that it detects effectively the soil layers with enhanced sensitivity. Pidlisecky et al. (2006) have developed 3-D distribution of electrical conductivity by the cone based electrical resistivity tomography, which integrates resistivity tomography with cone-penetration testing. Anderson et al. (2007) have ranked cross hole (CH), Multi-channel analysis of surface waves method (MASW), Refraction micro-tremor (ReMi) and SCPT methods in terms of accuracy, functionality, cost and overall utility. According to these authors, MASW is a better method. Schnaid and Yu (2007) have presented a simple theoretical approach to the interpretation of the seismic cone test in granular soils. Cardarelli et al. (2007) have assessed foundation stability of a damaged five-floor residential building through integrated geophysical methods (ERT, seismic refraction, MASW, cross-hole seismic

surveys). Sastry and Viladkar (2004) have assessed the stability of a multi-storeyed building on a hill slope through integrated geophysical approach. Dahlin et al. (2004) have indicated that RCPT (CPT with resistivity) is to be deployed at selected points for a refined interpretation of resistivity imaging and it can serve as a key for possible correlation between the resistivity and mechanical or chemical properties of the ground.

Marschall et al. (2007) have carried out seismic, DC resistivity and GPR techniques along with CPT to describe the subsurface structures of construction sites for traffic and transportation systems and they found out that such a combination of methods is cost-effective and reliable. The combination of geophysical data (2-D / 3-D ERT) and geotechnical measurements (Soupios et al., 2007a; Soupios et al., 2008) may greatly improve the quality of bridge under construction in civil engineering. Kim et al. (2006) have introduced SPT-Uphole tomography method for the evaluation of near subsurface shear wave velocity distribution map. Dahlin et al. (2004) recommend that ERT should preferably be carried out in the early stage of geotechnical pre-investigation and if the detailed investigations include Resistivity Cone Penetration Test, RCPT at selected points is to be used as the reference data for a refined interpretation of ERT data. Kemna et al. (2002) have assessed the usefulness of electrical resistivity tomography (ERT) in imaging and characterizing the subsurface solute transport in heterogeneous unconfined aquifers. Tomographic site characterization using CPT, ERT and GPR is attempted by Morey (1999). Endres and Clement (1998) have observed that the ratio of permittivity to the logarithm of resistivity is a good geophysical discriminator of the engineering soil classification. Dahlin and Bernstone (1997) have reported a roll-along technique for 3-D data acquisition by ERT. Griffiths and Barker (1993) described a system of automatic measurement of electrical resistivity pseudo-sections. Soils are polarizable when they contain clay minerals, which are the main causes of swelling and shrinkage. These two effects are a major concern for foundation engineering because they cause extensive damage to structures. IP response was dependent on the amount of water and cation exchange capacity (CEC), which is directly related to clay minerals (Kiberu, 2000) and IP method can be used to characterize clay and shaly sands in the subsurface. Geo-electromagnetic (GEM-AMT, TEM and DC resistivity methods) and seismic field

data (Mackie et al., 1997; Zelt and Barton, 1998) can be appropriately scaled to handle near-surface imaging problems.

2.2.2 Correlation of Geophysical and Geotechnical Test Data

The correlations amongst geotechnical test data, like SPT and CPT exist in literature (Akca, 2003; Danzinger et al., 1998; Edet et al., 1994; Robertson et al., 1983). According to Gay et al. (2006b), a linear relationship exists between seismic velocity and SPT 'N' blow counts and in turn SPT 'N' is better correlated with dynamic elastic modulus than with seismic velocity and further the seismically derived dynamic elastic modulus can accurately predict soil strength. Cosenza et al. (2006) have tried to establish qualitative and quantitative correlation between electrical and geotechnical data. No clear relationship between cone resistance and inverted resistivity extracted from ERT section has been observed by them. Braga et al. (1999) have correlated resistivity and IP data with SPT 'N' data. Anbazhagan and Sitharam (2008) and Lontzetidis et al. (1997) have attempted correlation of SPT 'N' with shear wave velocity. Anbazhagan et al. (2006) have attempted geophysical and geotechnical tests in understanding the site specific soil properties. Sudha et al. (2009) have observed a linear correlation between transverse resistances of soil with SPT 'N' and remarked that these linear relationships are site-specific and coefficients of linear relation are sensitive to lithology of subsurface formation. While attempting safety assessment of a central-core type earth-fill dam, Oh and Sun (2008) caution that one should correlate electrical resistivity and SPT 'N' carefully.

Hacikoylu et al. (2006) have revisited Faust's equation and used the available rock physics transforms between the velocity, porosity and mineralogy together with existing empirical and theoretical resistivity-porosity models to determine the range of its applicability in terms of rock type and lithology. Gallardo and Meju (2003) have developed a robust 2-D joint inversion scheme of electrical resistivity and seismic velocity for resistivity-velocity relationship in a complex near-surface environment. Weiher and Davis (2004) compared the theoretical soil modulus with measured penetration resistance.

Meju et al. (2003) present the results of coincident GEM and seismic experiment to the investigate near-surface resistivity-velocity relations at a selected area in Quorn in England. Their studies lend support to the hypothesis that porosity or fracture permeability may be the key function in understanding the electrical-seismic relations in both consolidated and unconsolidated crustal materials. Joint 2-D imaging of GEM and seismic profiling data may be a useful strategy for improved resistivity-velocity correlations in the near-surface studies.

Weiher and Davis (2004) have investigated some existing correlations between soil moduli and penetration resistance and have made the use of settlement data from case histories for both shallow and deep foundations over sandy soils. Knowledge of foundation dimensions, loads and measured settlements permitted the use of elasticity theory to calculate theoretical soil modulus. The computed modulus was then compared with measured penetration resistance. The resulting data set was used to assess the efficacy of two well-known correlations between soil moduli and penetration resistance. Hasancebi and Ulusay (2007) have analyzed the existing correlations between shear wave velocity and penetration resistance and developed regression equations for the same. Prediction of the ground shaking response at various soil sites requires knowledge of the soil expressed in terms of shear wave velocity. The regression equations developed in this study compare well (Hansancebi and Ulusay, 2007) with most of the previous equations and exhibit good prediction performance. It is noted that better correlations are observed when uncorrected blow counts (SPT) are used.

Tillmann et al. (2008) have estimated grain size distribution from CPT data, which were used in determining the hydraulic conductivity at a test site in Germany. The estimated hydraulic conductivity values were validated and the authors claim that CPT is a fast and inexpensive tool for the estimation of three-dimensional hydraulic conductivity fields with sufficient accuracy.

Ulugergerli and Uyanik (2006) opine that if a geotechnical parameter is required for the assessment of the soil condition, direct gathering from the field or core sample must be employed for a realistic evaluation. According to Anderson et al. (2008), geotechnical

geophysics is not a substitute for boring or testing, but is often a very cost-effective and reliable means of imaging the subsurface between and below boreholes and for determining the in-situ bulk properties of soil and rock.

2.3 GAPS IN STATE OF ART

The critical review of literature reveals the following:

- a) Only simple qualitative correlation studies were conducted between resistivity / seismic velocity with SPT / CPT with no clear conclusions.
- b) The available correlations (linear and non-linear) do not allow any quantitative geotechnical assessments even on prediction basis.
- c) For a civil engineering construction, a geotechnical engineer has to rely on point mode geotechnical tests leading to 1-D geotechnical models for site evaluations. At present, complex geological setting requires a lot of costly drilling followed by time-consuming geotechnical site tests.
- d) Even though exploration geophysics offers a wide variety of geophysical imaging methods, only shear wave images provided by MASW / SASW have received considerable attention.
- e) A geotechnical engineer needs comprehensive subsurface images of different formation parameters (porosity, water saturation, lithology etc.) and geotechnical parameters (unit weights of soils, angle of internal friction, compressive strength, and different types of bearing capacities). However, limited available studies at present do not meet these challenges at expected confidence levels.

2.4 OBJECTIVES OF THESIS

- i) To examine the feasibility of deriving site-specific correlations of true resistivity / chargeability / fictitious resistivity (product of resistivity and IP chargeability) with different geotechnical test data (SPT / DCPT / SCPT) and use them in inferring geotechnical test data at other locations where they are absent on the same geo-electrical profile.
- ii) To derive regression equations for formation and geotechnical parameters based on existing well established empirical relations / tables / curves in geotechnical literature.
- iii) To use the regression equations arrived in earlier phases for inferring 2-D lithology, formation and geotechnical parameter sections.
- iv) To suggest a better site investigation strategy involving both geo-electrical and geotechnical test studies in an optimal and cost-effective manner.

GEOELECTRICAL IMAGING

3.1 INTRODUCTION

Recently, geophysical techniques have been used to image or characterize the shallow subsurface of the Earth. These techniques are offered to improve the geotechnical models obtained by the geotechnical engineer, based on the geotechnical field measurements as well as laboratory tests.

There has been a revolutionary modification in the geoelectrical surveying method in the last decade. Until the early 1990's, the resistivity measurements were made using four electrodes which were enough to perform either the sounding or the profiling. Thus, the quantitative interpretation was confined to model the vertical and horizontal variation of resistivity distributions respectively (1-D). Modeling of both the variations together was not possible. However, due to recent developments of multi-electrode imaging equipments, two-dimensional (2-D) and even three-dimensional (3-D) geoelectrical surveys are now feasible for undertaking the environmental and engineering geophysical studies. Accordingly, there has been an explosive growth in the number of commercial multi-electrode resistivity and IP systems for the geoelectrical imaging surveys.

The second development that has made 2-D and 3-D electrical imaging surveys the practical tools is a fast inversion (RES2DINV and RES3DINV) and modeling (RES2DMOD & RES3DMOD) software (Loke and Barker, 1996).

RES2DINV, a 2-D resistivity and IP inversion software, also supports underwater and cross-borehole surveys. In addition to the standard Wenner (alpha, beta, gamma), Wenner-Schlumberger, pole-pole, pole-dipole, inline dipole-dipole, equatorial dipole-dipole arrays (Table 3.1), the program supports survey lines with up to 16000 electrodes and 27000 data points.

In the present study, geoelectrical method (2-D electrical resistivity imaging tomography (ERT) and 2-D induced polarization imaging (IPI)) have been used.

The relevant data acquisition details are provided in Chapters 6-9. Here, an outline of resistivity and IP imaging are included.

Table 3.1 Different Geoelectrical Arrays with Corresponding Geometrical Factors (Loke, 1999)

S. No.	Electrode Array	Geometrical Factor (K)
1	Pole-Dipole	$2\pi n(n+1)a$
2	Dipole-Dipole	$\pi n(n+1)(n+2)a$
3	Pole-Pole	$2\pi a$
4	Wenner -Alpha	$2\pi a$
5	Wenner -Beta	$6\pi a$
6	Wenner -Gamma	$3\pi a$
7	Schlumberger	$\frac{\pi \left(S^2 - \frac{a^2}{4} \right)}{a}$
8	Wenner-Schlumberger	$\pi n(n+1)a$

In Table 3.1, different geometric factors corresponding to several electrode configurations are included.

3.2 2-D - ELECTRICAL RESISTIVITY TOMOGRAPHY (ERT)

The ground resistivity is related to various geological parameters such as porosity, water content and degree of saturation etc in the rock. Initially, the resistivity imaging was developed for geo-hydrological and mining investigations but later on it has become an indispensable tool for various engineering and environmental applications. It is cost-effective and fast in the field survey for obtaining 2-D or 3-D subsurface data (Mondal, 2009; Overmeeren and Ritsema, 1988; Griffiths et al., 1990; Dahlin, 1996). In many geological settings, 2-D electrical imaging can give useful results that play a vital role in geotechnical engineering (Loke, 2002).

3.2.1 Basics of DC Resistivity Method

The governing DC conduction equation is given by

$$\nabla \cdot (\sigma \nabla U) = Q \quad (3.1)$$

where σ is the conductivity (mho/m), U is the electric potential (volts) and Q is the point current source (ampere). This is a basic equation controlling the direct current (dc) resistivity method.

Using Dirac delta function notation, source Q can be expressed as

$$Q = -I\delta(x - x_s)\delta(y - y_s)\delta(z - z_s) \quad (3.2)$$

where 3-D point current source is kept at (x_s, y_s, z_s) . For a real medium, conductivity, σ is a second order symmetric tensor. Hence, equation (3.2) can be represented as

$$\frac{\partial}{\partial x} \left(\sigma_{xx} \frac{\partial U}{\partial x} \right) + \frac{\partial}{\partial y} \left(\sigma_{yy} \frac{\partial U}{\partial y} \right) + \frac{\partial}{\partial z} \left(\sigma_{zz} \frac{\partial U}{\partial z} \right) = -I\delta(x - x_s)\delta(y - y_s)\delta(z - z_s) \quad (3.3)$$

where σ_{xx} , σ_{yy} and σ_{zz} are conductivity values along the three major axes.

If the medium is isotropic, then equation (3.3) reduces to

$$\sigma \left(\frac{\partial^2 U}{\partial x^2} + \frac{\partial^2 U}{\partial y^2} + \frac{\partial^2 U}{\partial z^2} \right) + \left(\frac{\partial \sigma}{\partial x} \frac{\partial U}{\partial x} + \frac{\partial \sigma}{\partial y} \frac{\partial U}{\partial y} + \frac{\partial \sigma}{\partial z} \frac{\partial U}{\partial z} \right) = -I\delta(x - x_s)\delta(y - y_s)\delta(z - z_s) \quad (3.4)$$

For obtaining numerical solution of equation (3.4), the boundary conditions imposed are the Neumann and Dirichlet boundary conditions, which are respectively,

$$\left(\frac{\partial U}{\partial z} \right) = 0 \quad (3.5)$$

at the air-earth interface, and

$$U(x, y, z) = 0 \quad (3.6)$$

at the outer boundaries. It may be mentioned that for 2-D case, right hand terms of equations (3.3 and 3.4) need to be suitably altered.

In the following, potential and potential difference expressions for both homogeneous and inhomogeneous cases are outlined.

Case I : Homogeneous and isotropic medium

The potential U , due to a point source of dc current, I over a semi-infinite homogeneous and isotropic medium is given by

$$U = \frac{\rho I}{2\pi r} \tag{3.7}$$

where r is the distance of the current electrode in the medium to potential electrode on air-earth interface and ρ is the resistivity of the medium.

In practice, four electrodes-arrangement is used in the resistivity surveys. For this case, the potential difference is given by

$$\Delta U = \frac{\rho I}{2\pi} \left(\frac{1}{r_{c1}p_1} - \frac{1}{r_{c2}p_1} - \frac{1}{r_{c1}p_2} + \frac{1}{r_{c2}p_2} \right) \tag{3.8}$$

where $r_{c1} p_1$, $r_{c1} p_2$, $r_{c2} p_1$ and $r_{c2} p_2$ are the distances of current electrodes from potential electrodes, p_1 and p_2 respectively.

Case II : Inhomogeneous medium

Usually, the field surveys are invariably conducted over an inhomogeneous medium, where the subsurface resistivity has a 3-D distribution. The resistivity measurements are still made by injecting the current into the ground through two current electrodes and measuring the resulting voltage difference at two potential electrodes (Fig. 3.1). Then from the current (I) and potential difference (ΔU), the apparent resistivity calculated as

$$\rho_a = K \frac{\Delta U}{I} \tag{3.9}$$

where geometrical factor $K = \frac{2\pi}{\left(\frac{1}{r_{c1}p_1} - \frac{1}{r_{c2}p_1} - \frac{1}{r_{c1}p_2} + \frac{1}{r_{c2}p_2} \right)}$

The calculated resistivity value is not the true resistivity of the subsurface but an apparent resistivity, which is the true resistivity of equivalent fictitious homogeneous medium.

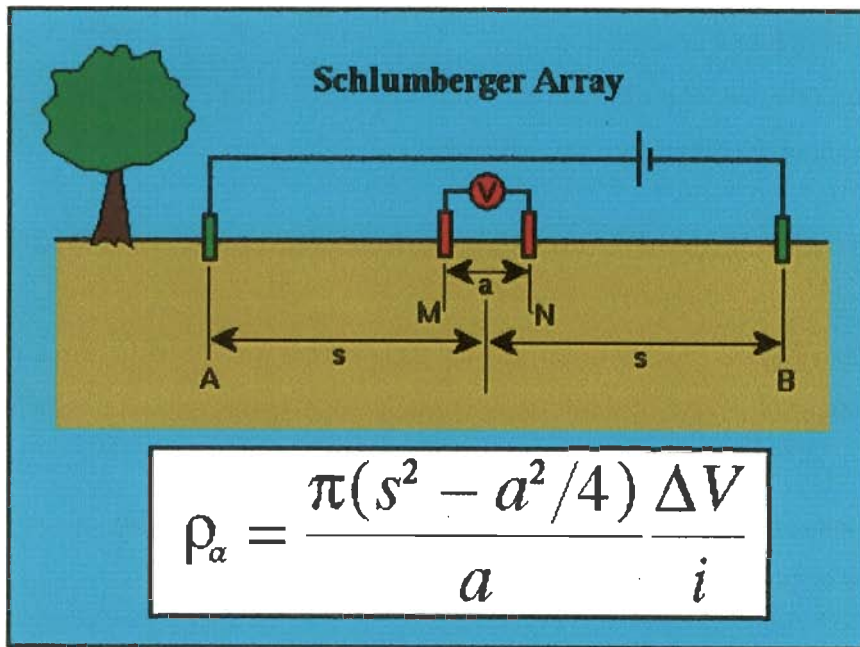


Fig. 3.1 Schlumberger Electrode Arrangements

3.3 INDUCED POLARIZATION METHOD

It has long been used in groundwater and environmental applications (Vacquier et al., 1957; Weller et al., 1996; Slater and Lesmes, 2002). Induced Polarization sounding (IPS) method can distinguish high salinity formations from clay horizons, where resistivity study fails (Dahlin et al., 2002).

3.3.1 IP Sources

Induced polarization (IP) method is based on polarizability property of earth materials. It is a geophysical phenomenon, where a slow decay of voltage (Fig. 3.2) in the subsurface after cessation of an excitation current pulse (time domain) is observed (Sumner, 1976). The rate of decay of induced polarization depends on the lithology of the rock, its pore geometry, degree of water saturation, cation exchange capacity (CEC), grain size and water content. Schlumberger (1920) observed that induced polarization was taking place in the bulk volume of rock and not on the field electrodes used to measure it.

The phenomenon of induced polarization and its electrochemical mechanism are extremely complex. The exact causes of induced polarization are still unclear but most probably induced polarization results from the combined effects of several physical and chemical processes. There are two primary mechanisms that are responsible for the occurrence of induced polarization.

- a) Grain (electrode) polarization
- b) Membrane (Electrolyte) polarization

The electrode polarization occurs when pore space is blocked by metallic particles and again charges accumulate when an electric field is applied. The result is two electrical double layers which add to the voltage measured at the surface of the particles. Membrane polarization occurs when pore space narrows to within several boundary layer thicknesses. Membrane polarization is most probably due to ionic exchanges and setting up of diffusion potentials and presence of clay is also responsible for this type of polarization.

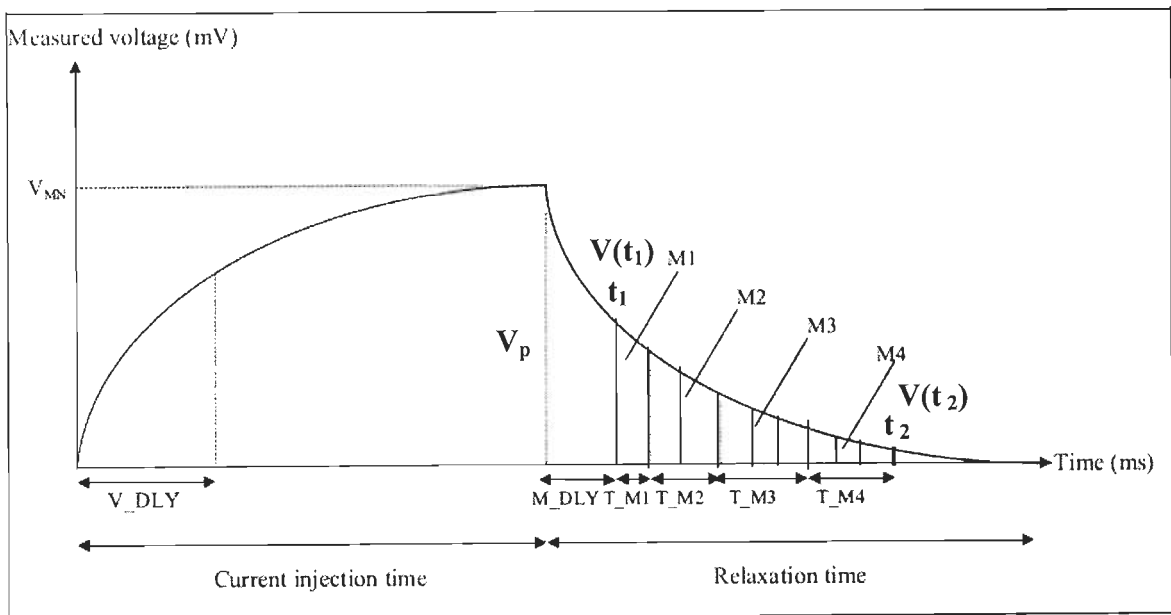


Fig. 3.2 Induced Polarization Decay Curve

3.3.2 Methods of Measurement of IP Effect

Induced polarization is a dimensionless quantity and it is measured as a change in voltage with time or frequency. Relevant details of time domain IP are discussed below:

3.3.2.1 Time domain

The direct current is injected into the subsurface through the current electrode and the decay of the voltage between the potential electrodes after the cut off current is recorded. The measured IP effect is the chargeability (mSec) (Siegel, 1959) and can be expressed as

$$M = \frac{V_s}{V_p} \text{ in } \frac{mv}{v} \quad (3.10)$$

where V_p and V_s are the on-time and off-time measured voltages respectively

The measured parameter in the time domain is the area under the decay curve of Voltage $V(t)$ corresponding to the time interval (t_1, t_2) . The integration of these values with respect to time gives the area under the curve (Fig. 3.2). The chargeability can be expressed as

$$m = \int_{t_1}^{t_2} V_{s(t)} dt = \frac{A}{V_p} \quad (3.11)$$

where V_s are the off-time measured voltage at time t and V_p the observed voltage with an applied current.

The conductivity, σ'_i in a polarizable medium (Siegel, 1959) is related to its counterpart, σ_i in the non-polarizable medium by the following relation:

$$\sigma'_i = \sigma_i(1 - m_i) \quad (3.12)$$

where σ'_i is the conductivity of the polarizable medium, σ_i is the conductivity of the non-polarizable medium and m_i is the chargeability of the polarizable medium. Hence, for a polarizable medium, the conductivity distribution in the subsurface can be attempted through equation 3.12. The time-domain IP has been used in this thesis, the frequency domain IP details are not included here.

3.4 2-D - MULTI-ELECTRODE GEOELECTRICAL SURVEYS

3.4.1 Instrument and Measurement Procedure

At present, equipment and field techniques to carry out geoelectrical measurement are well developed and commercially available. Figure 3.3 shows a typical setup for a 2-D survey with number of equi-spaced collinear electrodes attached to a multi-core cable. The micro-processor on the main panel automates the entire data acquisition as per the user's choice. The depth of investigation depends on the geometry of the electrodes.

A SYSCAL Jr *Switch-72* DC electrical resistivity imaging system of IRIS (Plate 3.1) make was used for geoelectrical imaging (ERT and IPI) surveys. It is a multi-node resistivity imaging system (www.iris-instruments.com) with an internal switching board for 72 electrodes and an internal 100 W power source. The output current is automatically adjusted (automatic ranging) to optimize the input voltage values and ensure the best measurement quality. The system is designed to automatically perform pre-defined sets of resistivity and IP measurements with roll-along capability. Six strings of heavy-duty seismic cable with 10 m electrode spacing and with 12 electrodes take-out are connected together on the backside of the resistivity meter. The system compensates SP (Self-potential) values through automatic linear drift correction (Mondal, 2009).



Plate 3.1 Electrical Resistivity Imaging System (IRIS)

The resistivity system (www.iris-instruments.com) used offers good opportunity to obtain resistivity as well as Induced Polarization images up to a reasonable depth of around 100 m.

The 2-D resistivity (ERT) and IP data were collected using a Wenner-Schlumberger array, as it will provide good vertical as well as lateral resolution. For each resistivity / IP profile, measurements were acquired at 529 to 1216 points using different inter-electrode spacing. Topographic correction and 2D inversion were performed on acquired ERT and IPI data using *Res2DInv* software of GEOTOMO.

3.4.2 Selection of Array

The choice of the “best” array for a field survey depends on the type of structure to be mapped, the sensitivity of the resistivity meter and the background noise level. In practice, the arrays that are most commonly used are given in Table 3.1. The following characteristics consider in the selection of the array:

- i) Depth of investigation (Barker, 1989)
- ii) The sensitivity of the array to vertical and horizontal changes in the subsurface resistivity,
- iii) Horizontal and vertical data coverage
- iv) The signal strength

Wenner-Schlumberger array has been used in the present work.

3.4.3 Wenner-Schlumberger Array

This is a combination of Wenner and Schlumberger arrays (Pazdirek and Blaha, 1996) used in electrical imaging surveys. The classical Schlumberger configuration is one of the most commonly used arrays for resistivity sounding surveys, while Wenner array is preferred for the resistivity profiling. The combination, Wenner-Schlumberger array provides 2-D variation of the resistivity, thereby providing the 2-D picture of the subsurface. A digitized form of this array is shown in Fig. 3.3. So that it can be used on a system with the electrodes arranged with a constant spacing. The “n” factor for this array is the ratio of the distance between the current and potential (C_1 - P_1 or P_2 - C_2) electrodes to the spacing between the P_1 - P_2 potential pair (Loke, 2002).

The Wenner-Schlumberger array is a reasonable all-round alternative if both good and vertical resolutions are needed, particularly if good signal strength is also required.

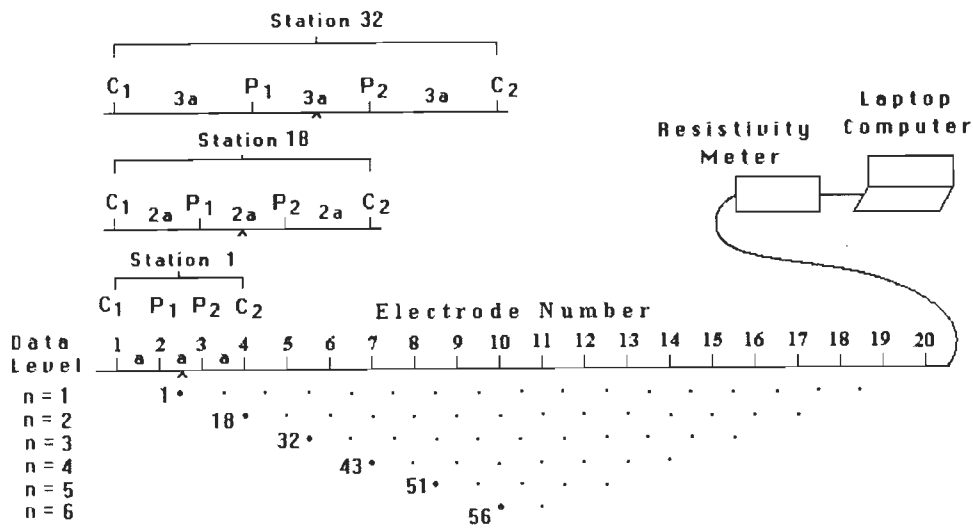


Fig. 3.3 Arrangement of Electrodes for 2-D Geoelectrical Survey and Sequence of Measurements Used to Build up a Pseudo-section (Loke and Barker, 1995)

3.4.4 Display of Pseudo-section Plots

To plot 2-D geoelectrical imaging data, the pseudo-section contouring method is commonly used. In this case, the horizontal location of the point is placed at the mid-point of the set of electrodes that are used to make that measurement. The vertical location of the plotting point is placed at a distance that is proportional to the separation between the electrodes.

Another method is to place the vertical position of the plotting point at the median depth of investigation (Edwards, 1977), or pseudo-depth, of the electrode array used. This pseudo-depth value is based on the sensitivity values or Frechet derivative for a homogeneous half space. This method is the mathematical basis for plotting the pseudo-sections. The pseudo-section plot obtained by contouring the collected data (apparent resistivity and chargeability) is a convenient means to display the data. The comparison of electrode arrangement as well as pseudo-section for Wenner and Schlumberger configuration has been show in Fig. 3.4.

The pseudo-section gives a very approximate picture of the true subsurface resistivity distribution and it is very helpful in the quantitative interpretation of the measured apparent resistivity values (Apparao and Sarma, 1983; Apparao et al., 1992; Roy and Apparao, 1971). One useful practical application of the pseudo-section is in picking out bad apparent resistivity measurements. Such bad measurements usually stand out as points with unusually high or low values (Loke, 2002).

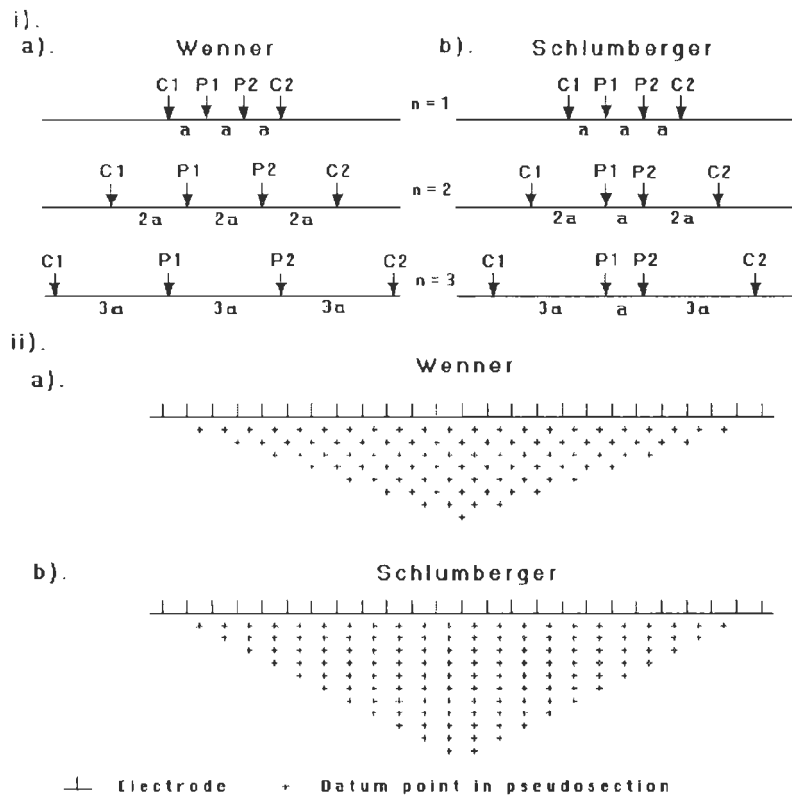


Fig. 3.4 Comparison of (i) Electrode Arrangement and (ii) Pseudo-section data Pattern for the Wenner and Wenner-Schlumberger Configurations

3.5 THEORITICAL ASPECTS OF RESISTIVITY AND IP IMAGING

Loke and Barker (1995) have attempted 2-D inversion of resistivity data by assuming a homogeneous conductive half-space as starting model for which the apparent resistivity and sensitivity matrix can be calculated analytically. The updates of resistivity within different 2-D rectangular blocks, which are arranged depth-wise as per the depth of investigation norms, produce a pseudo-section. The depths to the centre of block are usually set at median depth of investigation of the electrode array (0.5 times the electrode spacing for the Wenner array). Tests with a variety of models and data

from surveys show that this technique is insensitive to random noise, provided a large damping factor is used. Subsequently, Loke and Barker (1996a) considered quasi-Newton method due to Broyden (1972), which avoids the direct calculation of Jacobian by using an updating method. Dahlin (2001) has summarized the developments of DC resistivity imaging techniques. Dahlin et al. (2002) have elaborated measuring techniques in IP imaging. For inversion of IP data, earlier outlined resistivity inversion is valid, except for the fact that one has to use polarizable conductive earth model as per equation 3.12.

The details of resistivity inversion (Loke and Barker, 1995) are as per the following sub-sections:

3.5.1 Frechet Derivative for a Homogeneous Half-Space

The first two characteristics can be determined from the sensitivity function of the array for a homogeneous earth model. The higher the value of the sensitivity function, the greater is the influence of the subsurface region on the measurement. Mathematically, the sensitivity function is given by the Frechet derivative (McGillivray and Oldenburg 1990). Consider the simplest possible array configuration shown in Fig. 3.5 with just one current source located at the origin (0,0,0) and one potential electrode located at (a,0,0) with “a” meter spacing on the ground surface. Inject I_s ampere current into the ground through the C_1 current electrode that resultant potential, ϕ observed at the potential P_1 electrode. Suppose the resistivity within a small volume of the ground located at (x,y,z) by a small amount $\delta\rho$ were to be changed, the corresponding change in potential, $\delta\phi$ measured at P_1 can be shown (Park and Van, 1991) as

$$\delta\phi = \frac{\delta\rho}{\rho^2} \int \nabla\phi \cdot \nabla\phi' d\tau \quad (3.13)$$

where, the change in resistivity has a constant value in a volume element, $d\tau$ and zero elsewhere. For the a homogeneous half-space, the potential, ϕ at a point in the half-space due to a unit current source on the surface is:

$$\phi = \frac{\rho I_s}{2\pi(x^2 + y^2 + z^2)^{0.5}} \quad (3.14)$$

The parameter ϕ' is the potential resulting from a fictitious unit current source at the location of potential electrode. It can be expressed as

$$\phi' = \frac{\rho}{2\pi[(x-a)^2 + y^2 + z^2]^{0.5}} \quad (3.15)$$

Differentiating the equation (3.15) to obtain the divergence and substituting into equation (3.13), one gets

$$\frac{\delta\phi}{\delta\rho} = \int \frac{I_s}{4\pi^2} \cdot \frac{x(x-a) + y^2 + z^2}{[x^2 + y^2 + z^2]^{1.5} [(x-a)^2 + y^2 + z^2]^{1.5}} dx dy dz \quad (3.16)$$

The 3-D Frechet derivative is given in terms of integral as

$$F_{3D}(x, y, z) = \frac{I_s}{4\pi^2} \cdot \frac{x(x-a) + y^2 + z^2}{[x^2 + y^2 + z^2]^{1.5} [(x-a)^2 + y^2 + z^2]^{1.5}} \quad (3.17)$$

This gives the Frechet derivative or sensitivity function for the pole-pole array consisting of just one current and one potential electrode. To obtain the Frechet derivative for a general four electrodes array, one needs to just add up the contributions from the four current-potential pairs, as we have done earlier for the potential in Equation 3.14.

Loke and Barker (1999) have elaborately dealt with 2-D view of the sensitivity function. The 2-D partial derivative for a rectangular block of finite dimensions (Fig. 3.5) is given by

$$\frac{\partial\phi}{\partial\rho} = \frac{I_s}{4\pi^2} \int_{z_1}^{z_2} \int_{x_1}^{x_2} F_y dx dz \quad (3.18)$$

$$\frac{\partial\phi}{\partial\rho} = \frac{AI_s}{4\pi^2} \int_{-1}^{+2} \int_{-1}^{+1} F_y(u, v) dudv \quad (3.19)$$

$$\frac{\partial \phi}{\partial \rho} \approx \frac{AI_s}{4\pi^2} \sum_{l=1}^{n_z} \sum_{k=1}^{n_x} w_k w_l w F_y(u, v) \quad (3.20)$$

where

$$u = \frac{(2x - x_1 - x_2)}{(x_2 - x_1)}$$

$$v = \frac{(2z - z_1 - z_2)}{(z_2 - z_1)} \quad \text{and}$$

$$A = 0.25(x_2 - x_1)(z_2 - z_1)$$

The range of integration for the transformed abscissas, u and v is from -1 to +1. n_x and n_z are the number of function evolutions in the x and z directions respectively. These evolutions were adjusted depending upon the distance of the block from the electrodes (Loke and Barker, 1995).

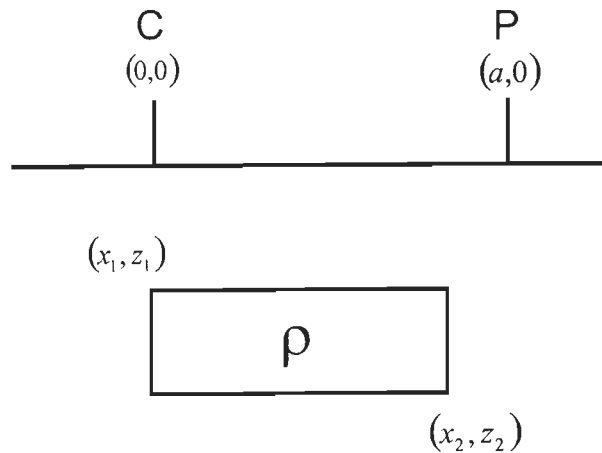


Fig. 3.5 Rectangular Block of Finite Dimension, C and P are the Current and Potential Electrode Respectively

Jacobian matrix computation in view of the reciprocity and certain symmetries in the problem is optimized stored them for the pole-pole array. Accordingly, for any four electrode configuration the partial derivative computation can easily be made.

The inversion is performed based on the following least-square equation:

$$(J^T J + \lambda C^T C)P = J^T g \quad (3.21)$$

where

J is the Jacobian matrix of partial derivatives,

λ is the damping factor,

g is the discrepancy vector containing the logarithmic differences between the measured and calculated apparent resistivity values, and

p is the correction vector to the model parameters.

2-D flatness filter, C is to constrain the smoothness of the model parameters (Sasaki, 1992). The logarithms of the model resistivity values are used in the calculation of the model correction vector, p .

3.5.2 Inversion Algorithm

Loke and Barker (1996a) used an inversion model where the arrangement of the model blocks directly follows the arrangement of the pseudo-section plotting points. This approach gives satisfactory results for the Wenner and Wenner-Schlumberger arrays where the pseudo-section point falls in an area with high sensitivity values. Their RES2DINV program uses a more sophisticated method to generate the inversion model where the arrangement of model blocks is not tightly bound to the pseudo-section.

The 2-D model used by this program divides the subsurface into a number of rectangular blocks (Fig. 3.6). The purpose of resistivity inversion is to determine the resistivity of the rectangular blocks that will produce an apparent resistivity pseudo-section which agrees with the actual measurements. For the Wenner and Schlumberger arrays, the thickness of the first layer of blocks is set at 0.5 times the electrode spacing. The optimization method basically tries to reduce the difference between the calculated and measured apparent resistivity values by adjusting the resistivity of the model blocks. A measure of this difference is given by the root-mean-square (RMS) error. However, the model with the lowest possible RMS error can sometimes show large and unrealistic variations in the model resistivity values and might not always be the "best" model from a geological perspective. In general, the most prudent approach is to choose the model at the iteration after which the RMS error does not change significantly. This usually occurs between the 3rd and 5th iterations.

The RES2DINV program (Loke and Barker, 1999) is designed to operate, as far as possible, in an automatic and robust manner with minimal input from the user.

Thus, the inversion method involves the following three basic types:

- a) To calculate the apparent resistivity values technique either finite-difference (Smith and Vozoff, 1984) or the finite element method (Sasaki, 1992).
- b) To calculate the Jacobian matrix of partial derivatives by equation (3.20).
- c) To solve the system of linear equations in the above equation (equation 3.21).

A number of numerical techniques, such as the modified Gram-Schmidt, Cholesky decomposition and singular-value decomposition methods (Golub and van Loan, 1989) can be used.

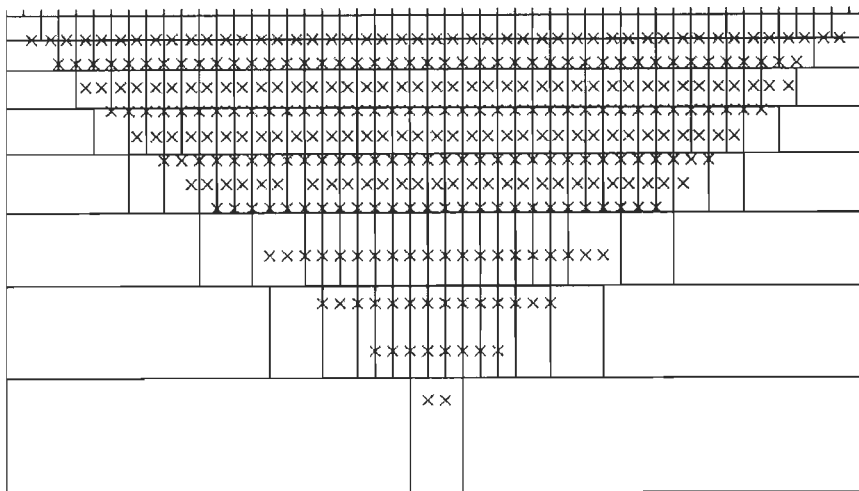


Fig. 3.6 Arrangement of the blocks used in a model together with data points in the pseudo-section.

3.6 SHALY SAND ANALYSIS USING IP

The presence of shale (clay minerals) within a formation can cause erroneous values for water saturation and porosity. Estimation of formation shaliness using SP and natural Gamma ray logs is well known in well logging literature. As polarizability of clay's and shale's is higher amongst the sedimentaries, IP method can also be used to assess shaliness of sub-surface. In the present work, an attempt has been made to evaluate relative shaliness of subsurface from true chargeability data using the following formula similar to the one proposed in well-logging literature (Mondal, 2009):

$$SHP = \frac{CHT - CHT_{Min}}{CHT_{Max} - CHT_{Min}} \% \quad (3.22)$$

where SHP is the Relative shaliness percentage, *CHT*, the True chargeability within the subsurface, CHT_{Min} , the Minimum true chargeability and CHT_{Max} is the Maximum true chargeability.

Table 3.2 is adopted for assigning the shaliness to concerned lithologies. The resulting shaliness plot can at best provide broad lithologies in terms of polarizability distribution only. It may not literally mean presence of clay / shale. These plots need to be analyzed by local geology of a site (Mondal, 2009).

Table 3.2 Percentage of Shaliness and Related Lithology (Mondal, 2009)

Shaliness %	Formation
0 – 20	Sand
20 – 50	Sandy Clay
50 – 70	Clayey Sand
70 – 100	Clay

3.7 PROCEDURE FOLLOWED IN THIS WORK

By considering all the theoretical aspects as described in earlier sections, in the present effort, Wenner-Schlumberger array has been adopted for gathering both resistivity and IP sections along different profiles in the study region. Effort was made to have these geoelectrical profiles in the vicinity of geotechnical field tests (SPT, DCPT and DCPT). By utilizing SYSCAL Jr *Switch-72* DC electrical resistivity imaging system of IRIS make having a provision of 72 electrodes, both resistivity and IP images of subsurface are gathered. For IP data acquisition, the default parameters have been used. The electrode spacing (2 m / 3 m / 5 m / 10 m) was usually selected to cover the target depth in SPT test. All relevant data acquisition details are included in respective case study chapters (Chapters 6 to 9).

GEOTECHNICAL PARAMETERS AND SITE TESTING

4.1 GENERAL

Soil mechanics and foundation engineering is a well established branch of civil engineering. The term soil mechanics is now accepted quite generally to designate that discipline of engineering science which deals with the properties and behavior of soil as a structural material (Murthy, 2008). The subject of foundation engineering deals with the design of various substructures under different soil and environmental conditions.

During the design, the designer has to make use of the properties of soils, the theories pertaining to the design and his own practical experience to adjust the design to suit to the field conditions. The foundation engineer must have the ability to interpret the principles of soil mechanics consistent with the field conditions. The success or failure of his design depends upon how much he is in tune with the real near surface earth (Murthy, 2008).

The present practice of soil investigations engineering provides point information depth-wise and involves digging and drilling, which are costly. It provides considerable detailed information needed for a foundation engineer and designer. However, as near surface soil conditions and earth materials are highly heterogeneous, simple point-wise soil investigations are not sufficient to meet the demands. e.g., collapsible soils, expansive soils and presence of organic clays etc. So, a detailed knowledge of 2-D / 3-D subsurface soil conditions is needed to enable a foundation engineer and designer to propose pragmatic solutions. The recent advances in geoelectrical imaging technology (Ward, 1990; Loke and Barker, 1995) if suitably transformed as per the tenets of soil mechanics and foundation engineering, can help meet the real demands of a civil engineer.

Here, pertinent to overall goal of this thesis, a brief summary of soil mechanics and foundation engineering is attempted. *This chapter ends with a table containing our derived transforms in the form of regression equations, which are used in later chapters.*

4.2 CLASIFICATION OF SOILS AND INDEX PROPERTIES OF SOILS

Classification of soils includes a number of geotechnical laboratory tests, which help to obtain the lithology variation with depth and this lithology variation is also known as the classification of the soils (Table 4.1). The samples collected from the borehole are subjected to various laboratory tests for soil classification. Soils usually may be classified as coarse or fine grained and cohesive or non-cohesive and on the basis of soil properties also may be divided into subgroups. Since soils include a wide range of engineering properties such as porosity, permeability, specific gravity, air content and degree of saturation etc., it is necessary to sub categorize the soil (Ranjan and Rao, 2005).

In the present study, the soil materials are classified on the basis of Indian Standard Soil Classification System outlined in Bureau of Indian Standard (BIS) codes (IS: 1498, 1970). The grain size distribution is carried out by the mechanical sieve analysis and the plasticity characteristics obtained via the Atterberg limits (for fine grained soil, Clay) method (Ranjan and Rao, 2005). A set of standard Sieves is used to perform mechanical sieve analysis (Plate 4.1). Accordingly, typical soil types are presented in Table 4.1.



Plate 4.1 Different Standard Sieves

Table 4.1 Nomenclature of Soils According to IS: 1498 (1970)

Group Letter Symbol	Typical Names
GW	Well graded gravels, gravel-sand mixtures little or no fines
GP	Poorly graded gravels or gravel-sand mixtures, little or no fines
GM	Silty gravels, poorly graded gravel sand-silt mixtures
GC	Clayey gravels, poorly graded gravel-sand-clay mixtures
SW	Well graded sands, gravelly sands, little or no fines
SP	Poorly graded sands or gravelly sands, little or no fines
SM	Silty sands, poorly graded sand-silt mixture
SC	Clays sands, poorly graded sands clay mixtures
ML	Inorganic silts and very fine sands, rock flour, silty or clayey fine sands or clayey silts with none to low plasticity
CL	Inorganic clays, gravelly clays, sandy clays, silty clays, lean clays of low plasticity
OL	Organic silts and organic silty clays of low plasticity
MI	Inorganic silts, silty or clayey fine sands or clayey silts of intermediate plasticity
CI	Inorganic clays, gravelly clays, sandy clays, silty clays, lean clays of intermediate plasticity
OI	Organic silts and organic silty clays of intermediate plasticity
MH	Inorganic silts of high compressibility, micaceous or diatomaceous fine sandy or silty soils, elastic silts
CH	Inorganic clays of high plasticity, fat clay
OH	Organic clays of high plasticity
Pt	Peat and other highly organic soils with very high compressibility

4.3 ESTIMATION OF SHEAR STRENGTH PARAMETERS

Widely in all the geotechnical problems concerning the foundations of various structures, earthquake construction etc., soil mass has to withstand the shearing stress. Shear strength is the most important engineering property of the soil; It is the capacity of soil to resist shearing stress. All stability analyses, which normally follow the limiting equilibrium approach, involve the determination of limiting shearing resistance i.e. the shear strength of the soil (Ranjan and Rao, 2005).

The fundamental shear strength equation, which is based on Mohr-Coulomb failure criterion, can be expressed as:

$$\tau_f = c + \sigma_n \tan \phi \quad (4.1)$$

where, τ_f , shear strength of the soil
 c , apparent cohesion
 σ_n , normal stress on the plane of rupture and
 ϕ , angle of internal friction

The graphical representation of Mohr-Coulomb equation (equation 4.1) is a straight line (Fig. 4.1). The intercept made by the straight line on the τ -axis represents the cohesion c and the slope of the plot gives the friction angle ϕ .

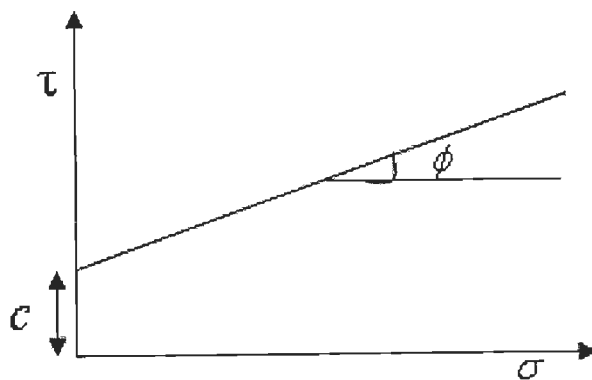


Fig. 4.1 Graphical Representation of Mohr-Coulomb Equation.

Shear strength parameters of soil contains the apparent cohesion (c) and angle of internal friction (ϕ). For the cohesionless soil, $c = 0$, Coulomb's equation becomes

$$\tau_f = \sigma_n \tan \phi \quad (4.2)$$

The shear strength parameters, c and ϕ of soils in undisturbed or remolded state may be determined by the laboratory tests such as Direct shear test, Triaxial compression test and laboratory Vane shear test as well as field Vane shear test.

4.4 SITE EXPLORATION AND GEOTECHNICAL TESTS

The in-situ tests in the field have the advantage of testing the soils in their natural, undisturbed condition. On the other hand laboratory tests having small size samples are obtained from boreholes and the reliability of these depend on the quality of the samples. It is a common practice to rely more on laboratory tests for cohesive soils. The Ultimate goal in carrying out the geotechnical investigation is to obtain various parameters for design of foundations. The field tests that are commonly used in the subsurface investigation (Ranjan and Rao, 2005) are included Table 4.2. The different geotechnical properties of soils and related laboratory tests are also included in Table 4.2.

Details of some of these are included here:

4.4.1 Standard Penetration Test (SPT)

This is the most extensively used penetrometer test in almost every country. The test employs a split-spoon sampler which consists of a driving shoe, a cylindrical split-barrel which is longitudinally split into two halves. IS: 2131-1981 suggests the standard procedure for carrying out the test.

The borehole is advanced to the required depth and its bottom cleaned. The split-spoon sampler attached to the standard drill rods of required length is lowered into the borehole and allowed to rest at the bottom. The split-spoon sampler is driven into

the soil for a distance of 450 mm by blows of a drop hammer of 65 kg falling vertically and freely from a height of 750 mm (Plate 4.2). The number of blows required to penetrate every 150 mm is recorded while driving the sampler. The number of blows required for the last 300 mm of penetration are added together and recorded as the N value at that particular depth of the borehole. The number of blows required to effect first 150 mm of penetration, called the seating derive, is disregarded. The split-spoon sampler is withdrawn, detached from the drill rods and disconnect the split-barrel from cutting shoe and the coupling. The soil sample is collected carefully from the split-barrel and transported to laboratory for classification tests.

The SPT is carried out at every 0.75 m vertical depth intervals in a borehole and this can be 1.50 m for large depth borehole. It does not perform well in rocky formation where the boring log shows *refusal* and the test is halted. In this case 50 blows required for any 150 mm and 100 blows for 300 penetration and 10 successive blows produce no advance (Plate 4.2). SPT values obtained in the field for sand have to be corrected. IS: 2131-1981 recommends that the field value N be corrected.



Plate 4.2 **Standard Penetration Test (SPT) in Progress**

4.4.1.1 Corrections to the observed SPT values

The standard penetration test provides representative soils samples both for visual inspection in the field and for laboratory testing. SPT is widely used in cohesionless soils and its application in cohesive soils is limited because the compressibility of such soils is not reflected by the N values. To avoid some pitfalls, proper precaution is required while SPT is carried out.

Normally the following three types of corrections (Plate 4.3) are applied to the observed N values:

- a) Correction for dilatancy
- b) Correction due to overburden pressure

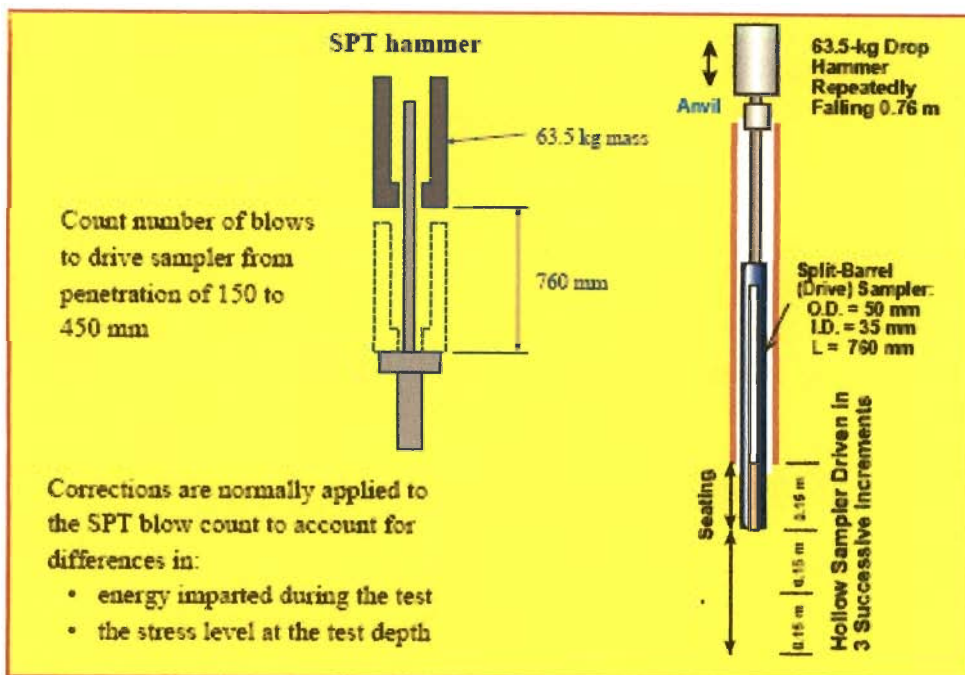


Plate 4.3 Standard Penetration Test-Details

4.4.1.2 SPT values related to relative density of cohesionless soils

Although the SPT is not considered as refined and completely a reliable method, the N-values give useful information with regard to consistency of cohesive soils and relative density of cohesionless soils. The correlation between corrected N-values and relative density of granular soils suggested by Terzaghi and Peck is given in Table 4.3.

Meyerhof (1956) has suggested the following equations for computing the internal friction angle from relative density.

For granular soils with fine sand and silt more than 5 percent,

$$\phi^0 = 25 + 0.15D_r$$

For granular soils with fine sand and silt less than 5 percent,

$$\phi^0 = 30 + 0.15D_r$$

where, D_r is relative density in percent and ϕ^0 is angle of friction

4.4.1.3 SPT values related to consistency of clay soil

Peck et al (1974) have developed correlations between N-values, unconfined compressive strength and consistency for saturated cohesive soils, which are included in Table 4.4 (Murthy, 2008).

$$q_u \propto N$$

$$q_u = \bar{k}N \quad \text{or} \quad \bar{k} = \frac{q_u}{N} \quad (4.3)$$

where \bar{k} is the proportionality factor.

Murthy (1982) investigated the relationship for the clay soil met at Farakka in West Bengal, India. An average value of $\frac{N}{q_u} = 7.5$ was assumed for this soil.

$$\text{or } q_u = \frac{N}{7.5} \text{ kg / cm}^2 = 13.33 \text{ N kPa} \quad (4.4)$$

The value of \bar{k} varies from 4 for clay soil to 7.5 for silty sandy soil (Sanglerat, 1972) Tables 4.3 and 4.4 respectively relate SPT 'N' with D_r , ϕ^0 and q_u .

Table 4.2 In-Situ Geotechnical Tests – Summary

S. No.	Geotechnical In-Situ Tests	Description	Geotechnical Parameters
1	Standard Penetration Test (SPT)	provides information of the penetration Resistance while also collecting a disturbed soil sample for grain-size analysis and soil classification	ϕ , E_s , μ etc.
2	Dynamic Cone Penetration Test (DCPT)	It is a quick test and helps to cover a large area. It provides the information of variability of the subsoil and unearth local soft pockets	Penetration Resistance
3	Static Cone Penetration Test (SCPT)	is performed using an instrumented probe with a conical tip, pushed into the soil hydraulically at a constant rate	tip resistance and friction resistance
4	Plate Load Test (PLT)	is usually performed in-situ to obtain load intensity versus settlement characteristics	Ultimate bearing capacity
5	Pressuremeter Test (PMT)	is a form of probe test, the load applied by uniform radial pressure to the sides of a borehole in which pressuremeter is placed	Soil deformation modulus, allowable soil pressure
6	Plate Dilatometer Test	is a plate probe often advanced using CPT rigs, but can also be advanced from conventional drill rigs	Strain with increasing the stress
7	Seismic Piezocone Penetrometer	SCPTu is advanced using the same equipment as a CPT or CPTu probe and also equipped with geophone	Detects the shear or pressure wave
8	Full Flow Penetrometers	These probes are used in extremely soft clay soils and are advanced in the same manner as the CPT	Penetration resistance
9	Visual Classification	is used to estimate soil characteristics such as the range of particle sizes and plasticity	Soil particles see by naked eye
10	In-Place Density Test	Usually used as part of a quality control/assurance plan for verifying if the compacted fill meets the required specifications	estimate unit weight and moisture content
11	Vane Shear Test	The shear vane consists of four steel blades at right angles to a steel rod. The vane gently pushed into the soil up to the required depth and measures torque by noting the angle of twist	Shear strength of soft clays

Table 4.3 Relation of N with Friction Angle (ϕ) and Relative Density, (Murthy, 2008)

S. No.	N	Compactness	Relative Density (D_r)	ϕ°
1	0-4	Very loose	0-15	< 28
2	4-10	Loose	15-35	28-30
3	10-30	Medium	35-65	30-36
4	30-50	Dense	65-85	36-41
5	> 50	Very Dense	> 85	> 41

Table 4.4 Relation between N and Unconfined Compressive Strength, q_u (Murthy, 2008)

S. No.	Consistency	N	q_u , kPa
1	Very soft	0-2	< 25
2	Soft	2-4	25-50
3	Medium	4-8	50-100
4	Stiff	8-15	100-200
5	Very Stiff	15-30	200-400
6	Hard	> 30	> 400

4.4.2 Dynamic Cone Penetration Test (DCPT)

In DCPT, a cone which has an apex angle 60° and attached to drill rods is driven into the soil by blows of a hammer of 65 kg, falling from a height of 750 mm (Plate 4.4). The blows are counted for every 150 mm penetration of the cone and the cone is driven till refusal or up to the required depth. The number of blows is required for 300 mm penetration as the dynamic cone penetration resistance N_{cd} . The number of blows provides an indication of uniformity or variability of the soils including the identification of any local soft pocket in the subsurface and no samples are recovered in this test. Dynamic cone penetration tests are performed either by using 50 mm diameter cone without bentonite slurry or 65 mm diameter cone with bentonite slurry. If the tests

are carried out close to a few boreholes, the data from DCPT can be compared with SPT data and correlation can be established between them for the particular site conditions (Ranjan and Rao, 2005).

4.4.3 Static Cone Penetration Test (SCPT)

The static cone penetration test is also known as cone penetration test (CPT) and is widely used in place of SPT for soft clay-silts and fine to medium sand deposits. The test was developed in Holland, and is therefore also called as Dutch cone test (Fig. 4.2). The penetrometer, uses a cone with apex angle of 60° and the base area of 10 cm^2 (Plate 4.4). CPT gives a continuous record of both the cone resistance and the friction resistance with depth. A disadvantage of this device is that no samples are obtained and the test is unsuitable for gravels, rocks and very dense sands owing to the difficulty experienced in pushing the cone. Cone penetration test is often used to estimate the point bearing resistance and skin friction resistance of a pile foundation. The correlation has been established between cone tip resistance, q_c and recorded number of blows, N for granular soils (Ranjan and Rao, 2005).

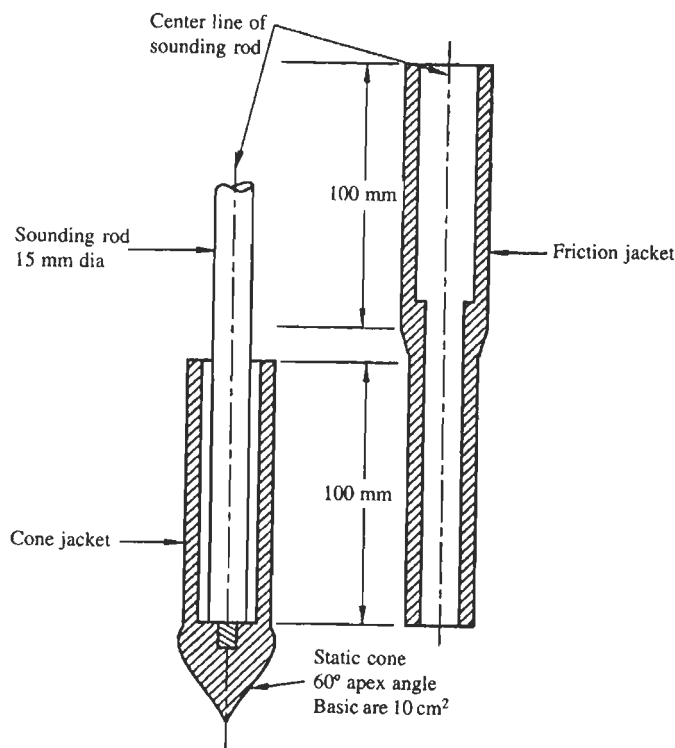


Fig. 4.2 Static Cone Penetration Equipment and Cone Assembly

Robertson and Campanella (1983a) have suggested a set of curves for normally consolidated clean sands that may be used to estimate relative density, D_r based cone resistance, q_c and effective overburden pressure. Robertson and Campanella (1983b) also provided the relationship between q_c and internal friction angle, ϕ (Murthy, 2008). Robertson (1990) and Zhang et al., 1996 have attempted soil classification based on CPT.

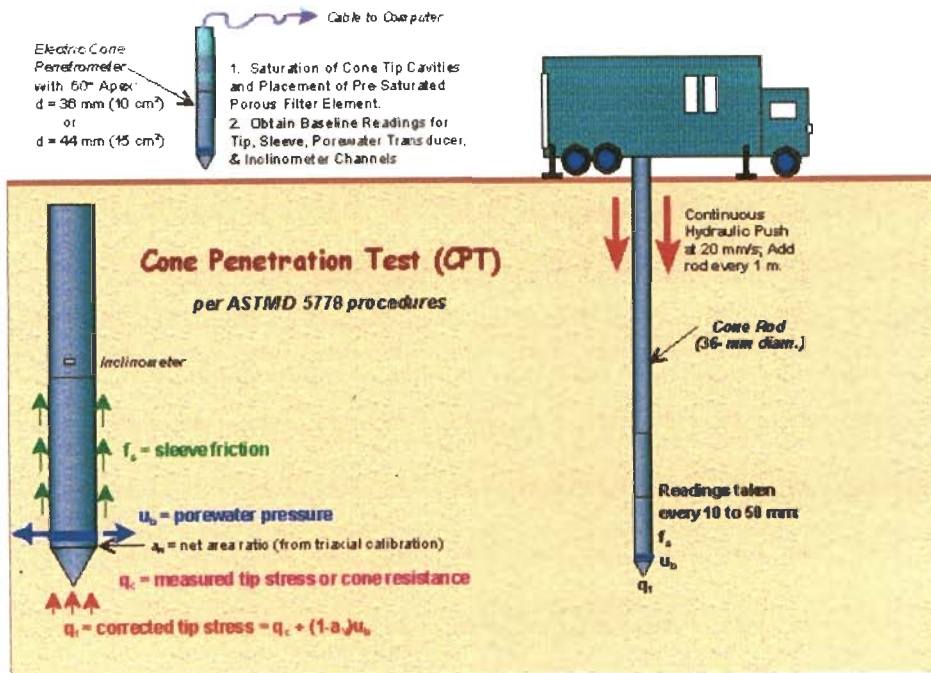


Plate 4.4 Setup and Procedure of Cone Penetration Test (CPT)

Table 4.5 Relationship between Relative Density (D_r) of Fine Sand, SPT (N), Static Cone Resistance (q_c) and Angle of Internal Friction (ϕ°) (Murthy, 2008)

S. No.	State of Sand	D_r	N	q_c	ϕ°
1	Very loose	< 0.2	< 4	< 2.0	< 30
2	Loose	0.2-0.4	4-10	2-4	30-35
3	Medium dense	0.4-0.6	10-30	4-12	35-40
4	Dense	0.6-0.8	30-50	12-20	40-45
5	Very dense	0.8-1.0	> 50	> 20	45

Table 4.6 Relationship between q_c and N (Murthy, 2008)

S. No.	Type of soil	$\frac{q_c}{N} = n$
1	Sand and gravel mixture	6
2	Sandy silts	3
3	Clay-silt-sand mixtures	2
4	Insensitive clay	1.5

4.4.4 Plate Load Test (PLT)

The plate load test is performed on either square or circular shape rigid steel plate. It is used as a model for the prototype foundation. The plate is located at proposed level of the foundation and is subjected to incremental loading (Plate 4.5). In IS: 1888-1982, the plate size varies from 30 cm to 75 cm square. The test is conducted by applying various increments of load through a hydraulic jack and the settlement at each increment of the loading is measured and the data is presented in the form of load intensity-settlement curve. The curve provides the value of ultimate bearing capacity of the test plate (Ranjan and Rao, 2005). It is also used to determine the modulus of sub grade reaction, which is very useful for design of raft foundation and design of pavements.

The ultimate bearing capacity of the foundation for cohesionless (granular) soils is given by

$$q_{uf} = q_{up} \left(\frac{B_f}{B_p} \right) \quad (4.5)$$

where

q_{up} : ultimate bearing capacity of test plate,

B_f : width of foundation in cm and

B_p : width of test plate in cm.

In cohesive soils

$$q_{uf} = q_{up} \quad (4.6)$$

If the plate load test is carried out above the water table, the settlement inferred from the load-settlement curve will have to be corrected. The actual settlement is calculated as

$$S_{act} = \frac{S_{PLT}}{C_{fac}} \quad (4.7)$$

where S_{PLT} is Settlement computed from plated load test (PLT) and C_{fac} is Correction factor.

The correction factor for water table is calculated using Peck, Hanson and Thornburn (1974).

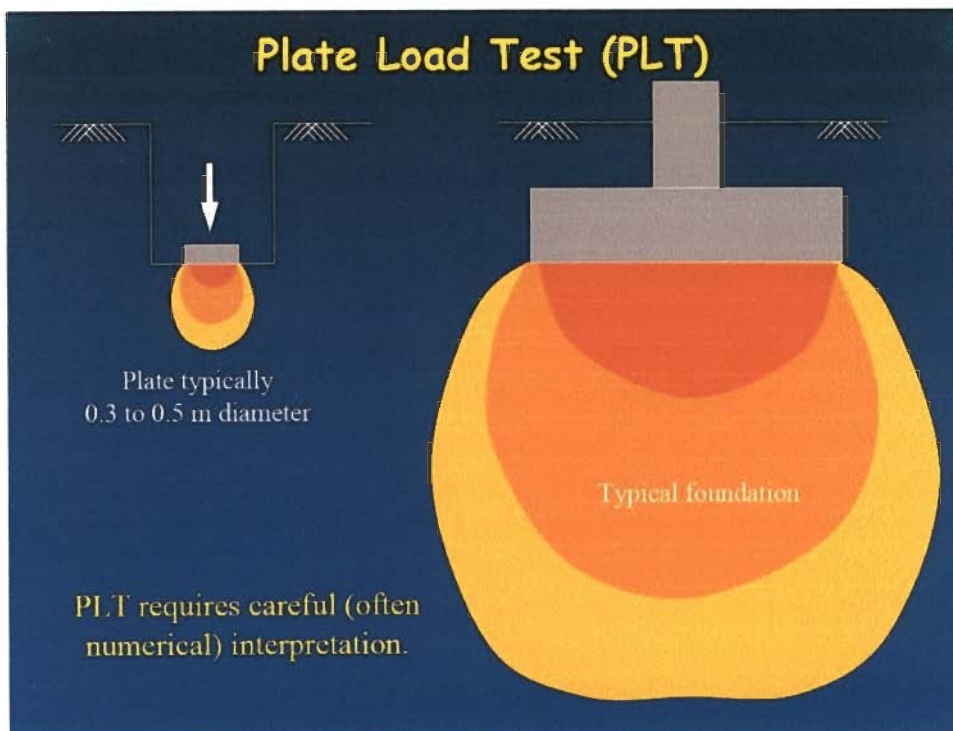


Plate 4.5 Plate load test (PLT)

4.5 LABORATORY TESTS

Laboratory testing is an essential requirement for the geotechnical engineer to examine the behavior of the subsoil. Field investigations include in-situ measurements, soil sample (Plate 4.6) collection for laboratory testing and other field observations related to the soils. Soil samples are generally of two types, namely the disturbed samples and the undisturbed samples. Disturbed samples are also known as representative samples and are useful for identification tests such as natural moisture content, grain size analysis, Atterberg limit and specific gravity etc (Table 4.7). Disturbed samples are altered due to mix up of other layer or mineral constituents and are called as non-representative samples. These are virtually of no use. Undisturbed samples have the original soil structure and material properties preserved. These are considered suitable for laboratory tests including shear strength, permeability and consolidation tests and triaxial tests. Since geotechnical tests are time consuming, the geotechnical engineer optimizes the tests according to the requirements. Only few selected geotechnical laboratory tests have been described in this chapter (Ranjan and Rao, 2005).

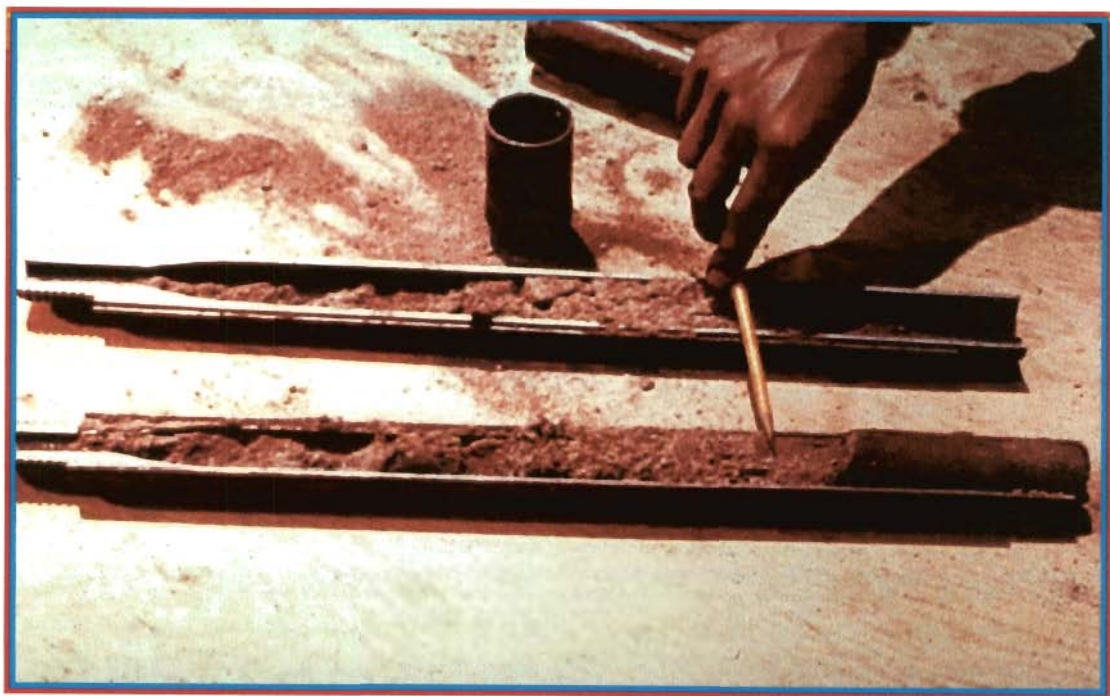


Plate 4.6 Sampling from SPT Split Spoon

Table 4.7 Geotechnical Properties and Related Laboratory Tests

S. No.	Geotechnical Properties	Description	Geotechnical Laboratory Tests
1	Grain size Analysis	It is sieving process, that perform to determine the soil gradation	Sieve Analysis / Hydrometer Analysis
2	Moisture Content	Also called the water content is the ratio of the weight of water to the weight of solids (%)	standard Proctor tests / Oven-drying / Pycnometer
3	Atterberg Limit	The Atterberg limits define the boundaries of plastic and liquid limit of the soil	Atterberg Limits Tests
4	Void ratio	is the ratio of volume of voids to the total volume of the soil (%)	Laboratory Testing
5	Specific Gravity	Is the ratio of the weight of a given volume of solids to the weight of an equivalent volume of water at 4° C.	Pycnometer
6	Permeability	Soil permeability relates to groundwater flow, and is a measurement of continuous void space within a soil medium	Constant head permeameters / falling head permeameter tests / auger hole method
7	Soil Compaction	The densification of the soil by the mechanical energy is called compaction	standard Proctor tests
8	Consolidation characteristics Compression Index Coefficient of Consolidation	This parameter controls the magnitude of consolidation in a soil is the coefficient of compressibility	Oedometer test
9	Relative Density	The degree of denseness or looseness of natural deposits	sand cone, nuclear densiometer
10	California Bearing Ratio (CBR)	is a laboratory test that is used to determine the suitability of a soil for use as a sub base in a pavement section.	CBR Test
11	Unconfined compression Test	is a laboratory test performed on undisturbed samples and estimate the unconfined compression strength q_c	Unconfined compression Test
12	In-situ Unit Weight	Unit weight of a soil mass is the ratio of the total weight of soil to the total volume of soil.	In laboratory by measuring the weight and volume of the undisturbed soil sample / In-Place Density Test
13	Shear Strength Parameters	Angle on the graph (Mohr's Circle) of the shear stress and normal effective stresses at which shear failure occurs	SPT / DST / TCT

4.6 BEARING CAPACITY

The earth provides the ultimate support to the structures such as bridges, earth fills, earth and concrete dams. The structural foundations are the substructure elements which transmit the structural load to the earth such that the supporting soil is not overstressed and does not undergo deformations that would cause excessive settlements of the structure.

The foundations can be broadly grouped into two categories:

- a) Shallow Foundations and
- b) Deep Foundations such as pile foundations

Terzaghi's (1943) definition shows that the ratio of depth to its width generally should lie in the range 1 to 15 for shallow foundations and greater than 15 for deep foundations. The foundation must satisfy the following criteria:

- a) Location and depth criteria
- b) Shear failure criterion or bearing capacity criterion
- c) Settlement criterion

The three above stated criteria are the general requirement of the foundation and must be satisfied separately.

4.6.1 Shallow Foundation

The foundation is said to be shallow if the depth of the foundation is less than or equal to the width of the foundation. In choosing the type of foundation, the design engineer has to implement the following measures:

- i. To gather the required information concerning the nature of the superstructure and the load to be transmitted to the foundation
- ii. To obtain the subsurface soil conditions
- iii. To take into account
 - a) The bearing capacity of the soil to carry the required load and
 - b) The adverse effects on the structure due to differential settlements
- iv. To undertake more detailed studies when one or two types of foundation are selected on the basis of preliminary studies
- v. To estimate the cost of the appropriate foundation and choose the optimal one

4.7 THE GENERAL BEARING CAPACITY EQUATION

The bearing capacity of soil can be determined either by analytical methods using bearing capacity equations or from the field test data.

The general bearing capacity equation developed by Terzaghi (1943) is for a strip footing under general shear failure. It has been modified for other types of foundations such as square, circular and rectangular by introducing shape factors. Meyerhof (1963) presented a general bearing capacity equation, which takes into account the shape and the inclination of load. This equation involves coefficients N_c , N_q and N_γ . Hansen (1970) has extended the work of Meyerhof by including in bearing capacity equation two additional factors to take care of tilt and foundation of slopes. Vesic (1973, 1974) used the same form of equation suggested by Hansen (1970). We have expressed the dependence of N_c , N_q and N_γ (Vesic) on shear angle of internal friction, ϕ analytically. The Indian Standard (IS) Code: 6403-1981 prescribes these bearing capacity coefficients. Terzaghi's (1943) ultimate bearing capacity q_μ equation is

$$q_\mu = cN_c + \gamma D_f N_q + \frac{1}{2} \gamma B N_\gamma \quad (4.8)$$

Where q_μ is the ultimate bearing capacity of footing.

c : unit cohesion, B : width of footing, γ : the effective unit weight of the soil,
 D_f : depth of foundation, N_c , N_q and N_γ : are the bearing capacity factors, and
 ϕ : friction angle.

The bearing capacity factors are the function of the friction angle (ϕ) and these factors can be expressed as the following equations

$$N_c = (N_q - 1) \cot \phi \quad (4.9)$$

$$N_q = \frac{a_\theta^2}{2 \cos^2 \left(45^\circ + \frac{\phi}{2} \right)} \quad (4.10)$$

$$N_\gamma = \frac{1}{2} \tan \phi \left(\frac{K_{py}}{\cos^2 \phi} \right) - 1 \quad (4.11)$$

$$a_{\theta} = \varepsilon^{\eta \tan \phi} \quad (4.12)$$

$$\eta = \left(0.75\pi - \frac{\phi}{2} \right) \quad (4.13)$$

Where $K_{p\gamma}$ = passive earth pressure coefficient

Terzaghi's bearing capacity equation has been modified for different other types of foundations such as square, circular and rectangular foundations. The local shear failure normally occurs in loose and general shear failure occurs in dense sand. The state of sand changes from loose to dense sand condition and is known as transition from local to general shear failure and there is no bearing capacity equation for this transition state. Terzaghi's bearing capacity factors for general shear failure is included in Fig. 4.3.

Peck et al., (1974) have presented the curves that provide values of bearing capacity factors (N_{γ} and N_q) and friction angle (ϕ) which can be obtained from SPT N-values for mixed (transition) state (Fig. 4.4). These curves have been developed on basis of the assumptions that (a) purely local shear failure occurs when $\phi \leq 28^\circ$ (b) purely general shear failure occurs when $\phi \geq 38^\circ$ (c) The transition curves for the values of ϕ between 28° and 38° represent the mixed state of local and general failures. Factors N_{γ} and N_q for $\phi \geq 38^\circ$ can be obtained from Table 4.8. The bearing capacity factors for local shear failure (\bar{N}_q and \bar{N}_{γ}) may also be obtained from the same table by using the relationship of shear parameters

$$\bar{\phi} = \tan^{-1} \left(\frac{2}{3} \right) \tan \phi \quad \text{and} \quad \bar{c} = \frac{2}{3} c \quad (4.14)$$

Under the general shear failure, cohesionless soil has $c = 0$, $N_c = 0$ and for cohesive soil $\phi = 0$, $N_c = 5.7$ and $N_q = 1$ for strip footing.

Dewaikar et al. (2008) have dealt with Terzaghi's bearing capacity factor, N_q and Prandtl Mechanisms in detail manner.

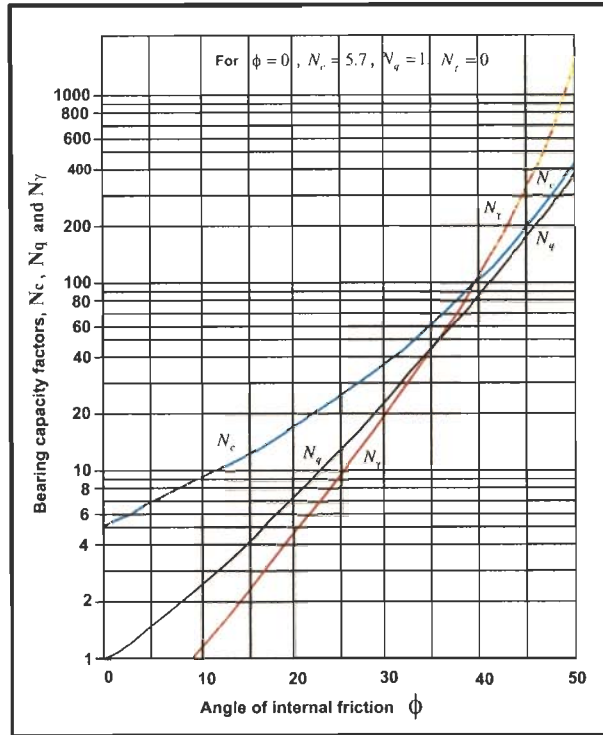


Fig. 4.3 Terzaghi's Bearing Capacity Factors for General Shear Failure (Murthy, 2008)

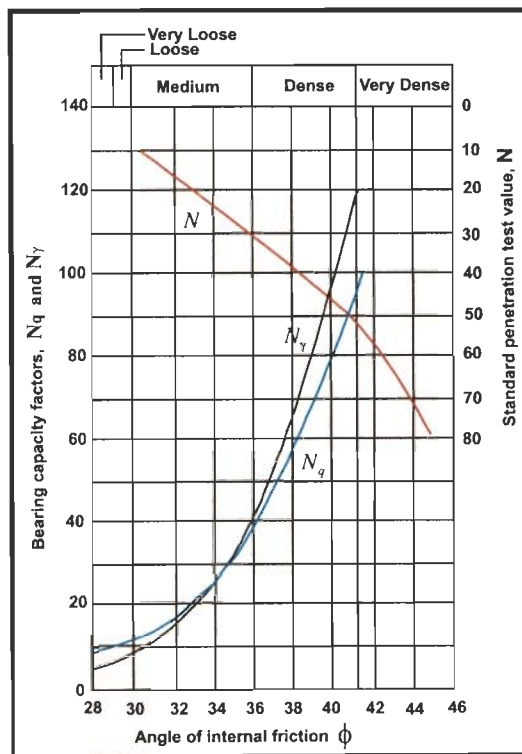


Fig. 4.4 Terzaghi's Bearing Capacity Factors for Mixed State of Local and General Shear Failures in Sand (Murthy, 2008)

Table 4.8 Bearing Capacity Factors of Terzaghi (Murthy, 2008)

S. No.	ϕ	N_c	N_q	N_γ
1	0	5.7	1.0	0.0
2	5	7.3	1.6	0.5
3	10	9.6	2.7	1.2
4	15	12.9	4.4	2.5
5	20	17.7	7.4	5.0
6	25	25.1	12.7	9.7
7	30	37.2	22.5	19.7
8	35	57.8	41.4	42.4
9	40	95.7	81.3	100.4
10	45	172.3	173.3	297.5
11	50	347.5	415.1	1153.0

Table 4.9 outlines the relationship between angle of internal friction, ϕ and N_c , N_q & N_γ Factors of Meyerhof (M), Hansen (H) and Vesic (V).

Table 4.9 The Value of N_c , N_q and N_γ Factors of Meyerhof (M), Hansen (H) and Vesic (V) (Murthy, 2008)

S. No.	ϕ	N_c	N_q	N_γ (H)	N_γ (M)	N_γ (V)
1	0	5.14	1.0	0.0	0.0	0.0
2	5	6.49	1.6	0.1	0.1	0.4
3	10	8.34	2.5	0.4	0.4	1.2
4	15	10.97	3.9	1.2	1.1	2.6
5	20	14.83	6.4	2.9	2.9	5.4
6	25	20.71	10.7	6.8	6.8	10.9
7	26	22.25	11.8	7.9	8.0	12.5
8	28	25.79	14.7	10.9	11.2	16.7
9	30	30.13	18.4	15.1	15.7	22.4
10	32	35.47	23.2	20.8	22.0	30.2
11	34	42.14	29.4	28.7	31.1	41.0
12	36	50.55	37.7	40.0	44.4	56.2
13	38	61.31	48.9	56.1	64.0	77.9
14	40	72.25	64.1	79.4	93.6	109.4
15	45	133.73	134.7	200.5	262.3	271.3
16	50	266.50	318.50	567.4	871.7	762.84

4.8 ULTIMATE BEARING CAPACITY OF FOOTINGS BASED ON SPT 'N'

For cohesionless soils, the relationship between N and ϕ established by Peck et al. (1974) is utilized in estimating ϕ , which in turn can be used for assessing the ultimate bearing capacity of soil.

For cohesive soils, the relationship between N and q_c (unconfined compressive strength) can be exploited to assess q_u . Then it is possible to estimate the net ultimate bearing capacity and the net allowable bearing pressure by following Skempton's (1951) approach.

$$q_u = 2c_u = \bar{k}NkPa \quad (4.15)$$

where, the value of the coefficient \bar{k} may vary from 12 to 25.

Analytical relations also exist for estimating the bearing capacity of soil based on CPT ' q_c ' values. The relationship between the cone penetration resistance, q_c and ϕ has been developed by Robertson and Campanella (1983b) and it can determine the values of ϕ with the known values of q_c as input. Further, by using the values of ϕ , bearing capacity factors can be determined and hence the ultimate bearing capacity.

4.9 DEEP FOUNDATION

There are three types of deep foundations

- i) Pile foundations
- ii) Wells or Caisson foundations
- iii) Drilled pier foundation

In this work, only the pile foundations have been considered. In case of deep foundations, following methods are available for determination of the ultimate load bearing capacity for the vertical pile.

- i) Static bearing capacity equation
- ii) SPT and CPT
- iii) Field load test
- iv) Dynamic method

The SPT and CPT methods have been employed to determine the bearing capacity factors for deep foundation. Figure 4.5 shows the relation of bearing capacity

with angle of internal friction for circular deep foundation and this figure is used to develop regression equation between bearing capacity factor and angle of internal friction (Table 4.10).

For deep foundations piles are used. Methods exist for determining the ultimate bearing capacity of a single vertical pile by using SPT ‘N’ and CPT ‘ q_c ’ values. In case of circular deep foundations (Bored and driven piles), several workers have proposed ultimate bearing capacity factor, N_q as a function of angle of internal friction, ϕ in the graphical form. We have expressed few of them in analytical form and included them in Table 4.10.

Meyerhof (1976) has dealt with bearing capacity and settlement of pile foundations. Murthy (2008) and Dewaikar et al. (2007) have outline non-linear 3-D finite element analysis of laterally loaded piles.

Expressions for bearing capacity of piles based on static cone penetration test (CPT) are also available. However, they are not being dealt here.

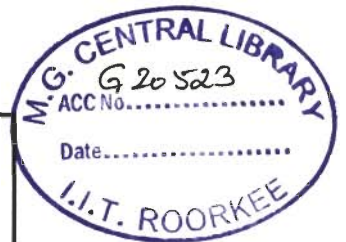
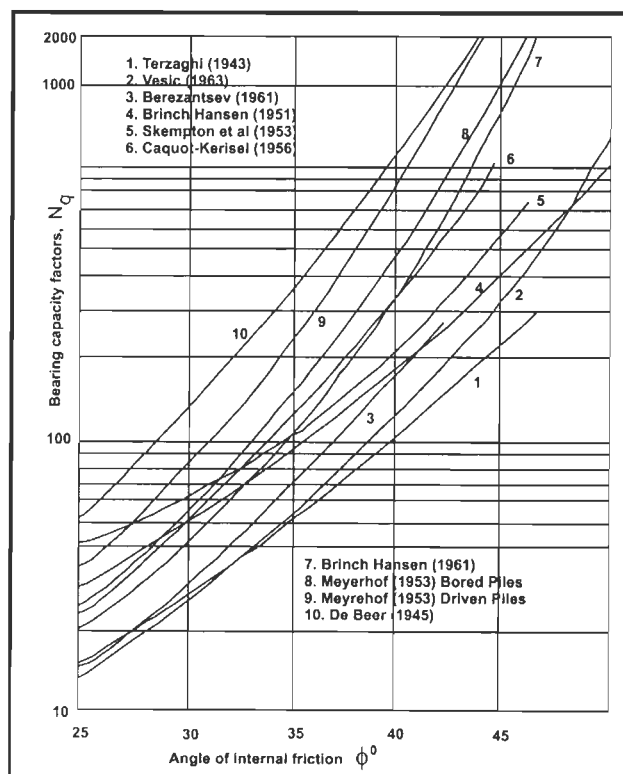


Fig. 4.5 Bearing Capacity Factors for Circular Deep Foundations (Murthy, 2008)

4.10 REGRESSION ANALYSIS

The material in Tables 4.1-4.9 and Figs. 4.1-4.5 were carefully analyzed and redrafted into Tables A.1-A.6 in Appendix A. These tables (A.1-A.6) formed the basis for the regression equations for both formation and geotechnical parameters in Table 4.10. Further, regression equations were used to infer different geotechnical parameter sections from geoelectric sections.

4.10.1 Inferring Prediction Equation for Angle of Internal Friction from SPT

Although SPT is not considered as refined and completely reliable method of soil investigation, the SPT 'N' values give useful information with reference to consistency of cohesive soils and relative density of cohesionless soils. Terzaghi and Peck (1967) have investigated the correlation between "N" values (corrected) and relative density of granular soils and the same is reproduced in Table A.1a & b.

Cohesionless soils

The relation between SPT, N and angle of internal friction, ϕ established by Peck et al. (1974) is given in graphical form (Fig. A.5a). The value of N for obtaining ϕ is a corrected value for standard energy. The angle of internal friction, ϕ obtained by this method can be used for obtaining the different bearing capacity factors of soil.

4.10.2 Prediction Equation for Unit Weight of Soil from Porosity / Water Saturation

By considering an empirical table (Table A.1a & b) prediction equations are developed for porosity versus unit weights of soil (both dry and saturated) and water saturation versus unit weights (both dry and saturated). These are included in Table 4.10.

4.10.3 Prediction Equation for Unconfined Compressive Strength from SPT 'N'

Peck et al. (1974) have given for saturated cohesive soils, correlations between 'N' value and unconfined compressive strength, q_u (k Pa) as per Table A.2. on basis of which the regression equation for q_u is predicted.

4.10.4 Prediction Equations for Terzaghi's General Bearing Capacity and Ultimate Bearing Capacity Factors (Strip Footings)

The ultimate bearing capacity factors of Terzaghi - N_c , N_q and N_γ versus angle of internal friction, ϕ for strip foundation were considered (Table A.3) and a prediction equation has been developed with ϕ as input.

Peck et al. (1974) have given curves for Terzaghi's bearing capacity factors N_γ and N_q and SPT 'N' versus shear angle, ϕ (Table A.4a, b & c) in case of transition from local to general shear failure in sand (Murthy, 2008). Prediction equations are developed for SPT 'N' versus ϕ and for N_γ , N_q versus ϕ as input.

The bearing capacity equation developed by Terzaghi for a strip footing under general shear failure has been modified by Meyerhof (1963). Its coefficients N_c , N_q and N_γ (Vesic) are correlated with shear angle, ϕ , as per Table A.5. The regression equations are respectively meant for these general bearing capacity factors with angle of internal friction, ϕ as input.

4.10.5 Prediction Equation for N_q Factor (Piles) Based on Shear Angle in Case of Deep Sub-Soil Investigations

For ultimate bearing capacity of driven and bored piles, the relation of bearing capacity factor N_q with angle of internal friction, ϕ is provided by several workers (Murthy, 2008). Here, our prediction equations for N_q are developed on the basis of correlations of Brinch Hansen (1961), Meyerhof (1953) for driven piles and Meyerhof (1953) for bored piles (Table A.7).

Table 4.10 summarizes the different geotechnical parameter prediction equations.

4.11 REMARKS

The estimation of bearing capacity factors based on CPT method is not attempted here. However, earlier outlined procedure for SPT 'N' can easily be extended to CPT method also.

Table 4.10 Inferred Predictive Equations of Different Geotechnical Parameters from Available Correlations in Literature (Murthy, 2008) for SPT.

S. No.	Formation Parameter/ Geotechnical Parameter	Regression equation $Y=a_1x^2+a_2x+a_3$ or $y=a_1\exp(a_2x)$	Regression equation $Y=b_1x^2+b_2x+b_3$ or $y=b_1\exp(b_2x)$
1	Unit weight of soil	Dry $a = \{24.809, -0.0181\}$ Input: Water saturation (%) Fig. A.1c $a = \{38.256, -0.0236\}$ Input: Porosity (%) Fig. A.1a	Saturated $b = \{24.901, -0.0094\}$ Input: Water saturation (%) Fig. A.1d $b = \{28.104, 0.0093\}$ Input: Porosity (%) Fig. A.1b
2	Friction angle, ϕ	Terzaghi's method $a = \{-0.0017, 0.3685, 26.4480\}$ Input: SPT 'N' Fig. A.4a	
3	Unconfined compressive strength, q_u	$a = \{0.0058, 12.771, 3.4342\}$ Input: SPT 'N' Fig. A.2	
4	Terzaghi's Bearing Capacity factors (Peck et al. 1974)	N_γ $a = \{0.0041, 0.2526\}$ Input: Friction angle, ϕ Fig. A.4c	N_q $b = \{0.0366, 0.1920\}$ Input: Friction angle, ϕ Fig. A.4b
5	Vesic (1973, 1974) bearing capacity factors	N_q $a = \{0.7706, 0.1108\}$ Fig. A.5b N_c $a = \{3.7368, 0.0749\}$ Input: Friction angle, ϕ Fig. A.5a	N_γ (Vesic) $b = \{0.2055, 0.1588\}$ Input: Friction angle, ϕ Fig. A.5c
6	Ultimate bearing capacity factors	N_q $a = \{0.8011, 0.1176\}$; Fig. A.3b N_c $a = \{4.266, 0.0797\}$ Input: Friction angle, ϕ Fig. A.3a	N_γ $b = \{0.1969, 0.1623\}$ Input: Friction angle, ϕ Fig. A.3c
7	Piles	Bored piles N_q (Vesic) $a = \{0.1566, 0.1696\}$ Fig. A.6a N_q (Meyerhof, 1953) $a = \{0.075, 0.2206\}$; Fig. A.6b Input: Friction angle, ϕ	Driven piles N_q (Meyerhof, 1953) $b = \{0.0999, 0.2244\}$ Input: Friction angle, ϕ Fig. A.6c

5.1 GENERAL

Here, an outline of methodology developed is attempted. However, for real demonstration, chapters 6-9 need to be consulted, where four case studies are included. Three of them (IIT Roorkee Campus (2No.) and Bhagawanpur about 20 kms from Roorkee) belong to Indo-Gangetic Alluvial Plains of Uttarakhand and fourth one belongs to Delhi Group of rocks (Piyala) in the vicinity of Delhi, India. In Chapter 6 the methodology is illustrated.

The entire methodology is based on regression equations between observed geophysical logs (selected columns of digital resistivity and IP images) and geotechnical data referred to a pair of boreholes. These equations in turn are validated at the same pair of boreholes in predicting lithology, water saturation, porosity depth profiles and geotechnical test results in terms of SPT, DCPT and SCPT. By considering the quality of match between actual and predicted values, one among the geo-electric sections such as earth resistivity tomogram (ERT), induced polarization image (IPI) and fictitious resistivity (Ficres) is identified for further analysis.

In the next stage, based on existing empirical relations / tables / graphical plots in geotechnical literature, regression equations have been developed between angle of internal friction and various categories of bearing capacity factors for both shallow and deep soil investigations (piles). These relations are used to transform the chosen geo-electric section into respective 2-D geotechnical sections along a geo-electric profile. Such profile sections in the study region may allow prediction of 3-D volumes of geotechnical parameters.

5.2 BASIC STEPS

- i) Development of regression equations that relate observed geo-electrical (Resistivity (Res), Induced Polarization (IP) and Fictitious Resistivity (Ficres)) logs from respective 2-D image data with geotechnical data are referred to boreholes at / in close proximity of geo-electrical profile. The geotechnical data includes SPT / DCPT / SCPT and formation parameters such as lithology, porosity, water saturation, sand and clay content.
- ii) Validation of respective regression equations referred to a pair of boreholes on the profile. By considering the quality of match between actual and predicted values, one among the geo-electrical sections such as ERT, IPI and Ficres is identified and used to convert the respective geo-electrical section to SPT / CPT section
- iii) Based on existing empirical relations / tables / graphical plots in geotechnical literature regression equations are developed between SPT / CPT with friction angle, unit weight of soil cover (dry & saturated), unconfined compressive strength and in turn angle of internal friction with various bearing capacity factors for both shallow and deep foundations.
- iv) The optimal correlation relations developed in Step 3 are in turn used to transform the SPT / CPT sections arrived in step 2 into respective 2-D geotechnical sections along the geo-electrical profile by using the respective correlation equations in Step 5.2.3.
- v) Steps i, ii and iv need to be repeated for each geo-electric profile in the study region, which in turn allow predicting probable 3-D volumes of geotechnical parameters.

5.3 BROAD DETAILS OF PROPOSED METHODOLOGY

5.3.1 Development of Regression Equations

The regression equations that relate observed geoelectrical (resistivity (Res), Induced polarization (IP) and fictitious resistivity (Ficres)) logs from respective 2-D image data with geotechnical data are referred to boreholes at / in close proximity of

geo-electrical profile. The geotechnical data includes SPT / DCPT / SCPT and formation parameters such as lithology, porosity, water saturation, sand and clay content derived from borehole samples.

5.3.2 Validation of Respective Regression Equations Referred to a Pair of Boreholes on the Profile

By considering the quality of match between actual and predicted values, one among the geo-electrical sections such as ERT, IPI and Ficles is identified and used to convert the respective geo-electrical section to SPT / CPT section

5.3.3 Development of Regression Equations for Geotechnical Parameters

Based on existing empirical relations / tables / graphical plots in geotechnical literature, regression equations have been developed between SPT / CPT with friction angle, unit weight of soil cover (dry & saturated), unconfined compressive strength and in turn friction angle with various bearing capacity factors for both shallow and deep foundations.

5.3.4 Generation of 2-D Geotechnical Parameter Sections

The optimal regression relations developed in Step 5.3 are in turn used to transform the SPT / CPT sections arrived in step 2 into respective 2-D geotechnical sections along the geo-electrical profile by using the respective regression equations in Step 5.3.

5.3.5 Prediction of 3-D Geotechnical Parameter Volumes

Steps 5.3.1, 5.3.2 and 5.3.4 need to be repeated for each geo-electric profile in the study region, which in turn allows predicting probable 3-D volumes of geotechnical parameters.

5.4 DETAILED PROCEDURE

5.4.1 Correlation of Normalized ERT, IPI, Ficles and SPT versus Depth Plots

Normalized plots of ERT, IPI, Ficles and SPT are made for different boreholes that lie in the vicinity of the geophysical profile in question. By a careful visual correlation, which of ERT, IPI and Ficles will be considered for further work is decided. In case of doubt, usually a pair will be considered, e.g., ERT and IPI or other pairs among the three. But the basic aim is to arrive at single geoelectrical investigation results, i.e. ERT / IPI / Ficles by carefully going through the validation results to be detailed in the following sub-sections.

5.4.2 Inferring Prediction Equations for ERT / IPI / Ficles versus SPT, DCPT and SCPT

For a pair of boreholes, regression equations have been generated by considering the correlation between geoelectrical log (a column in the image section against an appropriate electrode corresponding to the projected position of a borehole) and geotechnical field test results at a borehole. The process is repeated for the other borehole in the selected pair. Then an average relation is generated for predicting SPT at a borehole. The existing SPT 'N' values (normalized) and the predicted 'N' value decides the choice among the three contenders ERT, IPI and Ficles. Then this average relation will be used in converting the appropriate geoelectrical section into a predicted 2-D SPT section along the geo-electric profile in question.

The above procedure has been adopted for generating 2-D DCPT and SCPT sections also. But one has to take special care for depth-wise geo-electric data sampling by an interpolation scheme (spline procedure) at the initial stage of prediction equation development as sampling depths of SPT, DCPT and SCPT differ from each other. It is to be noted that resistivity / IP / Ficles values are available in logarithmic depth scale, while those of geotechnical test results are in different linear depth scales. So, a spline based interpolation scheme has been used for matching the depth scales before respective regression equation development.

5.4.3 Inferring Prediction Equations for ERT / IPI / Fictitious Resistivity versus Geotechnical Sand, Clay / Shale, Lithology, Water Saturation and Porosity

For a selected pair of boreholes, depth-wise variation of normalized values of resistivity / IP chargeability / Fictitious Resistivity from respective geo-electric sections are plotted against normalized values of sand, clay / shale, porosity, water saturation and lithology (Table 5.1) derived from geotechnical data after proper implementation of interpolation scheme in depth matching. In each correlation case, regression equations have been developed borehole-wise. Then average predictive equations have been developed for a chosen pair of boreholes. These can be used to transform the 2-D geo-electric sections into respective sand, clay / shale, porosity, water saturation and lithology sections. Further, for codifying lithology, Table 5.1, which was designed by considering the soil classification in geotechnical literature (Murthy, 2008) has been used.

5.4.4 Use of Regression Equations for Obtaining 2-D Sections of SPT, DCPT and SCPT

The regression equations developed in section 5.3 have been used in transforming the selected geoelectrical section into respective SPT / DCPT / SCPT sections.

5.4.5 Use of Regression Equations for Obtaining 2-D Sections of Angle of Internal Friction, Porosity, Water Saturation and Unconfined Compressive Strength

The earlier established regression equations (Table 4.10) of different geotechnical parameters (angle of internal friction, unconfined compressive strength, unit weights of soil (both dry & saturated) and bearing capacity factors) have been utilized in converting relevant resistivity / IP image data along a profile into respective geotechnical parameter sections.

5.4.6 Use of Regression Equations for Terzaghi's Bearing Capacity and Ultimate Bearing Capacity 2-D Sections for Strip Footings from Angle of Internal Friction

The regression equations for ultimate bearing capacity factors of Terzaghi - N_c , N_q and N_γ versus angle of internal friction, ϕ for strip foundation (Murthy, 2008) as input were considered (Table 4.10) and utilized in obtaining respective 2-D sections.

Regression equations developed for N_γ , N_q with ϕ as input (Table 4.10) have been utilized in obtaining respective 2-D sections.

Proposed regression equations respectively meant for general bearing capacity factors N_c , N_q and N_γ (Vesic) with shear angle, ϕ as input are utilized in obtaining respective 2-D sections.

5.4.7 Use of Regression Equation for N_q Factor 2-D Sections Based on Friction Angle in Case of Deep Sub-soil (Piles) Investigations

The regression equations for ultimate bearing capacity factors for driven and bored piles, N_q with angle of internal friction, ϕ as per Table 4.10 are utilized in obtaining respective 2-D sections. Here, proposed regression equations for N_q have been developed on the basis of correlations of Brinch Hansen (1961), Meyerhof (1953) for driven piles and Meyerhof (1953) for bored piles.

5.5 REMARKS

- i) Site and profile specific regression relations of resistivity / IP with various formation parameters need to be utilized in the generation of respective 2-D formation parameter sections.
- ii) Proposed Table 5.1 needs to be utilized in predicting the lithology section along a geoelectrical (Resistivity / IP / Ficsres) profile.
- iii) Table 4.10 summarizes different geotechnical parameter regression equations and these have been utilized in converting relevant resistivity / IP image data along a profile into respective bearing capacity factor sections.
- iv) The bearing capacity factors based on CPT method have not been attempted here. However, earlier outlined procedure for SPT 'N' can easily be extended to CPT method also.

Table 5.1 Resistivity / IP Values versus Lithology as per Geotechnical Soil Classification

Soil Type	Geotechnical Symbol	Resistivity Code	IP Code	Details
Gravels	GW	0.9	0.1	well graded gravels
Clean Sand	GP	0.8	0.2	poorly graded gravels
	GM	0.75	0.25	silty gravels
Gravel with fines	GC	0.7	0.3	clay gravels
	SW	0.85	0.15	well graded sands
Clean Sands	SP	0.72	0.28	poorly graded sands
	SM	0.65	0.35	silty sands
Sands with fines	SC	0.6	0.4	clay sands
	ML	0.45	0.55	inorganic silts and very fine sands
Silts and Clays with low compressibility	CL	0.4	0.6	inorganic clays, gravely clay
	OL	0.5	0.5	organic silts and organic silty clay
	MI	0.3	0.7	inorganic silts, clayey fine sands
Silts and Clays with medium compressibility	CI	0.35	0.65	inorganic clays, gravely clay
	OI	0.4	0.6	organic silts and organic silty clay
	MH	0.22	0.78	inorganic silts
Silts and Clays with high compressibility	CH	0.25	0.75	inorganic clays
	OH	0.3	0.7	organic clays
Highly organic soil	Pt	0.15	0.85	peat and other highly organic soils

GEOTECHNICAL CASE STUDIES-I

6.1 GENERAL

This study region namely the site of construction of New I.I.T Roorkee Library structure belongs to Indo-Gangetic Alluvial Plains and falls in Uttarakhand State, India. By using resistivity / IP image data the geotechnical site characterization has been attempted as per methodology detailed in Chapter 5. For geotechnical data, the geotechnical report of a civil engineering construction company was consulted.

6.2 GEOLOGY OF THE STUDY REGION

The vast Indo-Gangetic Alluvial plains are located to the south of the Sub-Himalaya and extend up to the Aravalli in the west, Satpura and Vindhya ranges in the south. This basin was considered to be a foredeep by Suess. The development and evolution of the fore deep into Indo-Gangetic basin has taken place in three stages related to different phases of Himalayan orogenic movements (Kumar, 2005). Major parts of Indogangetic plains are marked by relatively a sub-humid to humid climate and high rate of sedimentation (Parkash et al., 2001).

On the basis of surface and subsurface exploration carried out by various agencies for groundwater, oil and natural gas and general geologic mapping, four litho-successions ranging from Late Archaean to Proterozoic (Supersequence I, IIb, III and IV) and four from Upper Paleocene to Quaternary (Supersequence XII, XIII, XIV and XV) have been recognized. Of these, the last three sequences are exposed while knowledge about the other sequences is based on borehole data supplemented by geophysical surveys. The bulk of the exposed sediments range in age from Middle to Late Pleistocene (Super sequence XIV) and are generally referred to as the Older Alluvium. The relevant generalized stratigraphy of the Indo-Gangetic Plain, Uttar Pradesh is given in Table 6.1 (Kumar, 2005). By considering the depth of investigation, our three study regions (Table 6.1) belong to IGP (Holocene period).

The plains associated with the rivers (Ganga, Yamuna and its tributaries) are overlain by poorly to moderately developed soils and their clear association with some rivers can be identified from satellite images (Parkash et al., 2001). The Ganga plains have been divided into three soil-geomorphic units – the Old Ganga Plain, the Young Ganga Plain and the Ganga Flood plain (Fig. 6.1c). The first two form uplands, whereas the last one has a slightly entrenched nature. Further, the former two are marked by paleochannels, which on extension to the northwest meet the active channel at Haridwar. The Old Ganga Plain has heavy loamy soils, whereas the Young Ganga Plain has sandy soils. Aeolian activity has reworked alluvial soils of the Young Ganga Plain into sand mounds up to 3 m high.

The Ganga - Solani Plain is a small unit with sandy to loamy sand soils. It is marked by water logging due to high water table in the southern parts (Parkash et al., 2001). Our study region is on a river terrace of the Solani River.

6.3 SITE LOCATION MAPS

Figure 6.1(a) illustrates the position location of the study region. Different field geoelectrical and geotechnical study locations are included in Fig. 6.1(b). The geoelectrical investigations pertain to resistivity and IP imaging data acquisition.

6.4 GEOELECTRICAL AND GEOTECHNICAL DATA ACQUISITION

An attempt was made to acquire the geoelectrical data using a micro-processor controlled multi-electrode system of French make (SYSCAL system with 72-electrodes). Relevant details of this unit are included in Chapter 3. The geotechnical data was acquired by a civil engineering company entrusted with the task of multi-storeyed building construction at the site. The geotechnical data acquired by this company has been used here for analysis.

As per the methodology outlined in Chapter 5, for prediction of both formation and geotechnical parameters, a pair of boreholes in the vicinity of geoelectrical profile was selected. The resistivity and IP images are included in Fig. 6.2. Both geoelectrical image

data columns coinciding with projected borehole positions are correlated with formation and geotechnical data available at these boreholes. Here, electrodes E-16 and E-24 of profile A-B (Fig. 6.1b) respectively correspond to projected borehole locations B-1 and B-3. Figures 6.3a and 6.3b describe the observed SPT data at borehole locations B-1 and B-3 respectively. Further analysis is described in the following sections:

Table 6.1 Generalized Stratigraphy of the Indo-Gangetic Plain (After Kumar, 2005) Pertinent Study Region

Age	Super-Sequence	Litho-stratigraphy			
		Group	Formation		Lithology
Holocene	XV	Newer Alluvium	Fluvial deposits	Lacustrine sediments of lakes (tals)	Boulders, pebbles in unoxidised sand, silt, clays of fluvial deposits, unsorted boulders in colluvial fans, Dark clay and marl in lacustrine deposits
			Channel Alluvium and Colluvial Fans		
			Terrace Alluvium		
			Alluvial Fans		Boulders, cobbles, pebbles in unoxidised sand close to Himalaya, alteration of coarse to medium sand, unoxidised further downstream Bhat Alluvial fan and other alluvial fans close to Himalaya
Middle to Late Pleistocene
	XIV	Older Alluvium	Varanasi Alluvium		Polycyclic sequence of oxidized boulder / pebble / grit beds, sand, silt-clay with calcrete Kankar Conglomerate
Late Pliocene to Early Pleistocene
Early/Middle Miocene to Early Pliocene	XIII	Upper Siwalik/Banda	Unclassified Upper Siwalik; Banda Chitrakoot Group Variegated Clays		Boulder beds, coarse sand (morrum) alternating with red clays/silt Orange and red clays with reworked laterite at base
		Middle Siwalik	Unclassified		Sandstone grading from sub greywacke to arkose with calcareous matter, coarse to medium grained
		Lower Siwalik	Unclassified		Sandstone, hard grey, variegated claystone and siltstone

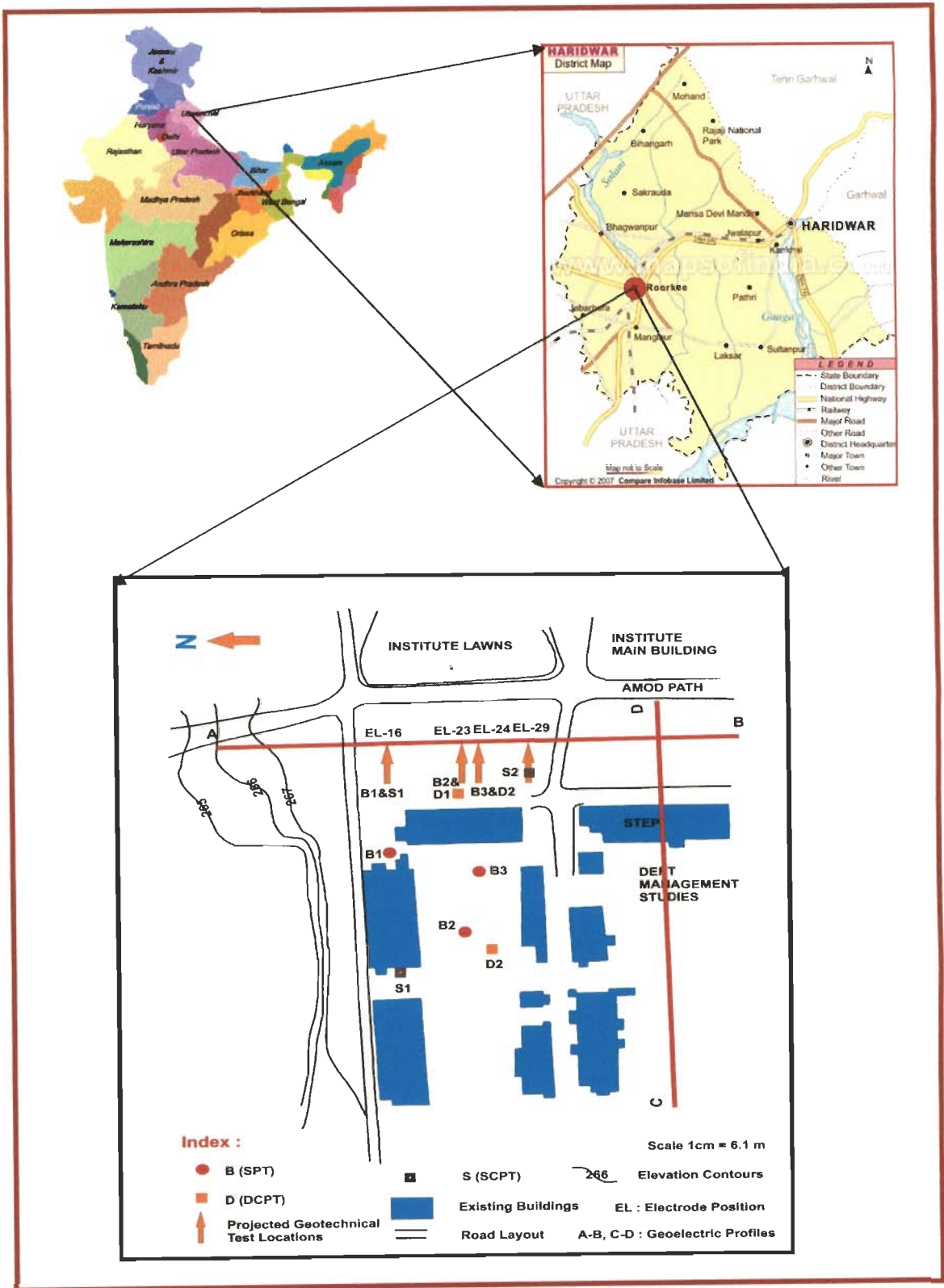


Fig. 6.1 a Location Map of Proposed Library Site, IIT Roorkee, Roorkee, India

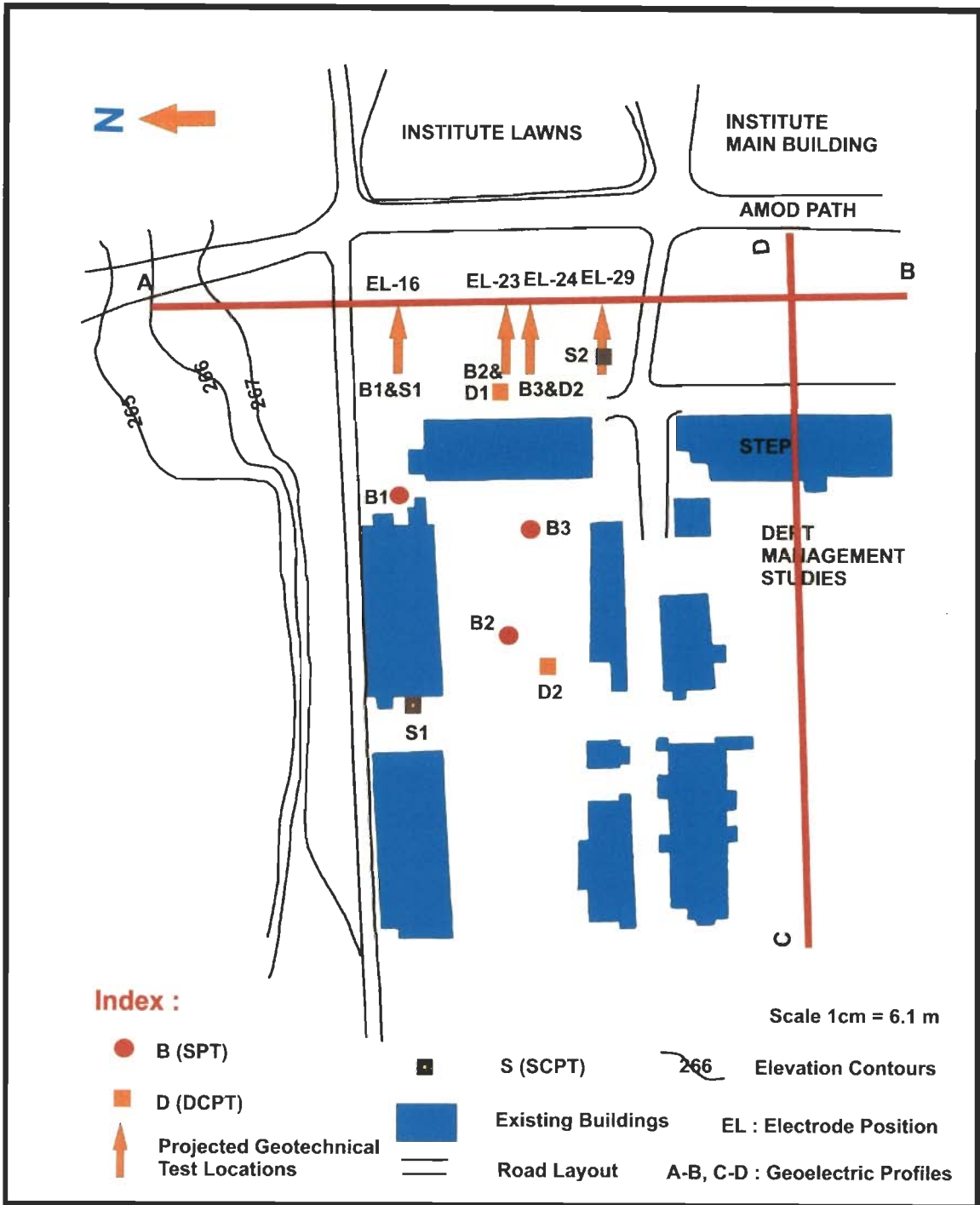


Fig. 6.1 b Map Showing the Location of ERT, IPI and Geotechnical Site Investigations

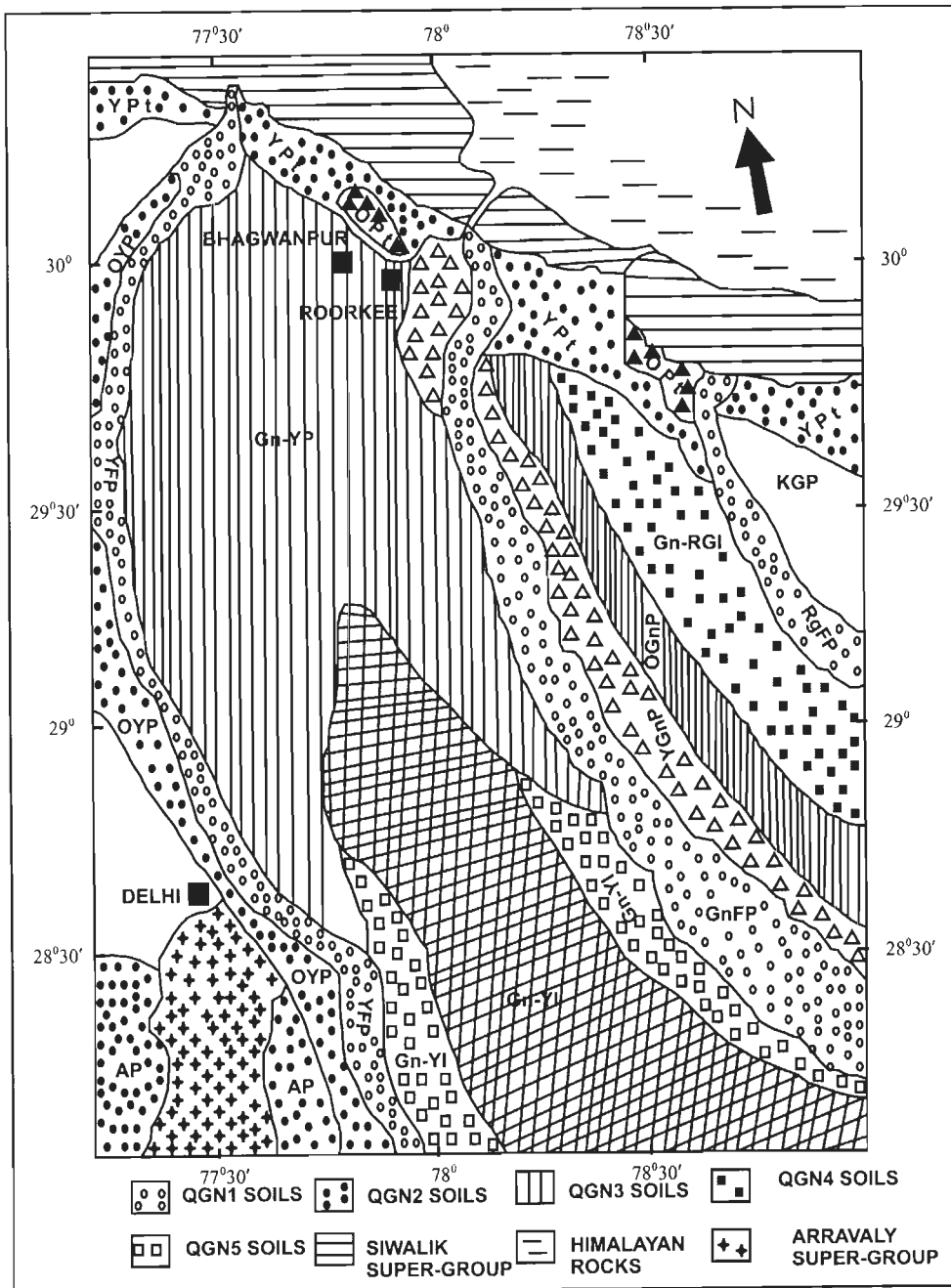


Fig. 6.1 c Geological (Soil-Geomorphic) Map of the Study Region. GnFP-Ganga Floodplain; YGP-Young Ganga Plain; OGnP-Old Ganga Plain; GnRGI-Ganga-Ramganga Interfluev; KGP-Kosi-Gola Plain; Gn-YP-Ganga-Yamuna Plain; Gn-YI-Ganga-Yamuna Interfluev, SA-Salt Affected, NSA-Not Salt-Affected, YPt-Young Piedmont, Opt-Old Piedmont (Parkash et al. 2000, 2001)

6.5 REGRESSION EQUATIONS FOR SPT AND SCPT

By utilizing the methodology outlined in Chapter 5, regression equations have been developed for both formation and geotechnical parameters for profile A-B (Fig. 6.1b). The involved procedure is explained below:

6.5.1 Regression Equation for SPT

In Figs. 6.4a and 6.4b normalized plots of SPT 'N', resistivity, IP and fictitious resistivity (Ficres) are made respectively for boreholes B-1 and B-3. These provide a general idea of available correlations of SPT 'N' with resistivity, IP and fictitious resistivity (Ficres) data. The regression equations for normalized SPT 'N' are developed based on both resistivity and IP data for borehole location B-1 in Figs. 6.4c and 6.4g respectively. Similar exercise has been carried out for borehole location B-3 in case of resistivity and IP (Figs. 6.4e and 6.4i) respectively. The predicted SPT on the basis of resistivity and IP for boreholes locations B-1 and B-3 are presented in Figs. 6.4d & f and 6.4h & j respectively. These clearly illustrate that resistivity based predicted of SPT values profile matches well with the observed profiles at boreholes B-1 and B-3 in comparison to that derived from IP data.

6.5.2 Regression Equation for SCPT

Figures 6.5a and 6.5b describe the observed SCPT data corresponding to the electrode location EL-16 and EL-29 of profile A-B. In Figs. 6.6a and 6.6b normalized plots of SCPT, resistivity, IP and fictitious resistivity (Ficres) are made respectively. These provide a general idea of the available correlations of SCPT with resistivity, IP and ficres data. The regression equations for normalized SCPT have been developed based on resistivity (Figs. 6.6g and 6.6i) and IP data (Figs. 6.6c and 6.6e) for electrode locations EL-16 and EL-29 respectively. The predicted SCPT on the basis of IP and resistivity for locations EL-16 and EL-29 are presented in Figs. 6.6d & 6.6f and 6.6h & 6.6j respectively.

6.6 REGRESSION EQUATIONS FOR SAND, CLAY, LITHOLOGY, POROSITY AND WATER SATURATION

Analysis of soil samples in geotechnical laboratory leads to estimation of sand (%), clay (%), lithology, porosity (%) and water saturation (%) for each borehole. For the soil types encountered in the study regions, a clear code varying within zero and unity is developed for resistivity and IP (Table 5.1).

Here, a pair of boreholes, B-1 and B-3 has been projected onto the geoelectrical profile A-B towards preparation of predicted sections of sand, shale, lithology, porosity and water saturation. Initially, correlations with normalized resistivity, IP and fictitious resistivity pertaining to B-1 and B-3 borehole positions on selected geoelectrical profile (profile A-B in Figs. 6.7a and 6.7b) have been developed.

Later, one of the geoelectrical options (IP / Resistivity / Fictives) is selected and regression equation was developed accordingly for each of the formation parameters. Then, the specific regression equation has been used in transforming the earlier opted geoelectrical image into formation parameter sections.

In Figs. 6.7a, 6.7g, 6.8a, 6.9a and 6.10a, normalized plots of sand, clay, lithology, porosity and water saturation versus resistivity, IP and fictitious resistivity (Fictives) have been presented respectively for borehole B-1. In Figs. 6.7b, 6.7h, 6.8b, 6.9b and 6.10b, normalized plots of sand, clay, lithology, porosity and water saturation versus resistivity, IP and fictitious resistivity (Fictives) have been made respectively for borehole B-3. These provide a general idea of available correlation of sand, clay, lithology, porosity, water saturation, resistivity, and IP and fictives data along chosen Profile A-B.

The regression equations have been developed as per earlier outlined procedure and included in Table 6.2. Accordingly, the predicted profiles for sand (Figs. 6.7c & 6.7d, 6.7e & 6.7f), clay (Figs. 6.7k & 6.7l, 6.7i & 6.7j), lithology (Figs. 6.8c & 6.8d, 6.8e & 6.8f), porosity (Figs. 6.9c & 6.9d, 6.9e & 6.9f), and water saturation (Figs. 6.10c & 6.10d, 6.10e & 6.10f) profiles have been developed based on IP and resistivity data for both boreholes B-1 and B-3.

Table 6.2 Inferred Regression Equations Based on Borehole and Geoelectrical Depth Profiles Gathered from Respective Geoelectrical Images at Projected Borehole Positions onto Geoelectrical Profile A-B at Library Site, IITR

S. No.	Formation Parameter / Geotechnical Parameter	Correlation equation based on IP at B-1 (EL-16) $Y=a_1x^2+a_2x+a_3$	Correlation equation based on IP at B-3 (EL - 24) $Y=b_1x^2+b_2x+b_3$	Average Correlation equation based on IP at B-1 & B-3 $Y=c_1x^2+c_2x+c_3$ [$c_1=av(a_1,b_1)$, $c_2=av(a_2,b_2)$, $c_3=av(a_3,b_3)$]
1	Sand	a = {0.0892, 0.0064, 0.8899} R2 = 0.3607	b = {-0.6573, 0.6526, 0.8194} R2 = 0.3219	a= {- 0.28405, 0.3231, 0.85475}
2	Clay / Shale	a = {-0.2641, 0.064, 0.3078} R2 = 0.3716	b = {1.6584, - 1.6466, 0.4966} R2 = 0.3219	a= {0.69715, - 0.7913, 0.4022}
3	Lithology	a = {1.434, 1.3844, 0.7582} R2 = 0.5247	b = {0.0504, 0.1187, 0.6244} R2 = 0.106	a={0.7422, - 0.63285, 0.6913}
4	SPT	a = {0.0744, 0.075, 0.7218} R2 = 0.0018	b = {-1.1981, 1.442, 0.4985} R2 = 0.6354	a= {- 0.56185, 0.5346, 0.61015}
5	DCPT	a = {18.654, - 3.286, 0.3783} R2 = 0.2769 DCPT 1 at EL-23	b = {1.8596, 0.8923, 0.1657} R2 = 0.4878 DCPT 2 at EL-24	a={10.2568, - 1.19685, 0.272}
6	SCPT	a = {0.1104, 0.3623, 0.2761} R2 = 0.4862 SCPT 1 at EL-16	b = {-2.1013, 2.3044, 0.3564} R2 = 0.5578 SCPT 2 at EL-29	a= {- 0.99545, 1.33335, 0.31625}
7	Porosity	a = {0.0867, - 0.0034, 0.8892} R2 = 0.3634	b = {-0.6352, 0.643, 0.8181} R2 = 0.3298	a={ - 0.27425, 0.3198, 0.85365}
8	Water saturation	a = {-2.5298, 3.0381, 0.0865} R2 = 0.6628	b={ -2.4126, 2.3639, 0.1511} R2 = 0.4649	a= {- 2.4712, 2.701, 0.1188}

6.7 REGRESSION EQUATIONS FOR UNIT WEIGHT OF SOIL (DRY & SATURATED), UNCONFINED COMPRESSIVE STRENGTH, q_u , INTERNAL FRICTION ANGLE, ϕ AND BEARING CAPACITY FACTORS (SHALLOW AND DEEP INVESTIGATIONS)

As detailed in Chapter 5, based on geotechnical literature (Murthy, 2008), the regression equations have been developed for i) unit weights of soil (both dry & saturated) versus water saturation and porosity, ii) unconfined compressive strength, q_u versus SPT 'N', iii) SPT 'N' versus internal angle friction, ϕ and in turn, iv) internal angle friction, ϕ versus Terzaghi's bearing capacity coefficients, Terzaghi's Bearing Capacity factors (Peck et al., 1974) N_γ & N_q , general bearing capacity factors, N_q , N_c & N_γ (Vesic), ultimate bearing capacity factors, N_q , N_c & N_γ , bearing capacity factor N_q (Vesic) for bored piles, bearing capacity factor N_q (Meyerhof, 1953) for bored piles and bearing capacity factor N_q (Meyerhof, 1953) for driven piles. All these regression equations have already been included in Table 4.10.

6.8 GENERATION OF FORMATION AND GEOTECHNICAL PARAMETER SECTIONS

The regression equations developed earlier (Tables 4.10 and 6.2) have been utilized to transform IP / resistivity sections along profile A-B into different formation and geotechnical parameter sections. All the illustrations are appended at the end of this chapter and Table 6.3 summarizes the salient features of them.

6.8.1 Formation Parameter Sections

Resistivity based lithology, porosity and water saturation sections are presented in Figs. 6.8g, 6.9g and 6.10g. In Figs. 6.11a & b and 6.13a & b, sand sections arrived at through IP and resistivity are presented. In Figs. 6.12a & b, 6.14a & b, clay sections arrived at through IP and resistivity means are presented.

6.8.2 Geotechnical Parameter Sections (SPT, SCPT)

As indicated earlier, in the validation phase, resistivity derived SPT (Figs. 6.4c & e) profiles match well with those of observed ones at borehole locations B-1 and B-3 in

comparison to those of IP (Figs.6.4h & j) respectively. So, the relevant regression equations (Figs. 6.4c & e) were used in deriving SPT section from resistivity section along Profile A-B (Fig. 6.15b). However, for completeness, IP derived SPT section is also included in Fig. 6.15a.

For SCPT case, in the validation phase, resistivity derived SCPT profiles (Figs. 6.6h & j) match well with those of observed ones at locations EL-16 and EL-29 in comparison to those of IP derived ones (6.6d & f). Figures 6.16a and 6.17b IP and resistivity derived SCPT sections are presented. However, resistivity derived SPT and SCPT sections (Figs. 6.15b and 6.16b) can be relied upon.

6.8.3 Unconfined Compressive Strength (q_u) and Internal Friction Angle (ϕ) Section

Using resistivity section, q_u section has been derived and presented in Fig. 6.20. As per section 6.7.2, resistivity derived SPT performs well in comparison to that of IP derived one. So, all geotechnical sections have been derived from resistivity section along Profile A-B using respective regression equations of Table 4.10. Accordingly, Fig. 6.17b represents predicted internal friction angle section along Profile A-B. Resistivity derived bearing capacity sections are discussed in the next section.

6.8.4 Bearing Capacity Sections

In Figs. 6.21-6.23 sections for general bearing capacity coefficients for general shear failure (N_c , N_γ (Vesic), and N_q) are presented. In Figs. 6.24-6.26, bearing capacity coefficients (N_c , N_γ , and N_q) sections are presented for strip footings. In Figs. 6.27-6.28, Terzaghi's bearing capacity coefficients (N_γ , N_q) sections are presented. In Figs. 6.29-6.30, sections for bearing capacity coefficients (N_q (Meyerhof, 1953), N_q (Vesic)) for bored piles are presented. Section for bearing capacity coefficient N_q (Meyerhof, 1953) for driven piles has been presented in Fig. 6.31.

Table 6.3 Details of Illustrations

S. No.	Formation / Geotechnical Parameter		Fig. No.		Remarks
			Resistivity	IP	
1.	Sand	Res. / IP derived	Fig. 6.11 b	Fig. 6.11 a	Based on borehole data, it is clear that resistivity data predicts better than IP. So, resistivity derived sand section in Fig. 6.13b predicts predominantly sand up to 30m depth. The presence of shaly sands around 12m depth is predicted by Fig. 6.11b.
		Geotechnical Derived	Figs. 6.7a & b,e,f, 6.13b	Figs. 6.7a & b, c, d, 6.13a	
2.	Clay / Shale	Res. / IP derived	Fig. 6.12 b	Fig. 6.12 a	Resistivity data predicts better than IP. Accordingly, Fig. 6.14b needs to be consulted for further analysis.
		Geotechnical Derived	Figs. 6.7g & h, i, j, 6.14b	Figs. 6.7g & h, k, l, 6.14a	
3.	Lithology		Figs. 6.8a & b, e, f, g	Figs. 6.8a & b, c, d	Resistivity data predicts lithology better than IP. So, Fig. 6.8g can be adopted as subsurface lithology section along Profile AB.
4.	SPT		Figs. 6.4a & b, 6.4c-f, 6.15b	Figs. 6.4a & b, 6.4g-j, 6.15a	Resistivity data predicts SPT better than that of IP (Ref. Figs. 6.4d & f and Figs. 6.4 h & j)
5.	SCPT		Figs. 6.6a & b, 6.6g-j, 6.16b	Figs. 6.6a & b, 6.6c-f, 6.16a	Resistivity data predicts SCPT better than that of IP
6.	Porosity		Figs. 6.9a & b, 6.9e, f	Figs. 6.9a & b, 6.9c, d	Resistivity data predicts porosity better than that of IP
7.	Water saturation		Figs. 6.10 a & b, 6.10e, f	Figs. 6.10 a & b, 6.10c, d	IP data predicts water saturation better than that of resistivity (Ref. Figs. 6.10c & d and Fig. 6.10e & f)
8.	Unit weight of soil	Dry	Fig.6.18b	Fig.6.18a	Resistivity derived unit weight sections are preferable
		Saturated	Fig.6.19b	Fig.6.19a	
9.	Angle of internal friction, ϕ		Fig. 6.17b	Fig. 6.17a	Resistivity derived ϕ section is preferable
10.	Unconfined compressive strength, q_u		Fig. 6.20		Since resistivity derived SPT scores over that of IP, q_u and all the bearing capacity sections are derived from resistivity section. IP derived bearing sections are not included for the same reason. The resistivity derived bearing capacity factor sections reveal a 4-layer structure with undulating 2-D interfaces unlike usual 1-D structures often adopted by geotechnical engineers.
11.	Terzaghi's Bearing Capacity factors (Peck et al. 1974)	N_y factor	Fig. 6.27		
		N_q factor	Fig. 6.28		
12.	Bearing capacity factors for general shear failure	N_c factor	Fig. 6.21		
		N_y (Vesic) factor	Fig. 6.22		
		N_q factor	Fig. 6.23		
13.	Ultimate bearing capacity factors	N_c factor	Fig. 6.24		
		N_y factor	Fig. 6.25		
		N_q factor	Fig. 6.26		
14.	Piles	Driven Piles N_q (Meyerhof, 1953) factor	Fig. 6.29		
		Bored Piles N_q (Meyerhof, 1953) factor	Fig. 6.30		
		Bored Piles N_q (Vesic, 1953) factor	Fig. 6.31		

6.9 RESULTS & DISCUSSION

The methodology adopted herein honors both geoelectrical and geotechnical data. The development of regression equations rests on a pair of boreholes that are projected onto the geoelectrical profile and the resistivity and IP data at those electrode positions. The regression equations are limited to 2nd degree polynomial only as higher order polynomial involves the usual mathematical difficulties as perceived in regional-residual separation for gravity data processing (Dobrin, 1976). In the present case study, excepting for prediction of water saturation, resistivity based prediction of formation and profiles for geotechnical parameter are better correlated with the actual ones in comparison to IP derived ones. However, for completeness sake, IP derived profiles and sections are also included here. In this regard, Table 6.3 contains all relevant details. Additionally, the followings remarks need to be considered:

- a) It is clear from Figs. 6.7 c, d, e & f that prediction based on resistivity data is better than IP in sand estimation. Further, resistivity derived sand section (Fig. 6.13b) shows the presence of sand up to 30 m depth; Whereas the presence of shaly sands around 12 m depth is indicated in Fig. 6.11b.
- b) Figures 6.7 i, j, and k and also clearly indicate that clay / shale prediction through resistivity is better than that of IP. So, predicted 2-D clay / shale section is worth considering.
- c) Figures 6.8 c, d, e and f demonstrate that resistivity derived lithology compares better with the real one (geotechnical borehole derived) than that of IP based one. So, resistivity predicted lithology section in Fig. 6.8 g can used for analysis.
- d) Figures 6.9c, d, e and f show that resistivity based predicted porosity profile matches well with that of actual ones. Accordingly, resistivity based 2-D porosity section (Fig. 6.9g) can be relied upon.
- e) Figures 6.10 c, d, e and f imply that resistivity based prediction profile for water saturation is better in comparison to that of IP derived. Hence, the 2-D water saturation section derived from resistivity is included here.
- f) For prediction of unit weight (dry & saturated) of soil sections, geotechnical literature based regression equations included in our Table 4.10 are utilized. Here,

water saturation has been used as basic input data. Even though, we present both resistivity (Fig. 6.18b & 6.19b) and IP derived (Fig. 6.18a & 6.19a) versions, resistivity derived unit weight sections can be adopted for use.

- g) Resistivity derived SCPT profiles (Figs. 6.6h, j) match with real ones in a better manner than IP derived ones (Figs. 6.6 d, f). Further, resistivity derived SCPT profiles exhibit a phase lag with respect to real ones.
- h) Figures 6.4d, f, h and j also show that resistivity derived SPT matches well with the actual ones for a pair of boreholes when compared to those derived from IP data. Accordingly, resistivity based (predicted) 2-D SPT section in Fig. 6.15b along Profile AB is better than that of IP derived one (Fig. 6.15a).
- i) Earlier resistivity derived SPT section has been utilized in arriving at unconfined compressive strength section (Fig. 6.20). As per geotechnical standards (Murthy, 2008), the achieved range of variation in q_u in Fig. 6.20 is well within the prescribed limits and it can be used.
- j) The 2-D section for angle of internal friction derived from resistivity (Fig. 6.17b) is recommended in comparison to that of IP derived one (Fig. 6.17a). All bearing capacity sections are predicted with this section as input and relevant regression equations included in Table 4.10 acting as transformations.
- k) Resistivity derived SPT section is used to derive angle of internal angle the section for friction section (Fig. 6.17b), which in turn is used to obtain sections different bearing capacity coefficients (Figs. 6.21-6.31) through the relevant regression equations tabulated in Table 4.10. Thus, sections of predicted bearing capacity factors (Figs. 6.21-6.31) broadly reveal a 4-layer structure with undulating 2-D interfaces. These in turn can be utilized to derive traditional 1-D geotechnical models, unlike usual 1-D structures often adopted by geotechnical engineers.
- l) No attempt has been made here to obtain sections for the bearing capacity factors based on CPT method. However, earlier outlined procedure for SPT 'N' can easily be extended to CPT method also.
- m) The present procedure is applicable to soil strata only, where conventional geotechnical tests are valid.

- n) The quality of input geo-electric sections affect inferred lithology, formation and geotechnical sections. So, basic data quality of geo-electrical data and attendant processing and inversion schemes has to be very high.
- o) The regression equations included in Table 4.10 have remained constant throughout the study and they are based on current geotechnical literature.
- p) The regression equations listed in Table 6.2 are site-specific and geo-electrical profile specific.
- q) All inferred 2-D sections clearly show that 1-D models often resorted to by geotechnical engineers are far from reality and efforts are needed to refine their quality or new procedures need to be evolved. The present effort is geared towards that goal.

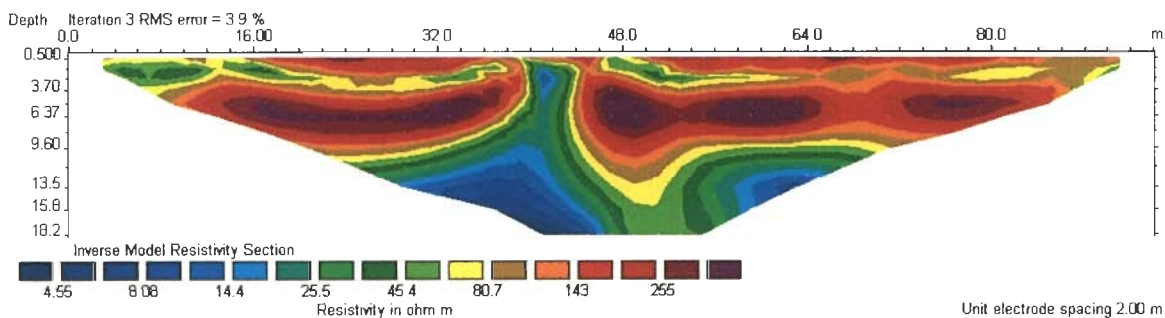


Fig. 6.2 a Resistivity Image (ERT) Along Profile A-B. The Resistivity (ohm-m) and Depth Scales are Logarithmic

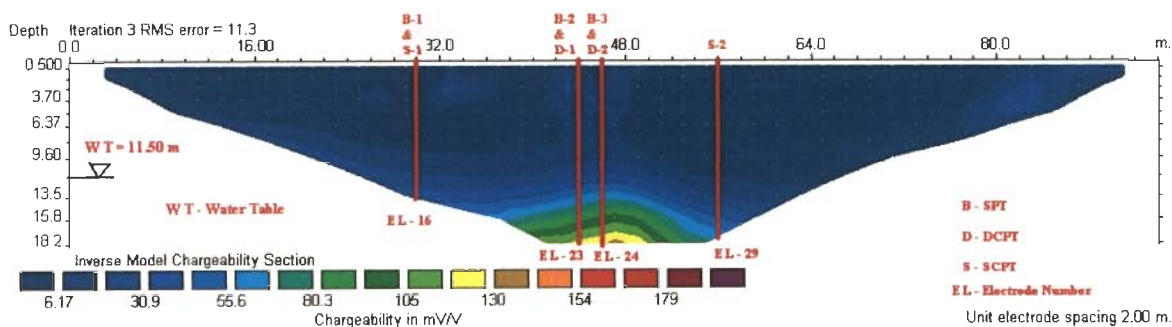
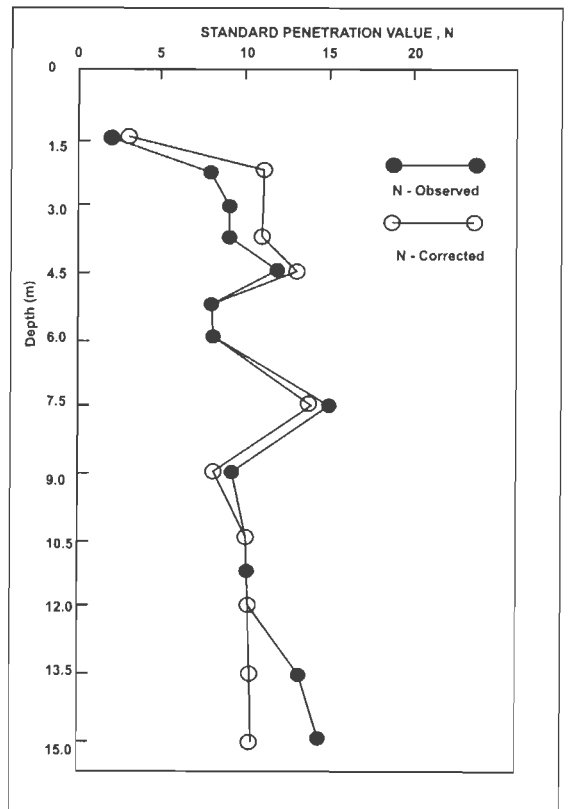


Fig. 6.2 b IP Image (IPI) Along Profile A-B. The IP Chargeability (mSec) and Depth Scales are Logarithmic

Depth (m)	Classification		Grain Size Distribution		Natural Water Content (%)	Calculated Porosity (Phi) (%)
	Symbol	Hatching	Sand (%)	Fines (%)		
1.5	SP-SM	[Hatching pattern]	88.2	11.1	6.2	38.81
3.0			89.8	10.2	8.0	39.51
4.5			90.4	9.6	7.1	39.78
6.0	SM	[Hatching pattern]	75.6	23.3	7.2	33.26
7.5	SP-SM	[Hatching pattern]	94.0	5.2	7.1	41.36
9.0	CI	[Hatching pattern]	88.1	11.9	28.1	38.76
10.5			5.1	94.9	38.2	2.24
12.0			10.0	90.0	39.9	4.40
13.5	SP	[Hatching pattern]	95.5	4.5	27.6	42.02
15.0			95.0	5.0	28.1	41.8
16.5						

Borehole B-1

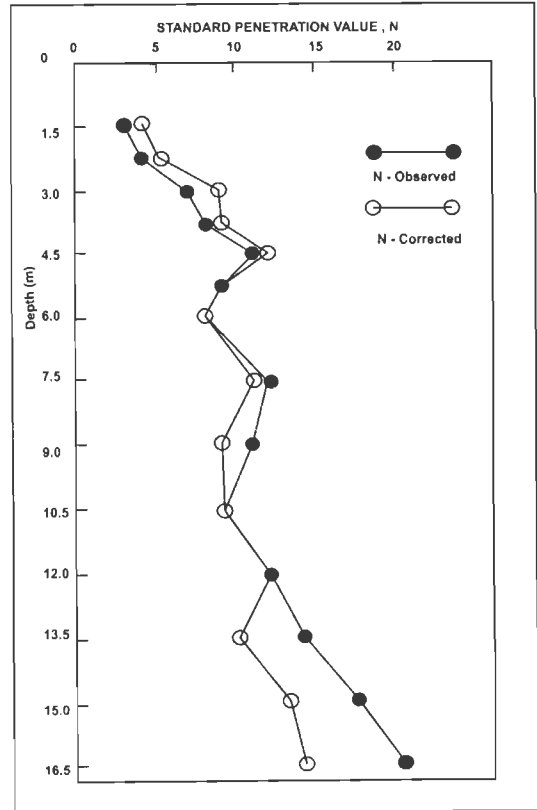


SPT DATA

Fig. 6.3 a Borehole Data at Location B-1. The Projected Borehole Position Coincides with Electrode, EL-16 of profile A-B

Depth (m)	Classification		Grain Size Distribution		Natural Water Content (%)	Calculated Porosity (Phi) (%)
	Symbol	Hatching	Sand (%)	Fines (%)		
1.5	SM	[Vertical lines]	70.7	29.3	9.8	31.11
			70.5	29.5	12.2	31.02
3.0			68.2	31.8	11.5	30.01
			87.9	12.1	6.8	38.68
4.5	SP-SM	[Diagonal lines]	85.0	15.0	6.5	37.4
			92.6	7.4	6.5	40.74
6.0			91.8	8.2	6.3	40.39
7.5	CI	[Cross-hatch]	94.5	5.5	29.7	41.58
9.0			6.8	93.2	19.9	2.99
10.5	SP-SM	[Diagonal lines]	89.5	10.5	27.0	39.38
12.0			95.0	5.0	30.8	41.8
13.5	SP	[Dotted]	95.8	4.2	30.4	42.15
15.0			97.0	3.0	24.3	42.68
16.5						

Borehole B-3



SPT DATA

Fig. 6.3 b Borehole Data at Location B-3. The Projected Borehole Position Coincides with Electrode, EL-24 of profile A-B

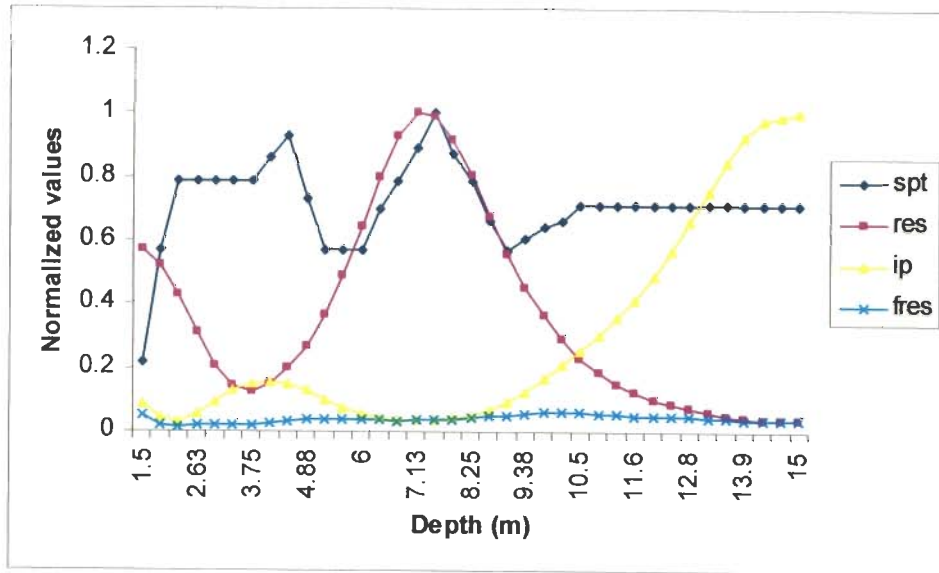


Fig. 6.4 a Plot of SPT N-Values versus Resistivity, IP and Fictitious Resistivity (EL-16) at Borehole Location- B-1 of Profile A-B

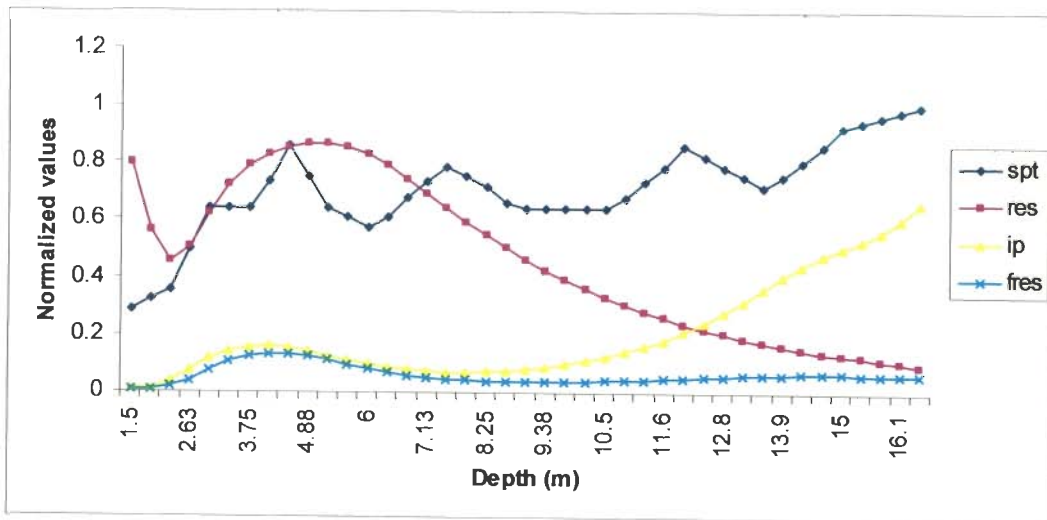


Fig. 6.4 b Plot of SPT N-Values versus Resistivity, IP and Fictitious Resistivity (EL-24) at Borehole Location- B-3 of Profile A-B

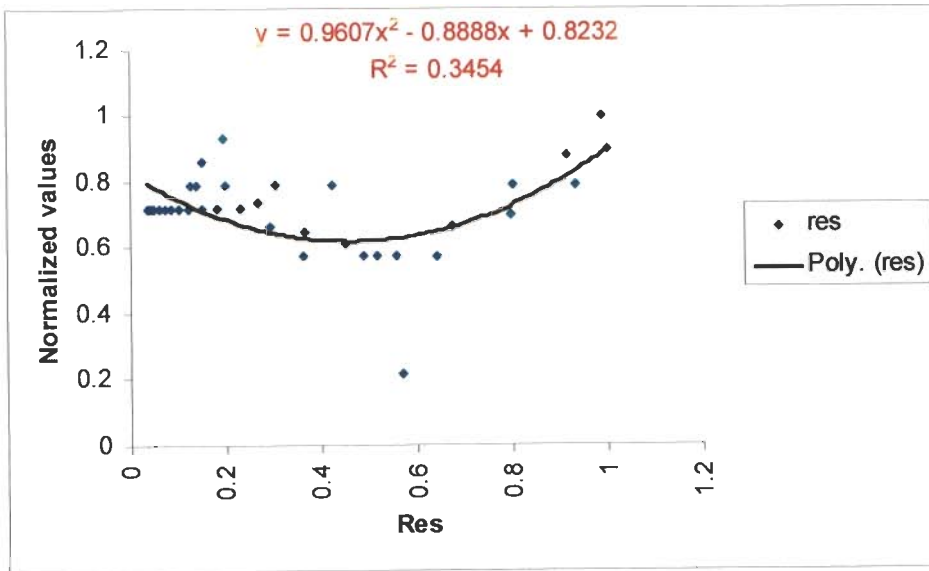


Fig. 6.4 c Plot of SPT N-Values versus Resistivity at Borehole Location- B-1

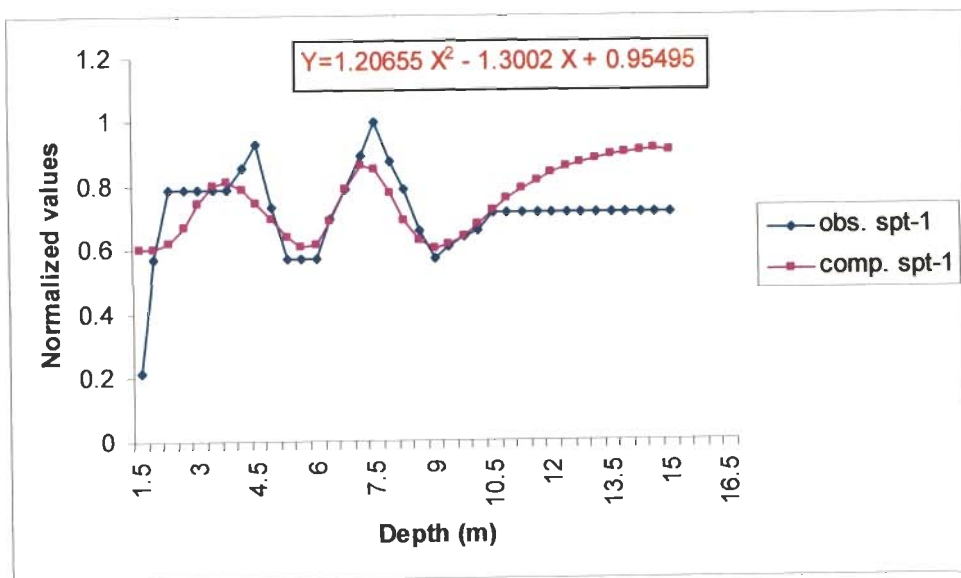


Fig. 6.4 d Plot of Observed versus Computed SPT Through Resistivity at Borehole Location- B-1

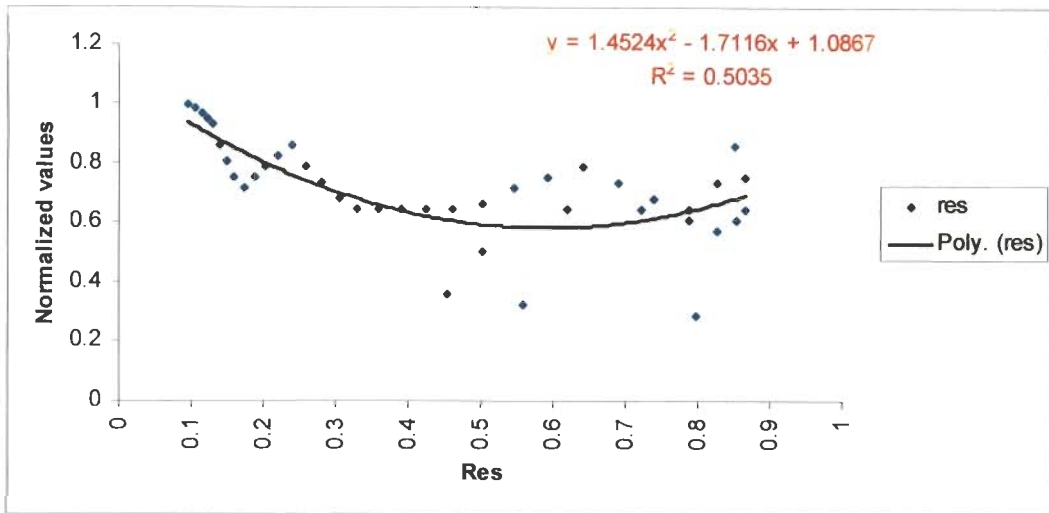


Fig. 6.4 e Plot of SPT versus Resistivity at Borehole Location- B-3

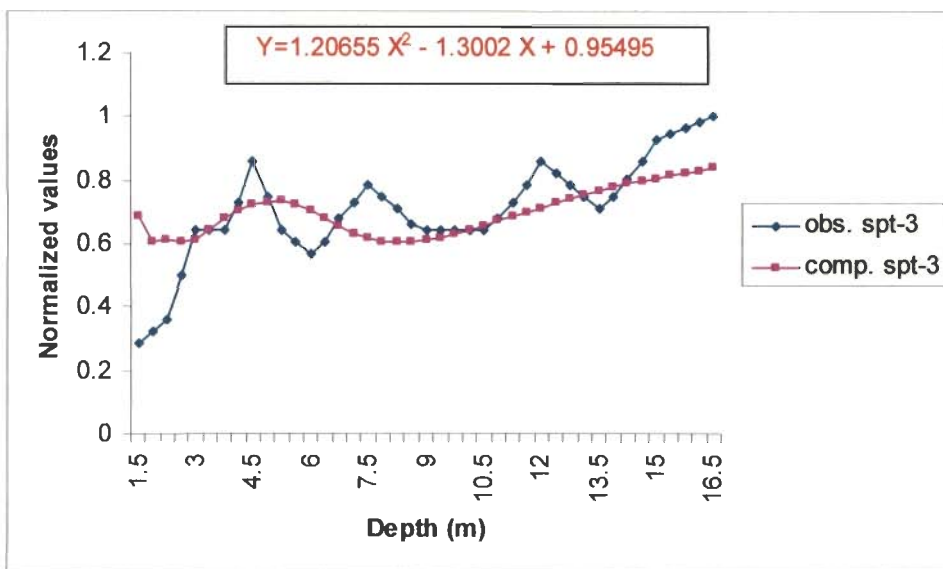


Fig. 6.4 f Plot of Observed versus Computed SPT Through Resistivity at Borehole Location- B-3

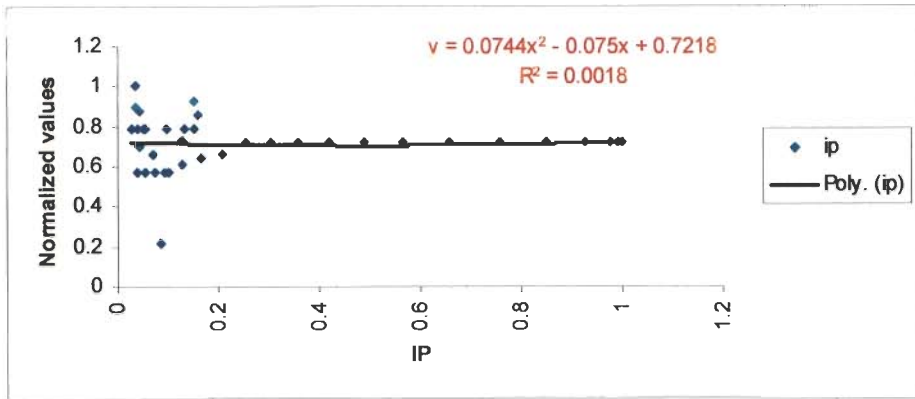


Fig. 6.4 g Plot of SPT N-Values versus IP at Borehole Location- B-1

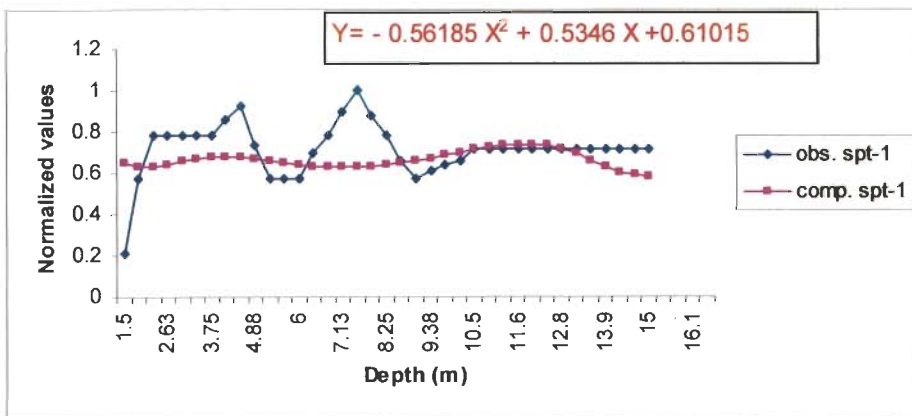


Fig. 6.4 h Plot of Observed versus Computed SPT Through IP at Borehole Location- B-1

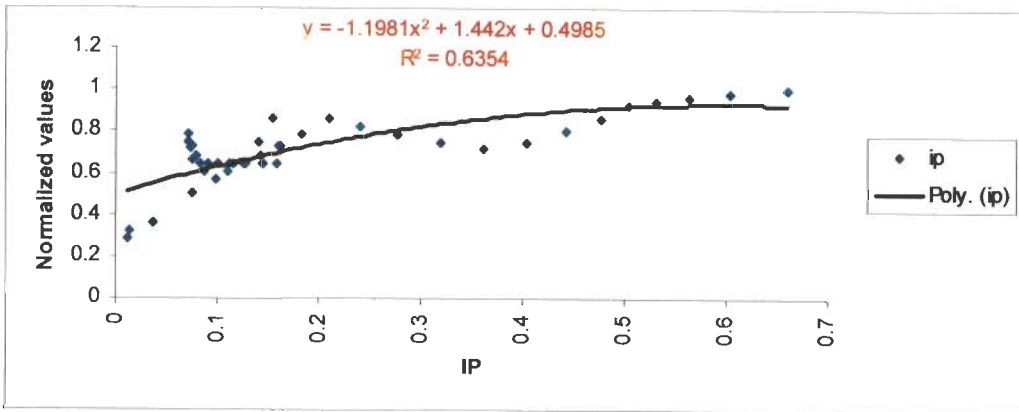


Fig. 6.4 i Plot of SPT N-Values versus IP at Borehole Location- B-3

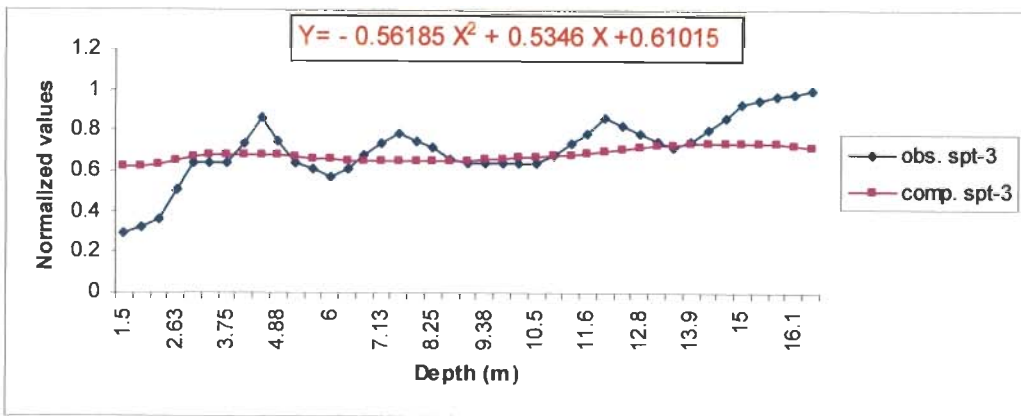
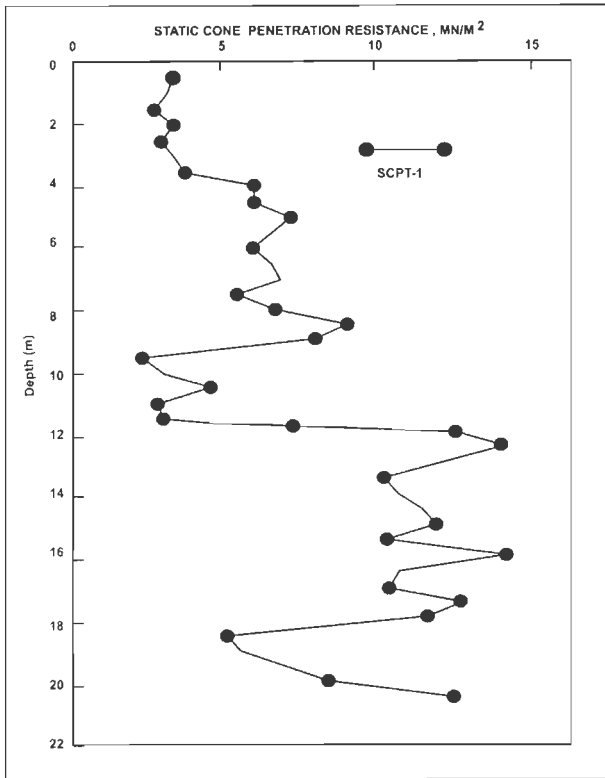
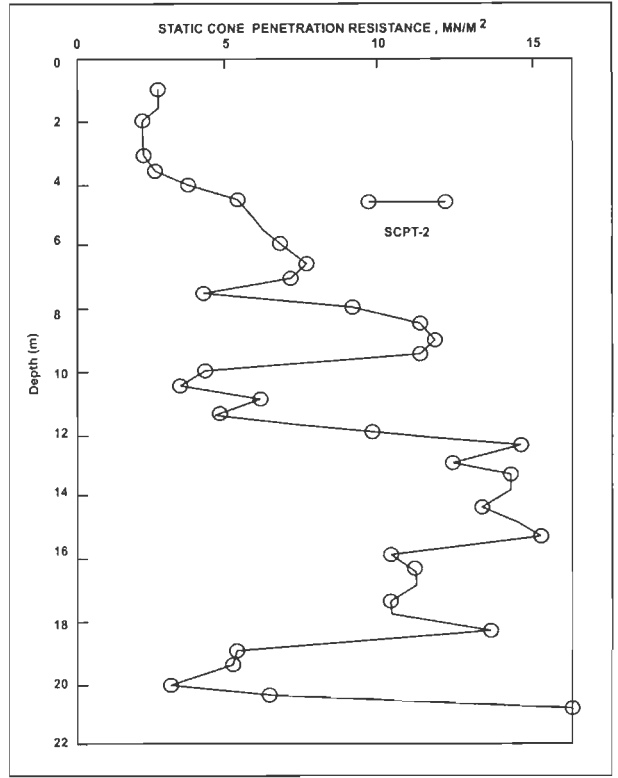


Fig. 6.4 j Plot of Observed versus Computed SPT Through IP at Borehole Location- B-3



a) SCPT-1



b) SCPT-2

Fig. 6.5 a) SCPT-1 Data. The Corresponding Electrode Position is EL-16 of Profile A-B

b) SCPT-2 Data. The Corresponding Electrode Position is EL-29 of Profile A-B

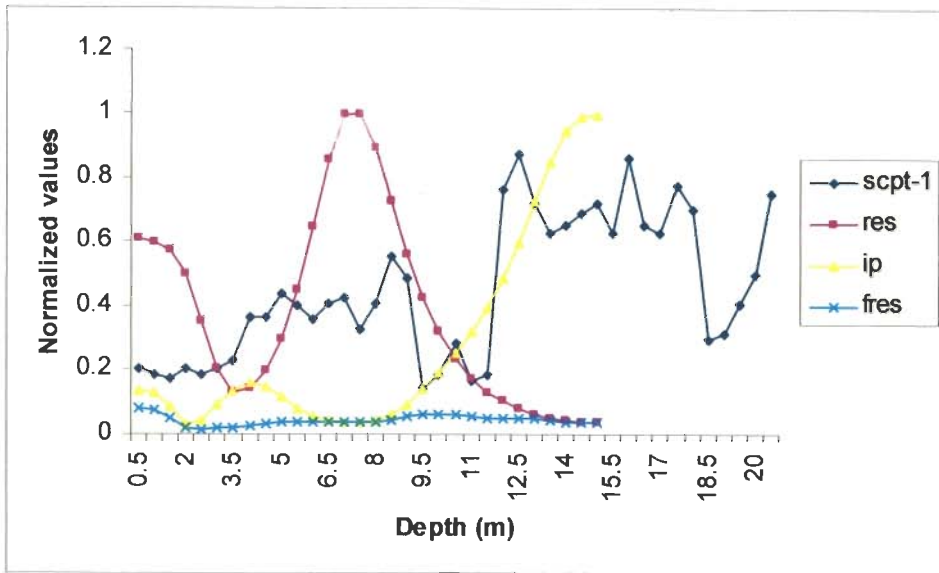


Fig. 6.6 a Plot of Observed SCPT-1, Resistivity, IP and Fictitious Resistivity at the Electrode Location- EL-16 of Profile A-B

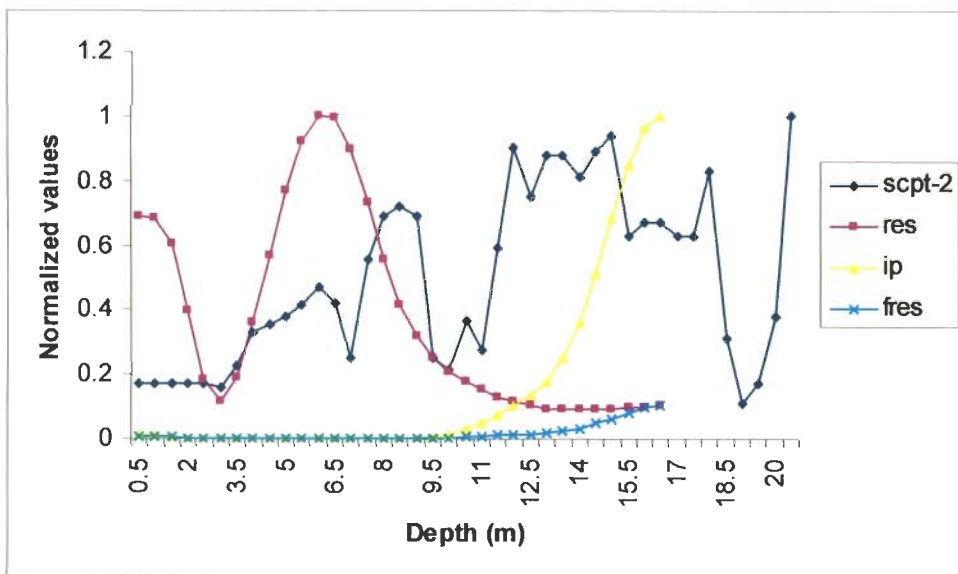


Fig. 6.6 b Plot of Observed SCPT-2, Resistivity, IP and Fictitious Resistivity at the Electrode Location - EL-29 of Profile A-B

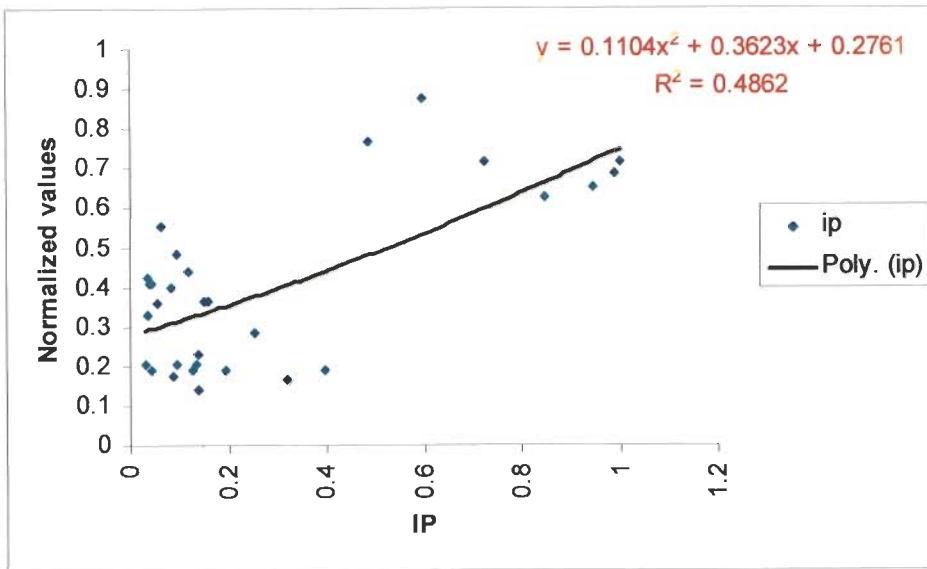


Fig. 6.6 c Plot of SCPT-1 versus IP at EL-16

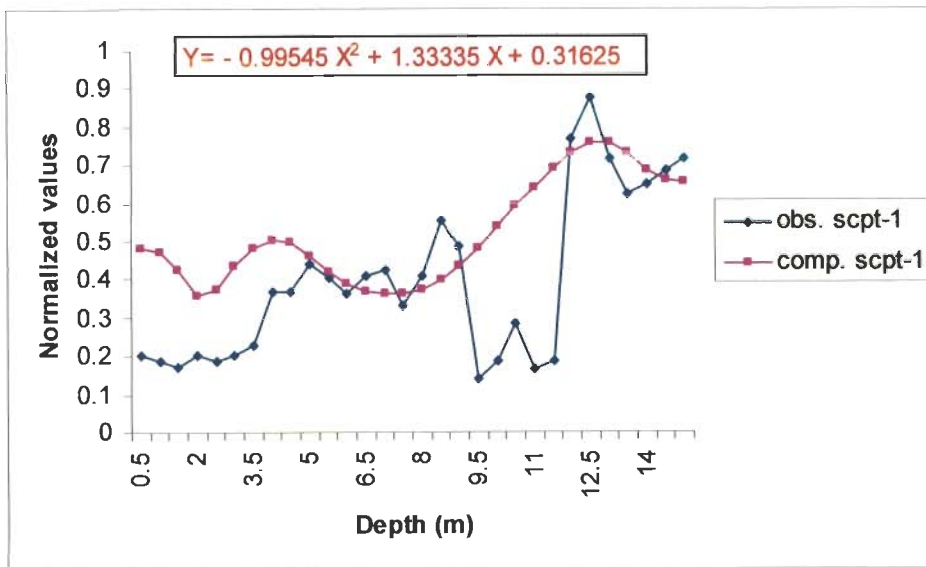


Fig. 6.6 d Plot of Observed versus Computed SCPT-1 at EL-16 Using IP

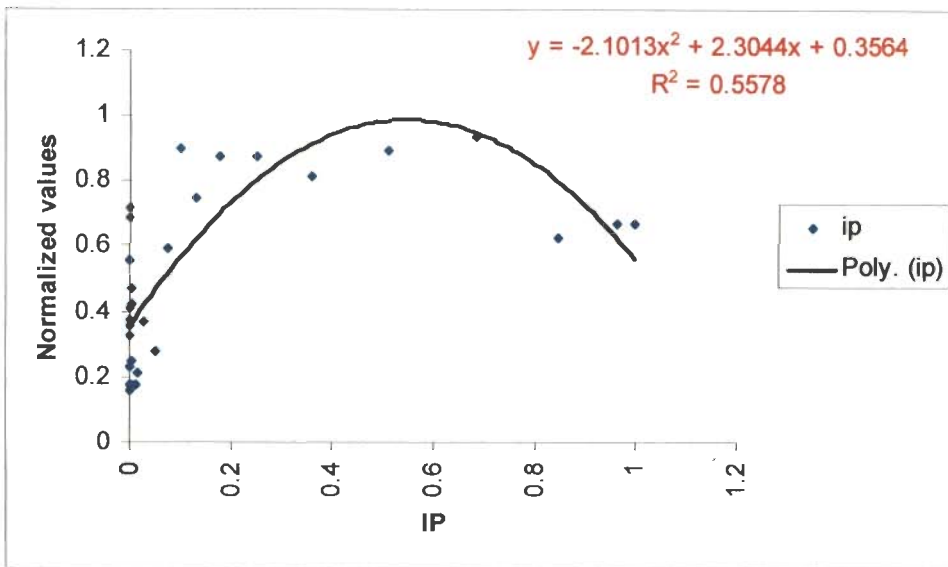


Fig. 6.6 e Plot of SCPT-2 versus IP at EL-29

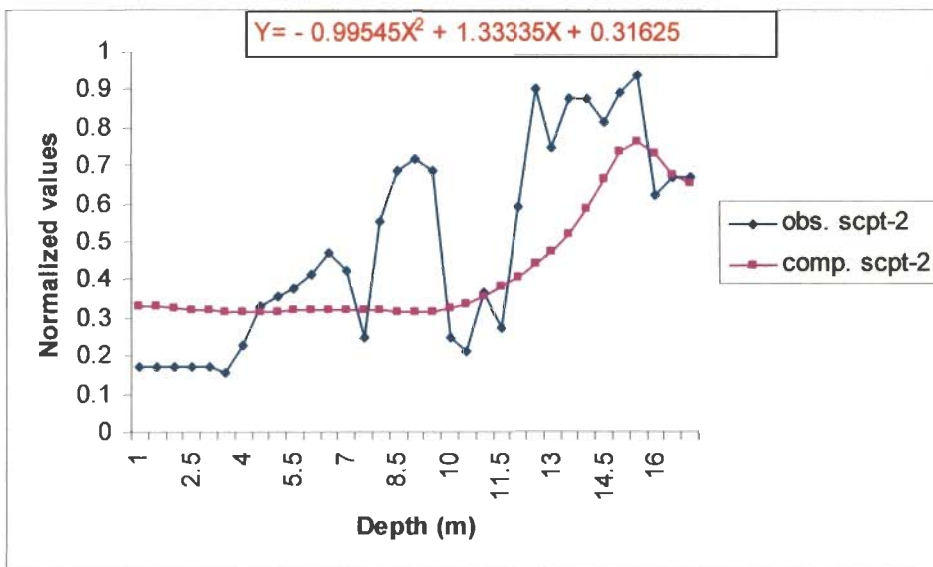


Fig. 6.6 f Plot of Observed versus Computed SCPT-2 at EL-29 Using IP

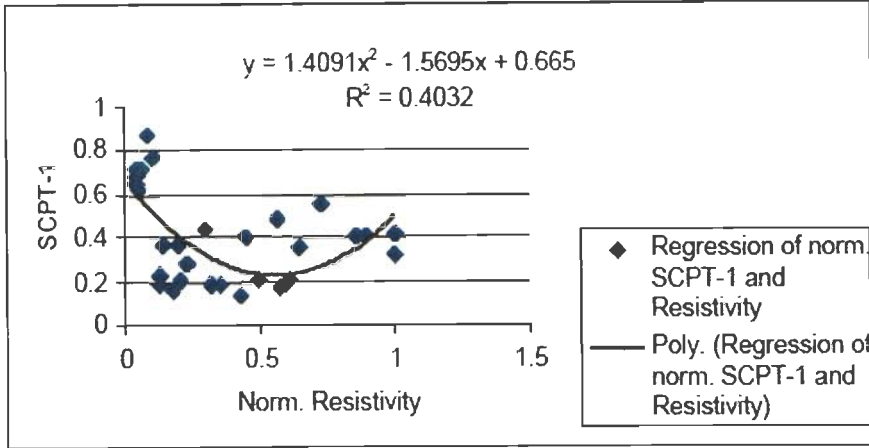


Fig. 6.6 g Regression of SCPT-1 with Normalized Resistivity

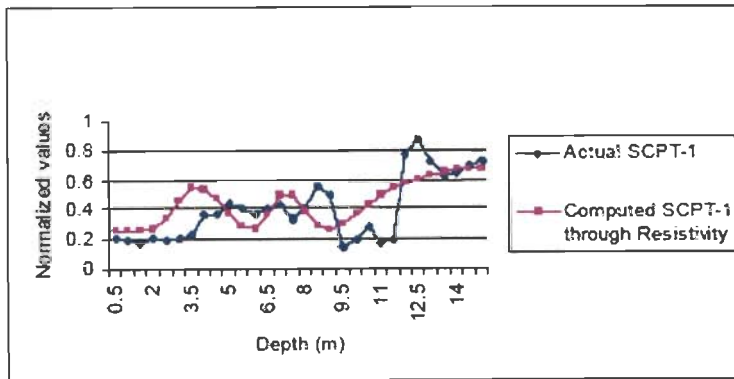


Fig. 6.6 h Comparison of Observed SCPT-1 and Computed One Using Resistivity

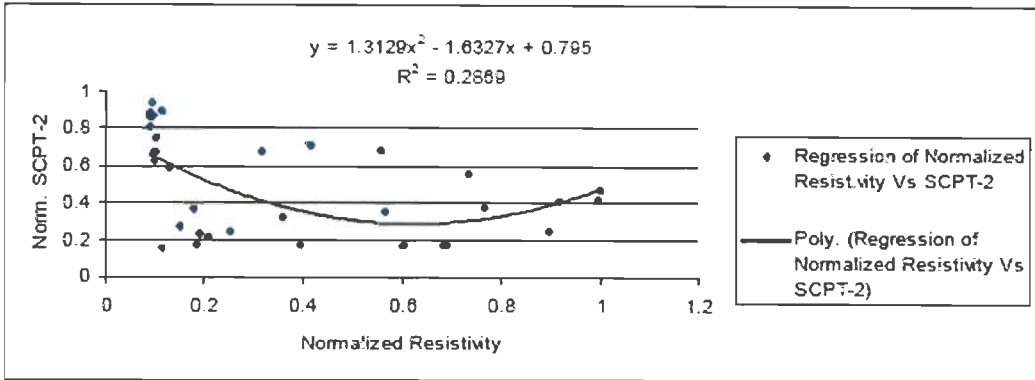


Fig. 6.6 i Regression of Normalized Resistivity with SCPT-2 of Profile A-B

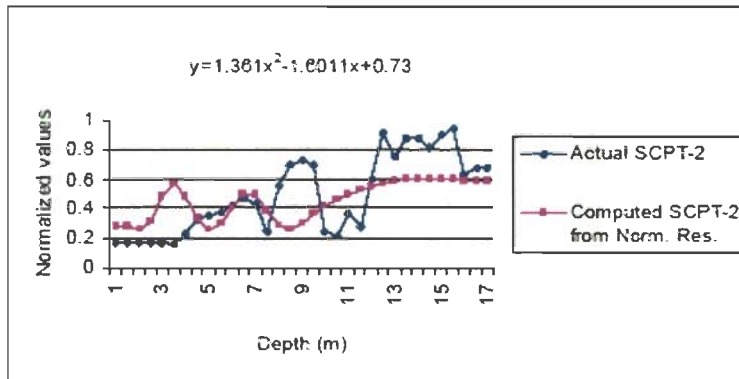


Fig. 6.6 j Comparison of Observed SCPT-2 with Computed One Using Resistivity

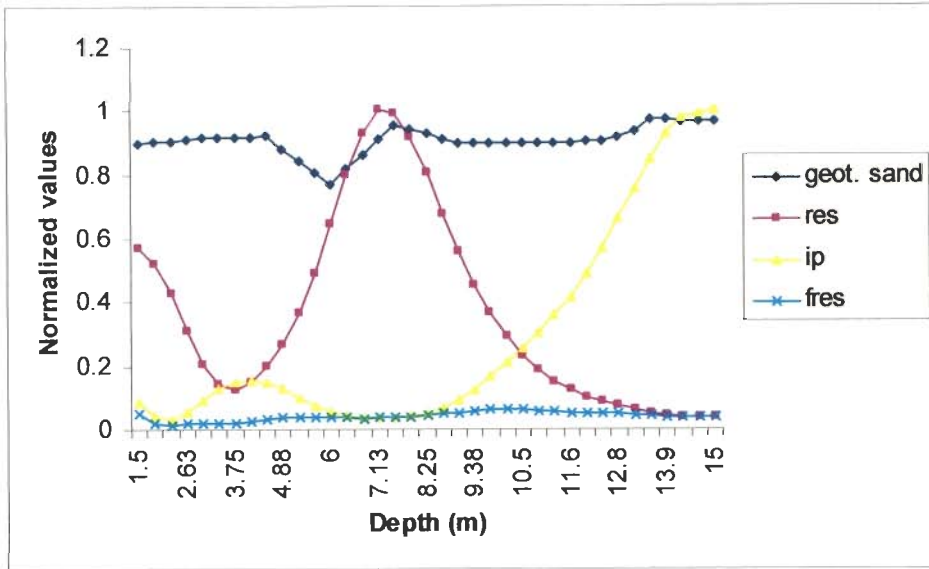


Fig. 6.7 a Plot of Geotechnical Sand, Resistivity, IP and Fictitious Resistivity at Borehole Location- B-1 (Electrode Location - EL-16) of Profile A-B

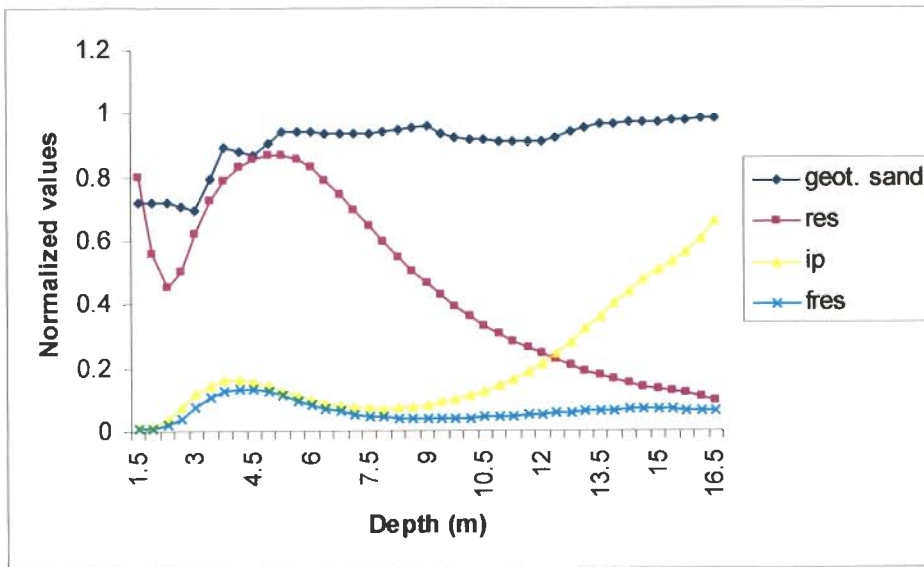


Fig. 6.7 b Plot of Geotechnical Sand, Resistivity, IP and Fictitious Resistivity at Borehole Location- B-3 (Electrode Location - EL-24) of Profile A-B

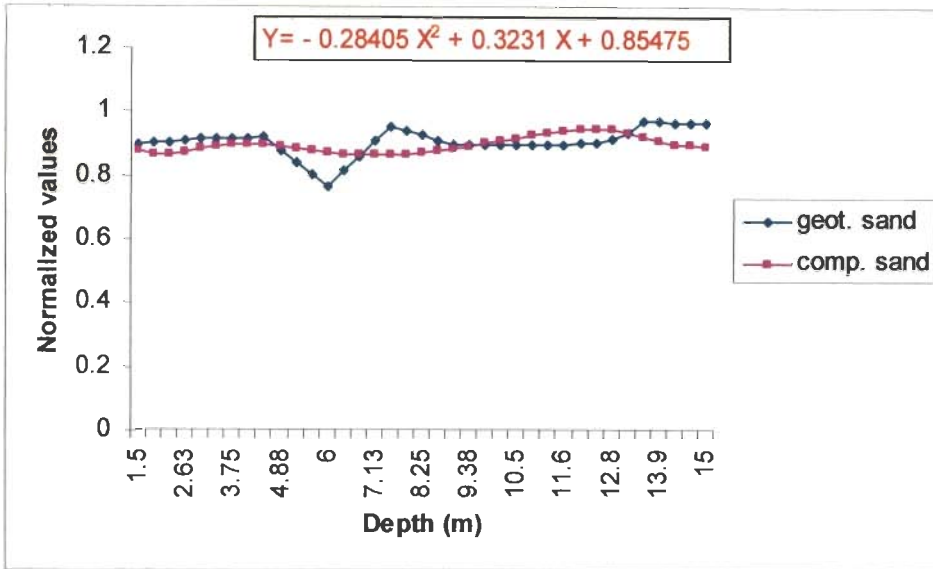


Fig. 6.7 c Plot of Geotechnical versus Computed Sand at Borehole Location- B-1 Using IP

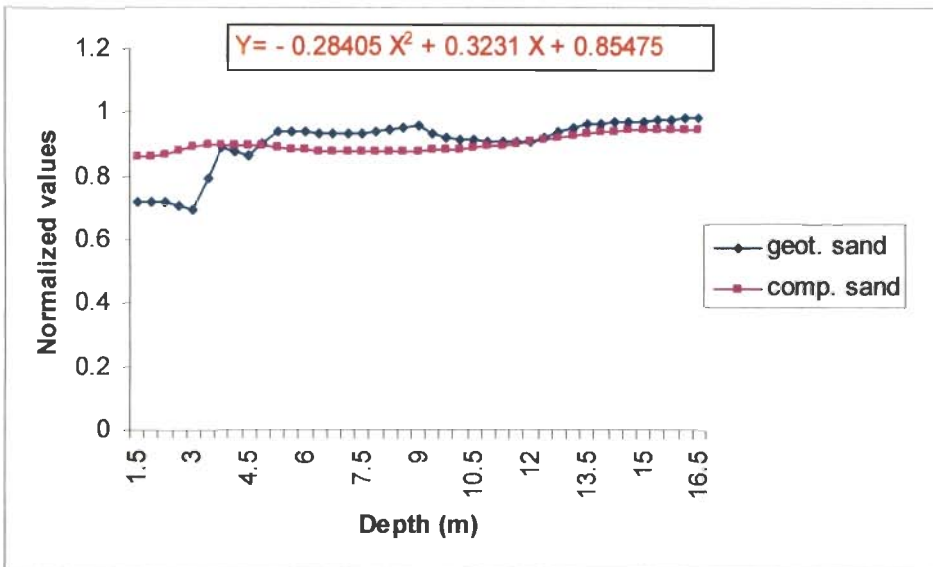


Fig. 6.7 d Plot of Geotechnical versus Computed Sand at Borehole Location- B-3 Using IP

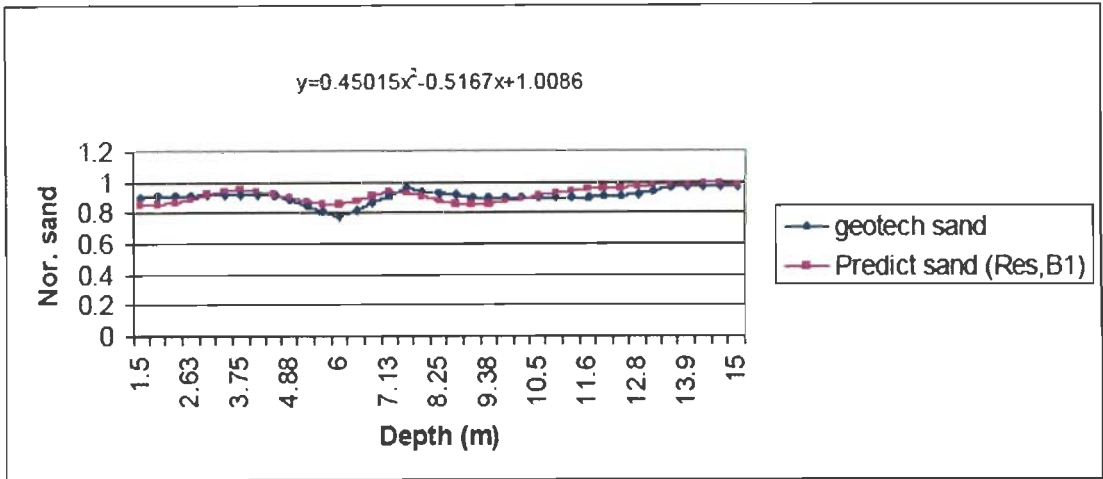


Fig. 6.7 e Comparison of Observed and Predicted Geotechnical Sand Through Resistivity at the Borehole Location-B-1

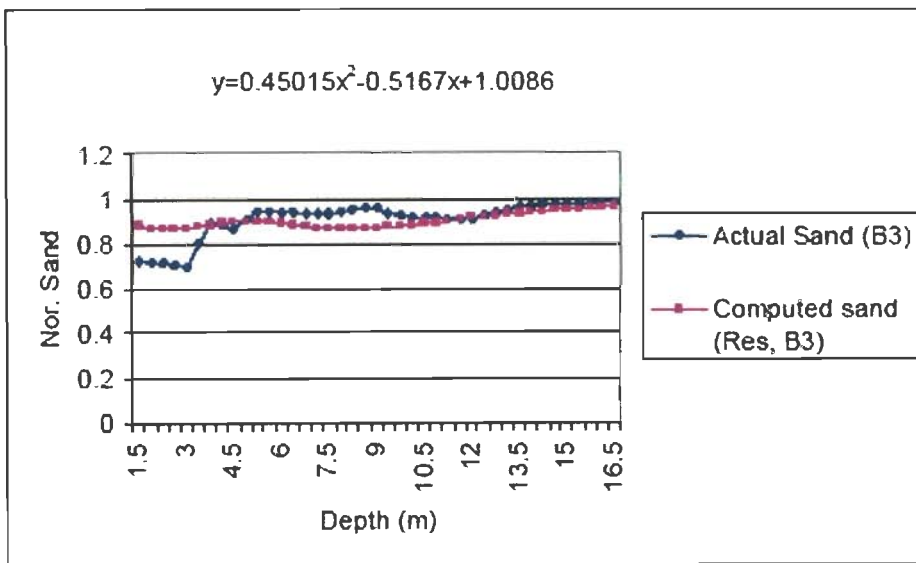


Fig. 6.7 f Comparison of Observed versus Computed Geotechnical Sand Through Resistivity at Borehole Location-B-3

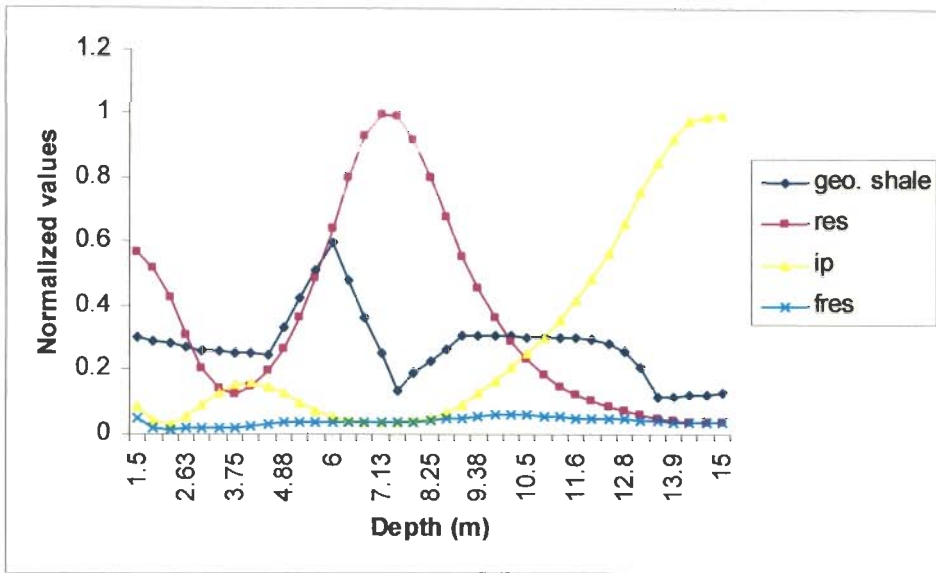


Fig. 6.7 g Plot of Geotechnical Shale, Resistivity, IP and Fictitious Resistivity at Borehole Location- B-1 (Electrode Location - EL-16) of Profile A-B

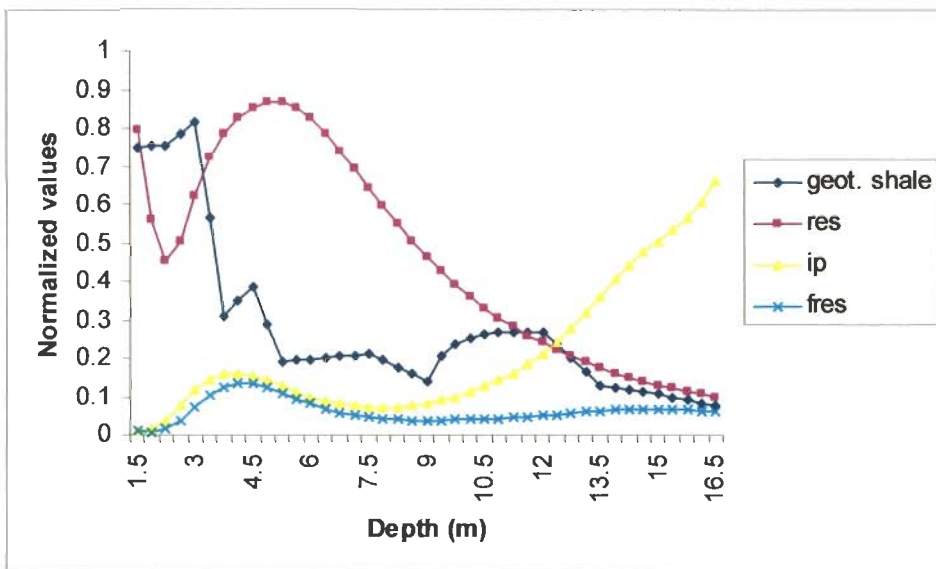


Fig. 6.7 h Plot of Geotechnical Shale, Resistivity, IP and Fictitious Resistivity at Borehole Location- B-3 (Electrode Location - EL-24) of Profile A-B

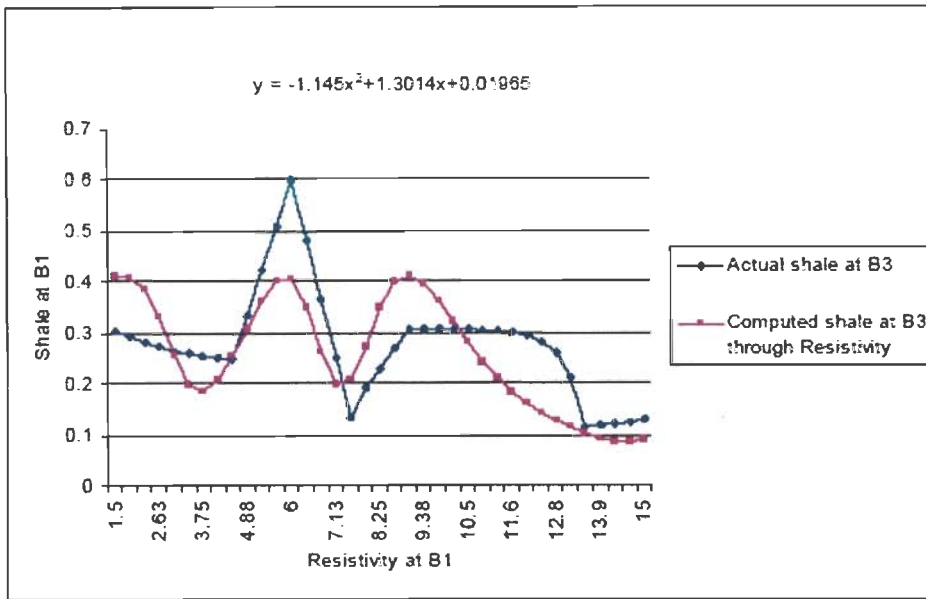


Fig. 6.7 i Comparison of Observed and Computed Shale Through Resistivity at Borehole Location- B1

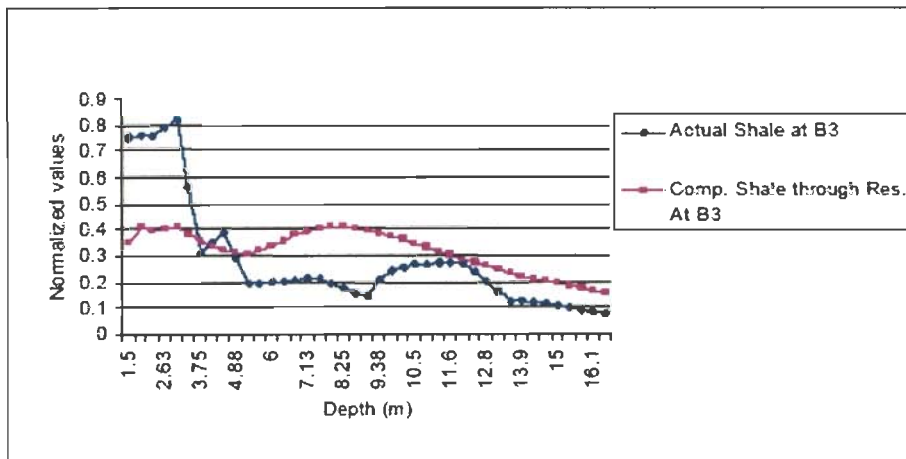


Fig. 6.7 j Comparison of Observed and Computed Shale Through Resistivity at Borehole Location-B-3

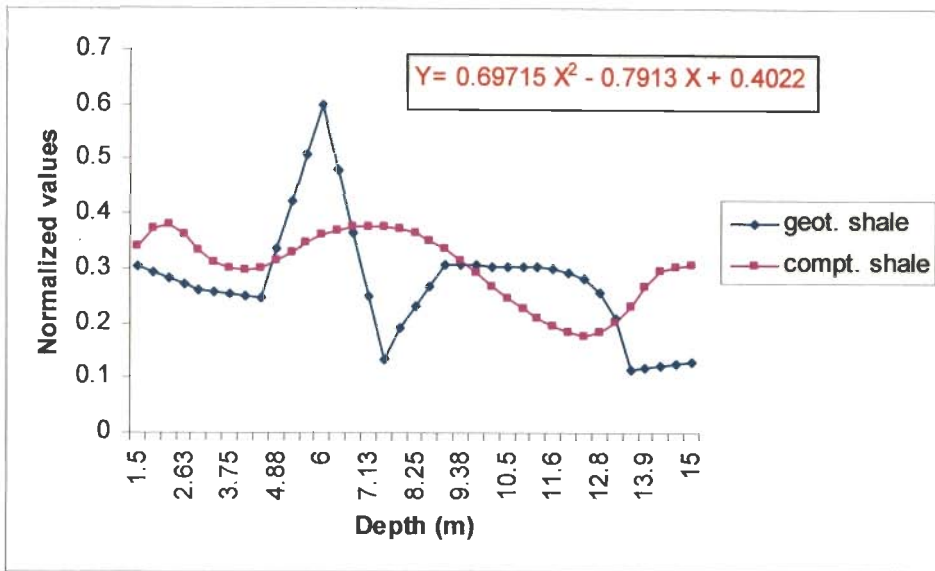


Fig. 6.7 k Plot of Geotechnical versus Computed Shale at Borehole Location- B-1 Using IP

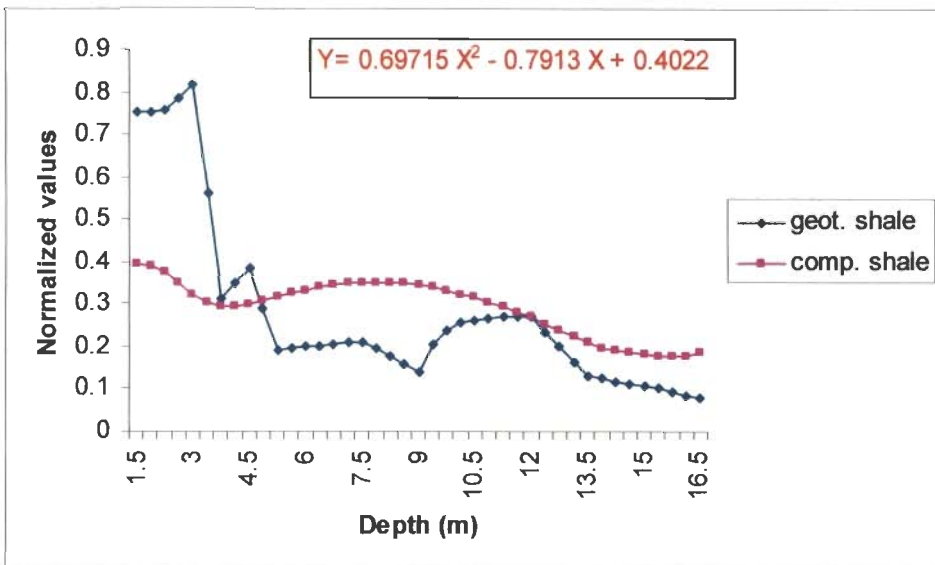


Fig. 6.7 l Plot of Geotechnical versus Computed Shale at Borehole Location- B-3 Using IP

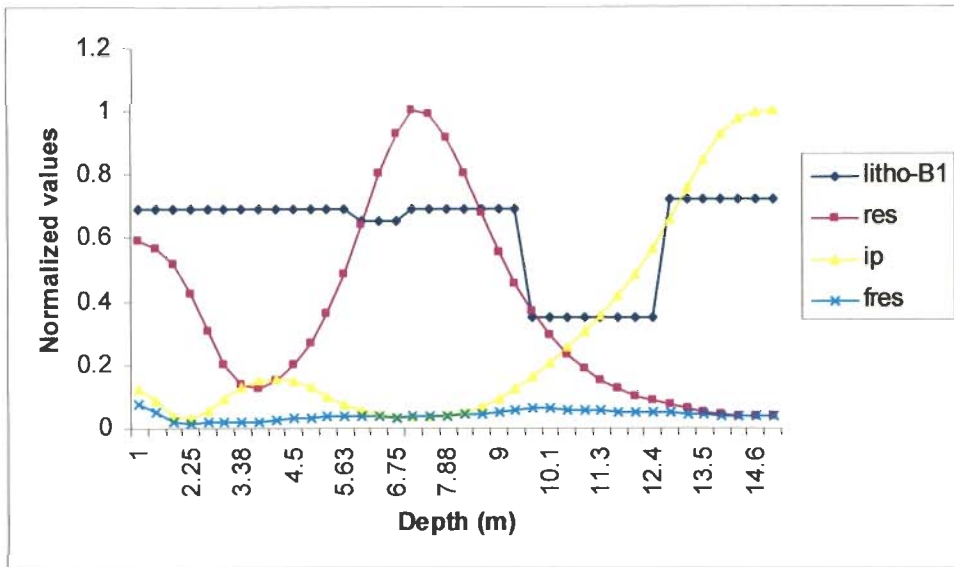


Fig. 6.8 a Plot of Observed Lithology, Resistivity, IP and Fictitious Resistivity at Borehole Location- B-1 (Electrode Location- EL-16) of Profile A-B

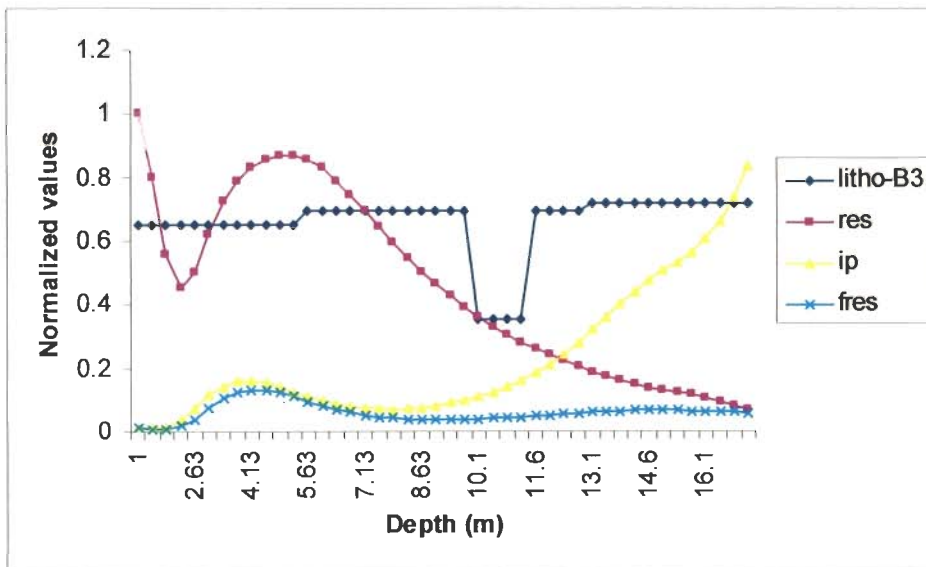


Fig. 6.8 b Plot of Lithology, Resistivity, IP and Fictitious Resistivity at Borehole Location- B-3 (Electrode Location- EL-24) of Profile A-B

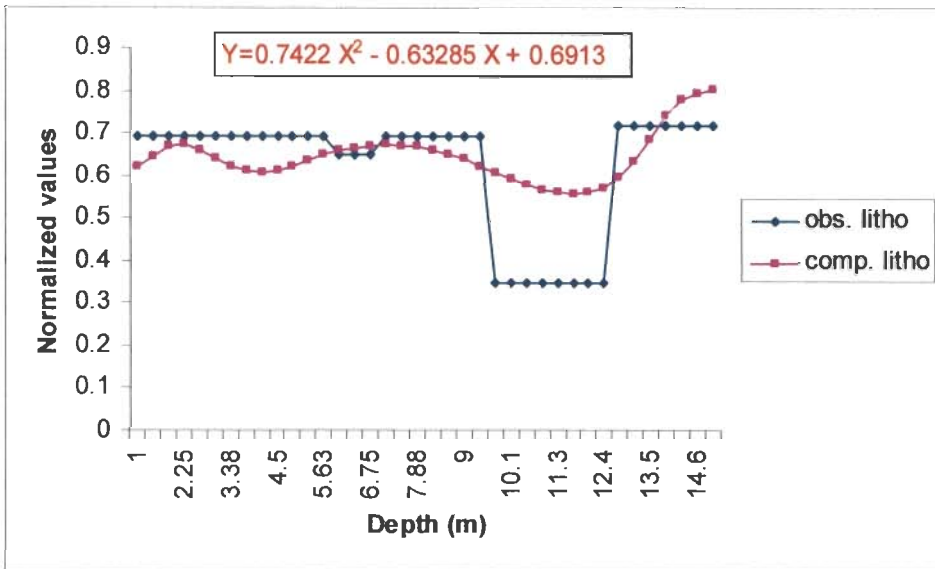


Fig. 6.8 c Plot of Observed versus Computed Lithology Through IP at Borehole Location- B-1

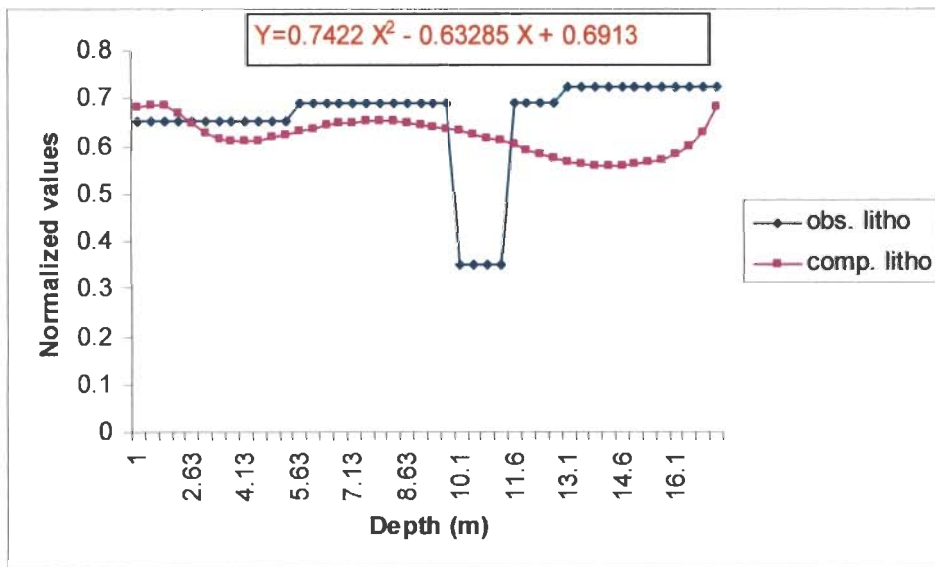


Fig. 6.8 d Plot of Observed versus Computed Lithology Through IP at Borehole Location- B-3

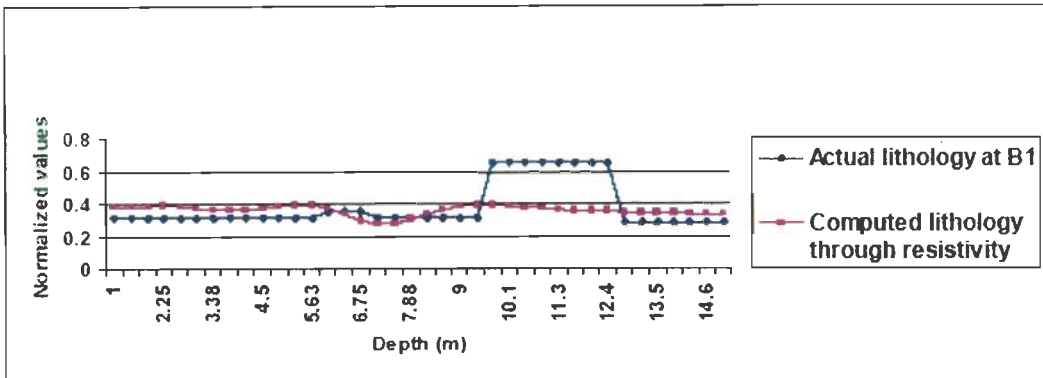


Fig. 6.8 e Comparison of Observed and Computed Lithology Through Resistivity at Borehole Location- B-1

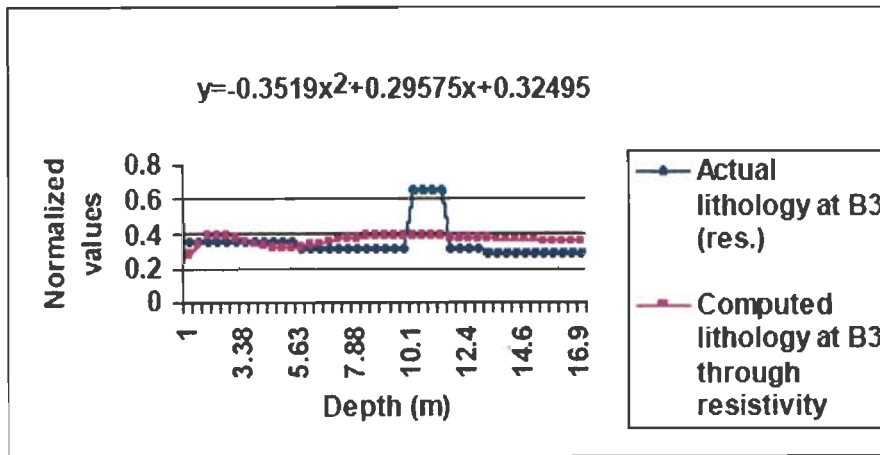


Fig. 6.8 f Comparison of Observed and Computed Lithology Through Resistivity at Borehole Location- B-3

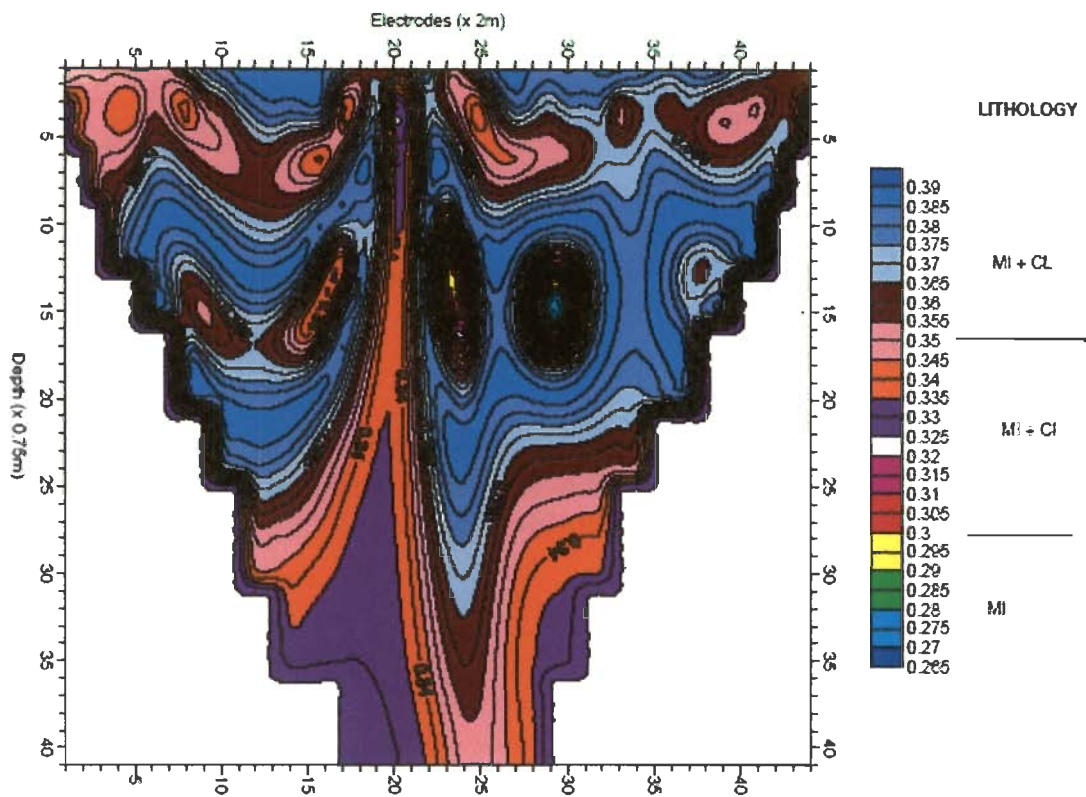


Fig. 6.8 g Inferred Lithology Section from Geotechnical and Resistivity Data Along Profile A-B, Library Site, IITR

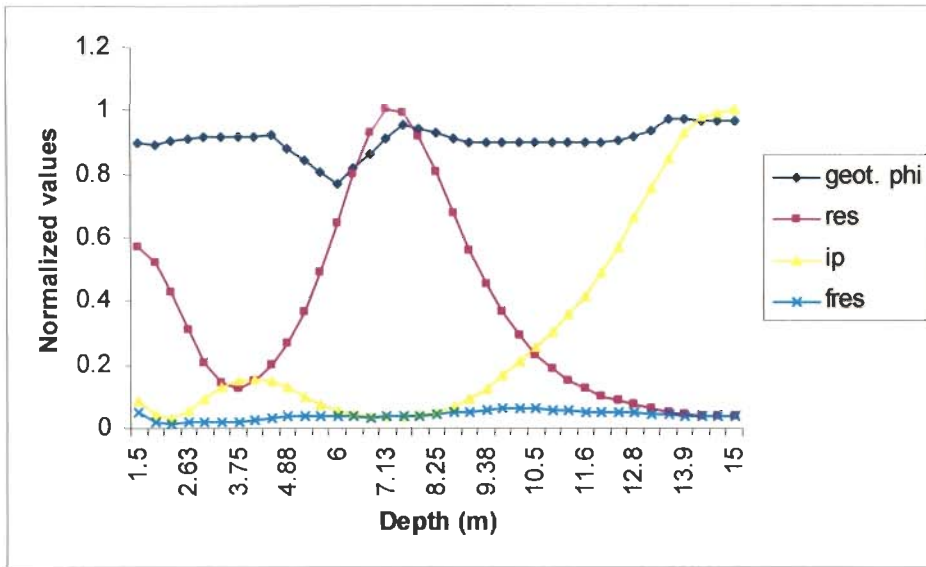


Fig. 6.9 a Plot of Observed Porosity, Resistivity, IP and Fictitious Resistivity at Borehole Location- B-1 (Electrode Location - EL-16) of Profile A-B

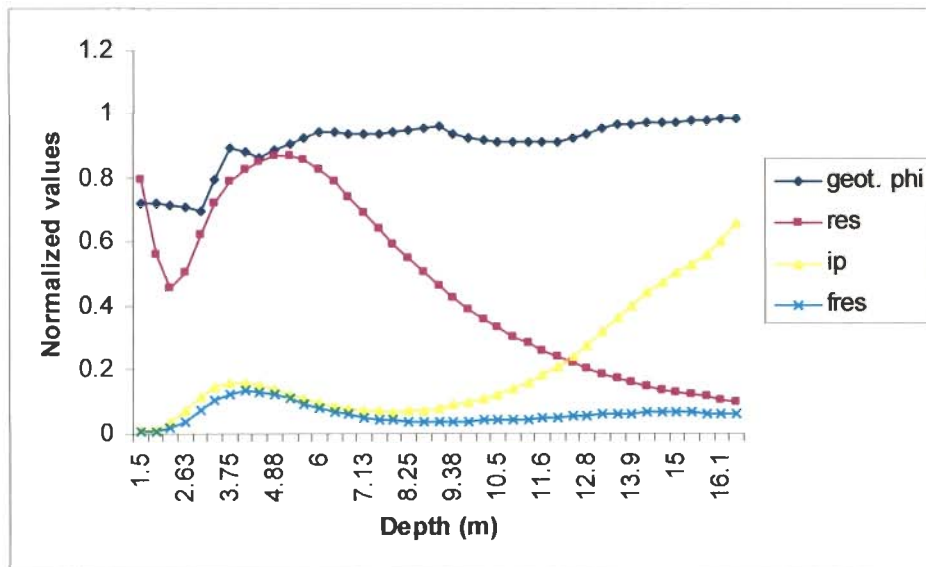


Fig. 6.9 b Plot of Observed Porosity, Resistivity, IP and Fictitious Resistivity at Borehole Location- B-3 (Electrode Location - EL-24) of Profile A-B

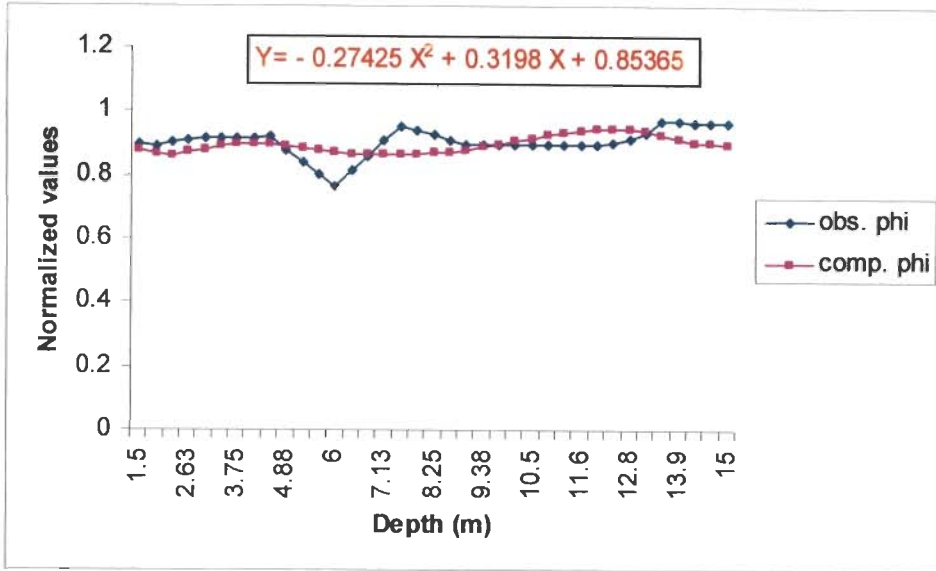


Fig. 6.9 c Plot of Observed versus Computed Porosity at Borehole Location- B-1 Using IP

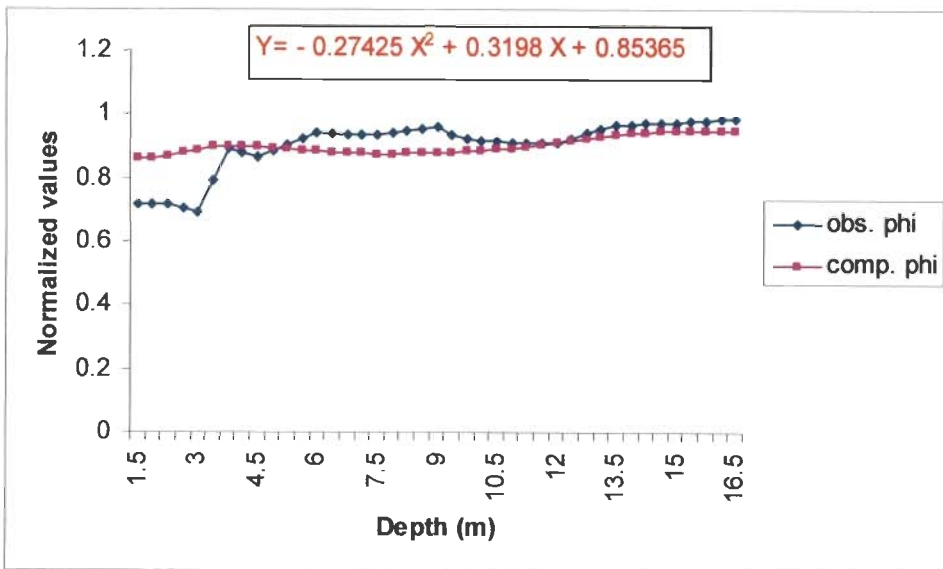


Fig. 6.9 d Plot of Observed versus Computed Porosity at Borehole Location- B-3 Using IP

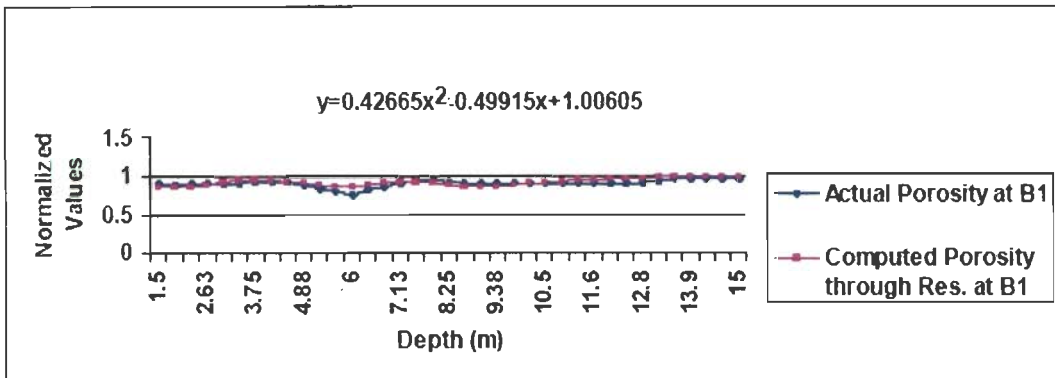


Fig. 6.9 e Comparison of Observed and Computed Porosity Through Resistivity at Borehole Location- B-1

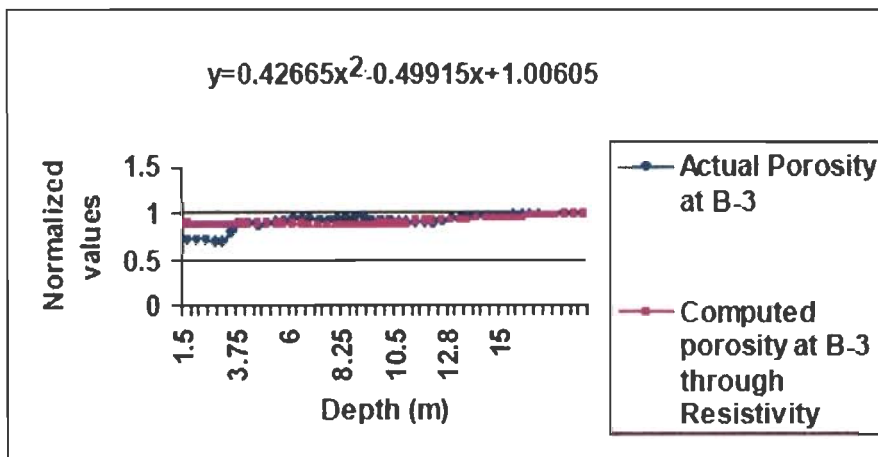


Fig. 6.9 f Comparison of Observed and Computed Porosity Through Resistivity at Borehole Location- B-3

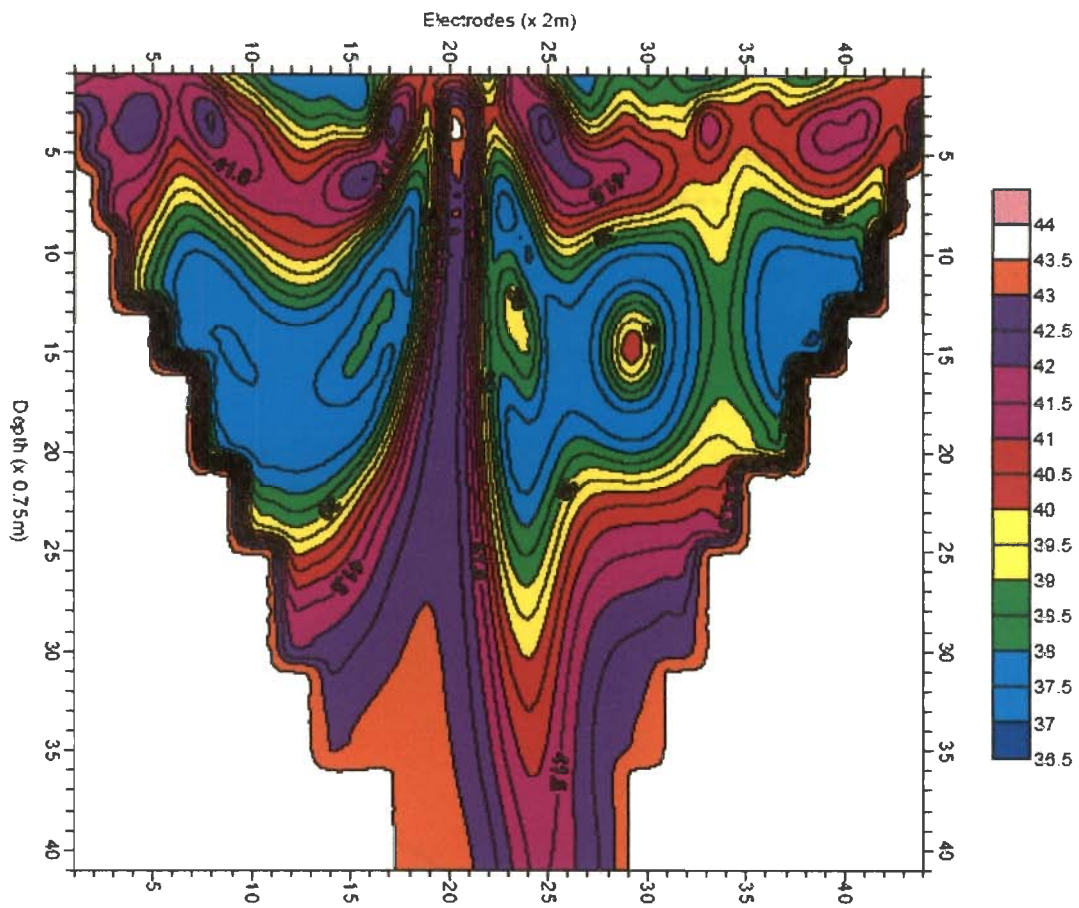


Fig. 6.9 g Predicted Porosity (%) Section from Resistivity and Borehole Data Along Profile A-B, Library Site, IITR

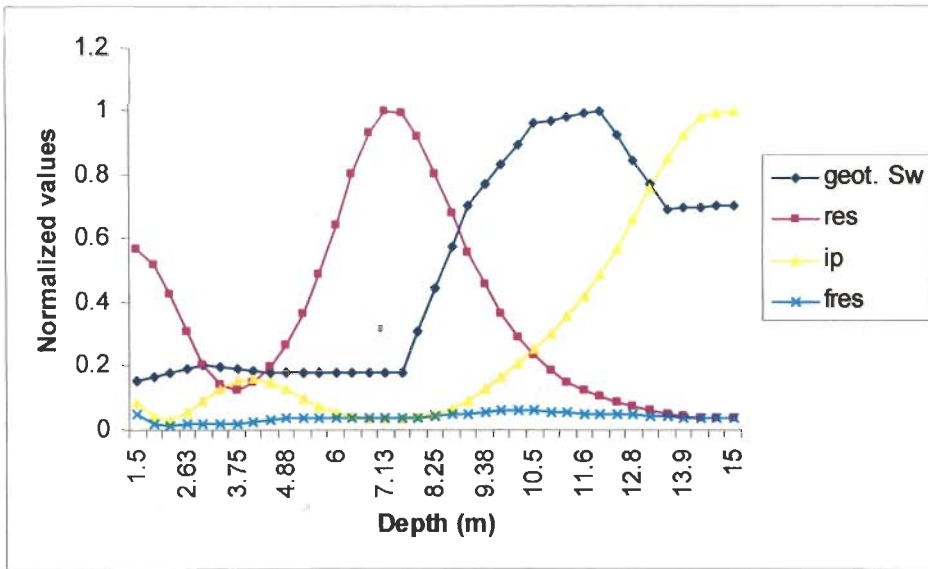


Fig. 6.10 a Plot of Water Saturation (S_w) versus Resistivity, IP and Fictitious Resistivity at Borehole Location- B-1 (Electrode Location - EL-16) of Profile A-B

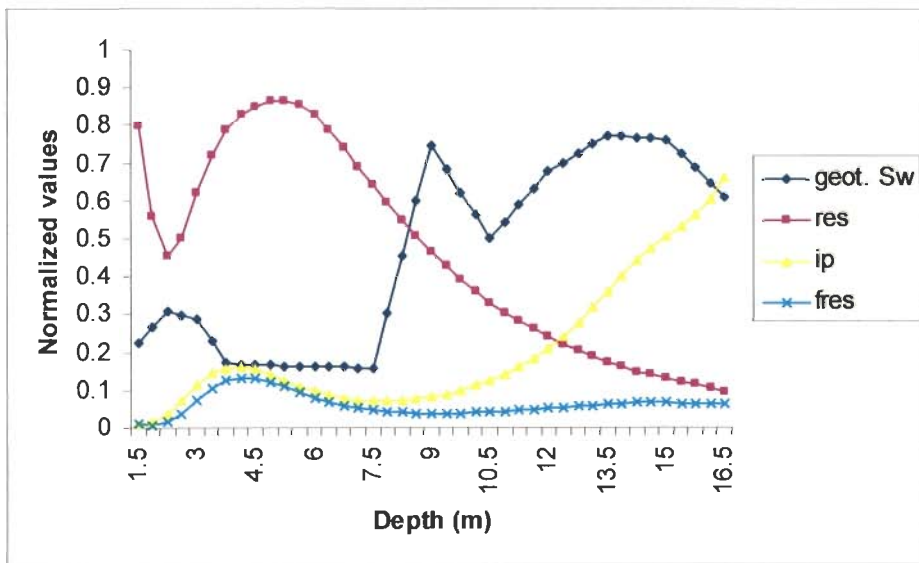


Fig. 6.10 b Plot of Water Saturation (S_w) versus Resistivity, IP and Fictitious Resistivity at Borehole Location- B-3 (Electrode Location - EL-24) of Profile A-B

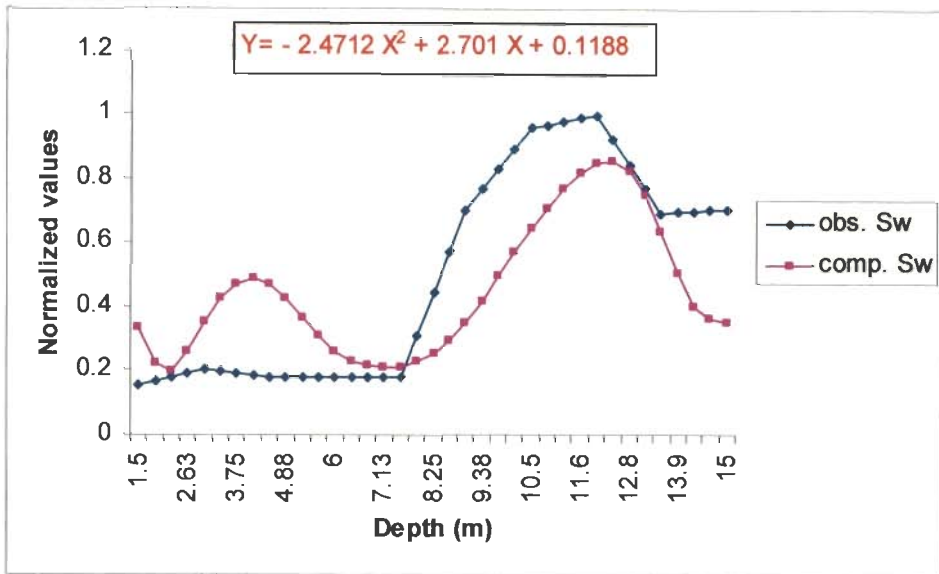


Fig. 6.10 c Plot of Observed versus Computed S_w at Borehole Location- B-1 Using IP

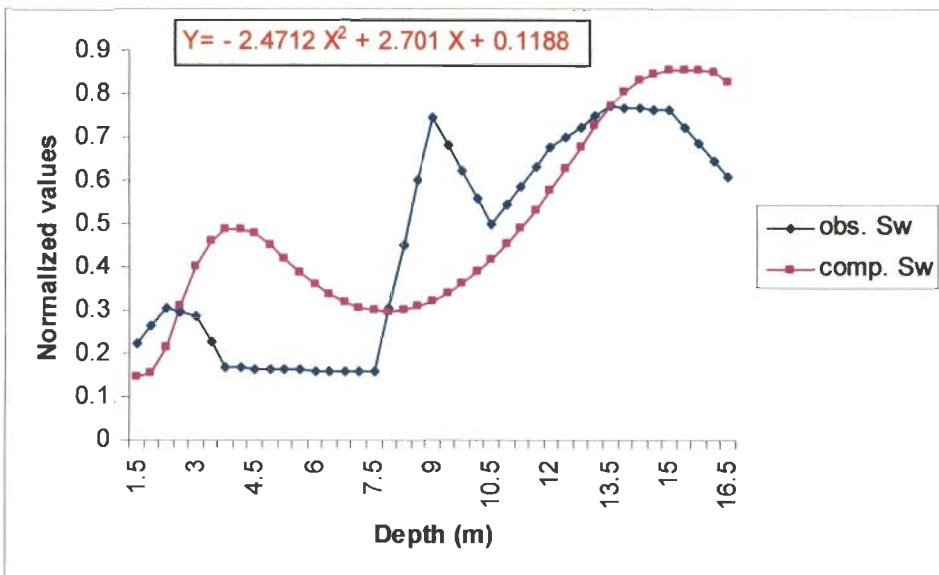


Fig. 6.10 d Plot of Observed versus Computed S_w at Borehole Location- B-3 Using IP

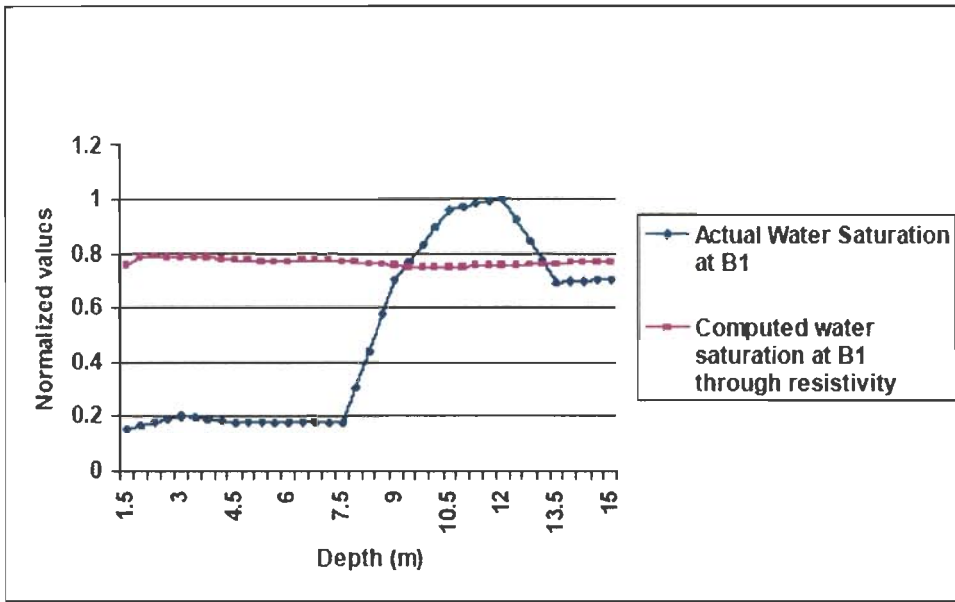


Fig. 6.10 e Comparison of Observed and Computed S_w at Borehole Location- B-1 Using Resistivity

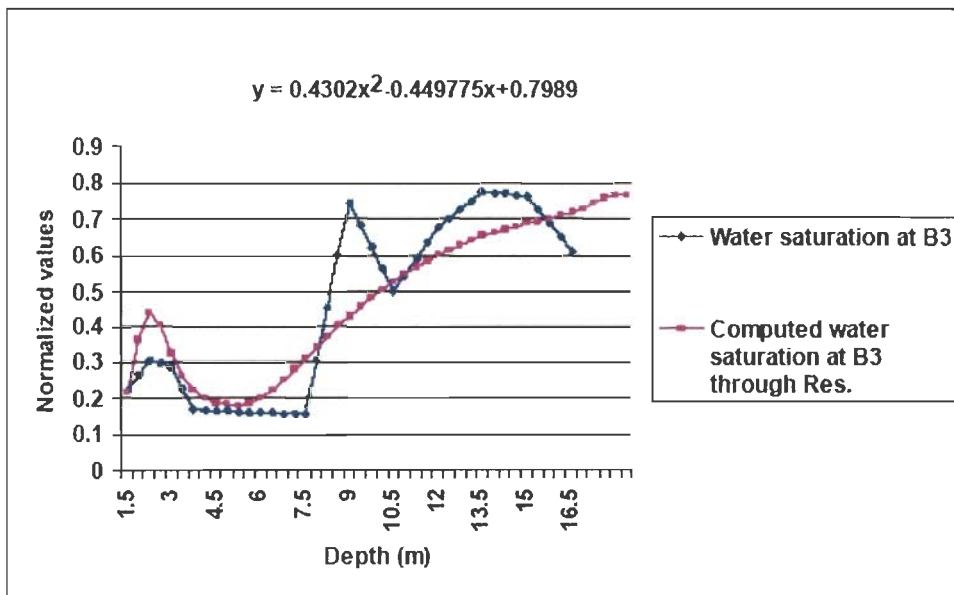


Fig. 6.10 f Comparison of Observed versus Computed S_w at Borehole Location- B-3 Using Resistivity

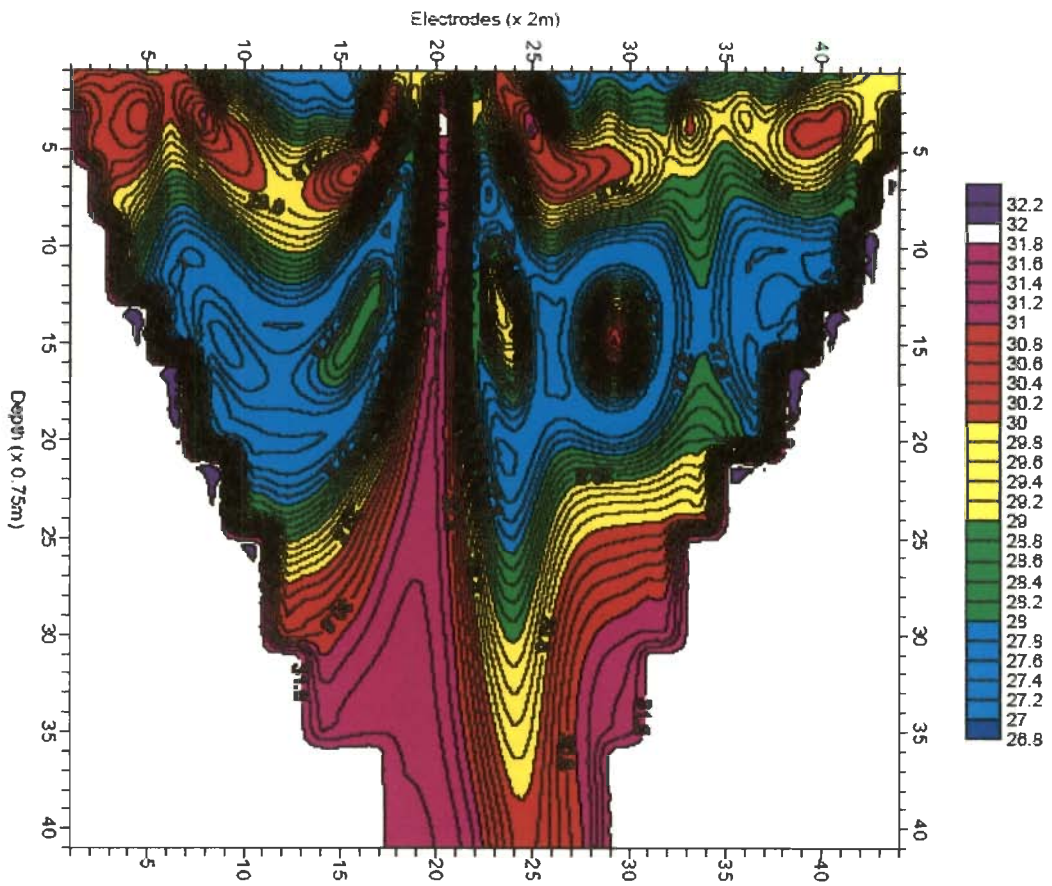


Fig. 6.10 g Predicted Water Saturation (%) Section from Resistivity and Borehole Data Along Profile A-B, Library Site, IITR

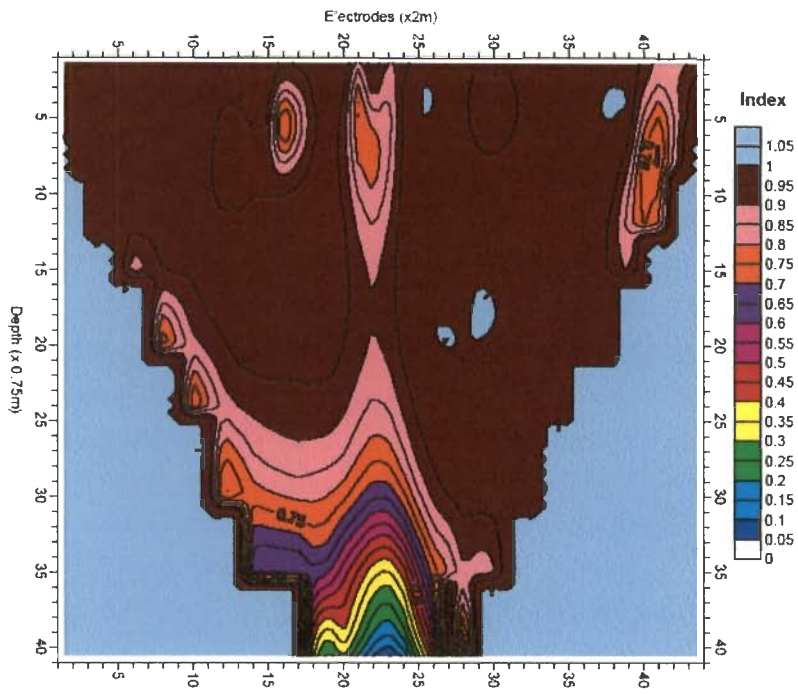


Fig. 6.11 a IP Derived Sand (%) Section Along Profile A-B, Library Site, IITR

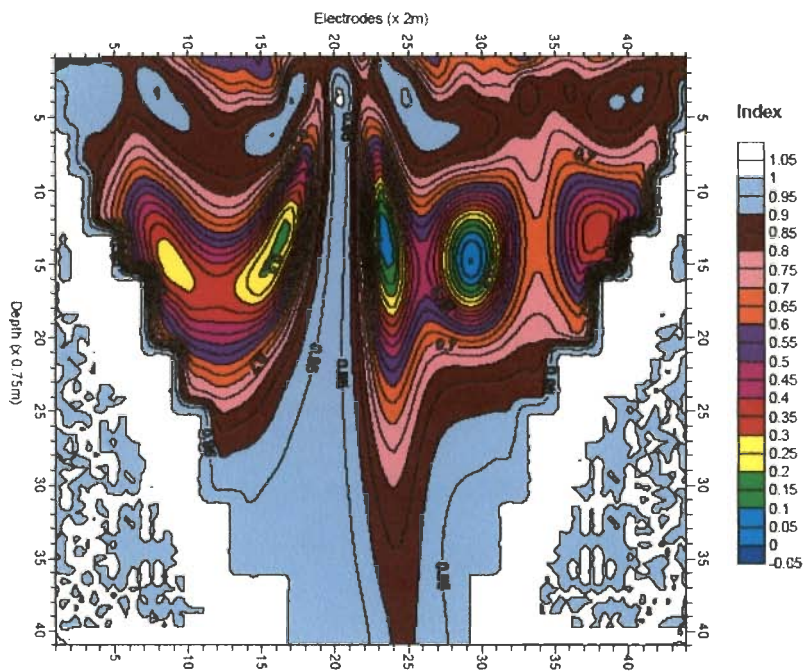


Fig. 6.11 b Resistivity Derived Sand (%) Section Along Profile A-B, Library Site, IITR

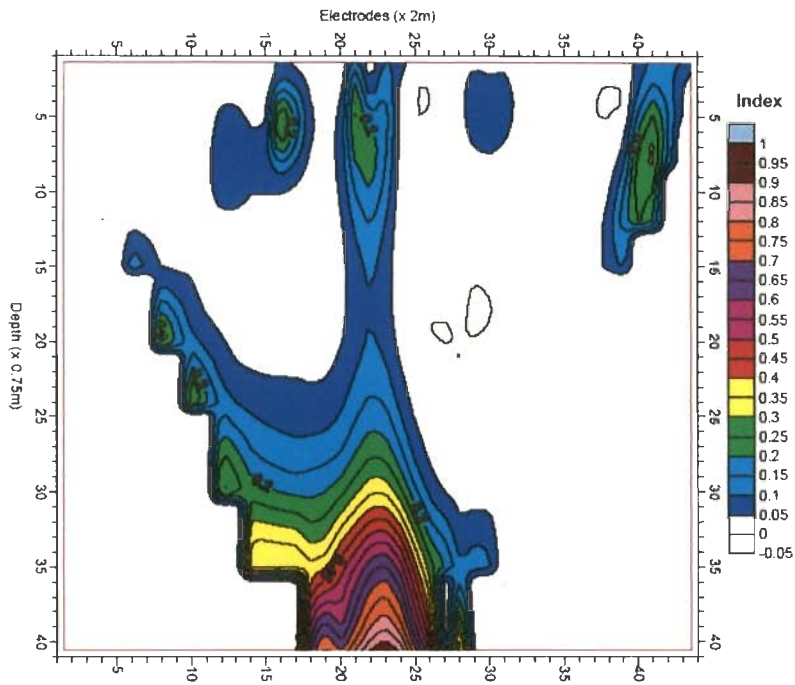


Fig. 6.12 a IP Derived Clay (%) Section Along Profile A-B, Library Site, IITR

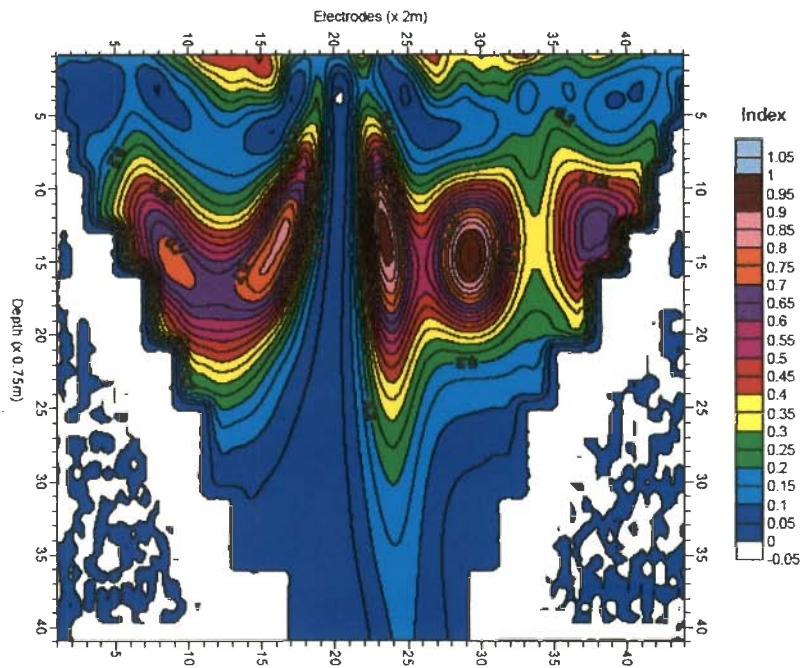


Fig. 6.12 b Resistivity Derived Clay (%) Section Along Profile A-B, Library Site, IITR

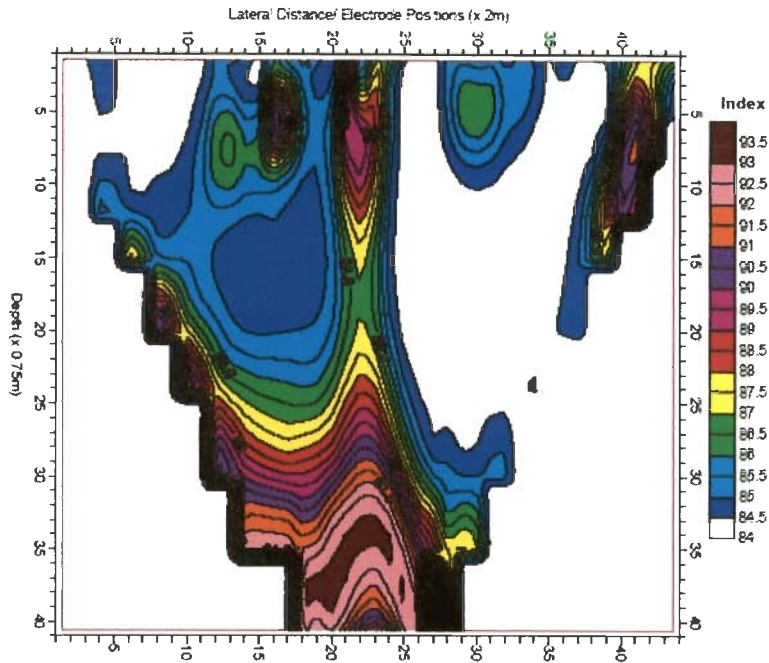


Fig. 6.13 a Predicted of Sand (%) Section from Geotechnical and IP Data Along Profile A-B, Library Site, IITR

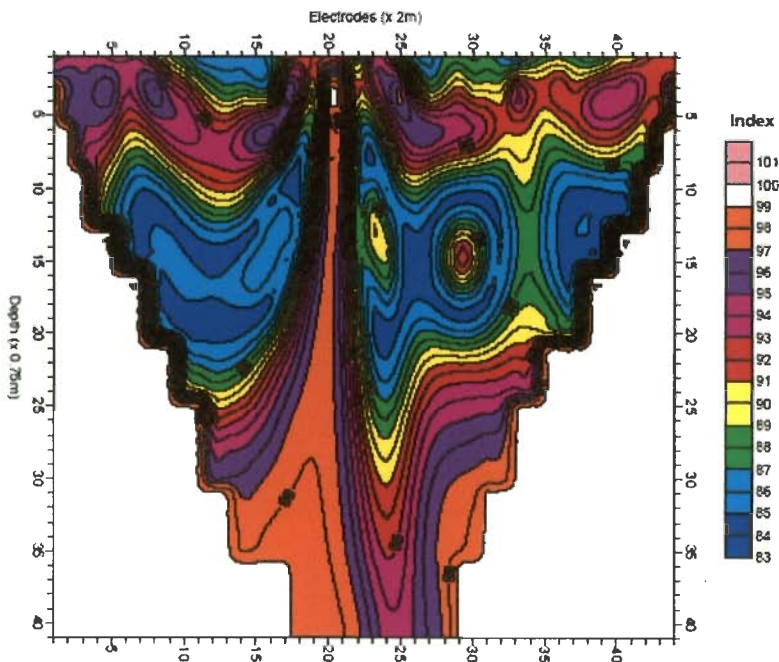


Fig. 6.13 b Predicted Sand (%) Section from Geotechnical and Resistivity Data Along Profile A-B , Library Site, IITR

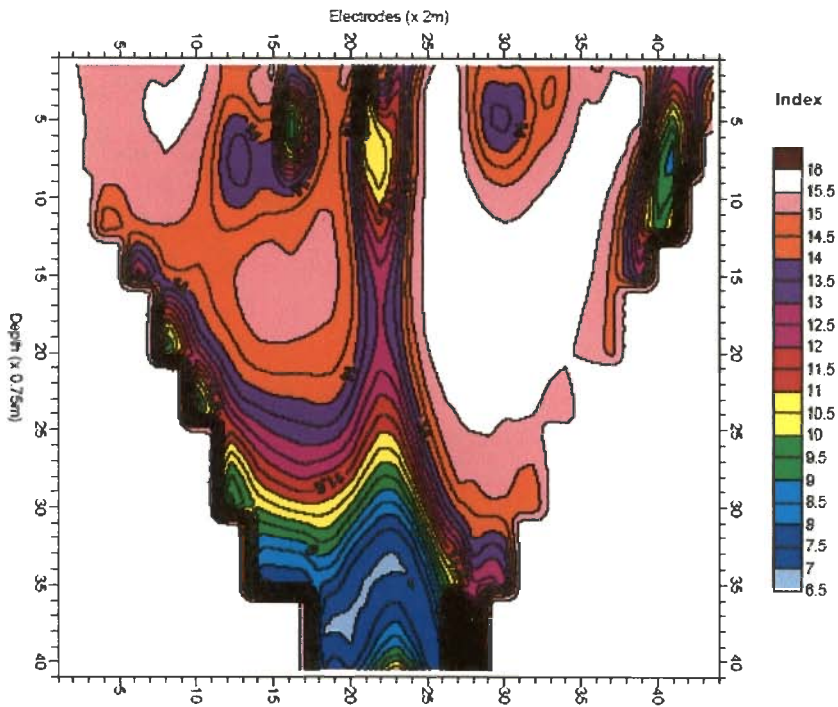


Fig. 6.14 a Predicted Clay (%) Section from Geotechnical and IP Data Along Profile A-B, Library Site, IITR

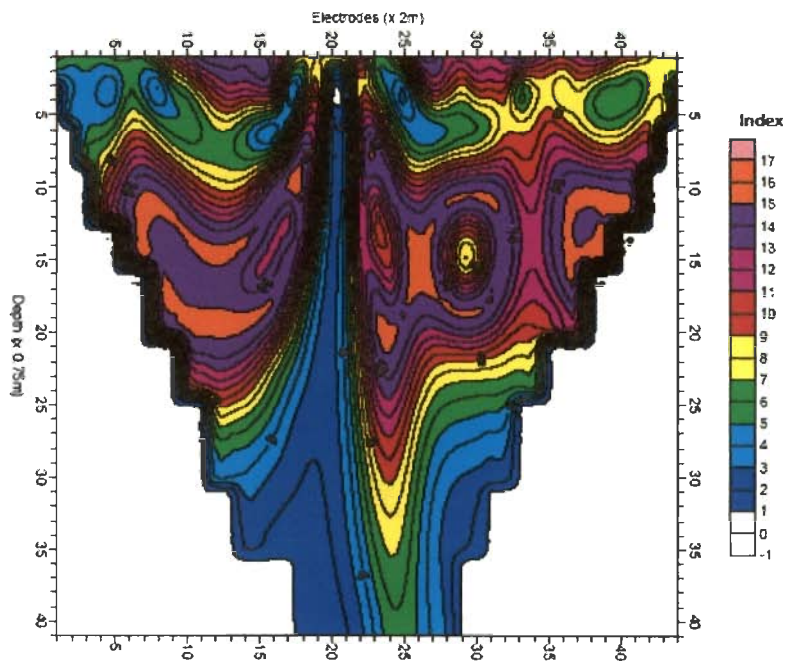


Fig. 6.14 b Predicted Clay (%) Section from Geotechnical and Resistivity Data Along Profile A-B, Library Site, IITR

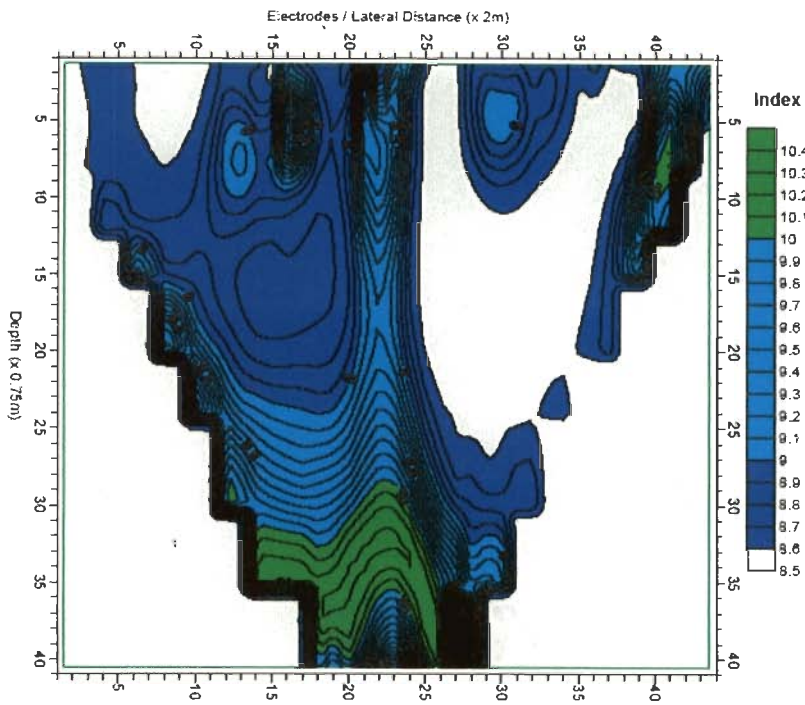


Fig. 6.15 a Predicted SPT Section from IP and Borehole Data Along Profile A-B, Library Site, IITR

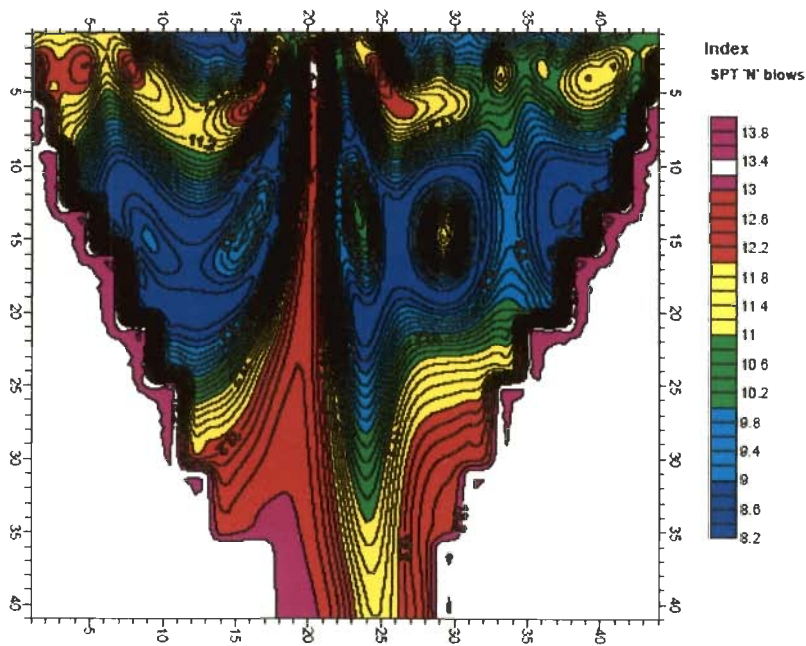


Fig. 6.15 b Predicted SPT Section from Resistivity and Borehole Data Along Profile A-B, Library Site, IITR

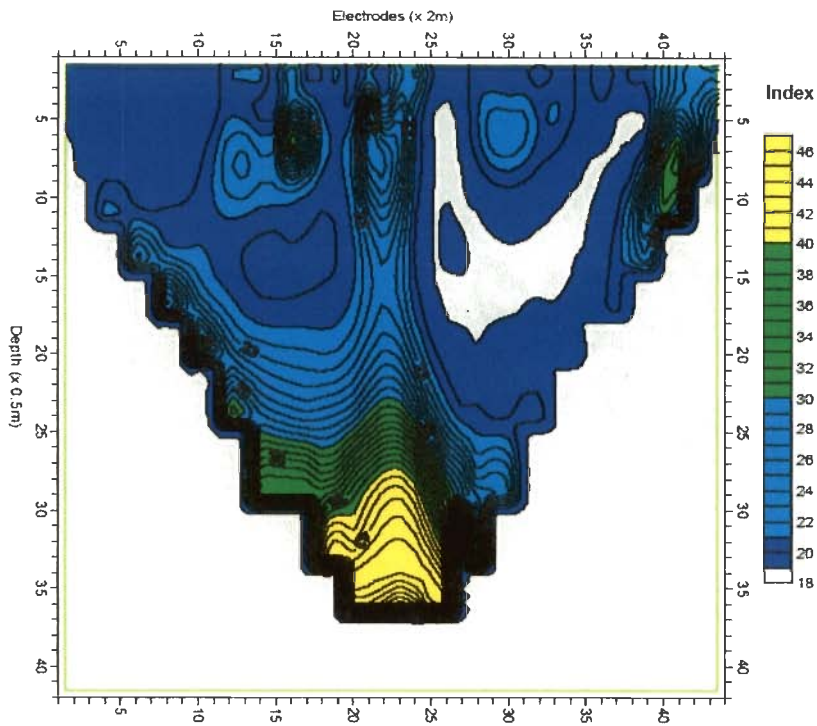


Fig. 6.16 a Predicted SCPT Section from IP and Borehole Data Along Profile A-B, Library Site, IITR

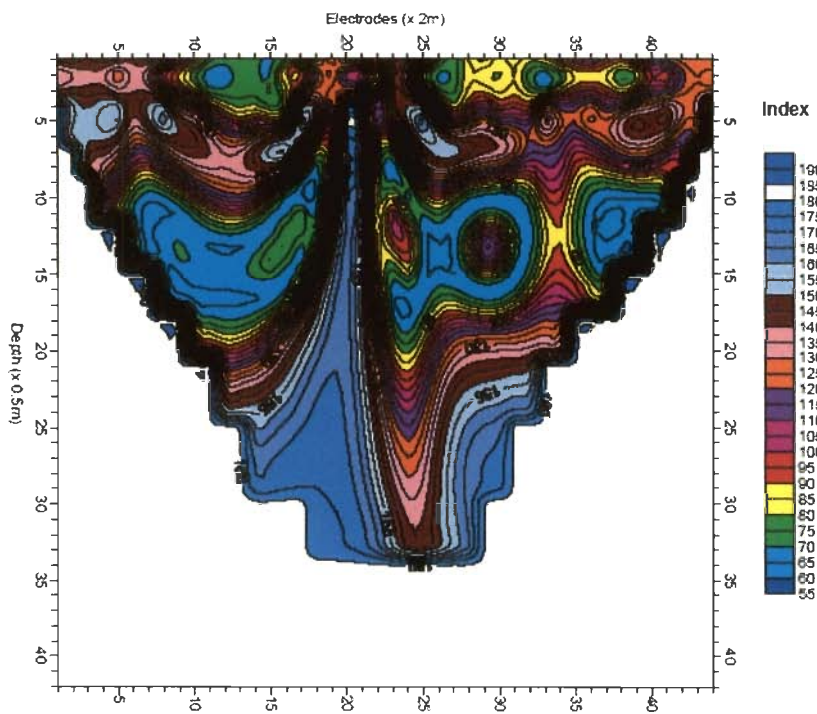


Fig. 6.16 b Predicted SCPT Section from Resistivity and Borehole Data Along Profile A-B, Library Site, IITR

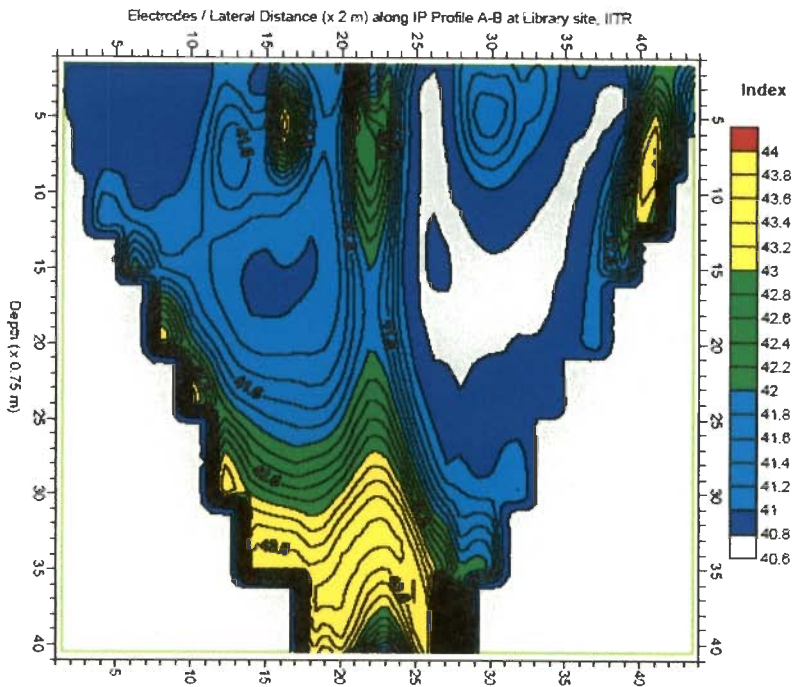


Fig. 6.17 a Predicted Internal Friction Angle Section from Synthetic SPT Section Using IP Along Profile A-B, Library Site, IITR

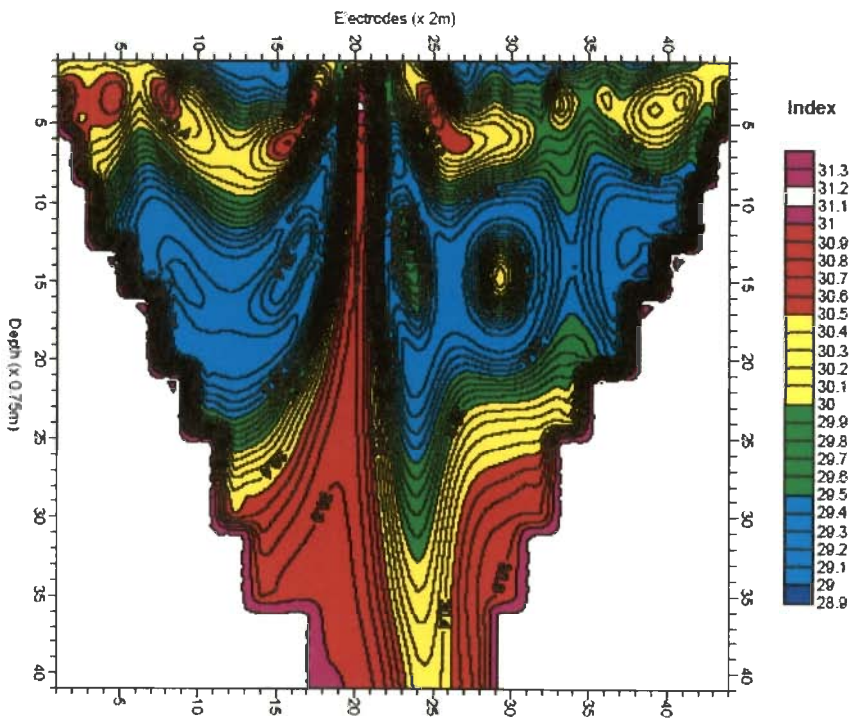


Fig. 6.17 b Predicted Internal Friction Angle Section from Synthetic SPT Section Using Rsistivity Along Profile A-B, Library Site, IITR

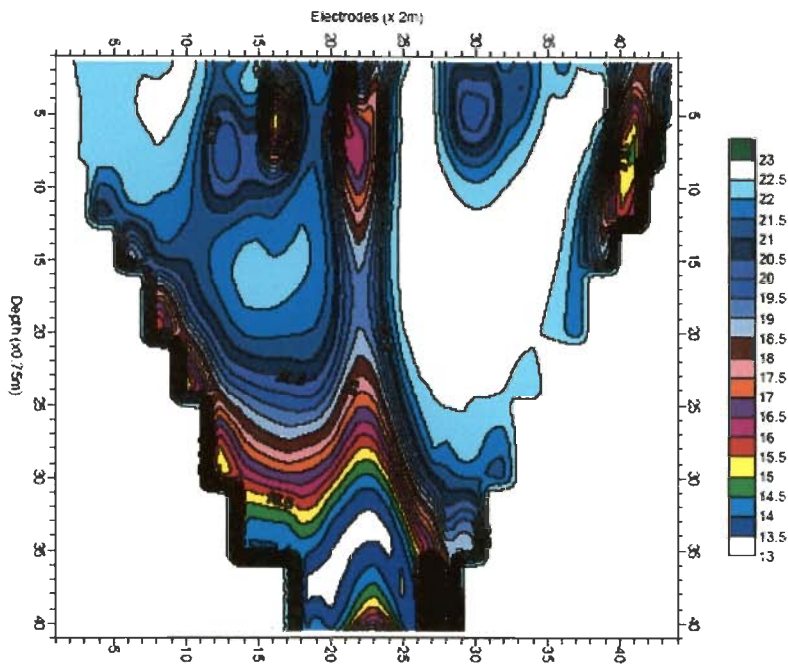


Fig. 6.18 a Predicted Unit Weight (Dry) in kN/m^3 Section from Water Saturation Section (Using IP) Along Profile A-B, Library Site, IITR

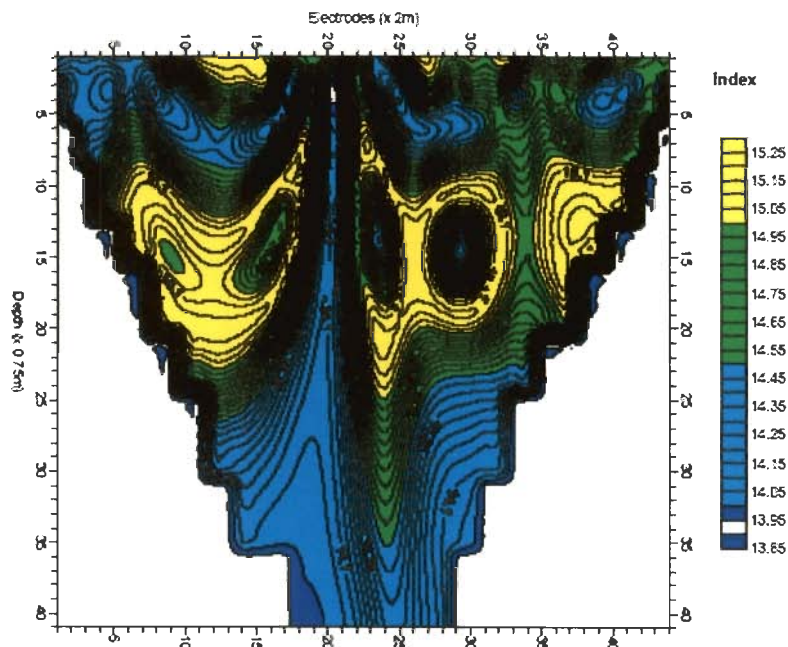


Fig. 6.18 b Predicted Unit Weight (Dry) in kN/m^3 Section from Water Saturation Section (Using Resistivity) Along Profile A-B, Library Site, IITR

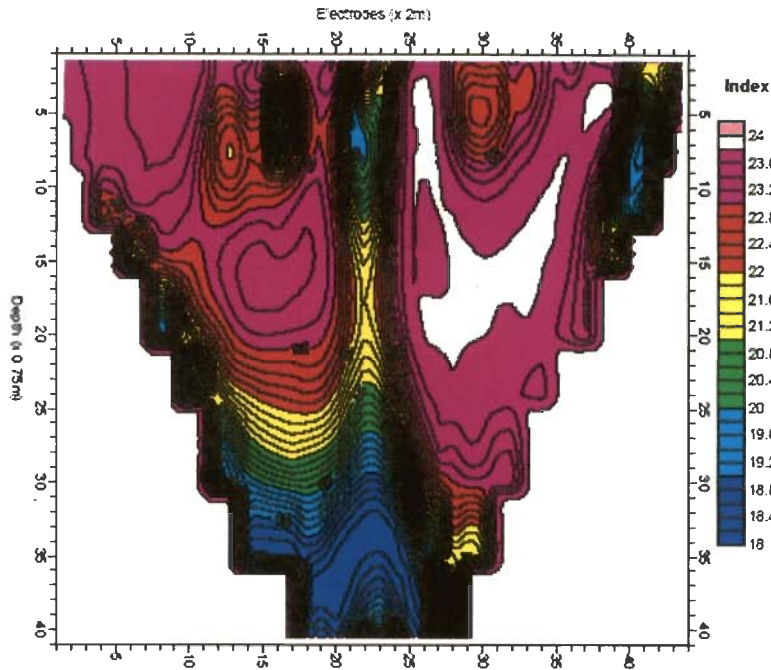


Fig. 6.19 a Predicted Unit Weight (Saturated) in kN/m^3 Section from Water Saturation (Using IP) Section Along Profile A-B, Library Site, IITR

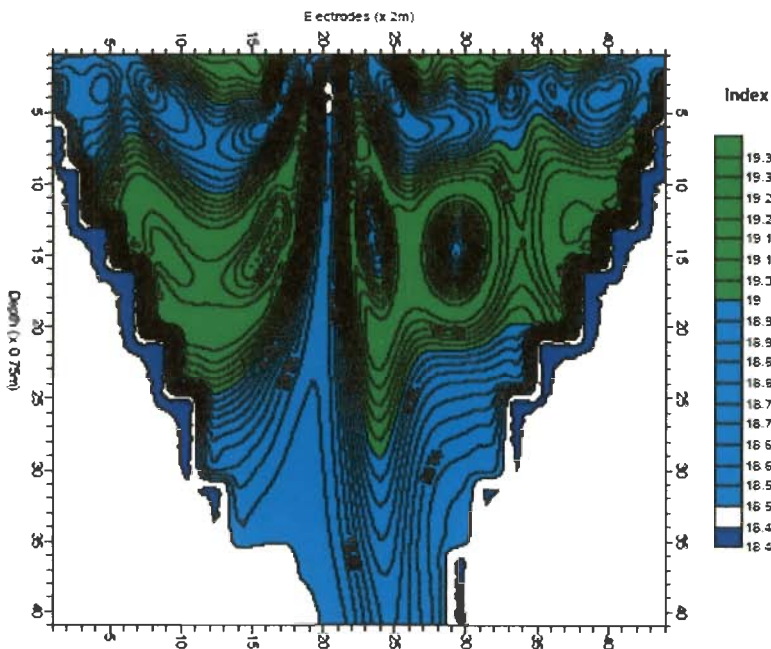


Fig. 6.19 b Inferred Unit Weight (Saturated) in kN/m^3 Section from Water Saturation (Using Resistivity) Section Along Profile A-B, Library Site, IITR

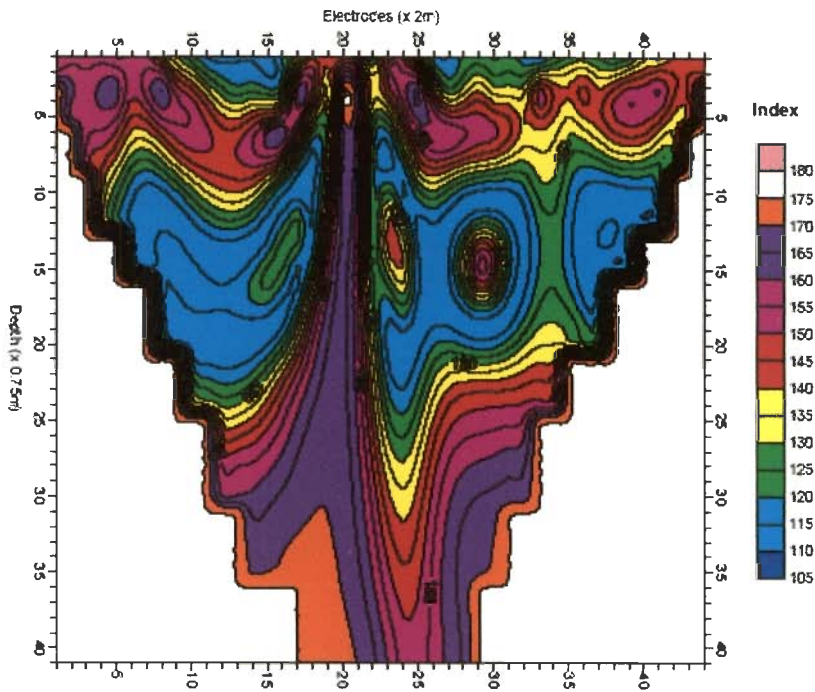


Fig. 6.20 Predicted Unconfined Compressive Strength, q_u Section from SPT 'N' Section (Using Resistivity) Along Profile A-B, Library Site, IITR

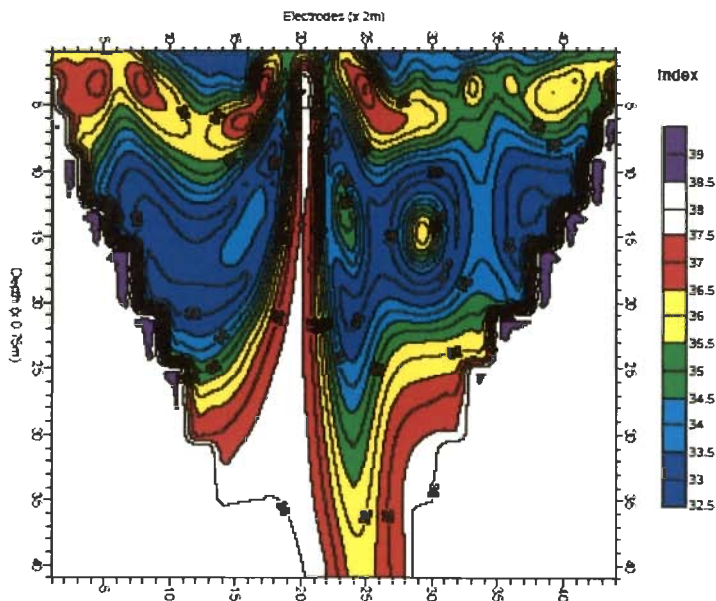


Fig. 6.21 Predicted Bearing Capacity Factor of General Shear Failure, N_c Section from Resistivity Derived Angle of Internal Friction Section Along Profile A-B, Library Site, IITR

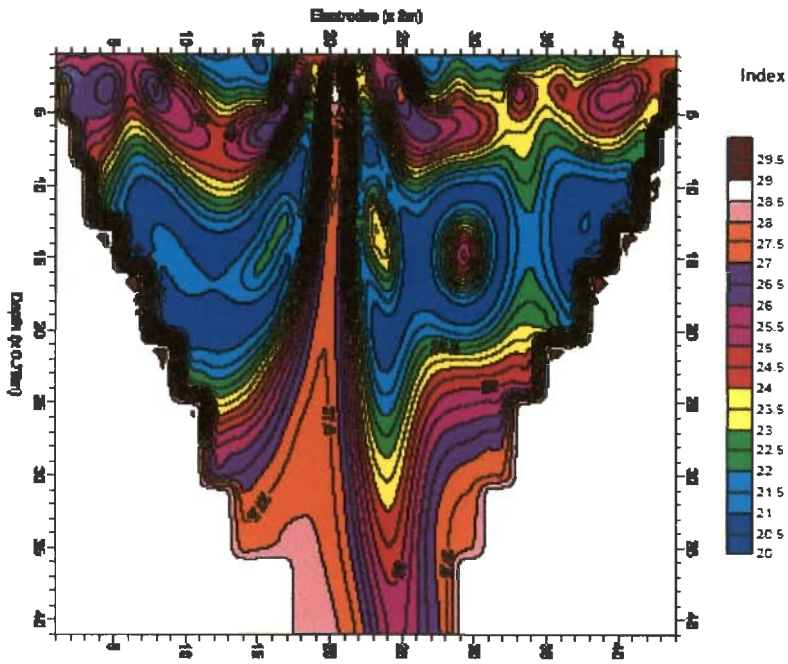


Fig. 6.22 Predicted Bearing Capacity Factor of General Shear Failure, N_γ (Vesic) Section from Angle of Internal Friction Section Along Profile A-B, Library Site, IITR

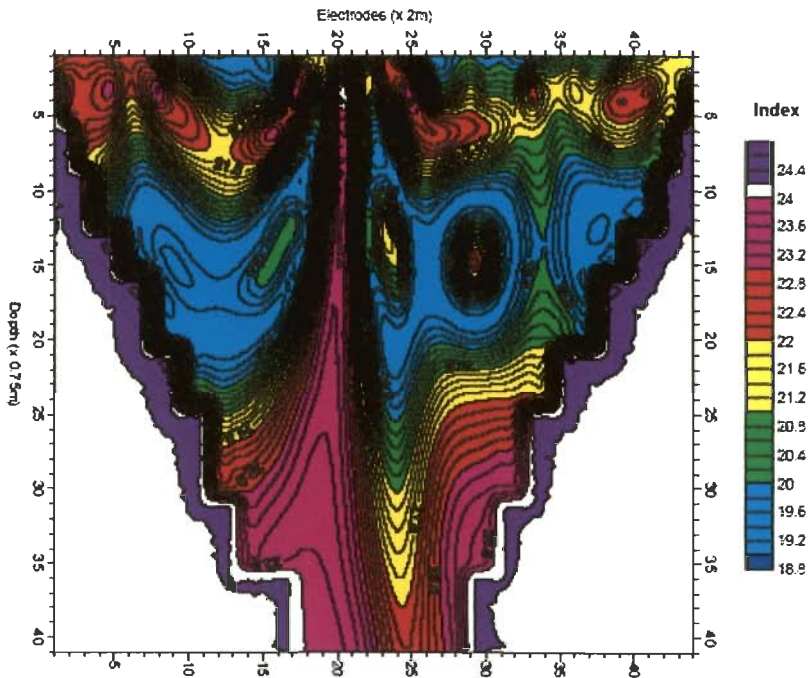


Fig. 6.23 Predicted Bearing Capacity Factor of General Shear Failure, N_q Section from Angle of Internal Friction Along Profile A-B, Library Site, IITR

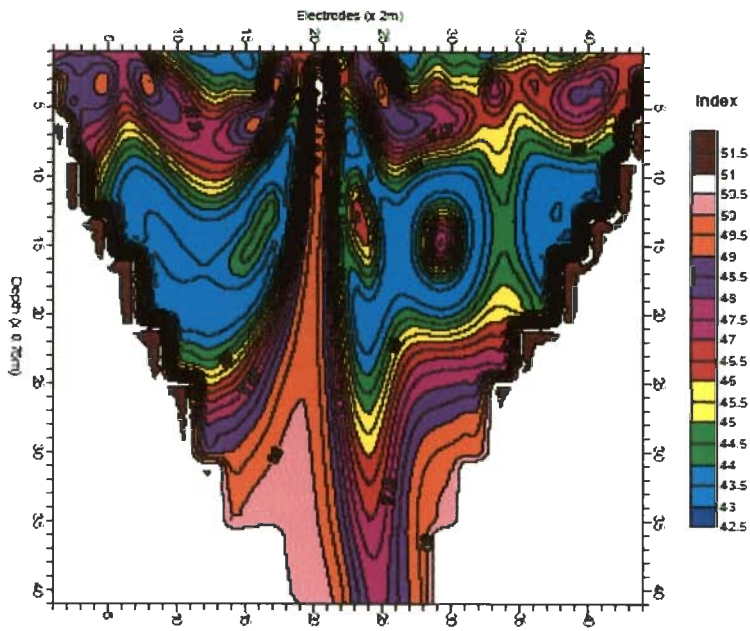


Fig. 6.24 Predicted Ultimate Bearing Capacity Factor, N_c Section for Strip Footings from Angle of Internal Friction Section Along Profile A-B, Library Site, IITR

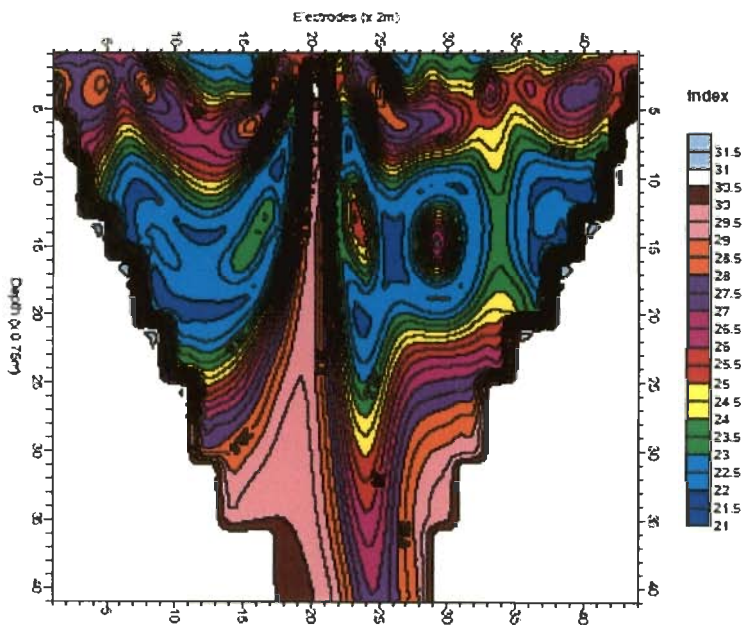


Fig. 6.25 Predicted Ultimate Bearing Capacity Factor, N_y Section for Strip Footings from Angle of Internal Friction Section Along Profile A-B, Library Site, IITR

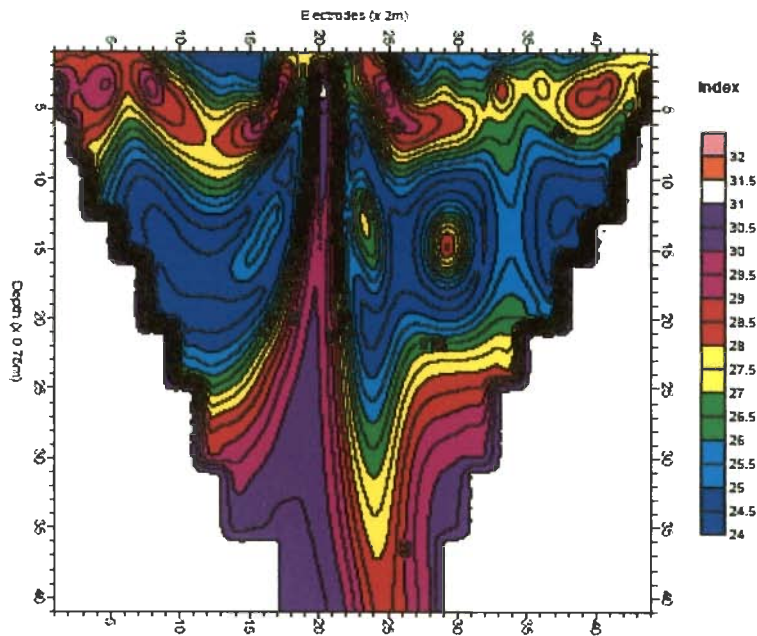


Fig. 6.26 Predicted Ultimate Bearing Capacity Factor, N_q Section for Strip Footings from Angle of Internal Friction Section Along Profile A-B, Library Site, IITR

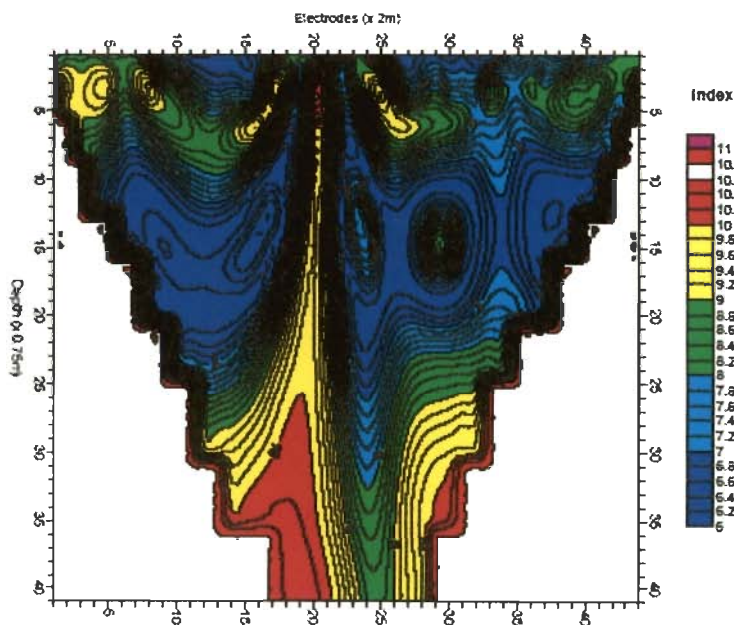


Fig. 6.27 Predicted Terzaghi's Bearing Capacity (Peck et al. 1974) N_γ Factor Section from Angle of Internal Friction Section Along Profile A-B, Library Site, IITR

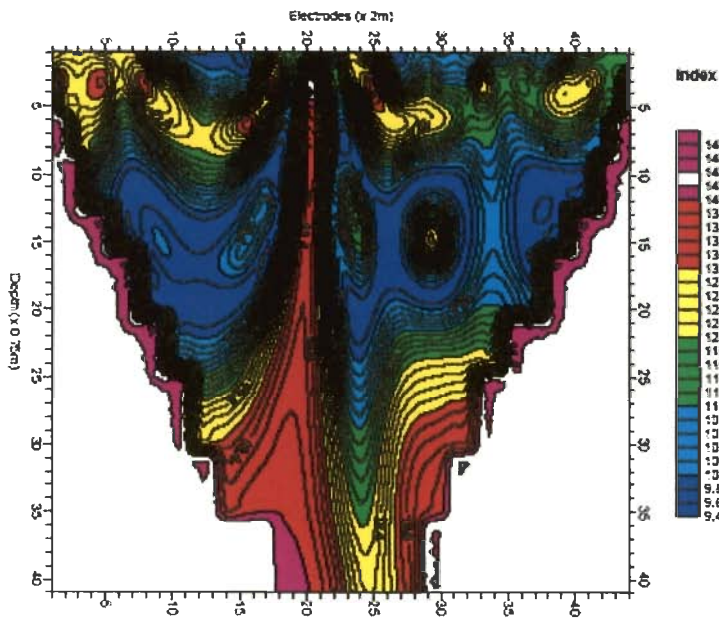


Fig. 6.28 Predicted Terzaghi's Bearing Capacity (Peck et al. 1974) Factor, N_q Section from Angle of Internal Friction Section Along Profile A-B, Library Site, IITR

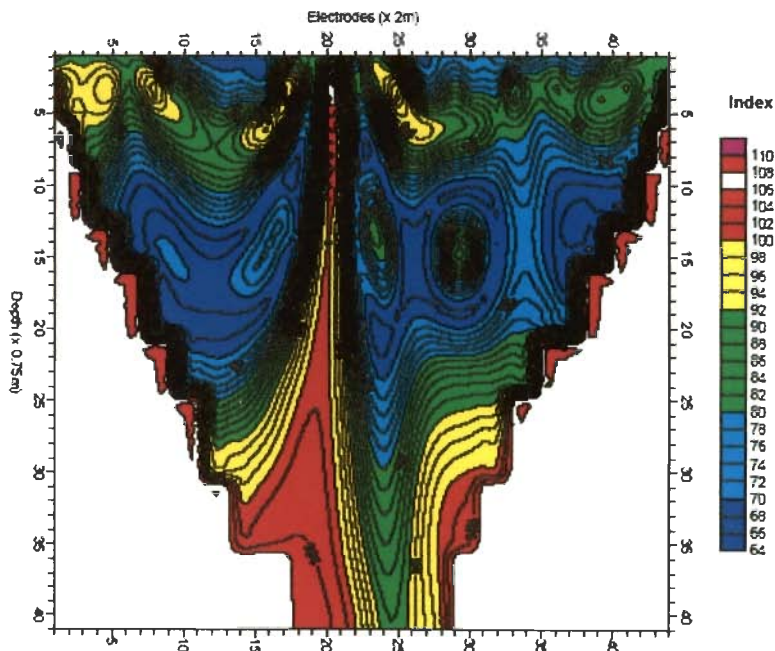


Fig. 6.29 Predicted N_q Factor (Meyerhof, 1953) Section for Driven Piles from Angle of Internal Friction Section Along Profile A-B, Library Site, IITR

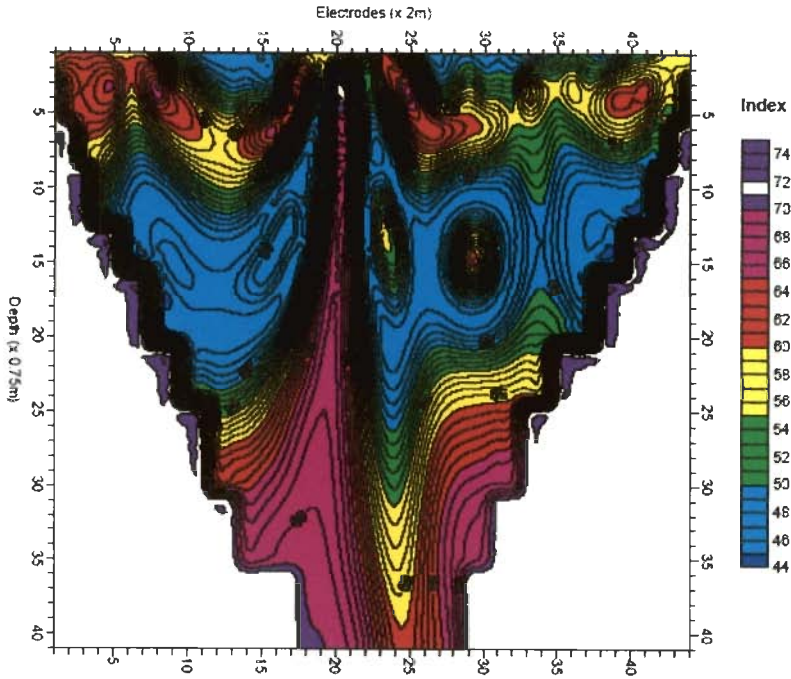


Fig. 6.30 Predicted N_q (Meyerhof, 1953) Factor Section for Bored Piles from Angle of Internal Friction Section Along Profile A-B, Library Site, IITR

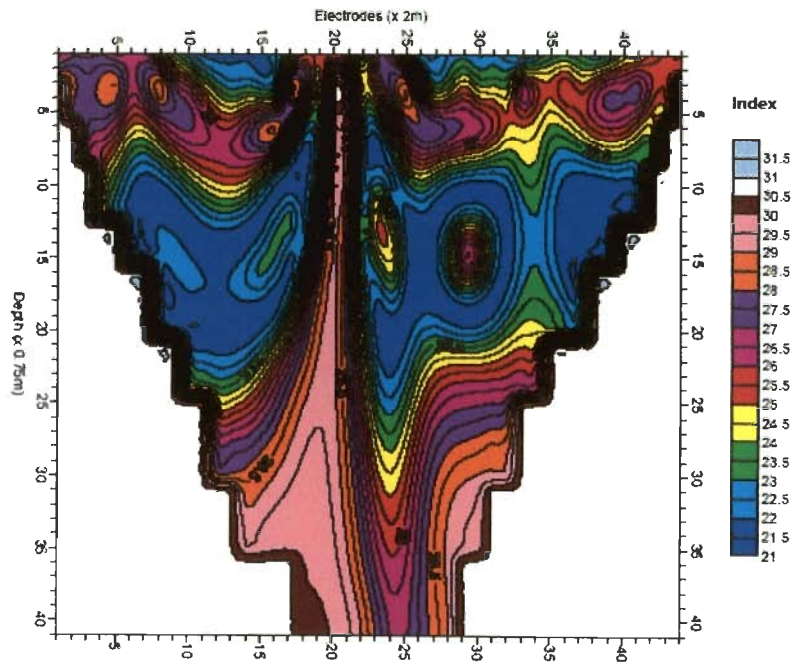


Fig. 6.31 Predicted N_q (Vesic) Factor Section for Bored Piles from Angle of Internal Friction Section Along Profile A-B, Library Site, IITR

GEOTECHNICAL CASE STUDIES-II

7.1 GENERAL

This study region namely construction of multistoried building of Hill-View Apartments (former East Punjab (E. P.) Hostel) structure, I.I.T. Roorkee falls in Uttarakhand State, India and it is in Indo-Gangetic Alluvial Plains. Here, the methodology detailed in Chapter 5 has been utilized in geotechnical site characterization using resistivity / IP image data. Geology of the study region (Table 6.1) remains same as that outlined in previous chapter.

7.2 SITE LOCATION MAPS

Figure 7.1(a) illustrates the position location of study region. Different field geoelectrical and geotechnical study locations are indicated in Fig. 7.1(b). The geoelectrical investigations refer to resistivity and IP imaging data acquisition.

7.3 GEOELECTRICAL AND GEOTECHNICAL DATA ACQUISITION

An attempt was made to acquire the geoelectrical data using a micro-processor controlled multi-electrode imaging system of French make (SYSCAL Jr. II of 72-electrodes). The relevant details of IP and resistivity images along chosen profile A-B (Fig. 7.1b) are included in Fig. 7.2.

The geotechnical data is acquired by a civil engineering company entrusted with a multi-storeyed building construction at this site. For our analysis we have consulted their report.

As detailed in Chapters 5 and 6, for generation of regression equations of both formation and geotechnical parameters, a pair of boreholes in the vicinity of geoelectrical profile was selected. Both geoelectrical image data columns coinciding with projected

borehole positions were correlated with both formation and geotechnical data available at those boreholes. The electrodes positions E-12 and EL-33 of profile A-B are correspond to the projected location of boreholes B-24 and B-29. Figs. 7.10a and 7.10b describe the observed SPT data at borehole location B-1 and B-2 respectively. Further analysis is described in the following sections:

7.4 REGRESSION EQUATIONS FOR FORMATION AND SITE GEOTECHNICAL TESTS

The complete methodology as outlined in Chapter 5 is implemented. Regression equations are developed for both formation and geotechnical parameters for profile A-B (Fig. 7.1b). For brevity sake, all those details are not included here. Table 7.1 contains all inferred regression equations (sand, clay, lithology, porosity, water saturation, SPT and SCPT) for this study region (Profile A-B in Fig. 7.1 b).

The observed SCPT data corresponding to the EL-15 and EL-33 have been shown in Figs. 7.14a and 7.14b respectively. On the basis of IP, predicted SCPT section has been presented in the Fig. 7.15.

7.5 PREDICTED 2-D SECTIONS FOR FORMATION AND SITE GEOTECHNICAL TESTS

As per methodology outlined in Chapter 5, by utilizing the appropriate regression equations that are included in Table 7.1, the digital IP values along section A-B (Fig. 7.2b) are converted to respective formation and field geotechnical sections. Accordingly, Figs. 7.3, 7.4, 7.7-7.9, 7.11 and 7.15 refer to predicted 2-D sections for sand, clay, lithology, porosity, water saturation, SPT and SCPT. IP derived sand and clay sections are included in Figs. 7.5-7.6 respectively. In Figs. 7.12 and 7.13, we compare inferred SPT with observed SPT for boreholes B-1 and B-2 respectively. As the number of illustrations is quite large, they are appended at the end of the chapter. Table 7.2 provides relevant details.

By utilizing the regression equations developed in Chapter 4 (Table 4.10), several geotechnical parameter sections are developed by considering IP section along profile A-B

(Fig. 7.2) as input. Accordingly, Figs. 7.16-7.30 respectively contain predicted 2-D sections of angle of internal friction (ϕ), unit weights of soil (dry & saturated), unconfined compressive strength(q_u), bearing capacity factors for general shear failure (N_c , N_γ (Vesic) and N_q), ultimate bearing capacity factors (N_c , N_γ and N_q), Terzaghi's bearing capacity (Peck et al. 1974) factors (N_γ and N_q), bored pile factors (N_q (Meyerhof, 1953) and N_q (Vesic)) and driven pile N_q factor (Meyerhof, 1953).

Table 7.1 Inferred Predictive Equations from Cross-correlation of Normalized Plots at Different Geophysical Sites Projected onto Profile A-B at E.P. Hostel, IITR

S. No.	Formation Parameter / Geotechnical Parameter	Correlation equation based on IP at B-1 (EL-24) $Y=a_1x^2+a_2x+a_3$	Correlation equation based on IP at B-2 (EL-29) $Y=b_1x^2+b_2x+b_3$	Average Correlation equation based on IP at B-1&B-2 $Y=c_1x^2+c_2x+c_3$ [$c_1=av(a_1,b_1)$, $c_2=av(a_2,b_2)$, $c_3=av(a_3,b_3)$]
1	Sand	$a = \{-0.2743, 0.4862, 0.772\}$ $R^2 = 0.3882$	$b = \{-0.0483, -0.0918, 0.9363\}$ $R^2 = 0.3841$	$c = \{-0.1613, 0.1972, 0.85415\}$
2	Clay / Shale	$a = \{0.3384, -0.5999, 0.3248\}$ $R^2 = 0.3882$	$b = \{0.0595, 0.1133, 0.122\}$ $R^2 = 0.3841$	$c = \{0.19895, -0.2433, 0.2234\}$
3	Lithology	$a = \{-1.4616, 1.6213, 0.1964\}$ $R^2 = 0.4473$	$b = \{0.6485, -0.7693, 0.5106\}$ $R^2 = 0.1942$	$c = \{-0.40655, 0.426, 0.3535\}$
4	SPT	$a = \{1.0069, -0.7463, 0.4039\}$ $R^2 = 0.5214$	$y = \{-0.4599, 0.3507, 0.3915\}$ $R^2 = 0.1385$	$c = \{-0.56185, 0.5346, 0.61015\}$ $c = \{0.2735, -0.1978, 0.3977\}$
5	SCPT	$a = \{0.3698, -0.6645, 0.4184\}$ $R^2 = 0.766$ SCPT 1 at EL-15	$b = \{0.2837, -0.4139, 0.3419\}$ $R^2 = 0.1436$ SCPT 2 at EL-33	$c = \{0.32675, -0.5392, 0.38015\}$
6	Porosity	$a = \{-0.2739, 0.486, 0.7719\}$ $R^2 = 0.3889$	$b = \{-0.0461, -0.094, 0.9366\}$ $R^2 = 0.3852$	$c = \{-0.16, -0.196, 0.85425\}$
7	Water Saturation	$a = \{-2.4243, 3.0389, 0.046\}$ $R^2 = 0.9159$	$b = \{0.1115, -0.567, 0.7094\}$ $R^2 = 0.2338$	$c = \{-1.1564, 1.23595, 0.3777\}$

7.2 Predicted 2D Geotechnical Parameter Sections

S. No.	Formation / Geotechnical Parameter		IP	Remarks
1.	Sand	IP derived	Fig. 7.3	Only IP derived sand section is presented. Predominantly, sand is present with pockets of shaly sands and clay
		Geotechnical & IP derived	Fig. 7.5	
2.	Clay / Shale	IP derived	Fig. 7.4	
		Geotechnical & IP derived	Fig. 7.6	
3.	Lithology		Fig. 7.7	Silt and clay dominate the section.
4.	SPT (N)		Figs. 7.11, 7.12, 7.13	Its range is 10 - 13. IP based SPT is validated against B1 and B2 data. It has an average performance. No resistivity derived SPT estimate has been tried.
5.	SCPT		Fig. 7.15	Predominantly, its range is 50-58; However, in deeper horizons, its value reduces to 24-30.
6.	Porosity		Fig. 7.8	For a major portion the range is 30-38%. A low porosity pocket (21-30%) in central region exists.
7.	Water saturation		Fig. 7.9	It exhibits inhomogeneous 2-D distribution, predominantly in the range, 15-28%.
8.	Unit weight of soil	Dry	Fig. 7.17	It exhibits 2-D variation and its range is 14.4-19 kN/m ³ .
		Saturated	Fig. 7.18	It exhibits 2-D variation and its range is 18.8-21.6 kN/m ³ .
9.	Angle of internal friction, ϕ		Fig. 7.16	Its range is 29.5 – 30.6°
10.	Unconfined compressive strength, q_u		Fig. 7.19	Its predominant range is 140-150 kN/m ² with few pockets in the range 132-150 kN/m ² .
11.	Terzaghi's Bearing Capacity factors (Peck et al. 1974)	N_γ factor	Fig. 7.26	All these bearing capacity factor sections exhibit 2-D variation. Depending on the proposed depth of foundation, the 2-D sections can be transformed into 1-D sections by an averaging process. These 1-D sections could of much help in the design of foundations of superstructures.
		N_q factor	Fig. 7.27	
12.	Bearing capacity factors of general shear failure	N_c factor	Fig. 7.20	
		N_γ (Vesic) factor	Fig. 7.21	
		N_q factor	Fig. 7.22	
13.	Ultimate bearing capacity factors	N_c factor	Fig. 7.23	
		N_γ factor	Fig. 7.24	
		N_q factor	Fig. 7.25	
14.	Piles	Driven Piles N_q (Meyerhof, 1953) factor	Fig. 7.28	
		Bored Piles N_q (Meyerhof, 1953) factor	Fig. 7.29	
		Bored Piles N_q (Vesic, 1953) factor	Fig. 7.30	

7.6 RESULTS & DISCUSSION

In the present case study, IP derived profiles and sections are included here. The prime reason behind such a decision is due to better quality of input IP section (Fig. 7.2b) over that of resistivity section (Fig. 7.2a). No inter-comparison studies are attempted here. In this regard, Table 7.2 contains all relevant details. The methodology adopted herein honors both geoelectrical and geotechnical data. The geotechnical data is obtained from the technical report of Civil Engineering Company. As per methodology outlined in Chapter 5, the development of regression equations rested on a pair of boreholes that are projected onto the geoelectrical profile, A-B (Fig. 7.1b) and the IP data at those electrode positions. The regression equations are limited to 2nd degree polynomial only as higher order polynomial involves the usual mathematical difficulties as perceived in regional-residual separation for gravity data processing (Dobrin, 1976). Additionally, the followings remarks need to be considered:

- a) In Fig. 7.3 sand section is directly derived from IP section by using equation 3.20, whereas Fig. 7.5 is derived from IP through the use of regression equation included in Table 7.1. As revealed in Fig. 7.5, the subsurface section is predominantly sandy. This is also corroborated by Fig. 7.6, wherein the clay amount is included.
- b) Contrary to earlier sand and clay sections, the lithology section (Fig. 7.7) derived from IP seems to indicate predominance of fines (silt and clay).
- c) The predicted porosity section (Fig. 7.8) along Profile A-B indicates a moderate porosity variation in the range 21-38 %.
- d) The predicted water saturation section infers the water table at 7.5 m depth and the low water saturation distribution (Fig. 7.9) is typical of shaly / clayey / silty sands.
- e) Water saturation based regression equation in Table 4.10 has allowed to predict unit weights of soil (both dry and Saturated) in Figs. 7.17 and 7.18.
- f) In Figs. 7.12 and 7.13, it is clear that IP based SPT prediction can at best lead to an average estimation only.
- g) Figure 7.15 depicts predicted SPT section on the basis of IP and regression equation outlined in Table 7.1. On an average, SPT 'N' varies in the range 10-13. On the

contrary, as predicted SCPT section provides a better resolution with the values ranging from 24-60.

- h) Unconfined compressive strength, q_u derived from SPT 'N' section is included in Fig. 7.19. Predominantly, q_u ranges from 132-170 kN/m³ with a 2-D distribution.
- i) The angle of internal friction, ϕ section derived from SPT reveals that it varies over a narrow zone of 29.5-30.5.
- j) All bearing capacity coefficient sections (Figs. 7.20-7.30), which are derived from angle of internal friction, ϕ section show a 2-D distribution. The traditional 1-D geotechnical models can be developed on their basis. It is expected that such sections are more likely to be better than those of the current practice at a proposed depth of foundation.
- k) All inferred 2-D sections clearly show that 1-D models often resorted to by geotechnical engineers are far from reality and efforts are needed to refine their quality or new procedures need to be evolved.
- l) The regression equations of Table 4.10 have been utilized throughout the study and they are based on current geotechnical literature.
- m) The regression equations listed in Table 7.2 are site-specific and geo-electrical profile specific.
- n) The quality of input geo-electric sections affect the inferred lithology, formation and geotechnical sections. So, basic data quality of geo-electrical data and attendant processing and inversion schemes has to be very high.
- o) The present procedure is applicable to soil strata only, where conventional geotechnical tests are valid.
- p) The bearing capacity factors based on CPT method is not attempted here. However, earlier outlined procedure for SPT 'N' can easily be extended to CPT method also.

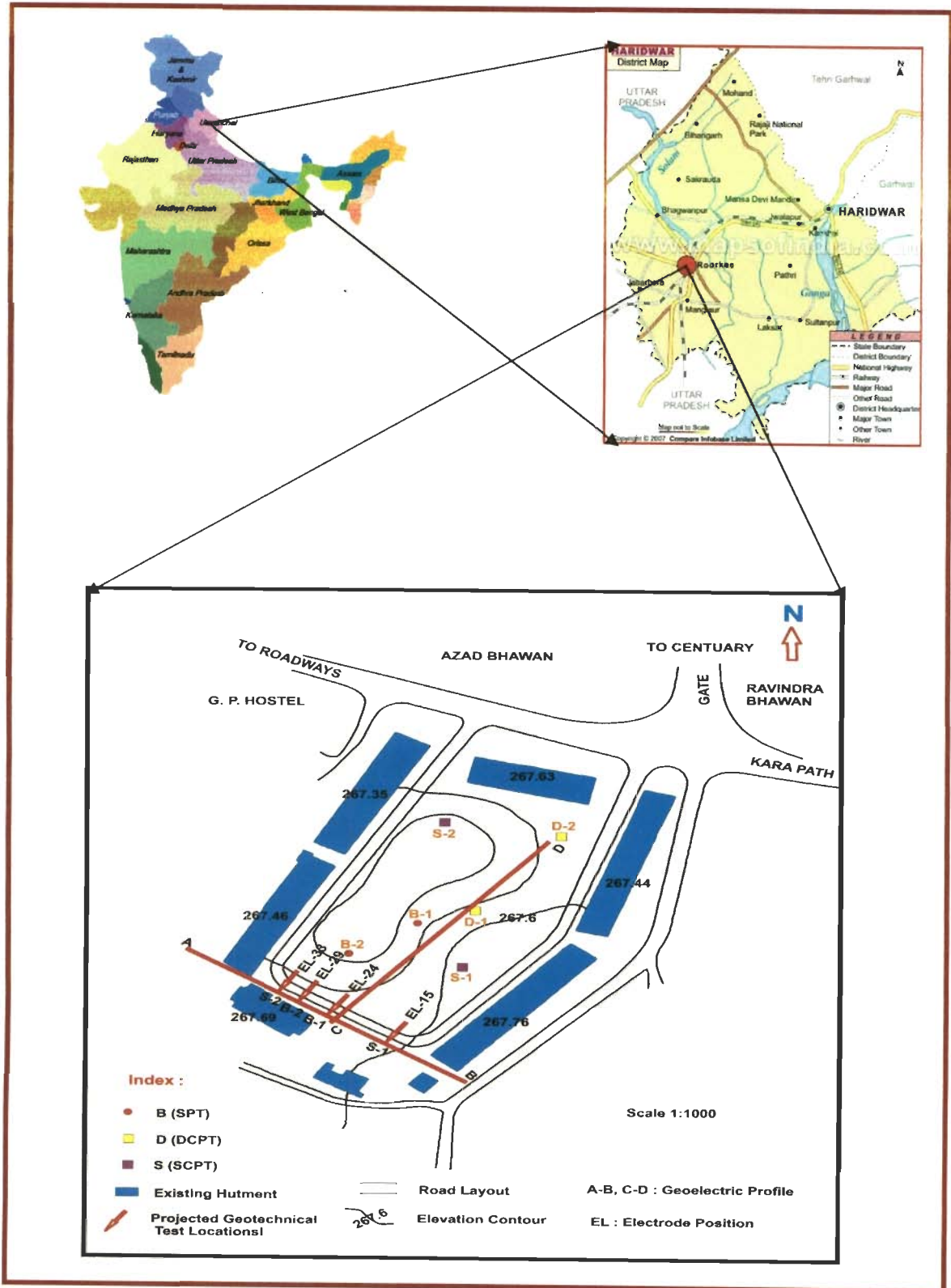


Fig. 7.1 a Location Map of Proposed Multi-storied Structure at E. P. Hostel Site, IIT Roorkee, Roorkee, India

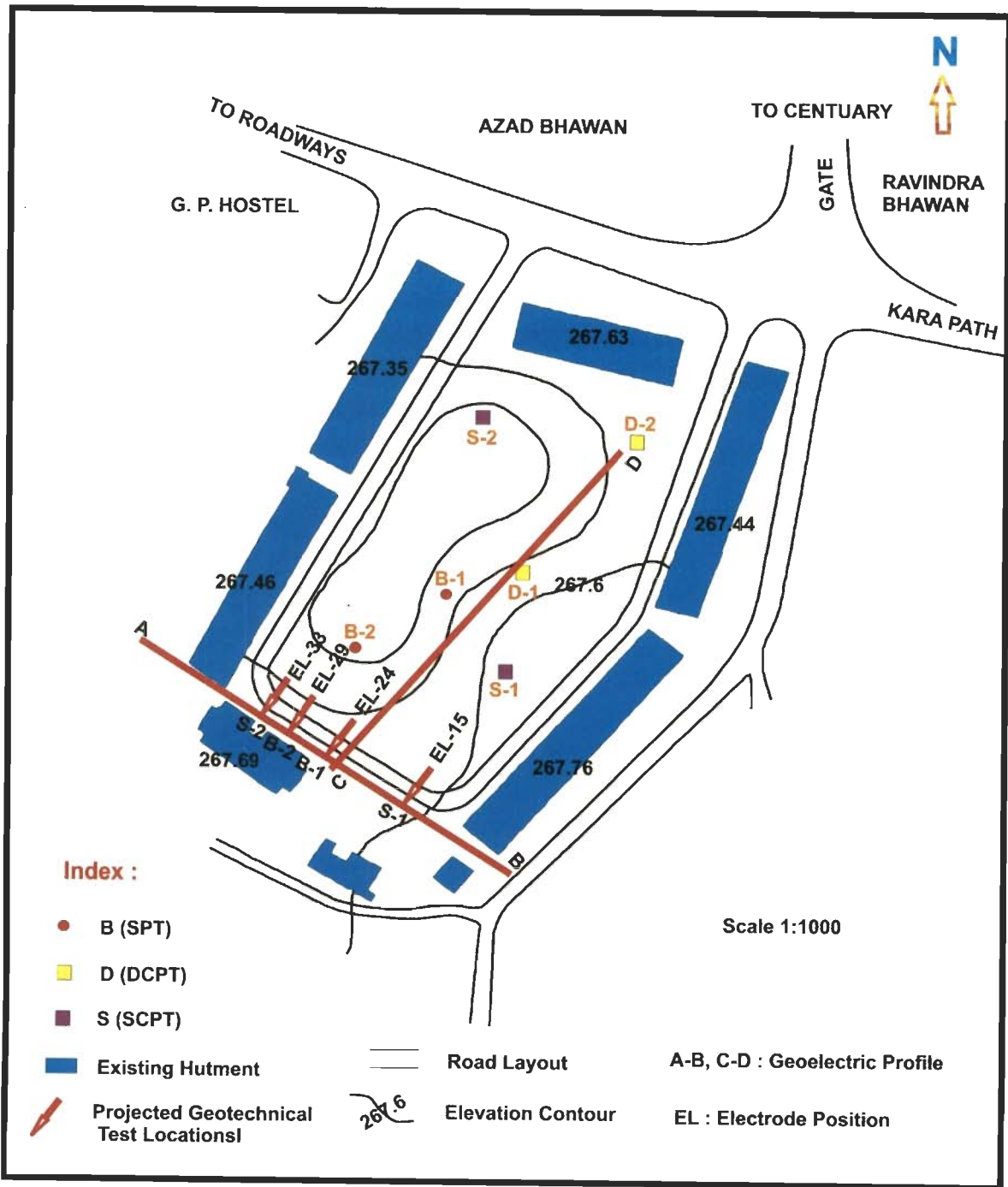


Fig. 7.1 b Map Showing the Location of ERT, IPI and Geotechnical Site Investigations

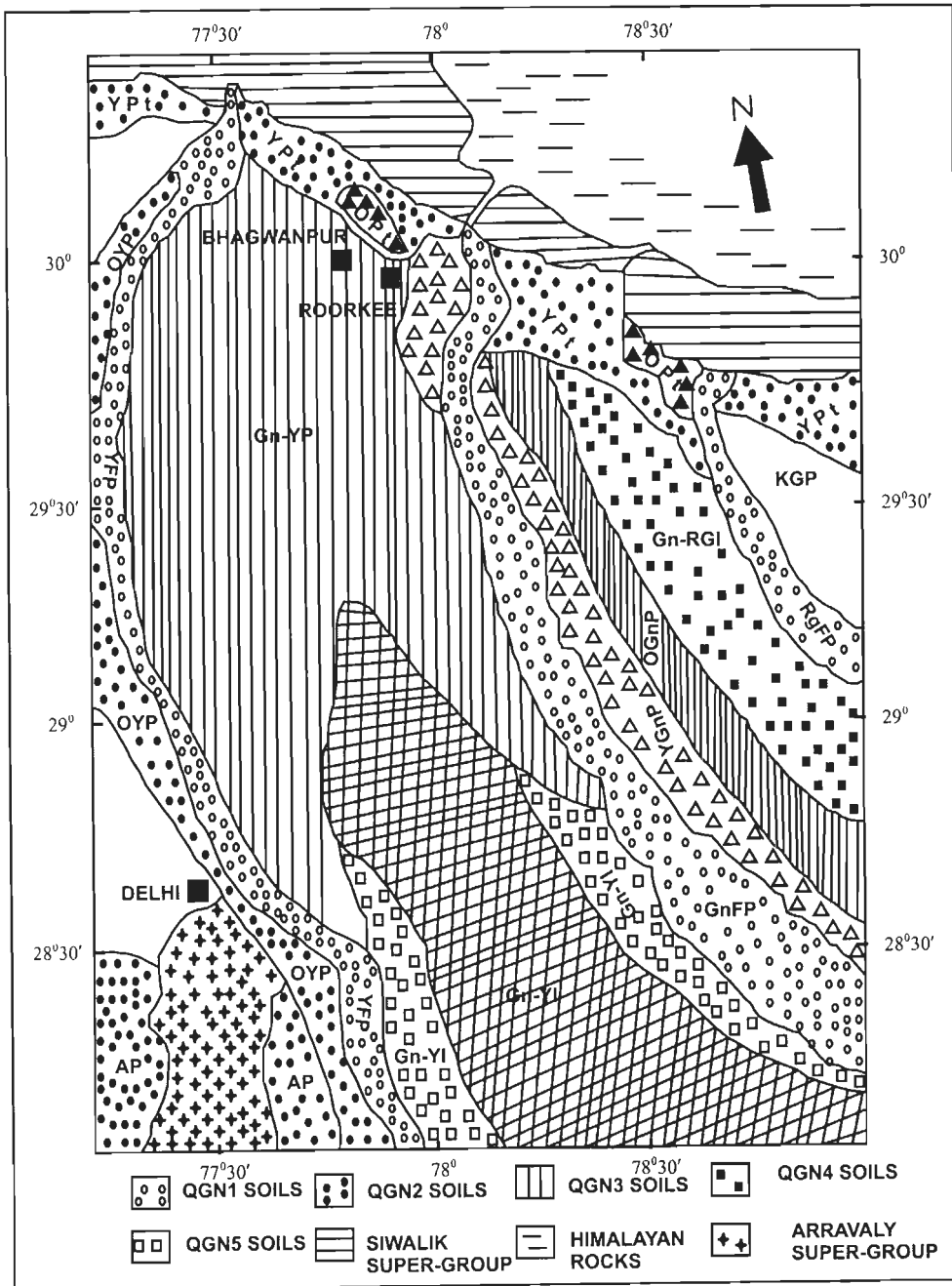


Fig. 7.1 c

Geological (Soil-Geomorphic) Map of the Study Region. GnFP-Ganga Floodplain; YGP-Young Ganga Plain; OGnP-Old Ganga Plain; GnRGI-Ganga-Ramganga Interfluev; KGP-Kosi-Gola Plain; Gn-YP-Ganga-Yamuna Plain; Gn-YI-Ganga-Yamuna Interfluev, SA-Salt Affected, NSA-Not Salt-Affected, YPt-Young Piedmont, Opt-Old Piedmont (Parkash et al. 2000, 2001)

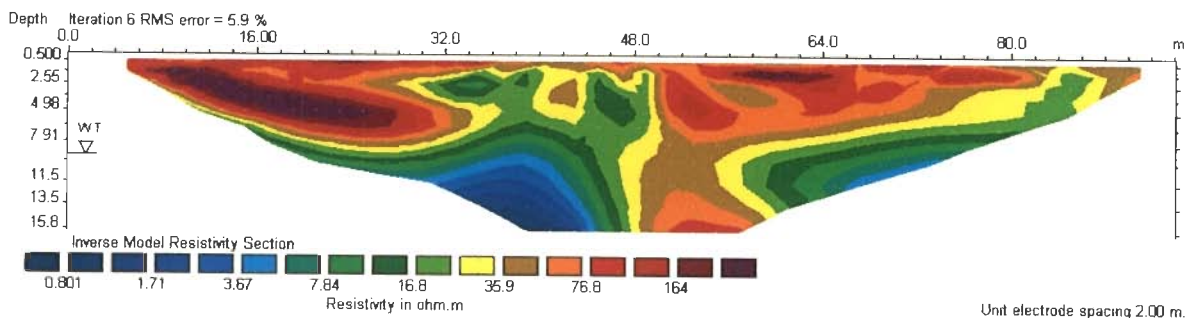


Fig. 7.2 a Resistivity Image (ERT) Along Profile A-B. The Resistivity and Depth Scales are Logarithmic.

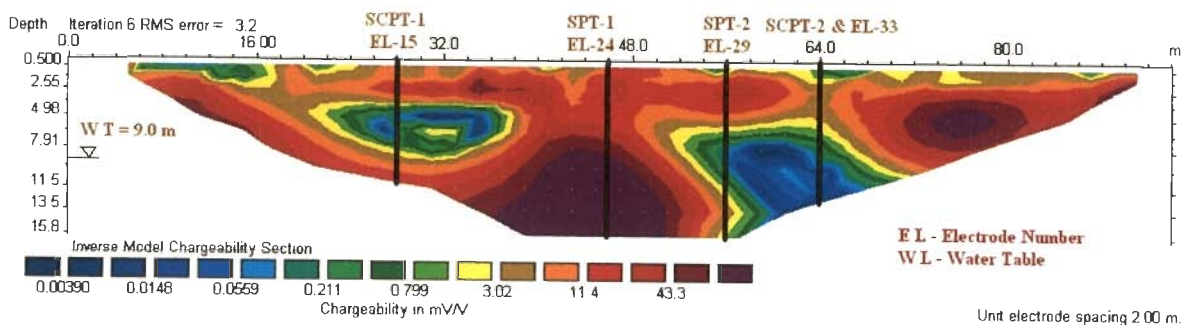


Fig. 7.2 b IP Image (IPI) Along Profile A-B. The Resistivity and Depth Scales are Logarithmic.

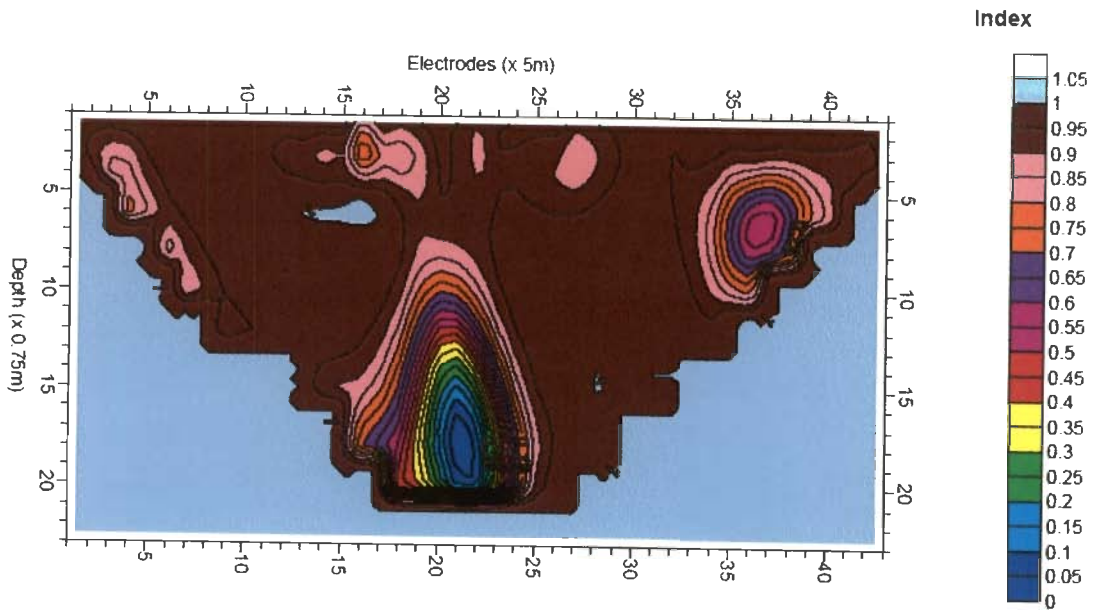


Fig. 7.3 IP Derived Sand (%) Section Along Profile A-B, E. P. Hostel, IITR

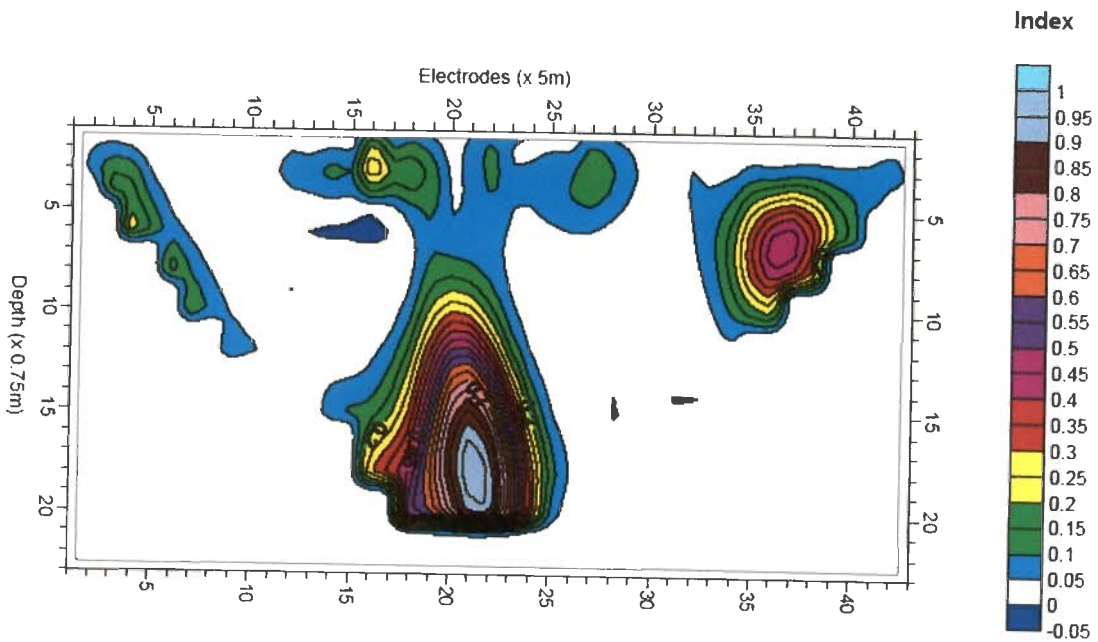


Fig. 7.4 IP Derived Clay (%) Section Along Profile A-B, E. P. Hostel, IITR

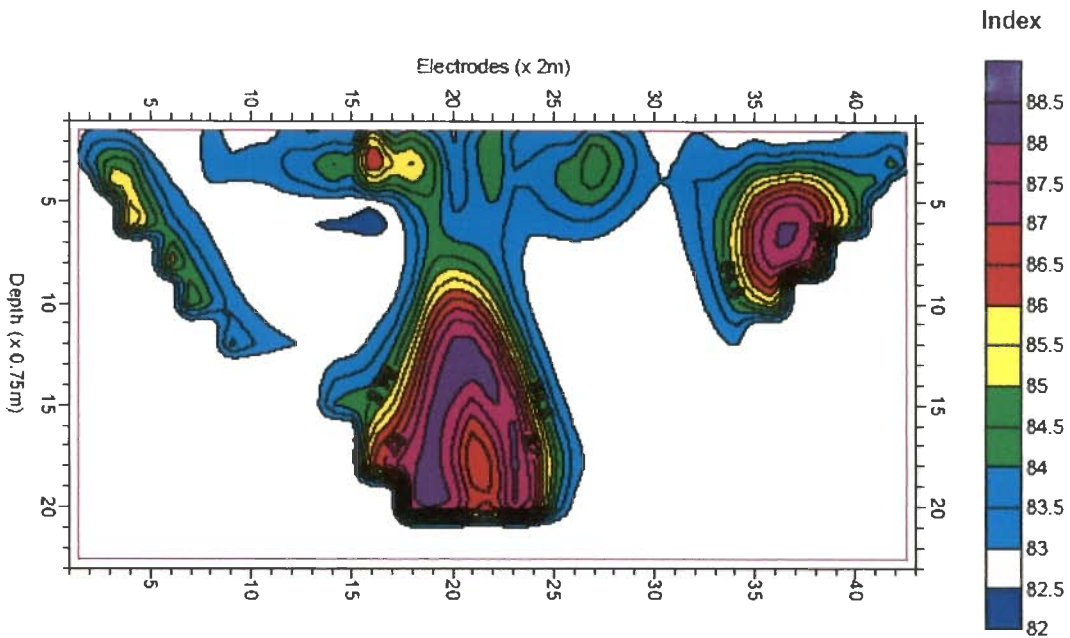


Fig. 7.5 Predicted Sand (%) Section from Geotechnical and IP Data Along Profile A-B, E. P. Hostel, IITR

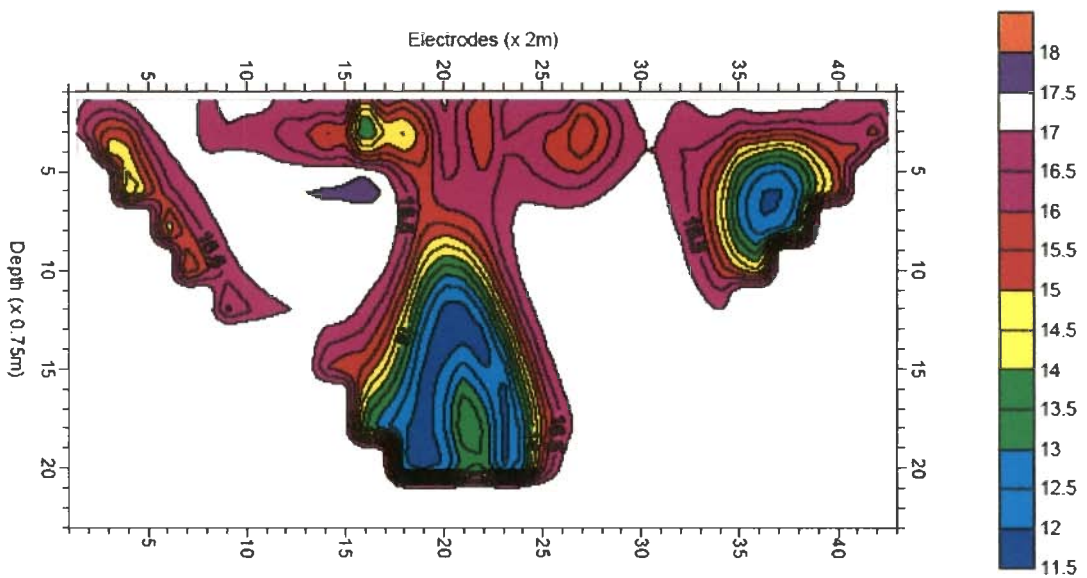


Fig. 7.6 Predicted Clay (%) Section from Geotechnical and IP data along Profile A-B, E. P. Hostel, IITR

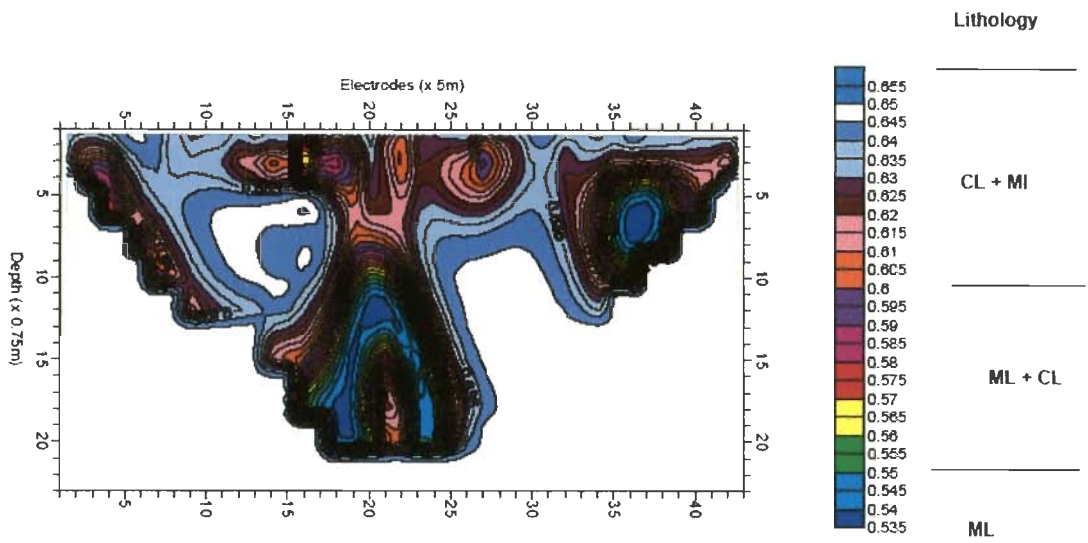


Fig. 7.7 Predicted Lithology Section from Geotechnical and IP Data Along Profile A-B, E. P. Hostel, IITR

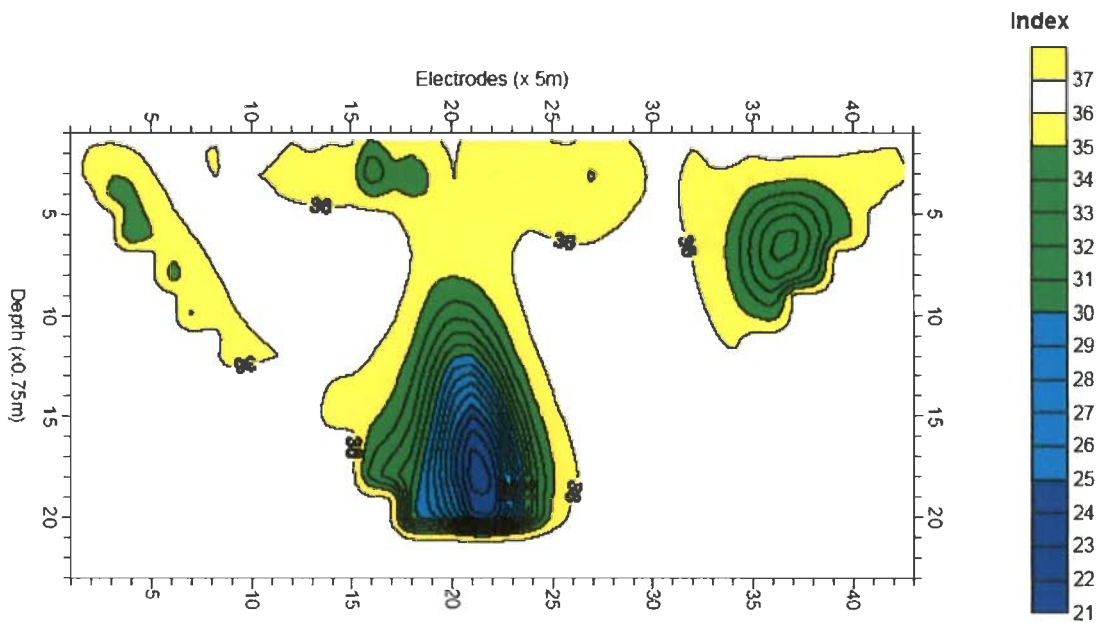


Fig. 7.8 Predicted Porosity (%) Section from IP and Geotechnical Data Along Profile A-B, E. P. Hostel, IITR

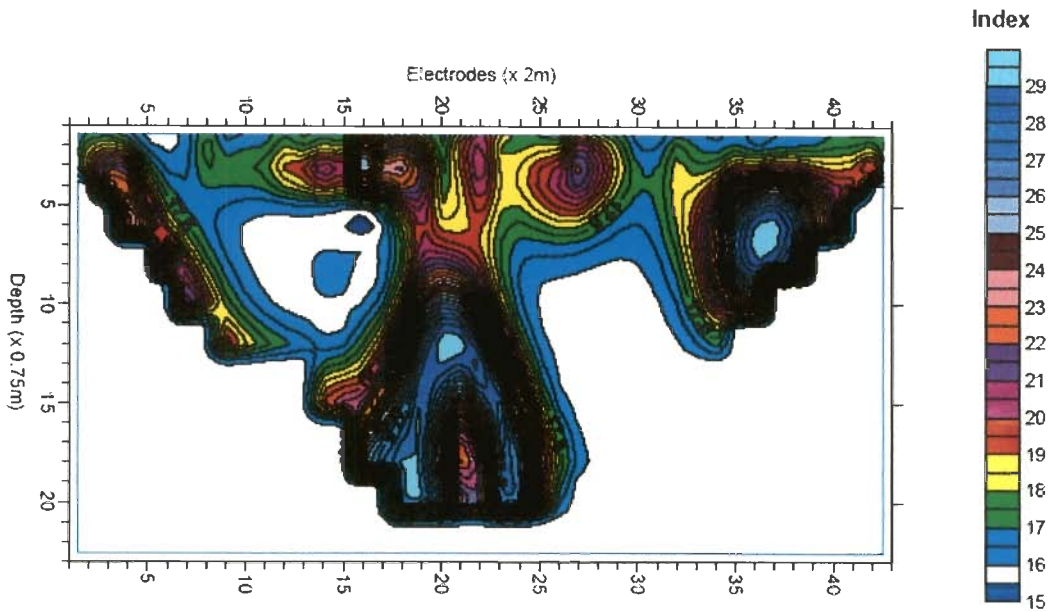
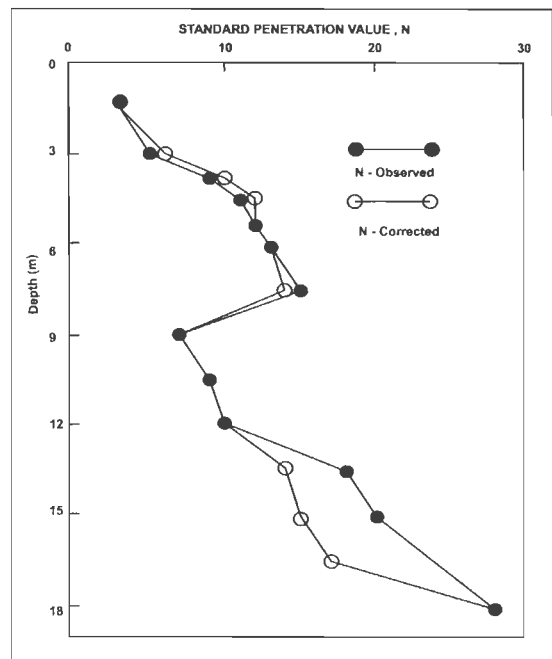


Fig. 7.9 Predicted Water Saturation (%) Section from IP and Geotechnical Data Along Profile A-B, E. P. Hostel, IITR

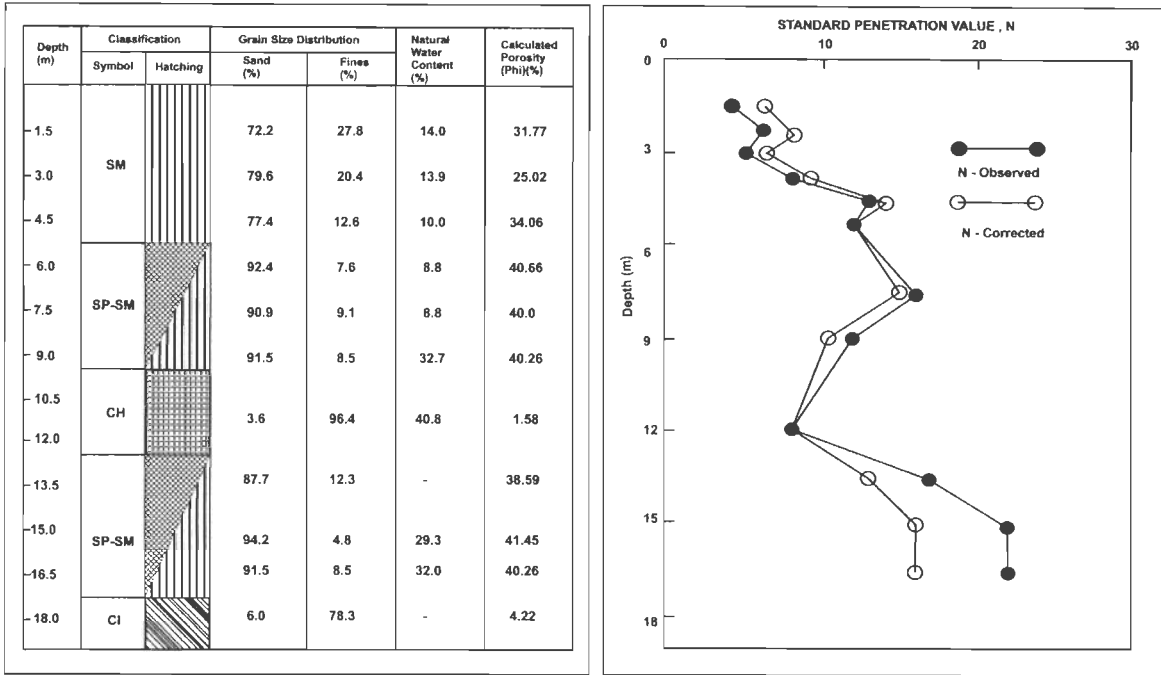
Depth (m)	Classification		Grain Size Distribution		Natural Water Content (%)	Calculated Porosity (P _n)(%)
	Symbol	Hatching	Sand (%)	Fines (%)		
1.5	CL	[Cross-hatch]	48.4	51.6	14.9	21.3
3.0	SM	[Vertical lines]	69.1	30.9	11.8	30.4
4.5	SP-SM	[Diagonal lines]	91.4	8.6	6.1	40.22
6.0	SM	[Vertical lines]	92.1	7.9	6.0	40.52
7.5	SM	[Vertical lines]	87.4	12.6	26.6	38.46
9.0	MI	[Dotted]	11.8	88.2	37.9	5.19
10.5	CH	[Horizontal lines]	7.0	93.0	41.6	3.08
12.0	CI	[Diagonal lines]	7.3	92.7	38.6	3.21
13.5	SP	[Dotted]	95.5	4.5	28.9	42.02
15.0			96.6	3.4	27.5	42.5
16.5	CI	[Diagonal lines]	96.0	4.0	26.3	42.24
18.0			9.1	76.6	36.9	4.0



a) Borehole B-1

SPT-DATA

Fig. 7.10 a Borehole Data at Location B-1. The Projected Borehole Position Coincides with Electrode, EL-24 of profile A-B



b) Borehole B-2

SPT-DATA

Fig. 7.10 b Borehole Data at Location B-2. The Projected Borehole Position Coincides with Electrode, EL-29 of profile A-B

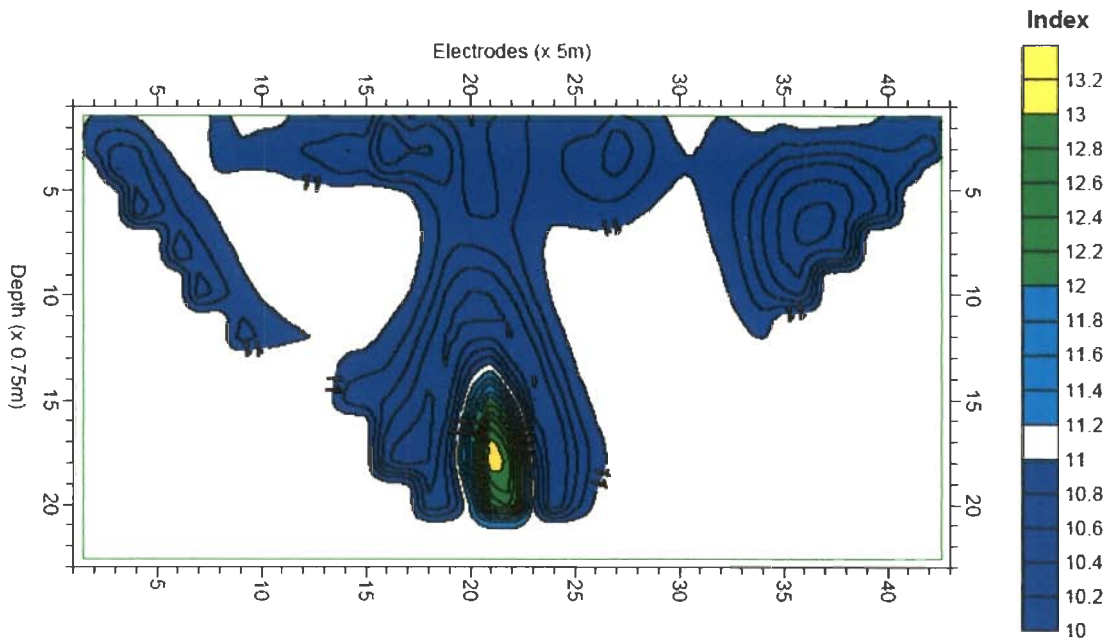


Fig. 7.11 Predicted SPT Section from IP and Borehole Data Along Profile A-B, E. P. Hostel, IITR

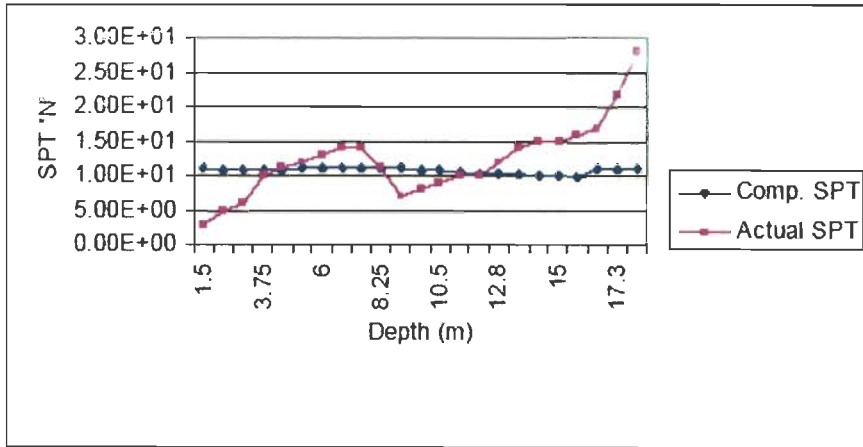


Fig. 7.12 Comparison of Observed and Predicted SPT 'N' through IP at Borehole Location – B-1

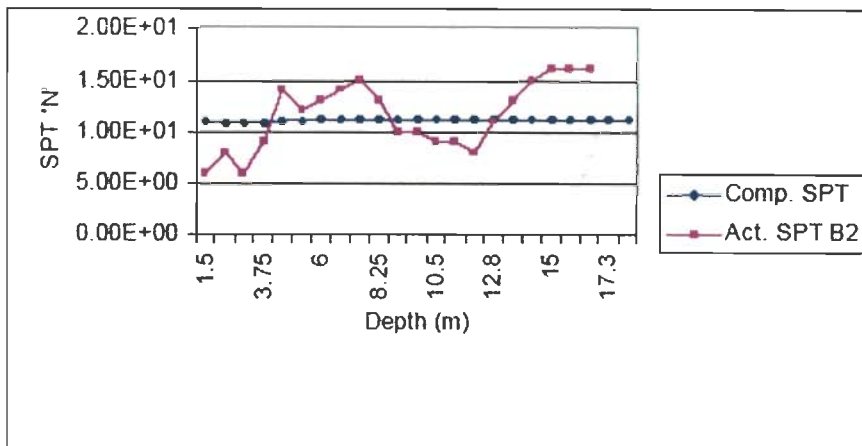
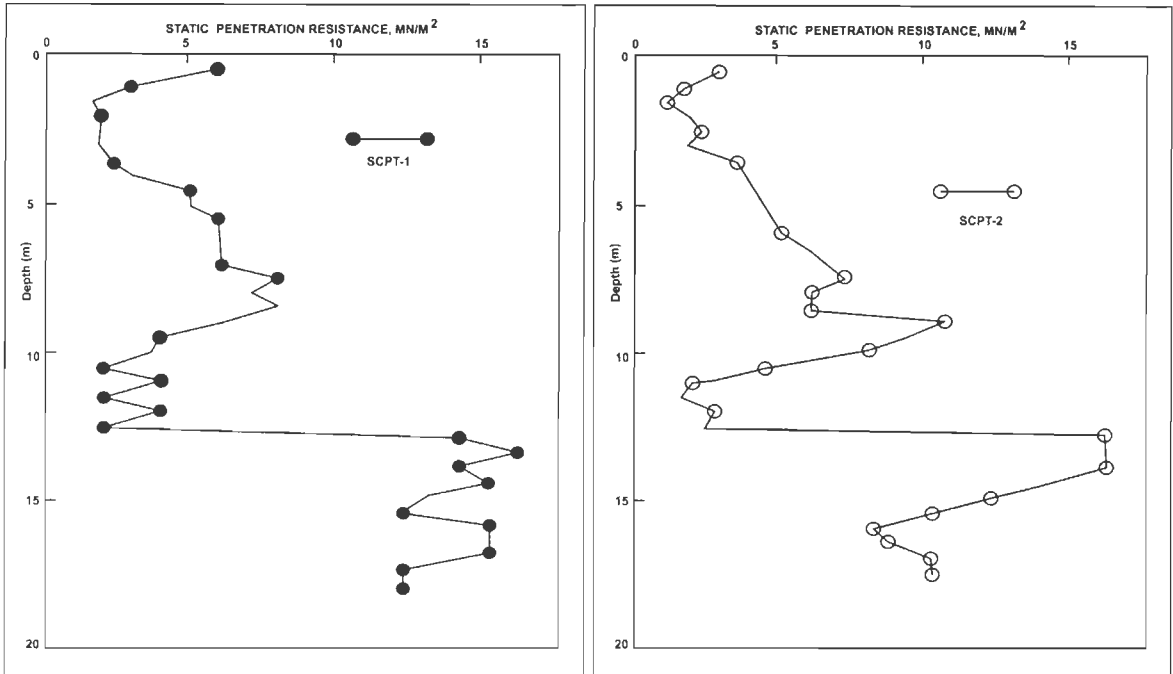


Fig. 7.13 Comparison of Observed and Predicted SPT 'N' through IP at Borehole Location- B-2



a) SCPT-1

b) SCPT-2

Fig. 7.14 a) SCPT-1 Data. The Corresponding Electrode Position is EL-15 of Profile A-B

b) SCPT-2 Data. The Corresponding Electrode Position is EL-33 of Profile A-B

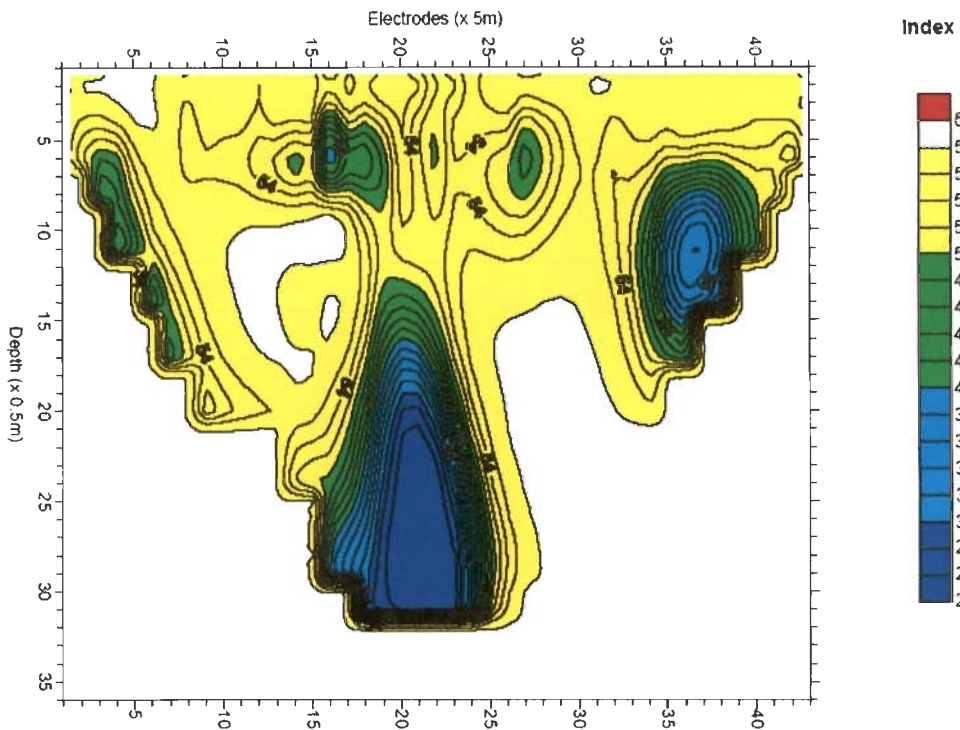


Fig. 7.15 Predicted SCPT Section from IP and Borehole Data Along Profile A-B, E. P. Hostel, IITR

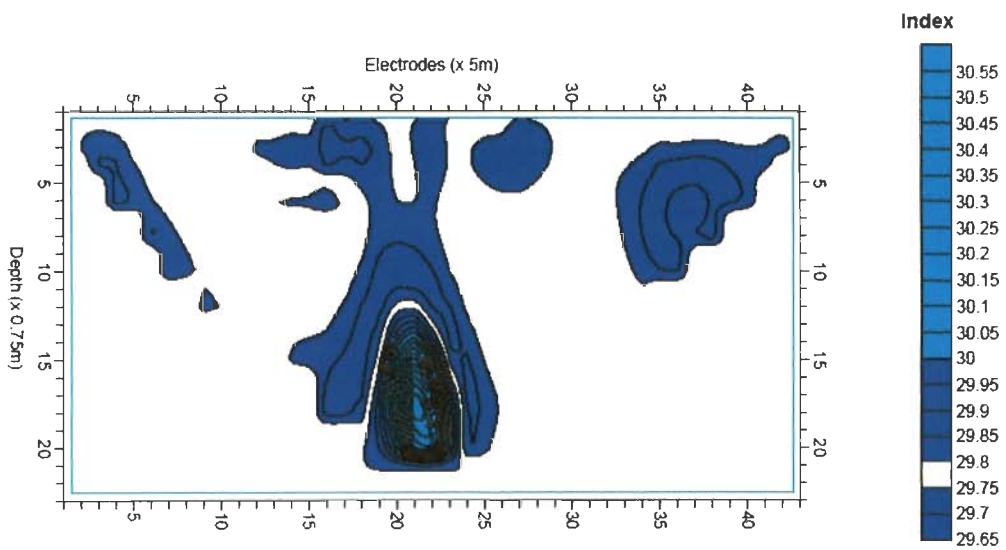


Fig. 7.16 Predicted Internal Friction Angle Section from Synthetic SPT Section Using IP Along Profile A-B, E. P. Hostel Site, IITR

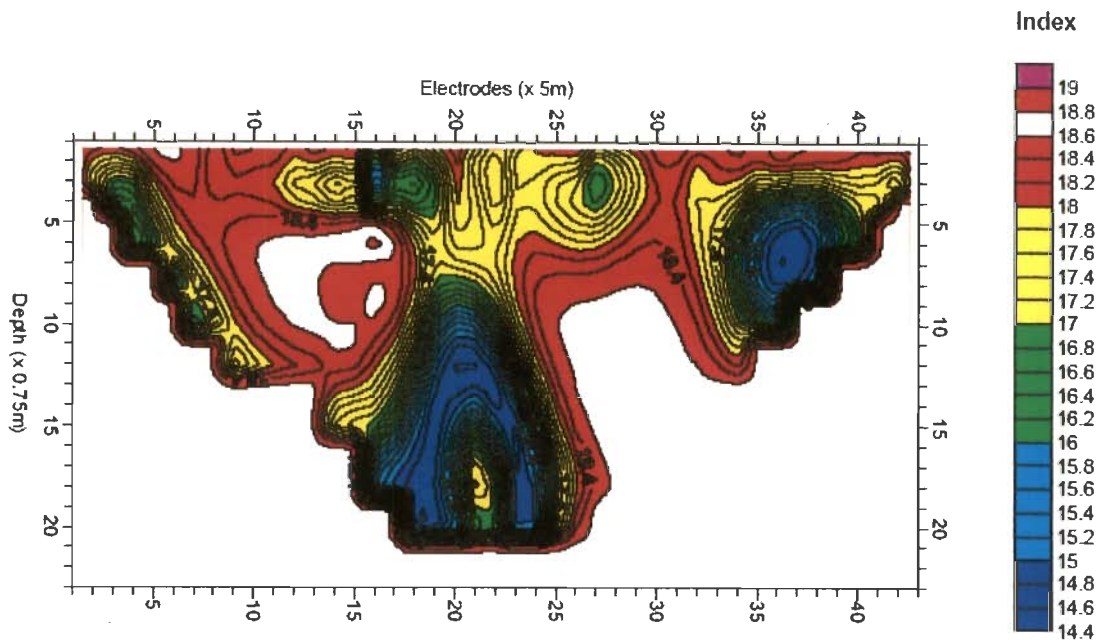


Fig. 7.17 Predicted Unit weight (Dry) in kN/m^3 Section from Water Saturation Section Using IP Along Profile A-B, E. P Hostel Site , IITR

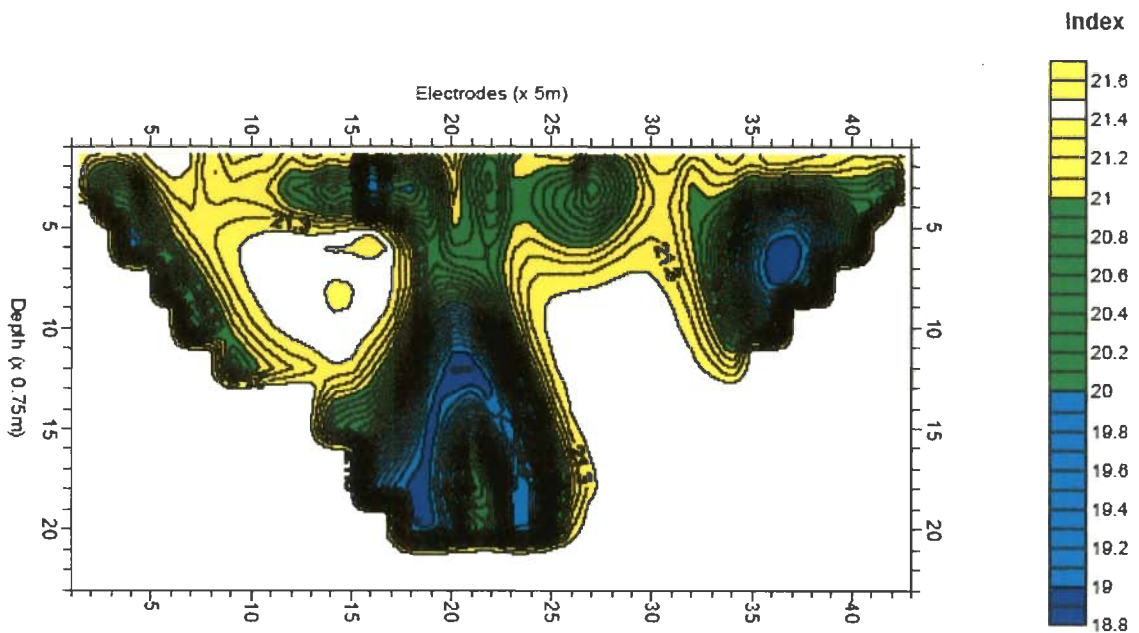


Fig. 7.18 Predicted Unit Weight (Saturated) in kN/m^3 Section from Water Saturation Section Using IP Along Profile A-B, E. P. Hostel, IITR

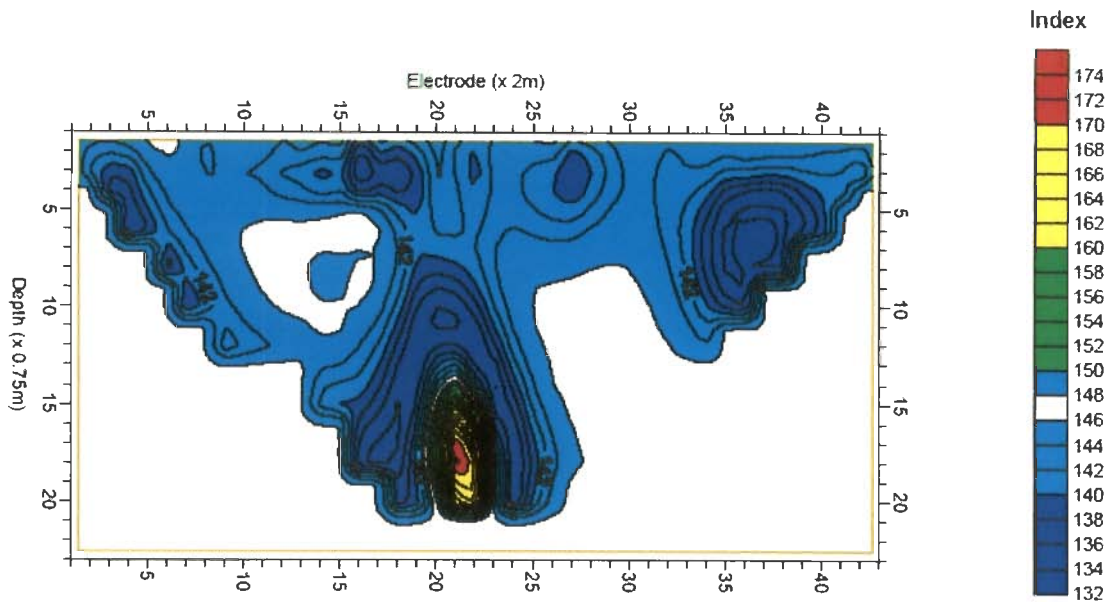


Fig. 7.19 Predicted Unconfined Compressive Strength, q_u Section from SPT 'N' Section Using IP Along Profile A-B, E. P. Hostel, IITR

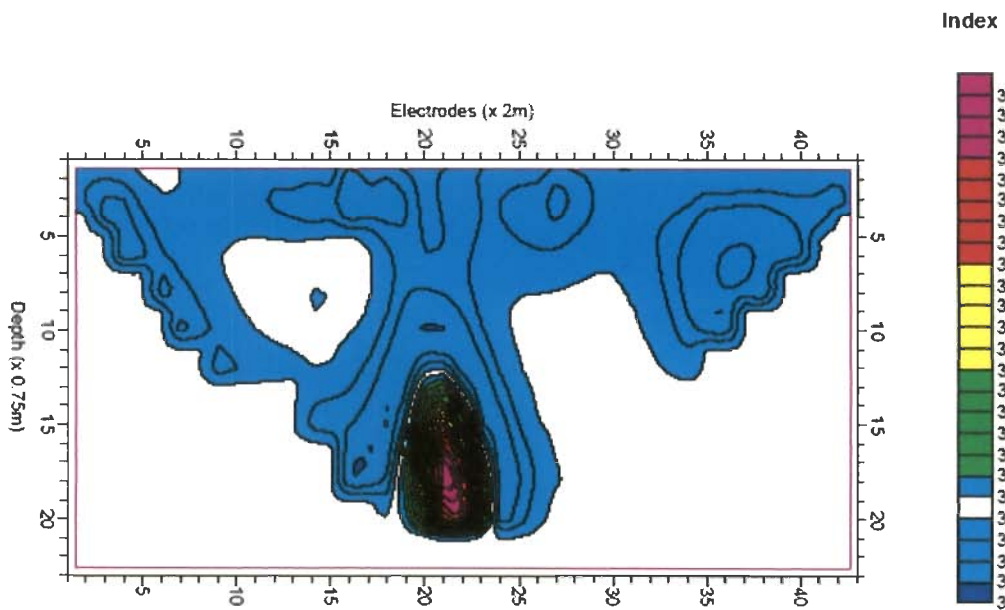


Fig. 7.20 Predicted Bearing Capacity Factor of General Shear Failure, N_c Section from IP Derived Angle of Internal Friction Section Along Profile A-B, E. P. Hostel, IITR

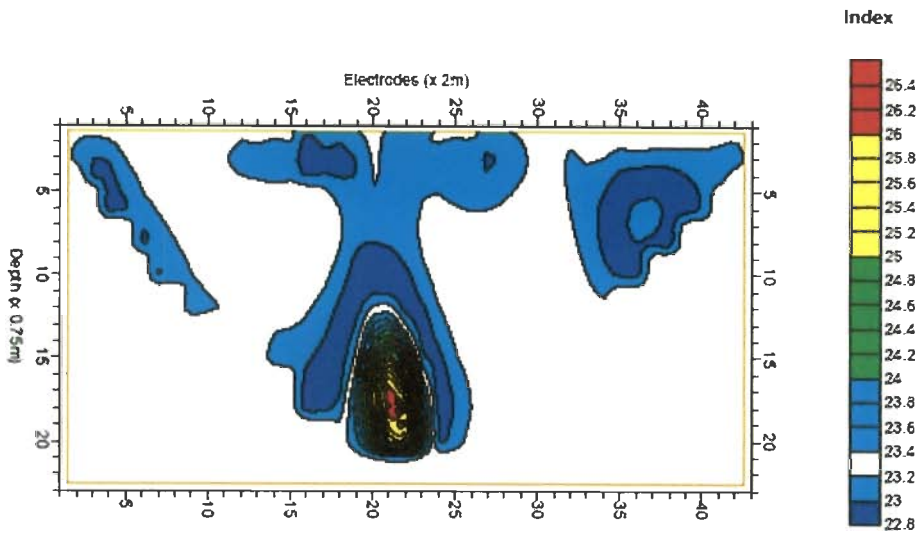


Fig. 7.21 Predicted Bearing Capacity Factor of General Shear Failure, N_γ (Vesic) Section from Angle of Internal Friction Section Along Profile A-B, E. P. Hostel, IITR

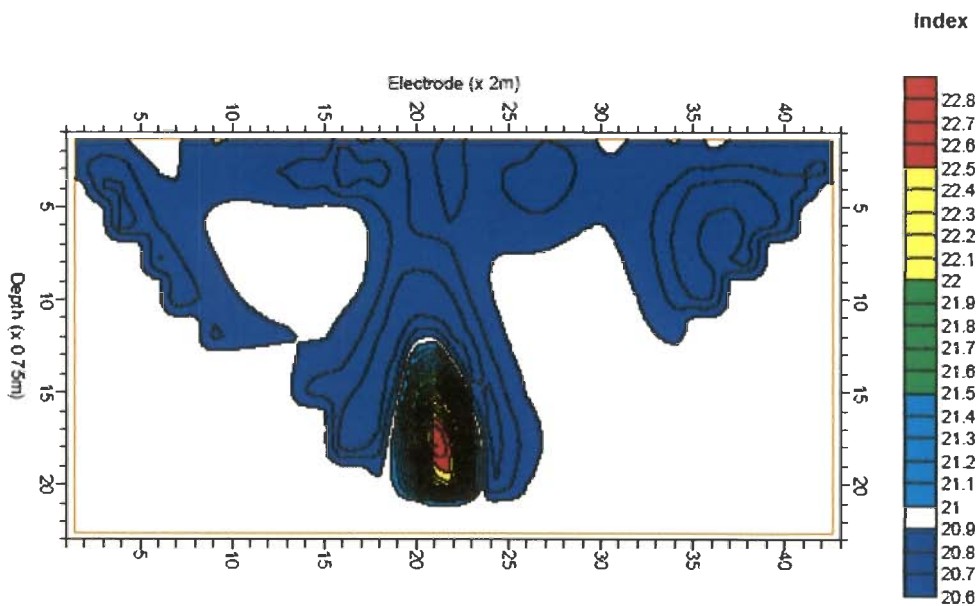


Fig. 7.22 Predicted Bearing Capacity Factor of General Shear Failure, N_q Section from Angle of Internal Friction Along Profile A-B, E. P. Hostel, IITR

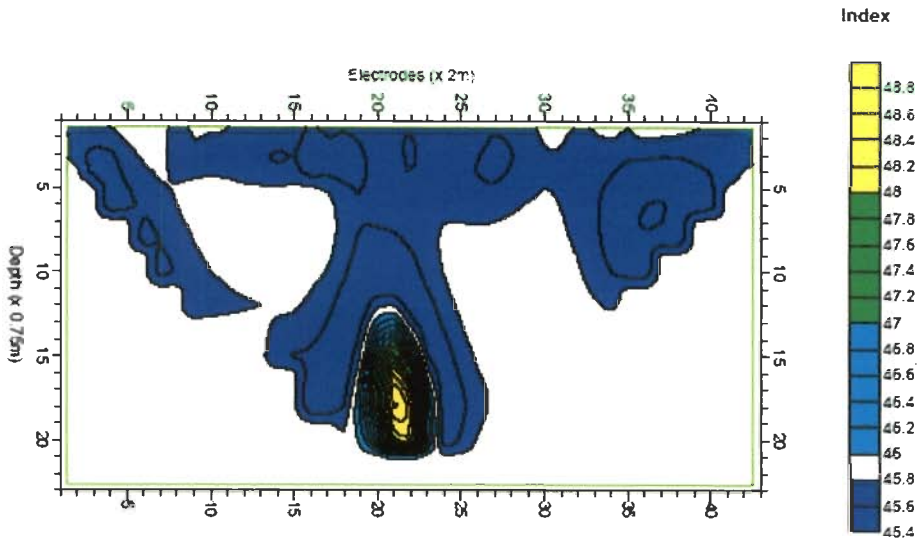


Fig. 7.23 Predicted Ultimate Bearing Capacity Factor, N_c Section for Strip Footings from Angle of Internal Friction Section Along Profile A-B, E. P. Hostel, IITR

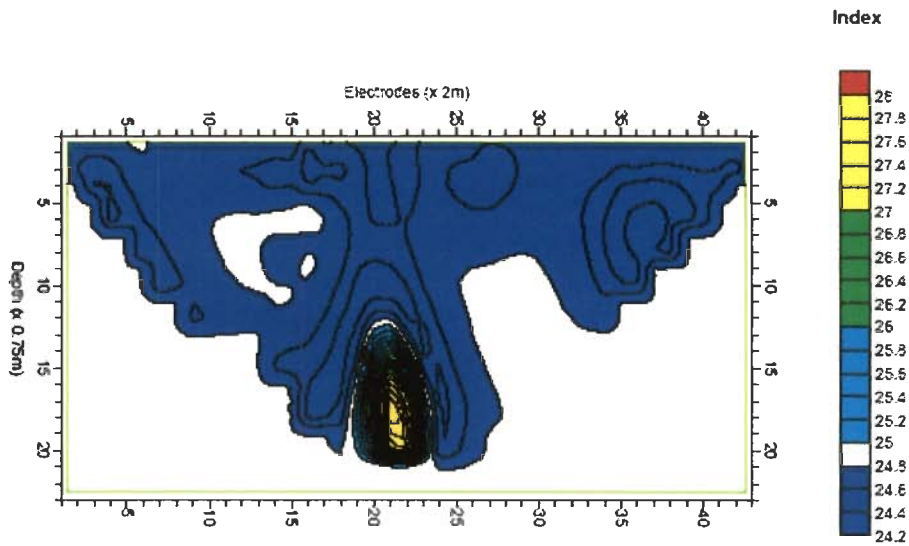


Fig. 7.24 Predicted Ultimate Bearing Capacity Factor, N_y Section for Strip Footings from Angle of Internal Friction Section Along Profile A-B, E. P. Hostel, IITR

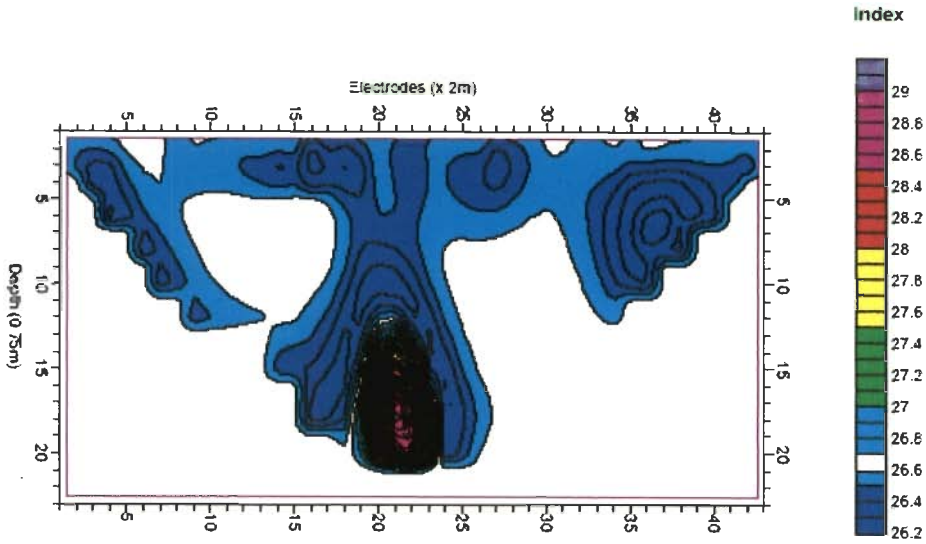


Fig. 7.25 Predicted Ultimate Bearing Capacity Factor, N_q Section for Strip Footings from Angle of Internal Friction Section Along Profile A-B, E. P. Hostel, IITR

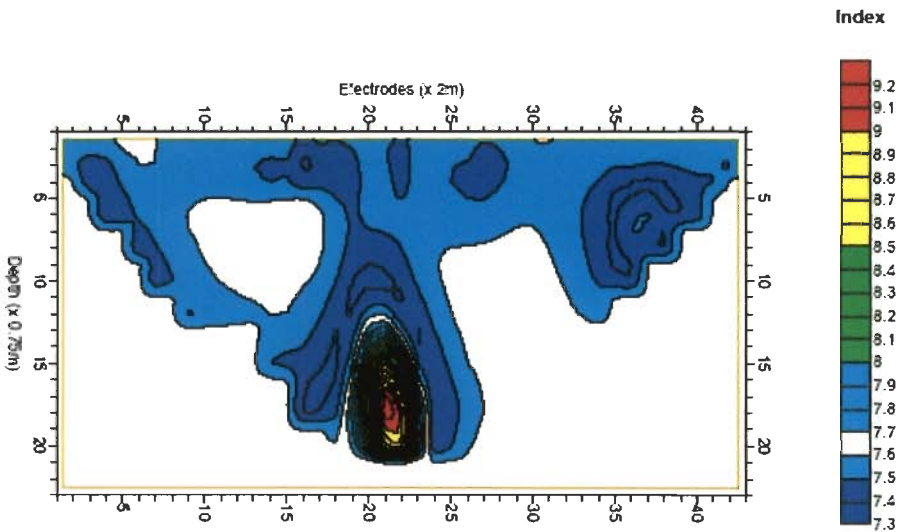


Fig. 7.26 Predicted Terzaghi's Bearing Capacity (Peck et al. 1974) Factor, N_γ Section from Angle of Internal Friction Section Along Profile A-B, E. P. Hostel, IITR

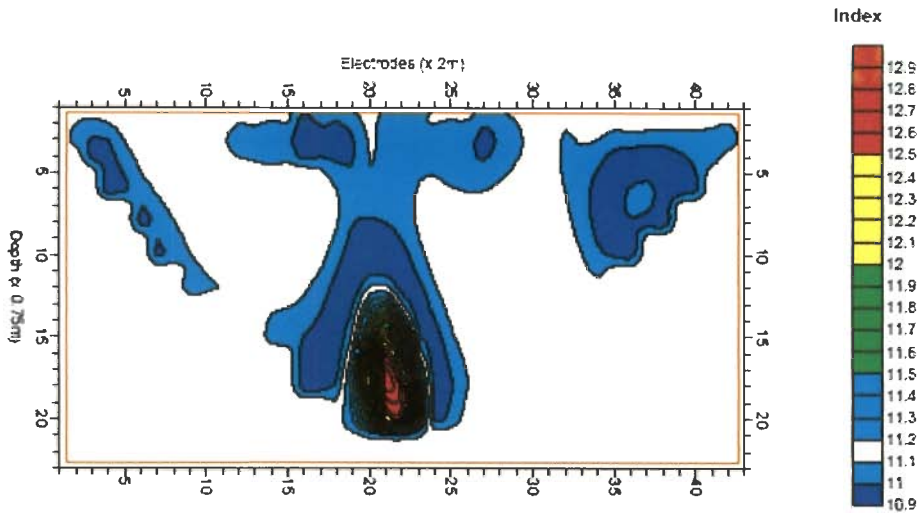


Fig. 7.27 Predicted Terzaghi's Bearing Capacity (Peck et al. 1974) Factor, N_q Section from Angle of Internal Friction Section Along Profile A-B, E. P. Hostel, IITR

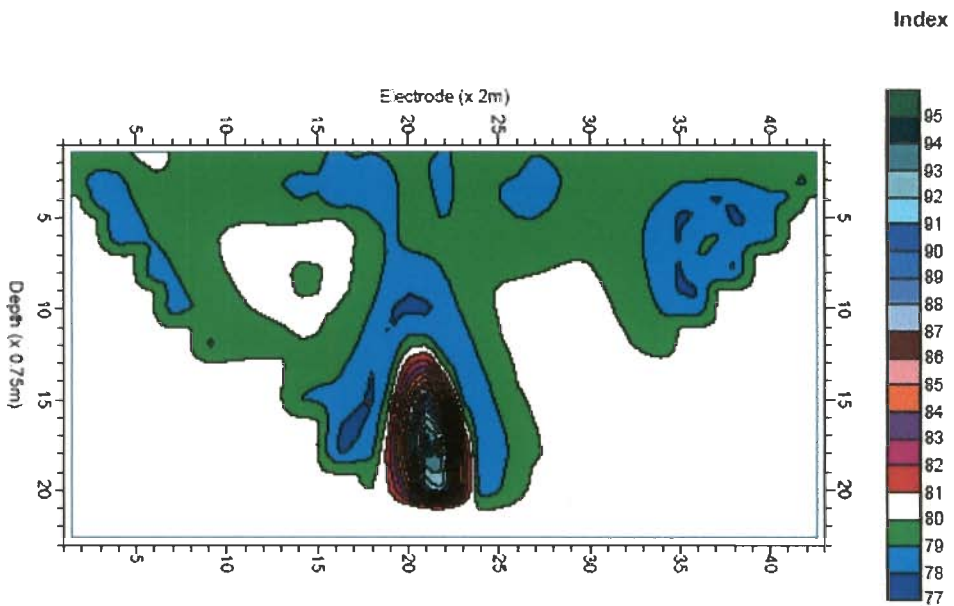


Fig. 7.28 Predicted N_q Factor (Meyerhof, 1953) Section for Driven Piles from Angle of Internal Friction Section Along Profile A-B, E. P. Hostel, IITR

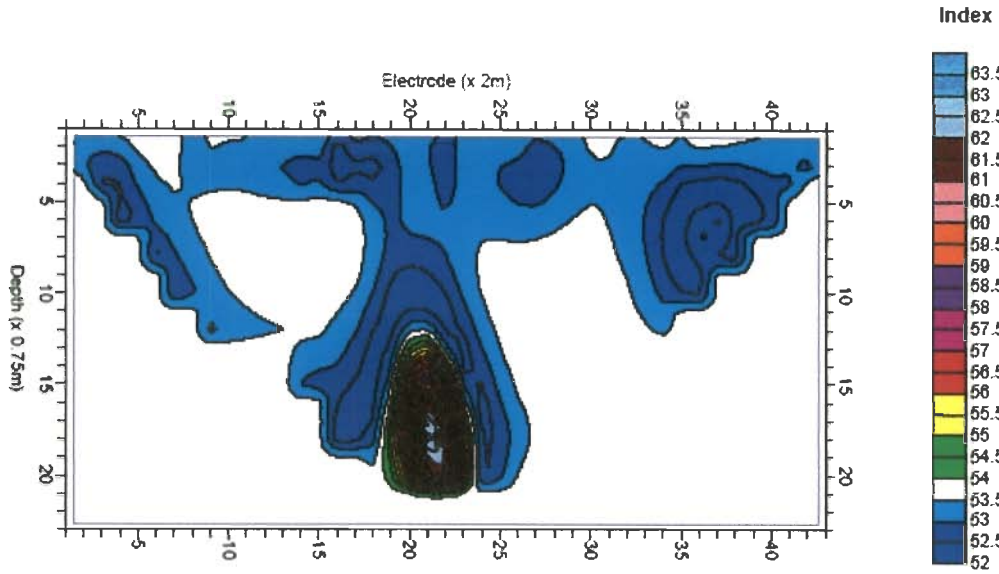


Fig. 7.29 Predicted N_q (Meyerhof, 1953) Factor Section for Bored Piles from Angle of Internal Friction Section Along Profile A-B, E. P. Hostel, IITR

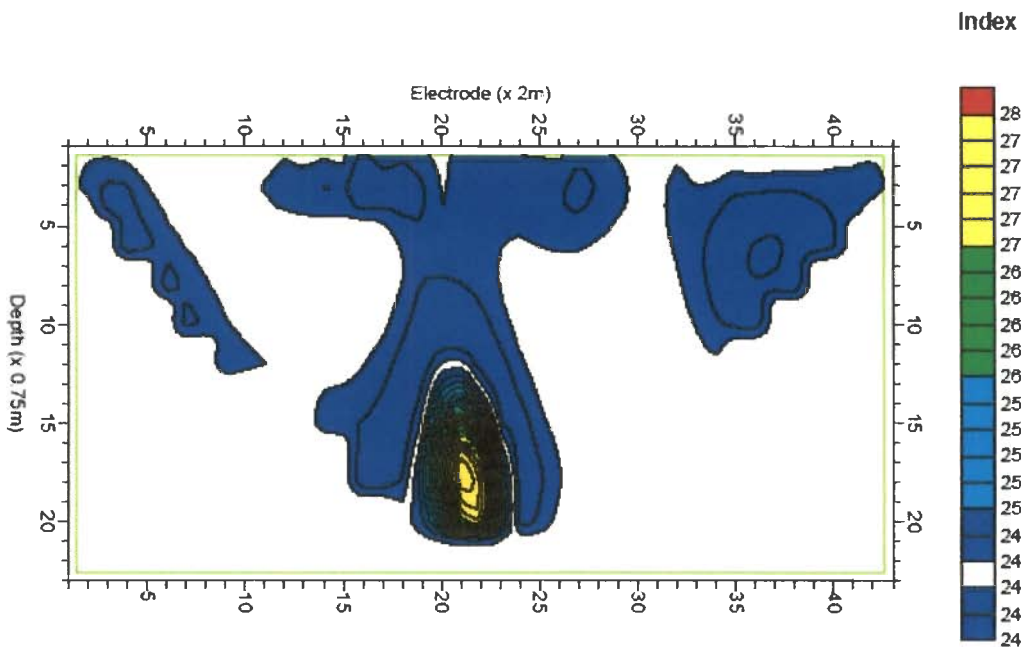


Fig. 7.30 Predicted N_q (Vesic) Factor Section for Bored Piles from Angle of Internal Friction Section Along Profile A-B, E. P. Hostel, IITR

GEOTECHNICAL CASE STUDIES-III

8.1 GENERAL

This study region namely construction of proposed structures of clinker grinding unit of Ambuja Cements Ltd (ACL), at Lakeshari (Bhagwanpur) near Roorkee falls in Uttarakhand State, India. It belongs to Indo-Gangetic Alluvial Plains. The methodology detailed in Chapter 5 has been utilized in geotechnical site characterization using resistivity / IP image data. For geotechnical data, the geotechnical report of Civil Engineering Department, IIT Roorkee was consulted.

8.2 SITE LOCATION MAPS

Figure 8.1 illustrates the location of study region. Different field geoelectrical and geotechnical study locations are indicated in both Fig. 8.1 and Fig. 8.2. The geoelectrical investigations refer to multi-electrode resistivity and IP data acquisition. Geology of the study region remains same as that outlined in Chapter 6 and broad lithology is included in Fig. 8.3.

8.3 GEOELECTRICAL AND GEOTECHNICAL DATA ACQUISITION

An attempt was made to acquire the geoelectrical data acquisition using a micro-processor controlled multi-electrode imaging system of French make (SYSCAL Jr. II of 72 electrode system). The relevant details of resistivity and IP images along chosen Profile A₃–B₃ (Fig. 7.1b) are included in Fig. 8.4.

As detailed in Chapters 5, for generation of regression equations of both formation and geotechnical parameters, a pair of boreholes in the vicinity of geoelectric profile is selected. Both geoelectric image data columns coinciding with projected borehole positions

(B-3 and B-6) were correlated with both formation and geotechnical data available at those boreholes. In the chosen geoelectric profile A₃-B₃ (Fig. 8.2), electrodes E-60 and E-52 respectively correspond to projected borehole locations B-3 and B-6. The observed SPT data at borehole location B-3 and B-6 have been described in Figs. 8.11a and 8.11b respectively. Further analysis is described in the following sections:

8.4 REGRESSION EQUATIONS FOR FORMATION AND SITE GEOTECHNICAL TESTS

The methodology as outlined in Chapter 5 is implemented. Accordingly, regression equations were developed for both formation and geotechnical parameters for Profile A₃-B₃ (Fig.8.2). Table 8.1 contains all regression equations (sand, clay, lithology, porosity, SPT and DCPT) that are developed for this study region (Profile A₃-B₃ in Fig.8.2).

Figures 8.15a and 8.15b describe the observed DCPT data corresponding to the electrode location EL-62 and EL-49 of profile A₃-B₃. On the basis of IP, predicted DCPT section has been presented in Fig. 8.16.

8.5 REGRESSION EQUATIONS FOR UNIT WEIGHT OF SOIL (DRY & SATURATED), UNCONFINED COMPRESSIVE STRENGTH, q_u , INTERNAL FRICTION ANGLE, ϕ AND BEARING CAPACITY FACTORS (SHALLOW AND DEEP INVESTIGATIONS)

As per Table 4.10 , the regression equations that were developed for i) unit weight of soil (both dry & saturated) versus porosity, ii) unconfined compressive strength, q_u versus SPT 'N', iii) SPT 'N' versus internal angle friction, ϕ and in turn, iv) internal angle friction, ϕ versus Terzaghi's bearing capacity coefficients, Terzaghi's Bearing Capacity factors (Peck et al., 1974) N_γ & N_q , bearing capacity factors for general shear failure, N_q , N_c & N_γ (Vesic), ultimate bearing capacity factors, N_q , N_c & N_γ , bearing capacity factor N_q (Vesic) for bored piles, bearing capacity factor N_q (Meyerhof, 1953) for bored piles and bearing capacity factor N_q (Meyerhof, 1953) for driven piles have been utilized here. All the relevant illustrations are appended at the end of this chapter and Table 8.2 summarizes the salient features of them.

Table 8.1 Inferred Predictive Equations from Cross-correlation of Normalized Plots at Different Geophysical Sites Projected onto Profile A₃-B₃ at Bhagawanpur

S. No.	Formation Parameter / Geotechnical Parameter	Correlation equation based on IP at B3 (EL-60) $Y=a_1x^2+a_2x+a_3$ or $y=a_1\exp(a_2x)$	Correlation equation based on IP at B6 (EL-52) $Y=b_1x^2+b_2x+b_3$ or $y=b_1\exp(b_2x)$	Average Correlation equation based on IP at B3 & B6 $Y=c_1x^2+c_2x+c_3$ or $y = c_1 \exp(c_2x)$ [$c_1=av(a_1,b_1)$, $c_2=av(a_2,b_2)$, $c_3=av(a_3,b_3)$]
1	Sand	$a = \{0.0234, 2.776\}$ $R2 = 0.5297$	$b = \{0.0845, 2.5412\}$ $R2 = 0.382$	$c = \{0.05395, 2.6586\}$
2	Clay / Shale	$a = \{0.1728, -0.4556, 0.9835\}$ $R2 = 0.4009$	$b = \{0.2204, -0.9629, 0.8762\}$ $R2 = 0.2921$	$c = \{0.1966, -0.70925, 0.92985\}$
3	Lithology	$a = \{-0.0401, 0.3254, 0.3906\}$ $R2 = 0.871$	$b = \{-1.1235, 1.5214, 0.2252\}$ $R2 = 0.6248$	$c = \{-0.5818, 0.9234, 0.3079\}$
4	SPT	$a = \{0.0234, 2.776\}$ $R2 = 0.5297$	$b = \{0.0845, 2.5412\}$ $R2 = 0.382$	$c = \{0.05395, 2.6586\}$
5	DCPT	$a = \{-0.667, 0.6556, 0.1336\}$ $R2 = 0.3364$ DCPT 3 at EL-62	$b = \{10.686, 9.2445, 2.1888\}$ $R2 = 0.6189$ DCPT 6 at EL-49	$c = \{5.0095, 4.29445, 1.1612\}$
7	Porosity	$a = \{0.0234, 2.776\}$ $R2 = 0.5297$	$b = \{0.0845, 2.5412\}$ $R2 = 0.382$	$c = \{0.05395, 2.6586\}$

8.6 INFERRED 2-D SECTIONS OF FORMATION PARAMETERS

As per methodology outlined in Chapter 5, by utilizing the appropriate regression equations that are included in Table 8.1, the digital IP values (Fig. 8.4b) along Profile A₃-B₃ (Fig. 8.3) have been converted to respective formation parameter sections.

Accordingly, Figs. 8.7-8.12 and 8.16 refer to predicted 2-D sections for sand, clay, lithology, porosity, SPT and DCPT. IP derived sand and clay sections are included in Figs. 8.5-8.6 respectively. In Figs. 8.13 and 8.14, we compare inferred SPT with observed SPT for boreholes B-3 and B-6 using resistivity and IP and it clearly shows that IP based SPT is preferable. The table provides relevant details.

Table 8.2 Details of Illustrations

S. No.	Formation / Geotechnical Parameter		Fig. No.	Remarks
1	Sand	IP derived	Fig. 8.5	Predominantly, it is a sandy section with shaly sand and clay pockets.
		Geotechnical Derived	Fig. 8.7	
2	Clay / Shale	IP derived	Fig. 8.6	Predominantly, it is a clayey section with occasional shaly sand pockets.
		Geotechnical Derived	Fig. 8.8	
3	Lithology		Fig. 8.9	The lithology section is dominated by silty and clayey sands and it can be considered for analysis.
4	SPT		Figs. 8.12, 8.13 a & b, 8.14 a & b	Figures 8.13-8.14 reveal that resistivity derived SPT matches with the actual ones. The corresponding SPT section is included in Fig. 8.12. The normalizing factor is 43.
5	DCPT		Fig. 8.16	It ranges from 30 to 200.
6	Porosity		Fig. 8.10	Low porosity ($\leq 9\%$) shaly sands have been inferred in the subsurface.
7	Unit weight of soil	Dry	Fig. 8.18	Its range is 6-23 kN/m ³ .
		Saturated	Fig. 8.19	Its range is 12.5-23.5 kN/m ³ .
8.	Angle of internal friction, ϕ		Fig. 8.17	Predominantly, it is in the range 26.5-27 ⁰ .
9	Unconfined compressive strength, q_u		Fig. 8.20	Its range is 130-220 kN/m ² .
10	Terzaghi's Bearing Capacity factors (Peck et al. 1974)	N_γ factor	Fig. 8.27	All these bearing capacity factor sections exhibit 2-D variation. Depending on the proposed depth of foundation, the 2-D sections can be transformed into 1-D sections by an averaging process. These 1-D sections could of much help in the design of foundations of superstructures.
		N_q factor	Fig. 8.28	
11	General bearing capacity factors	N_c factor	Fig. 8.21	
		N_γ (Vesic) factor	Fig. 8.22	
		N_q factor	Fig. 8.23	
12.	Ultimate bearing capacity factors	N_c factor	Fig. 8.24	
		N_γ factor	Fig. 8.25	
		N_q factor	Fig. 8.26	
13	Piles	Driven Piles N_q (Meyerhof, 1953) factor	Fig. 8.29	
		Bored Piles N_q (Meyerhof, 1953) factor	Fig. 8.30	
		Bored Piles N_q (Vesic, 1953) factor	Fig. 8.31	

8.7 GENERATION OF GEOTECHNICAL PARAMETER SECTIONS

The regression equations developed earlier in chapter 4 (Tables 4.10) have been utilized to transform IP section along Profile A₃-B₃ into different geotechnical parameter sections. Accordingly, Figs. 8.17 to 8.31 respectively contain predicted 2-D sections of angle of internal friction, unit weights of soil (dry & saturated), unconfined compressive strength (q_u), bearing capacity factors for shear failure (N_c , N_γ (Vesic) and N_q), ultimate bearing capacity factors (N_c , N_γ and N_q), Terzaghi's bearing capacity (Peck et al., 1974) factors (N_γ and N_q), bored pile factors (N_q (Meyerhof, 1953) and N_q (Vesic)) and driven pile N_q factor (Meyerhof, 1953).

8.8 RESULTS & DISCUSSION

In the present case study, IP based prediction of formation and geotechnical parameter profiles are better correlated with the observed ones (For example, Figs. 8.13 & 8.14) in comparison to resistivity derived ones. As a result, IP section (Fig. 8.4b) formed the basis for prediction of both formation and geotechnical parameter sections. Further, Unit weight of soil (dry & saturated) sections are derived based on the regression equation (Table 4.10) connecting them with porosity parameter (Murthy, 2008) as water saturation parameter was not available in the geotechnical report for the study region. All illustrations are appended at the chapter end and Table 8.2 contains all relevant details in this regard.

Additionally, the followings remarks need to be considered:

- a) The inferred lithology section (Fig. 8.9) clearly outlines the predominance of silty / clayey sand in the subsurface within the probed depth of 24 m.
- b) Except for a small pocket, the predicted porosity section (Fig. 7.8) along Profile A-B indicates a low porosity variation in the range of 5-10 %, which is typical silty / clayey sand.
- c) Porosity based regression equation in Table 4.10 has allowed to predict unit weights of soil (both dry & Saturated) in Figs. 8.18 and 8.19. The dry and saturated unit weights of soil are in the ranges 6-23 & 12.5-24 kN/m³ respectively.

- d) In Figs. 8.13 and 8.14, it is clear that IP based SPT prediction is better than that of resistivity based ones. So, for geotechnical parameter section predictions, the SPT section (Fig. 8.12) derived from IP is used. For a major portion of subsurface section (depth up to 24 m) along Profile A₃-B₃ the predicted SPT 'N' (Fig. 8.12) lies in the range 10-16.
- e) The predicted DCPT section provides a better resolution with the values in the range 30 to 200 up to a depth of 48 m.
- f) Unconfined compressive strength, q_u derived from SPT 'N' section is included in Fig. 8.20. Predominantly, q_u is in the range ranges from 130 to 250 kN/m³ with a 2-D distribution.
- g) The angle of internal friction, ϕ section (Fig. 8.17) derived from SPT reveals that it varies over a narrow zone of 26.5-28.
- h) All bearing capacity coefficient sections (Figs. 8.21-8.31), which are derived from angle of internal friction, ϕ section show a 2-D distribution. The traditional 1-D geotechnical models can be developed on their basis. It is expected that such sections are more likely be better than that of the current practice at a proposed depth of foundation.
- i) The bearing capacity factors based on CPT method is not attempted here. However, earlier outlined procedure for SPT 'N' can easily be extended to CPT method also.
- j) The regression equations that are included in Table 4.10 have remained constant throughout the study and they are based on current geotechnical literature.
- k) The regression equations listed in Table 8.1 are site-specific and geo-electrical profile specific.
- l) All inferred 2-D geotechnical sections clearly show that 1-D models often resorted to by geotechnical engineers are far from reality and are needed to refine their quality or new procedures need to be evolved. The present effort is geared towards that goal.

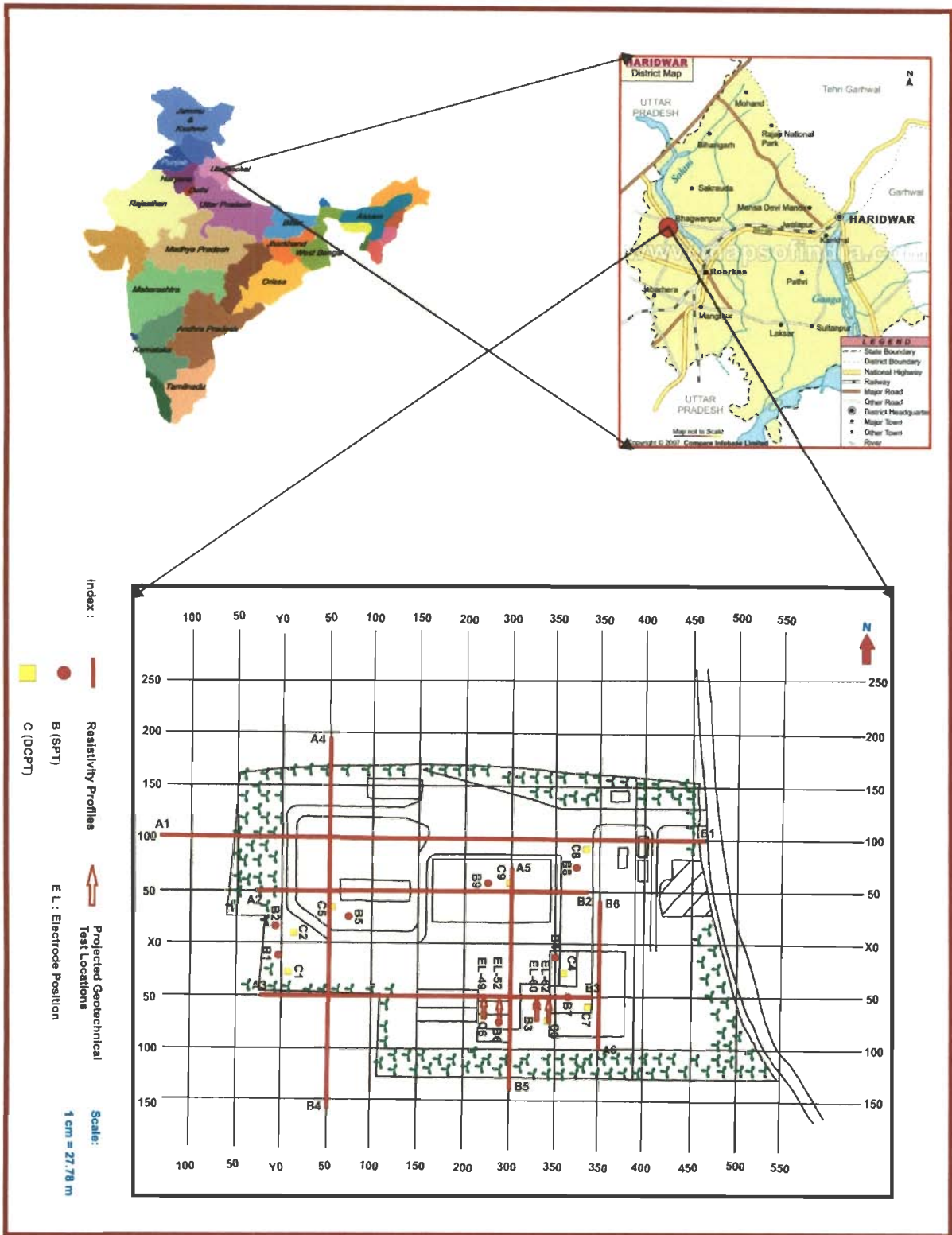


Fig. 8.1 Location Map of Proposed Structure of ACL at Bhagwanpur Site, Uttarakhand, India

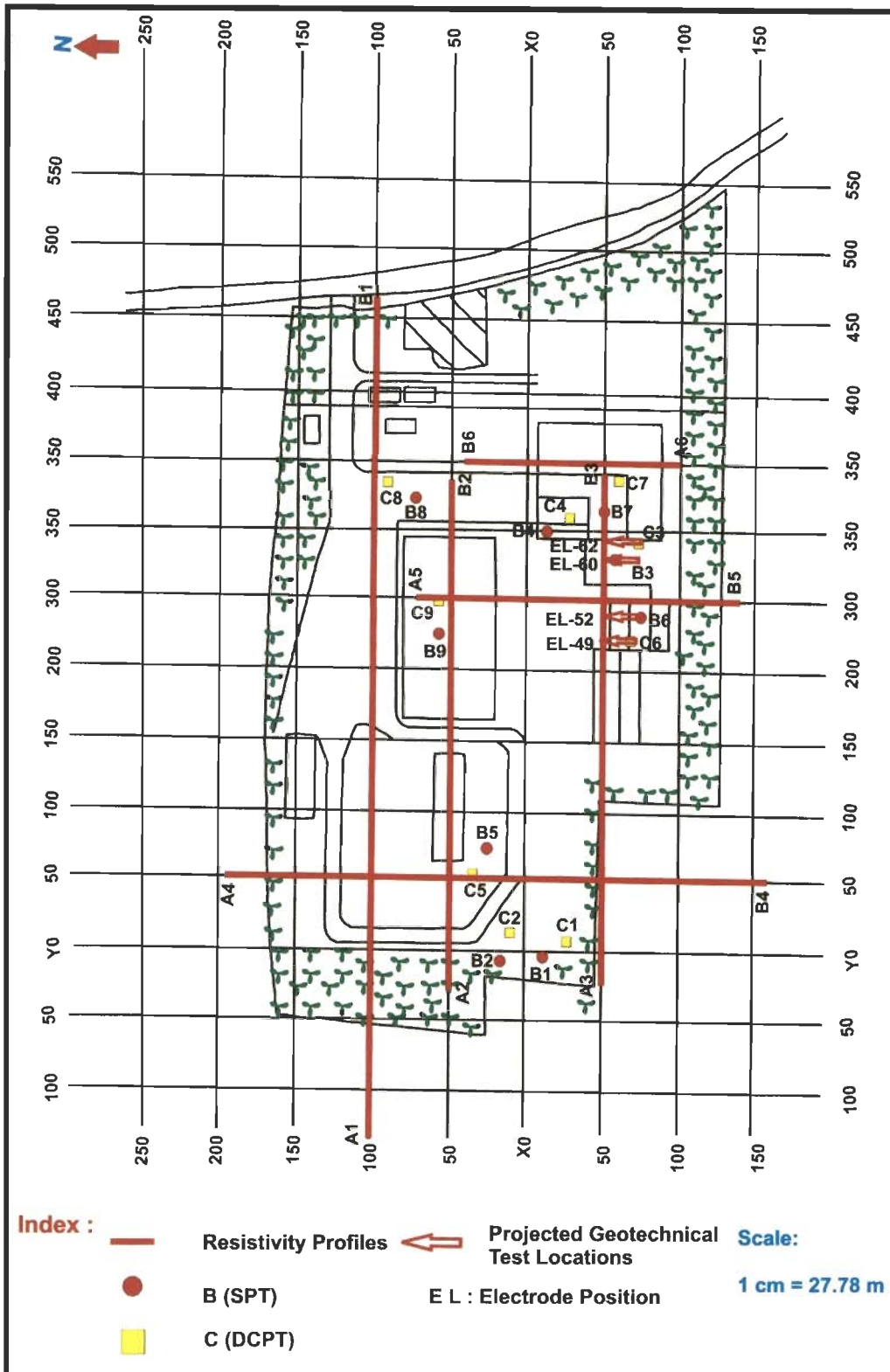


Fig. 8.2 Map Showing the Location of ERT, IPI and Geotechnical Site Investigations

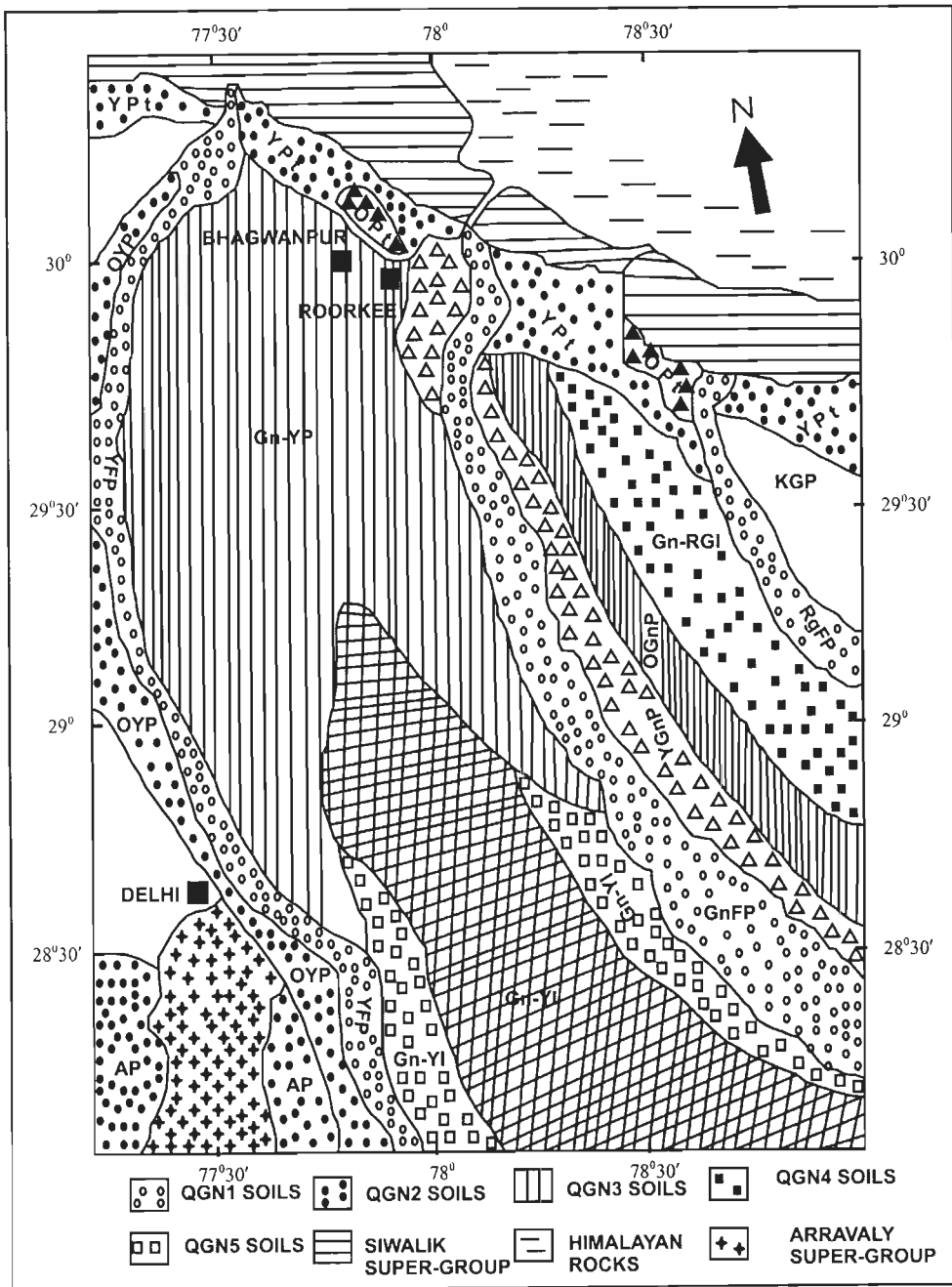


Fig. 8.3

Geological (Soil-Geomorphic) Map of the Study Region. GnFP-Ganga Floodplain; YGP-Young Ganga Plain; OGnP-Old Ganga Plain; GnRGI-Ganga-Ramganga Interfluv; KGP-Kosi-Gola Plain; Gn-YP-Ganga-Yamuna Plain; Gn-YI-Ganga-Yamuna Interfluv, SA-Salt Affected, NSA-Not Salt-Affected, YPt-Young Piedmont, Opt-Old Piedmont (Parkash et al. 2000, 2001)

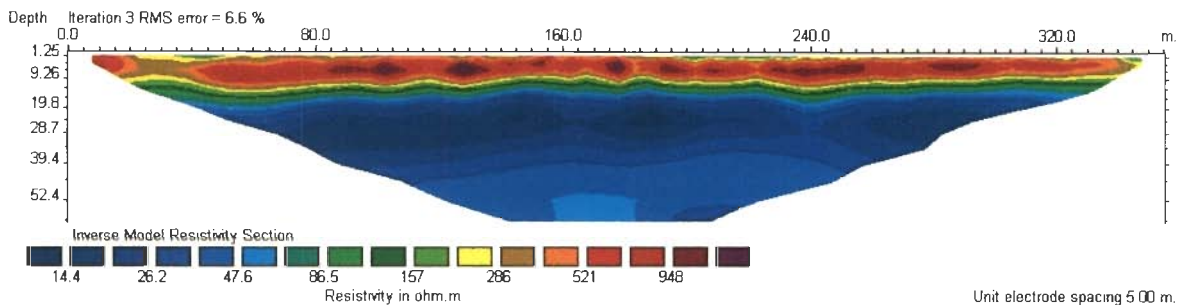


Fig. 8.4 a Resistivity Image (ERT) Along Profile A₃-B₃. The Resistivity (ohm-m) and Depth Scales are Logarithmic.

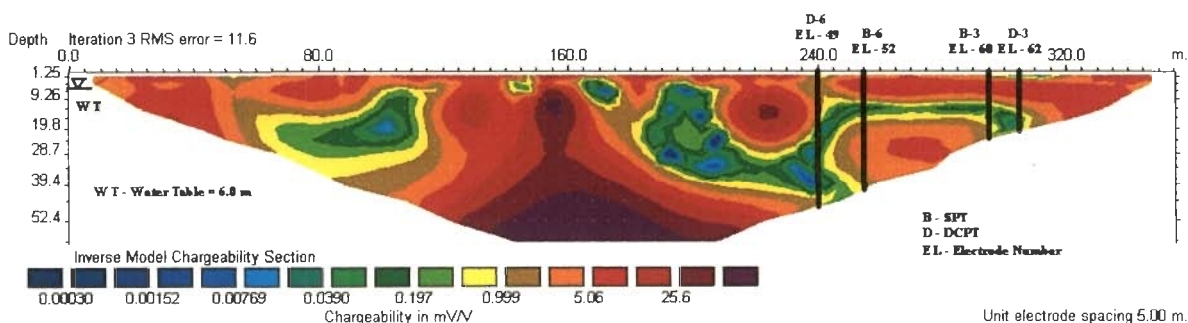


Fig. 8.4 b IP Image (IPI) Along Profile A₃-B₃. The Chargeability (mSec) and Depth Scales are Logarithmic.

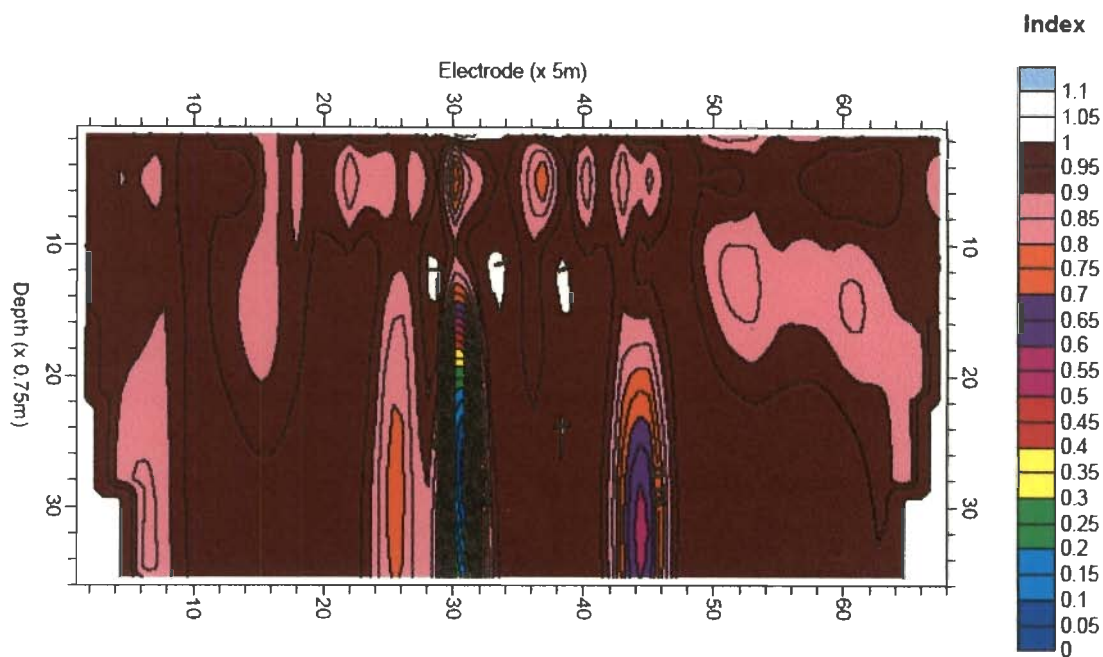


Fig. 8.5 IP Derived Sand (%) Section Along Profile A₃-B₃ , Bhagwanpur

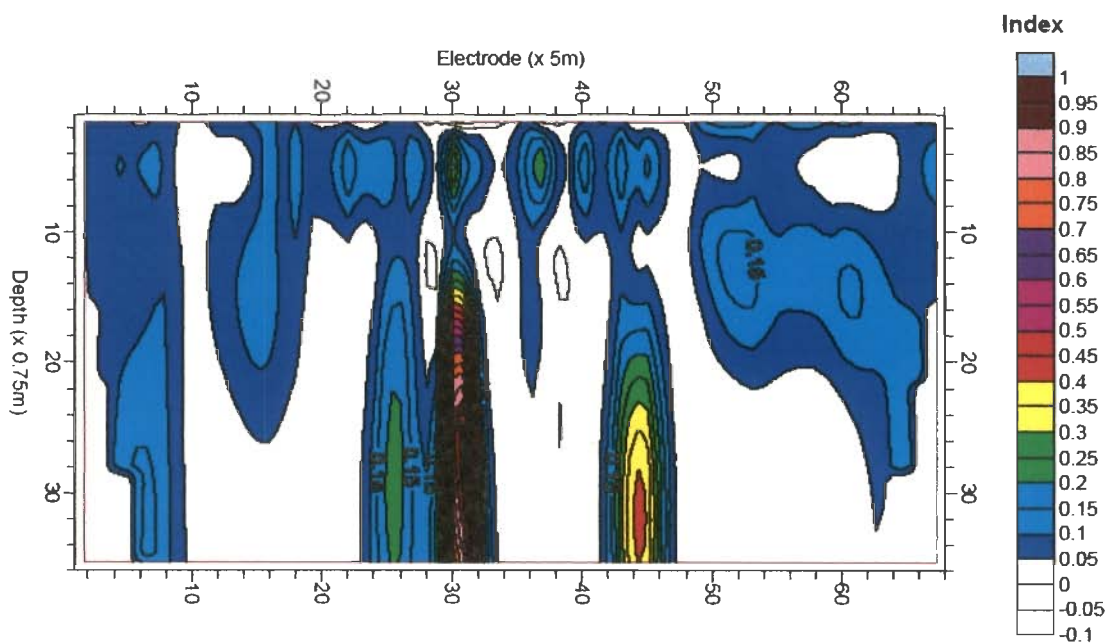


Fig. 8.6 IP Derived clay (%) Section Along Profile A₃-B₃, Bhagwanpur

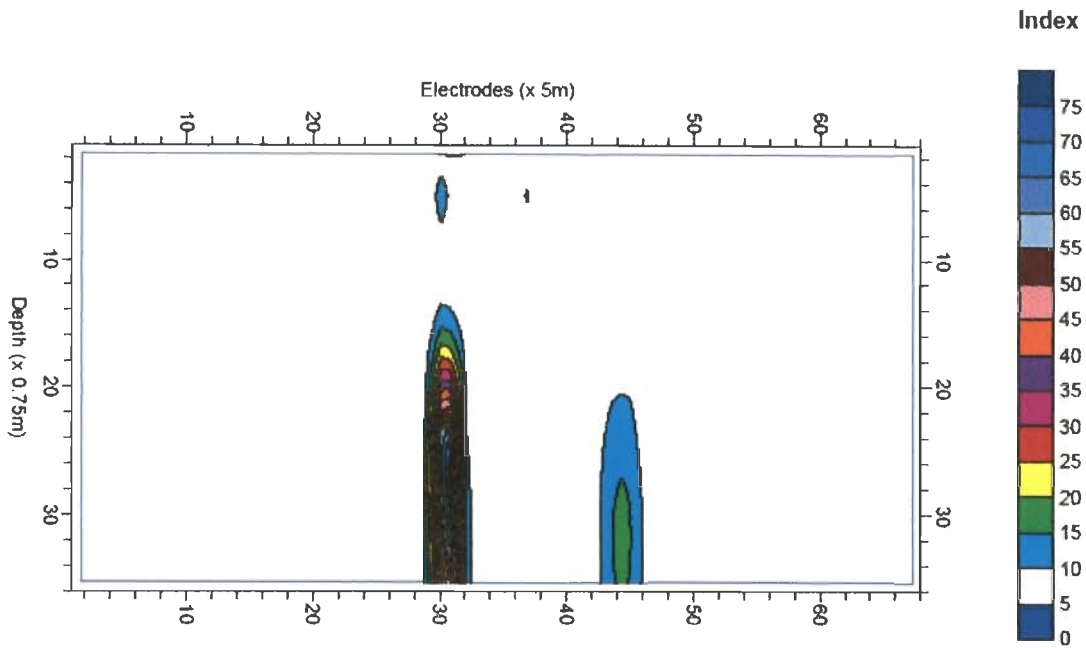


Fig. 8.7 Predicted Sand (%) Section from Geotechnical and IP Data Along Profile A₃-B₃, Bhagwanpur

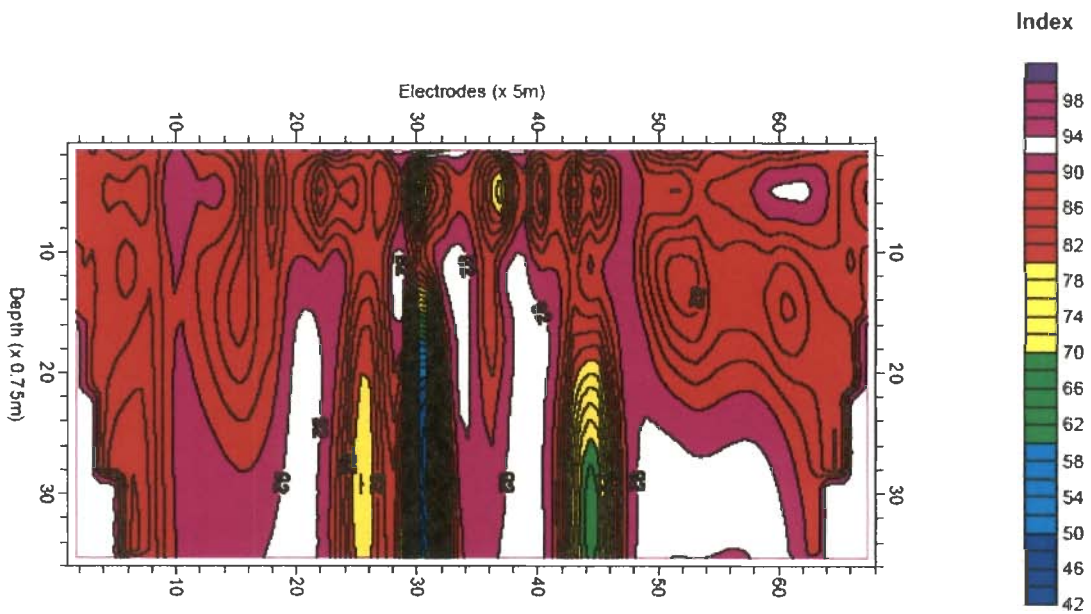


Fig. 8.8 Predicted Clay (%) Section from Geotechnical and IP Data Along Profile A₃-B₃ , Bhagwanpur

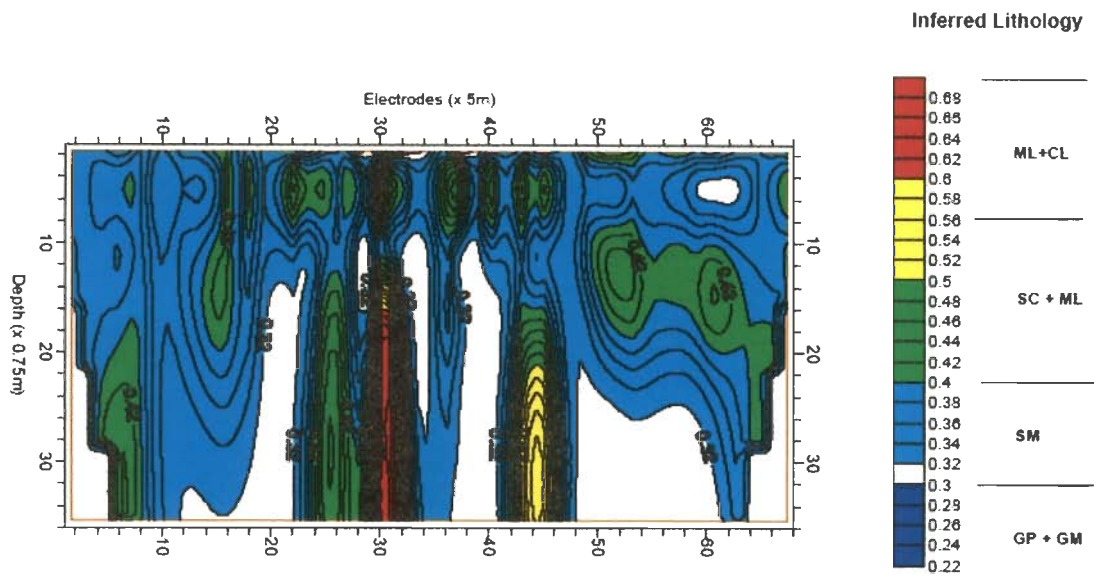


Fig. 8.9 Predicted Lithology Section from Geotechnical and IP Data Along Profile A₃-B₃, Bhagawanpur

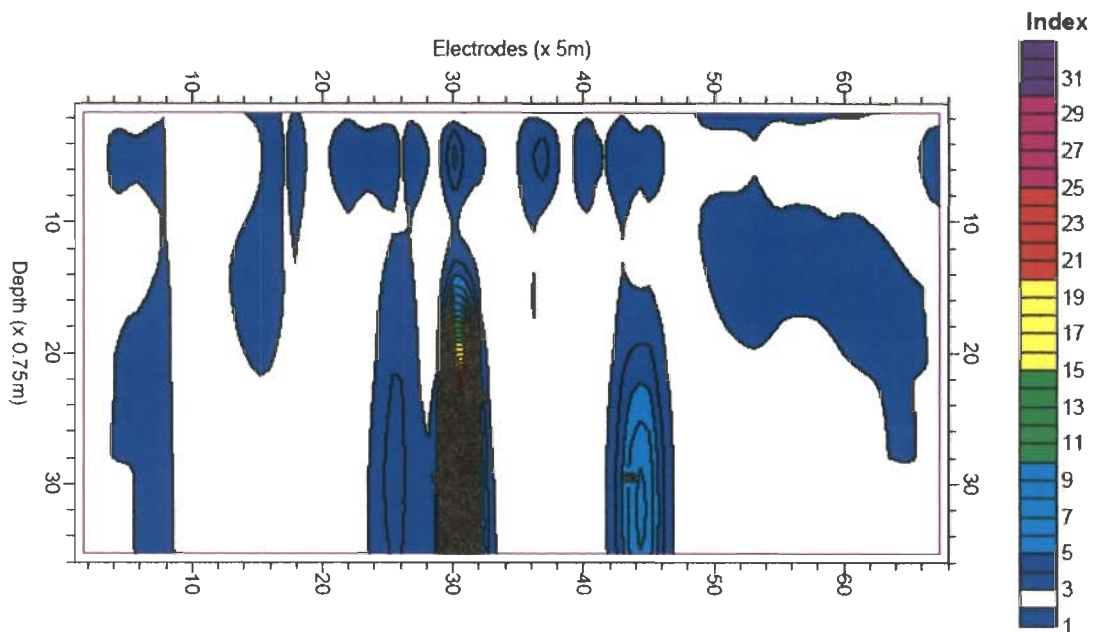
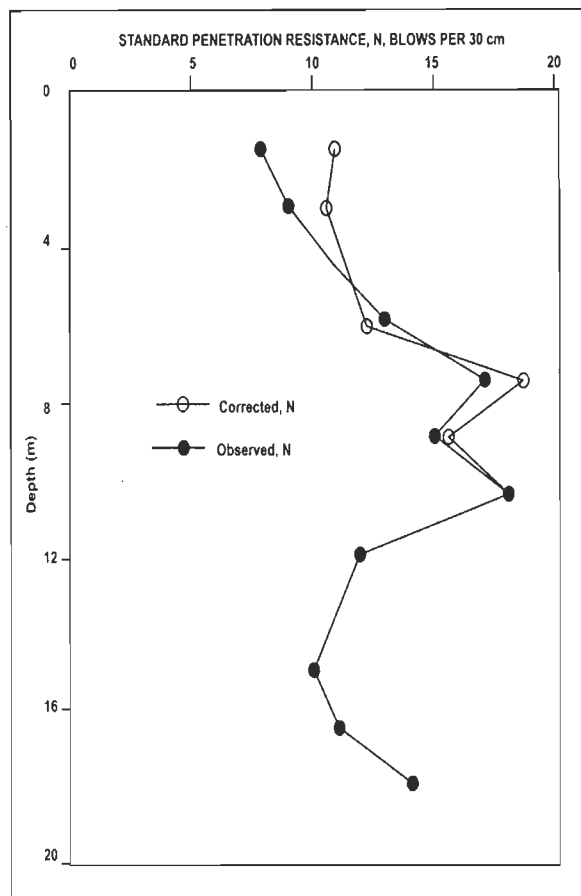


Fig. 8.10 Predicted porosity (%) Section from IP and Borehole Data Along Profile A₃-B₃, Bhagawanpur

Depth (m)	Classification		Grain Size Distribution	
	Symbol	Hatching	Sand (%)	Fines (%)
1.5	SM	Vertical lines	34.6	65.4
3.0			40.3	59.7
4.5			30.9	69.1
6.0			39.9	60.2
7.5			36.6	63.4
9.0	ML	Hexagonal pattern	2.9	97.1
10.5				
12.0	CI	Diagonal lines	3.0	97.1
13.5			1.3	98.7
15.0			3.0	97.0
16.5			1.3	98.2
18.0	CI	Diagonal lines	2.9	97.1
19.5				

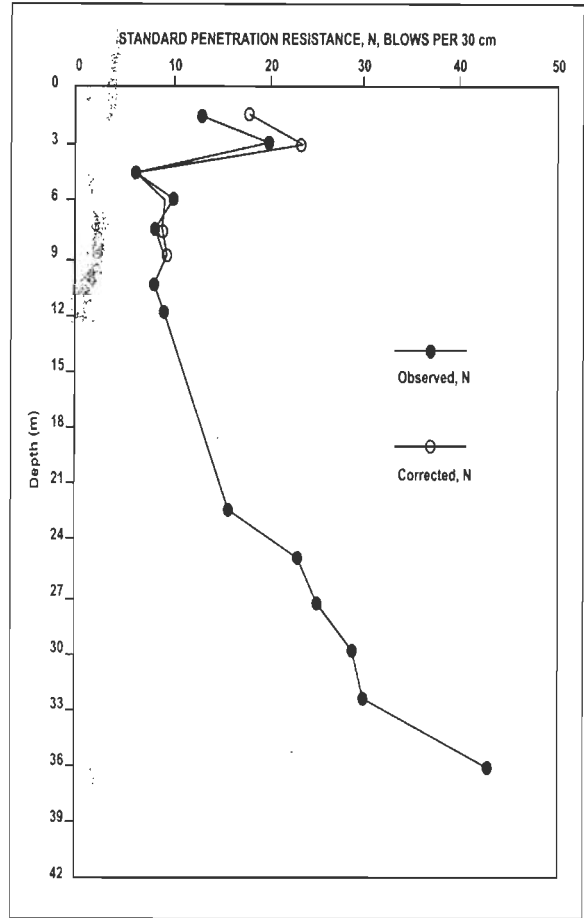


a) Borehole B-3

SPT-DATA

Fig. 8.11 a Borehole Data at Location B-3. The Projected Borehole Position Coincides with Electrode, EL-60 of profile A₃-B₃

Depth (m)	Classification		Grain Size Distribution	
	Symbol	Hatching	Sand (%)	Fines (%)
1.5	SP	[Cross-hatch]	95.3	4.7
3.0	SM	[Vertical lines]	95.8	4.2
4.5		[Diagonal lines]	83.9	16.1
6.0	SP-SM	[Cross-hatch]	92.3	7.7
7.5		[Vertical lines]	84.7	15.3
9.0	CI	[Diagonal lines]	3.7	96.3
10.5		[Diagonal lines]		
12.0		[Diagonal lines]		
13.5			7.1	92.9
15.0				
16.5				
18.0				
19.5				



b) Borehole B-6

SPT-DATA

Fig. 8.11 b Borehole Data at Location B-6. The Projected Borehole Position Coincides with Electrode, EL-52 of profile A₃-B₃

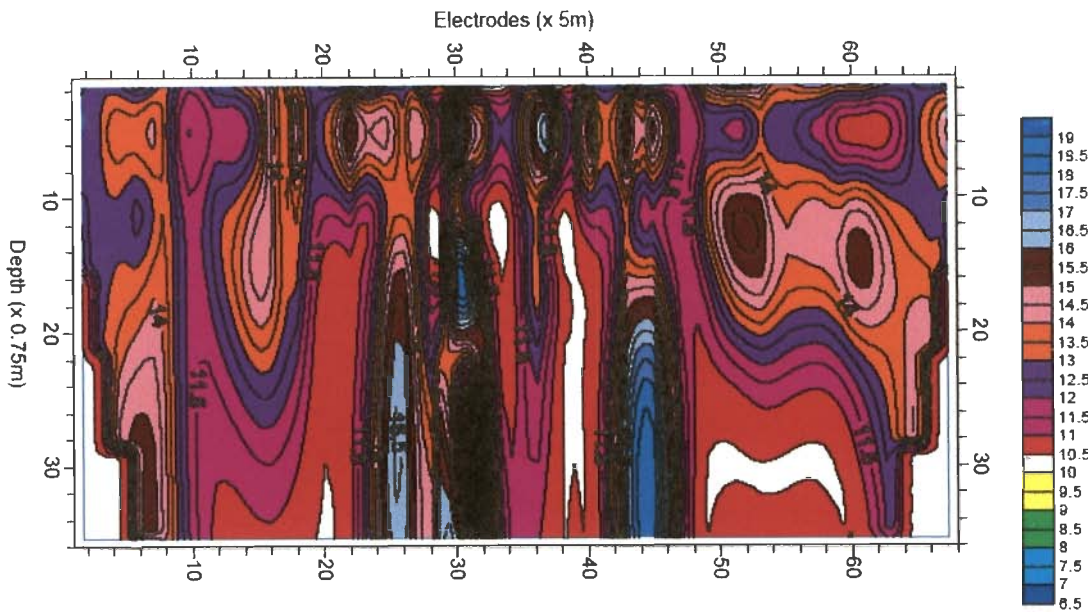


Fig. 8.12 Predicted SPT Section from IP and Borehole Data Along Profile A₃-B₃, Bhagawanpur

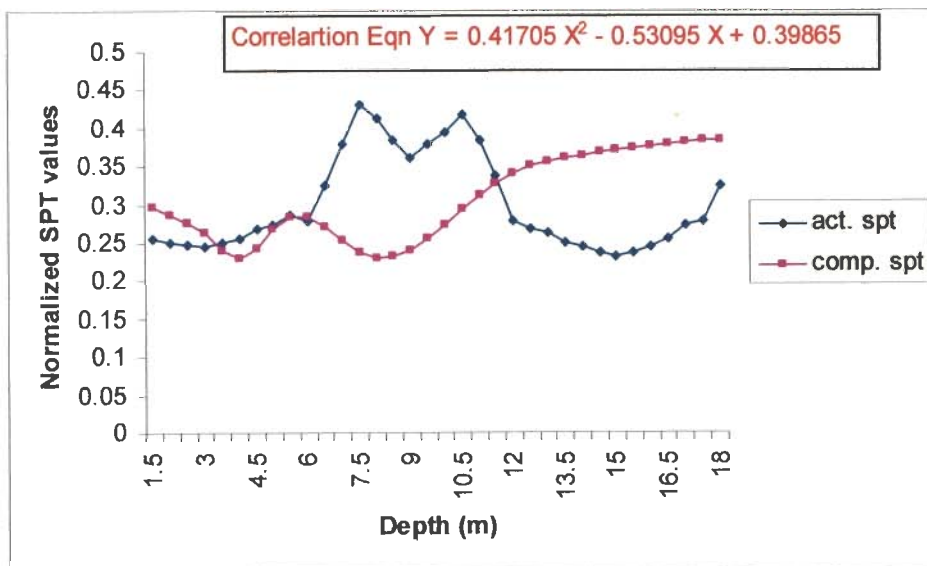


Fig. 8.13 a Comparison of Observed and Computed SPT 'N' Through Resistivity at Borehole location - B-3

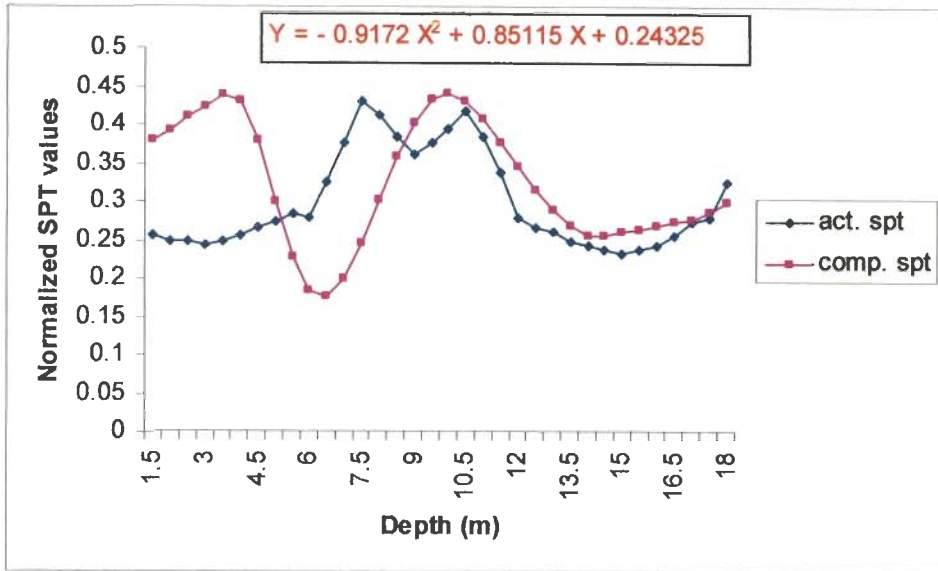


Fig. 8.13 b Comparison of Observed and Computed SPT 'N' Through IP at Borehole Location - B-3

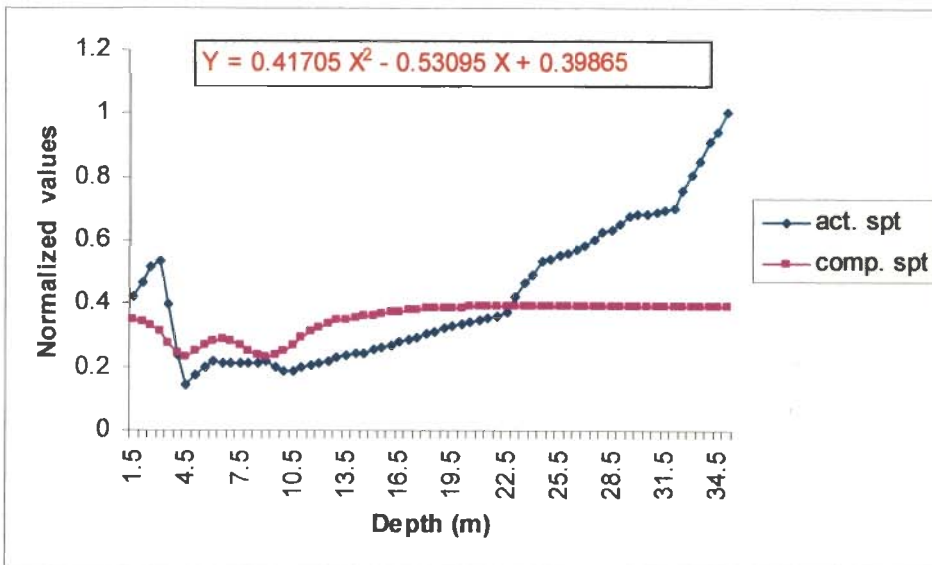


Fig. 8.14 a Comparison of Observed and Computed SPT 'N' Through Resistivity at Borehole Location - B-6

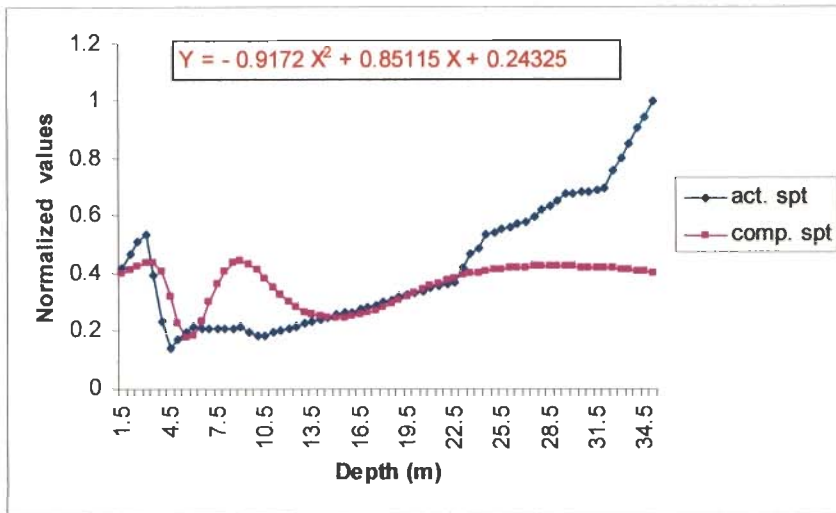


Fig. 8.14 b Comparison of Observed and Computed SPT 'N' Through IP at Borehole Location- B-6

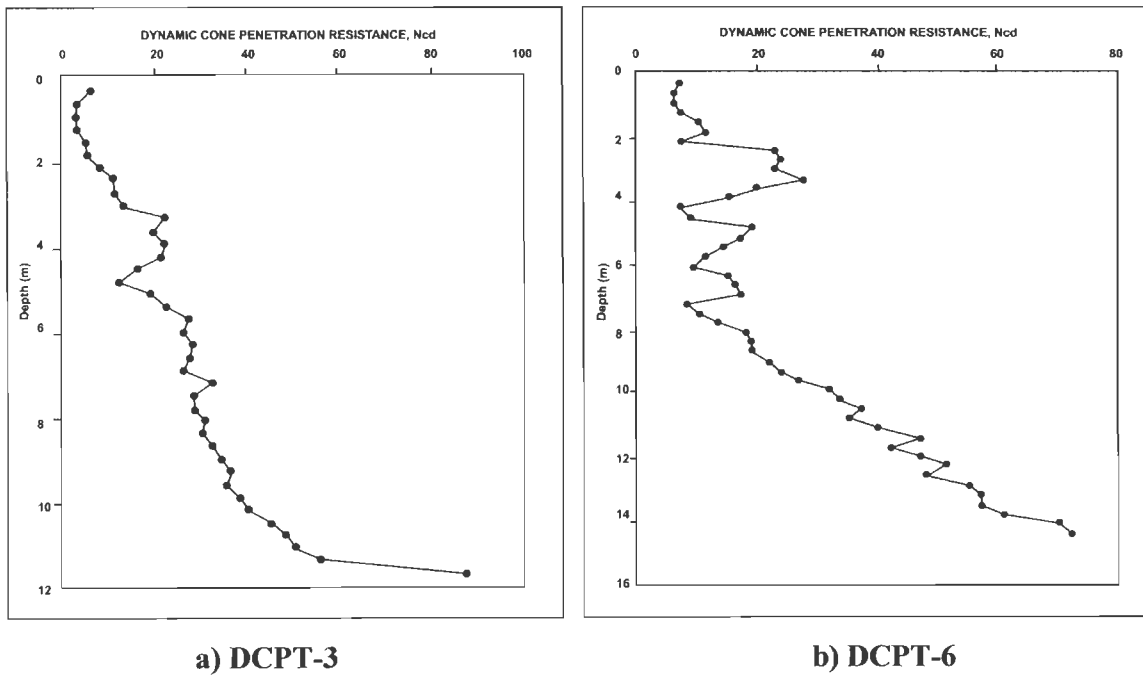


Fig. 8.15 a) DCPT-3 Data. The Corresponding Electrode Position is EL-62 of Profile A₃-B₃

b) DCPT-6 Data. The Corresponding Electrode Position is EL-49 of Profile A₃-B₃

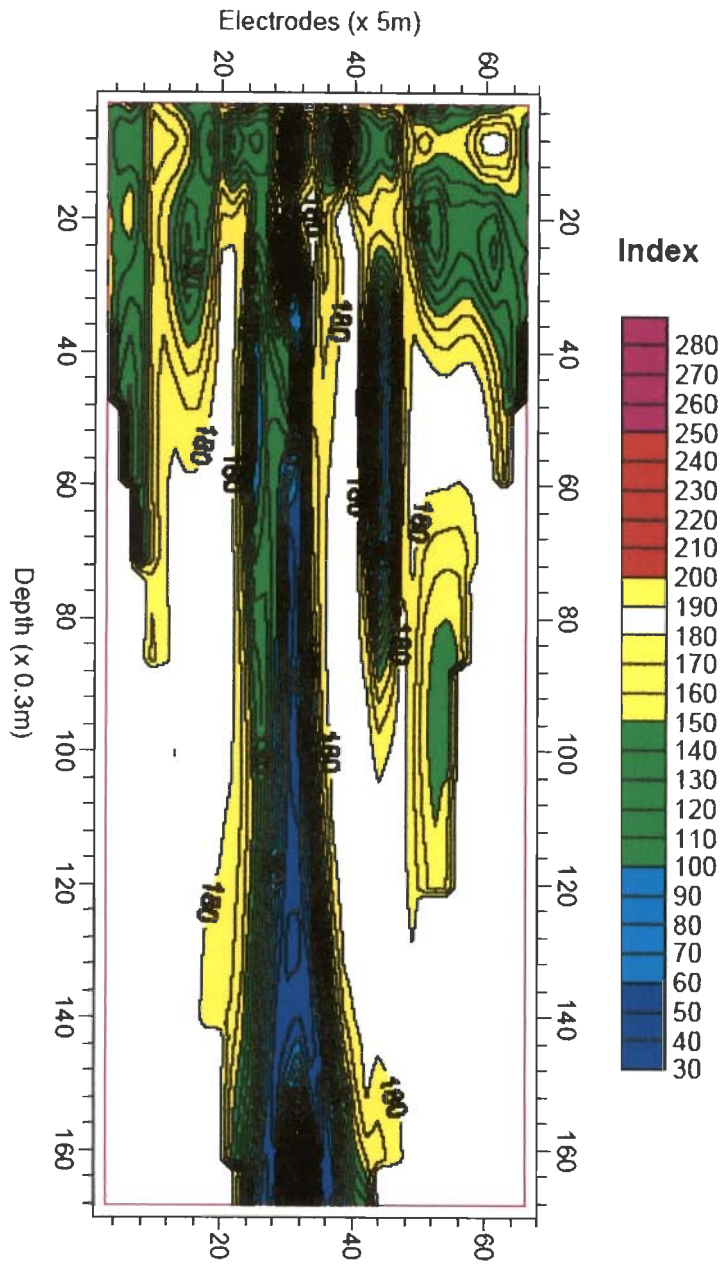


Fig. 8.16 Predicted DCPT Section from IP and Borehole Data Along Profile A₃-B₃, Bhagawanpur

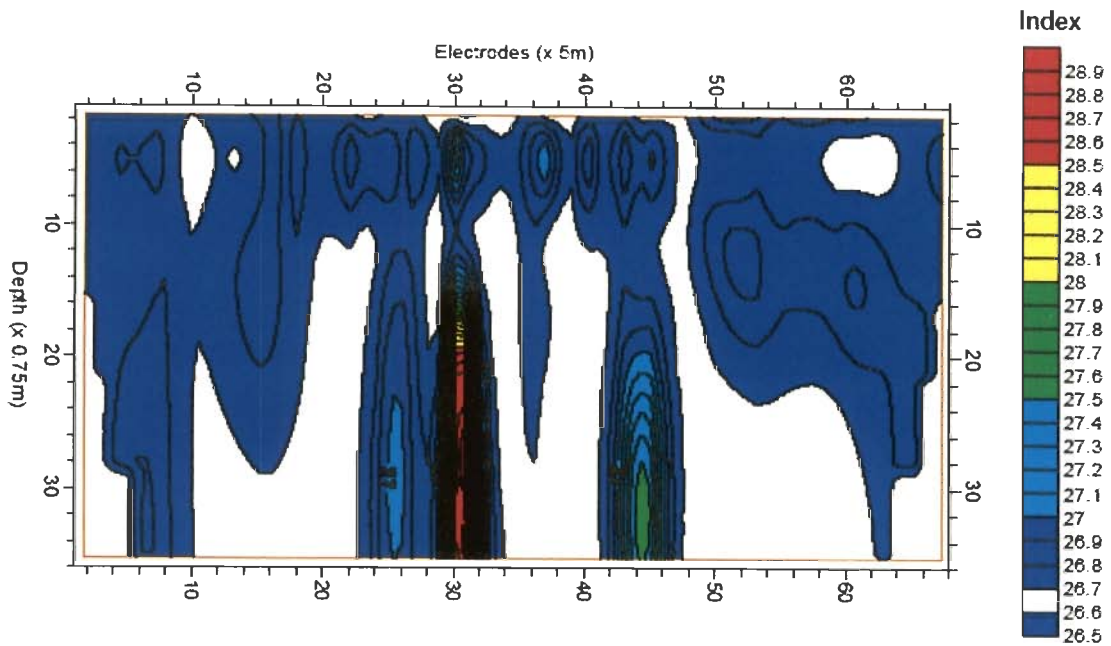


Fig. 8.17 Predicted Internal Friction Angle Section from Synthetic SPT Section Using IP Along Profile A₃-B₃, Bhagwanpur

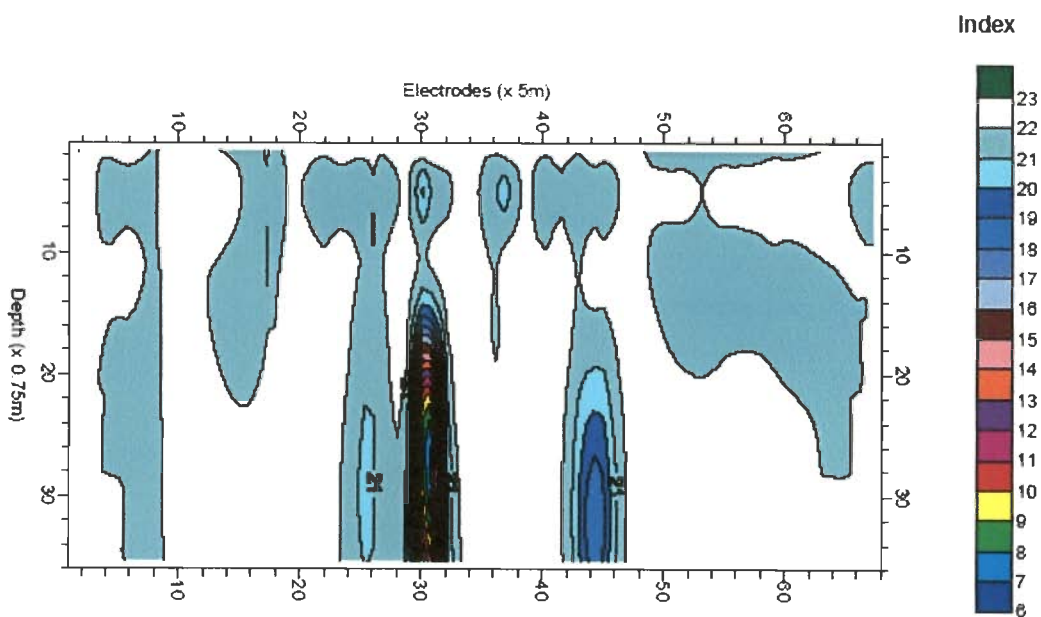


Fig. 8.18 Predicted Unit Weight (Dry) in kN/m^3 Section from Porosity Section Using IP Along Profile A₃-B₃, Bhagwanpur

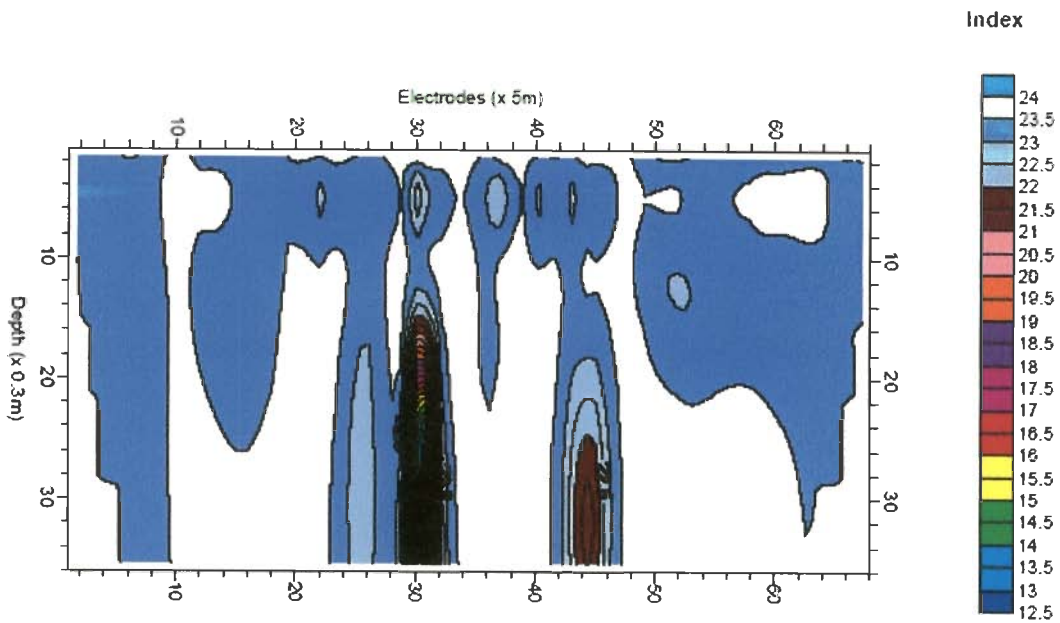


Fig. 8.19 Predicted Unit Weight (Saturated) in kN/m^3 Section from Porosity Section Using IP Along Profile A_3-B_3 , Bhagwanpur

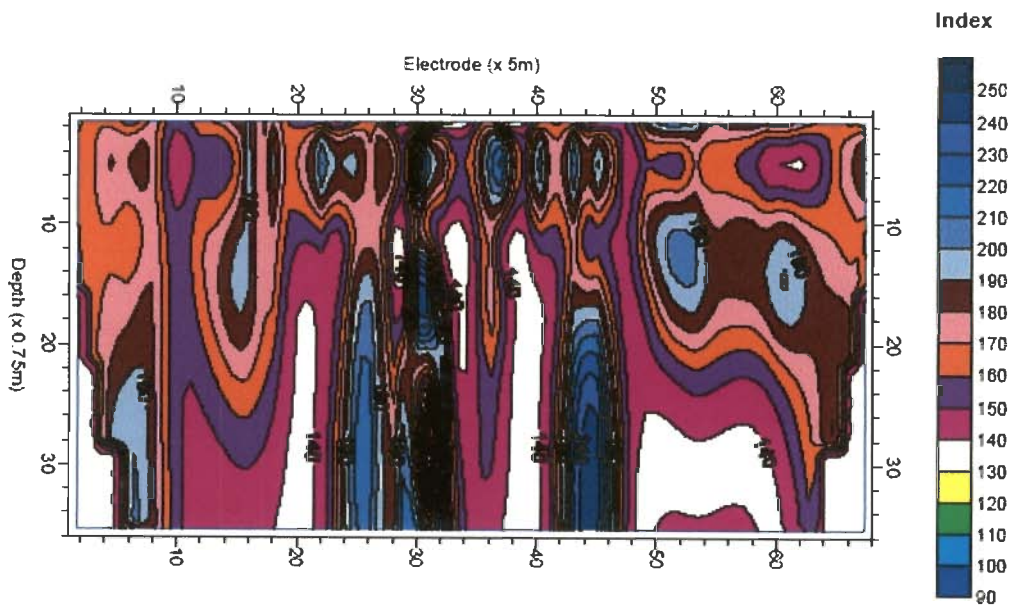


Fig. 8.20 Predicted Unconfined Compressive Strength, q_u Section from SPT 'N' Section Using IP Along Profile A_3-B_3 , Bhagwanpur

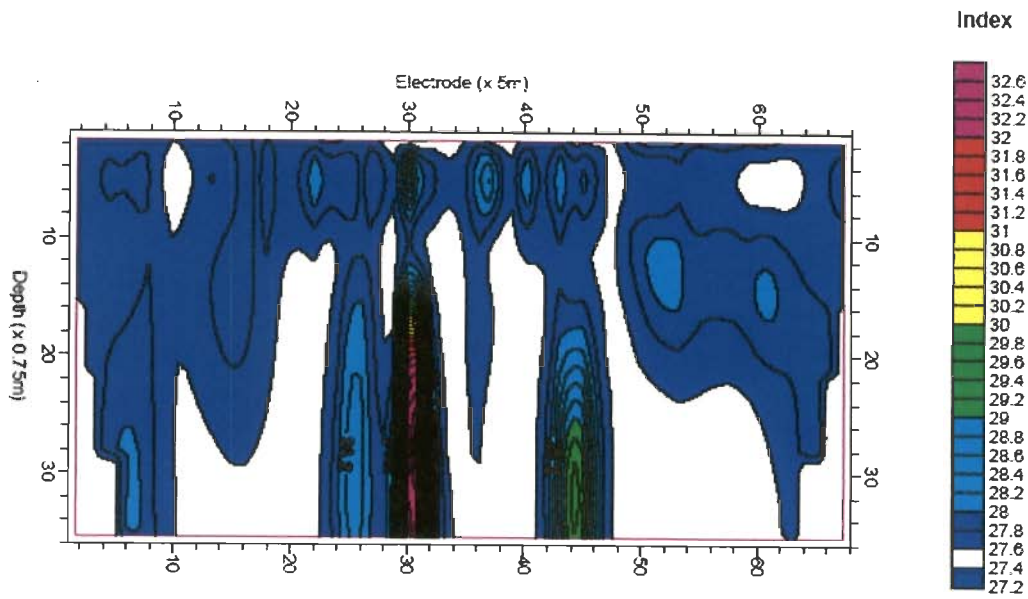


Fig. 8.21 Predicted Bearing Capacity Factor of General Shear Failure, N_c Section from IP Derived Angle of Internal Friction Section Along Profile A₃-B₃, Bhagwanpur

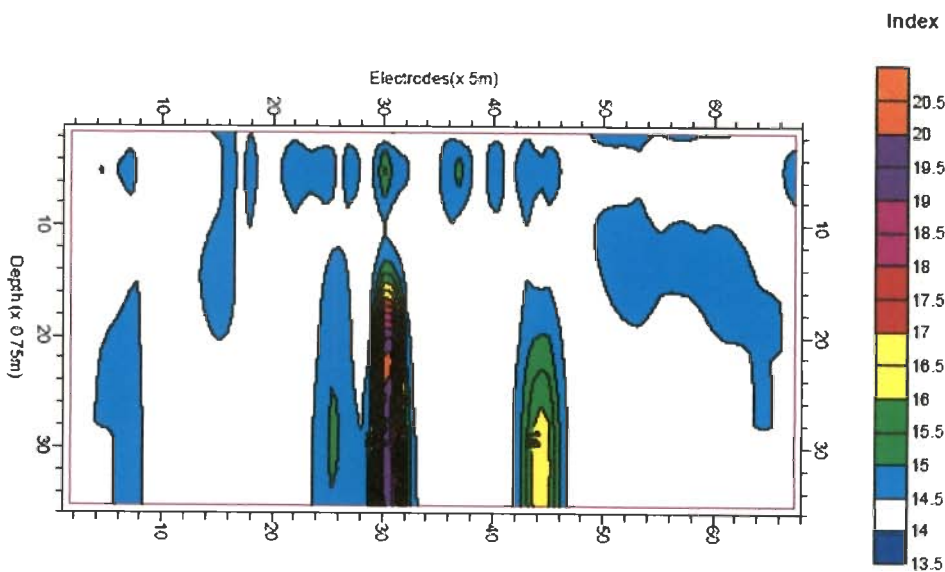


Fig. 8.22 Predicted Bearing Capacity Factor of General Shear Failure, N_v (Vesic) Section from Angle of Internal Friction Section Along Profile A₃-B₃, Bhagwanpur

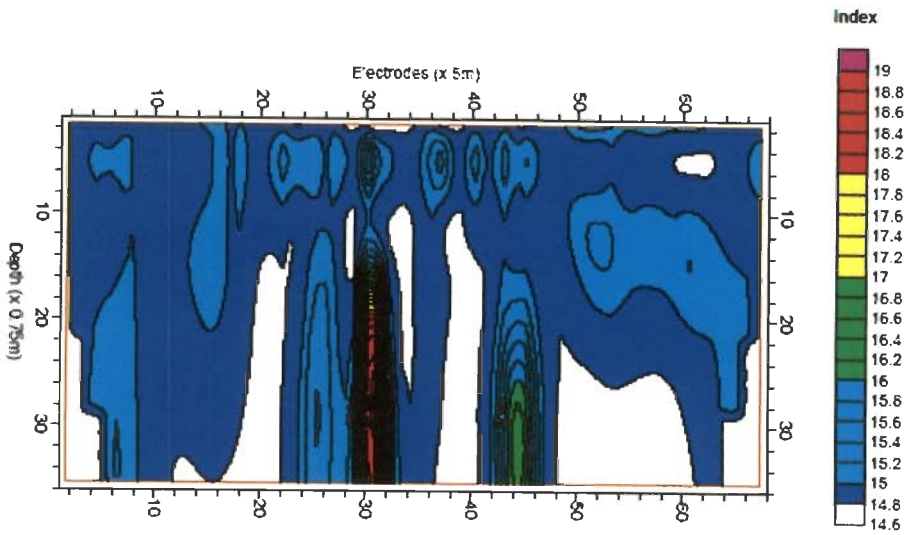


Fig. 8.23 Predicted Bearing Capacity Factor of General Shear Failure, N_q Section from Angle of Internal Friction Along Profile A₃-B₃, Bhagwanpur

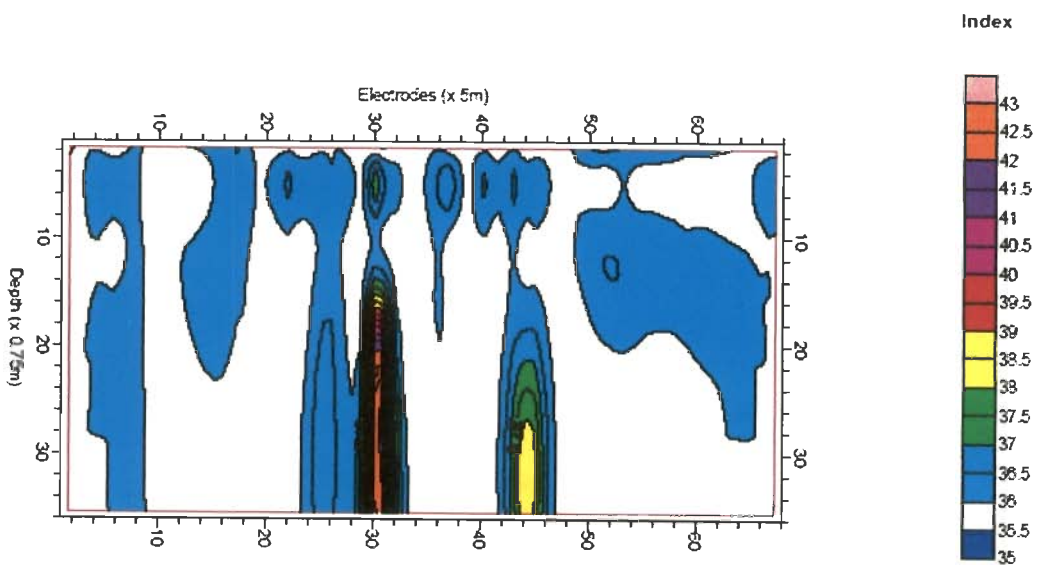


Fig. 8.24 Predicted Ultimate Bearing Capacity Factor, N_c Section for Strip Footings from Angle of Internal Friction Section Along Profile A₃-B₃, Bhagwanpur

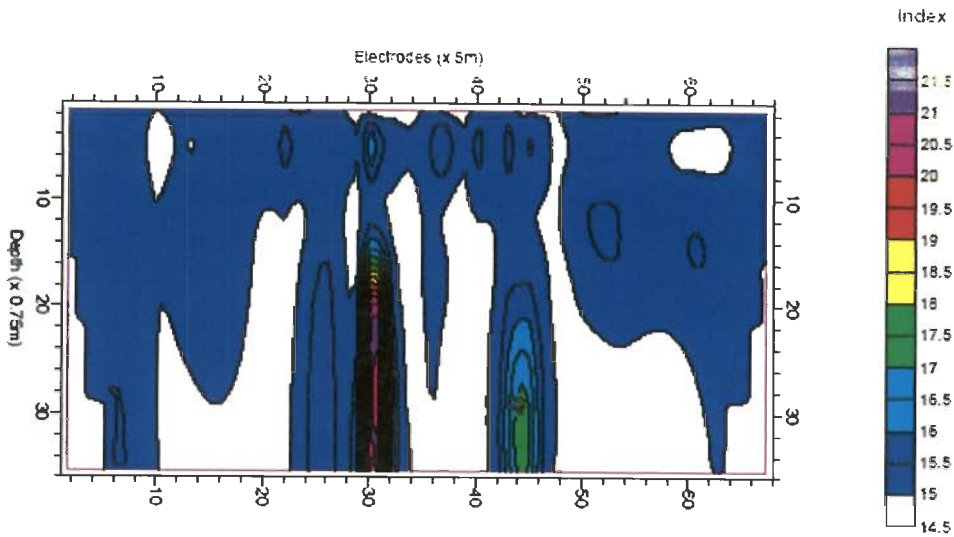


Fig. 8.25 Predicted Ultimate Bearing Capacity Factor, N_γ Section for Strip Footings from Angle of Internal Friction Section Along Profile A₃-B₃, Bhagwanpur

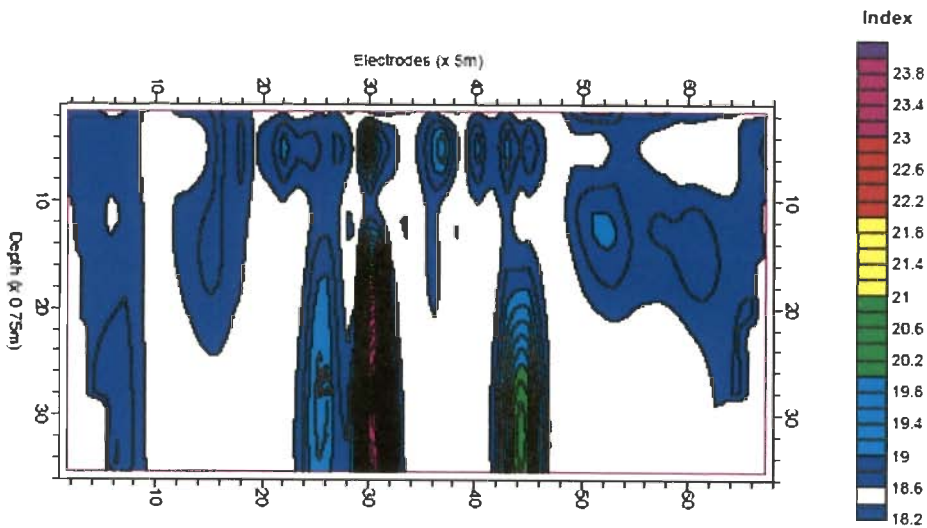


Fig. 8.26 Predicted Ultimate Bearing Capacity Factor, N_q Section for Strip Footings from Angle of Internal Friction Section Along Profile A₃-B₃, Bhagwanpur

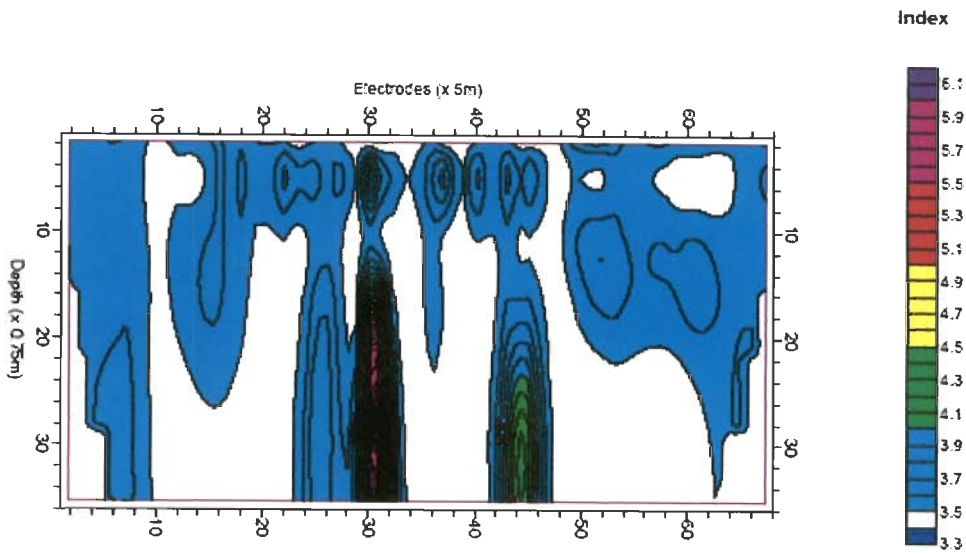


Fig. 8.27 Predicted Terzaghi's Bearing Capacity (Peck et al., 1974) N_γ Factor
Section from Angle of Internal Friction Section Along
Profile A₃-B₃, Bhagawanpur

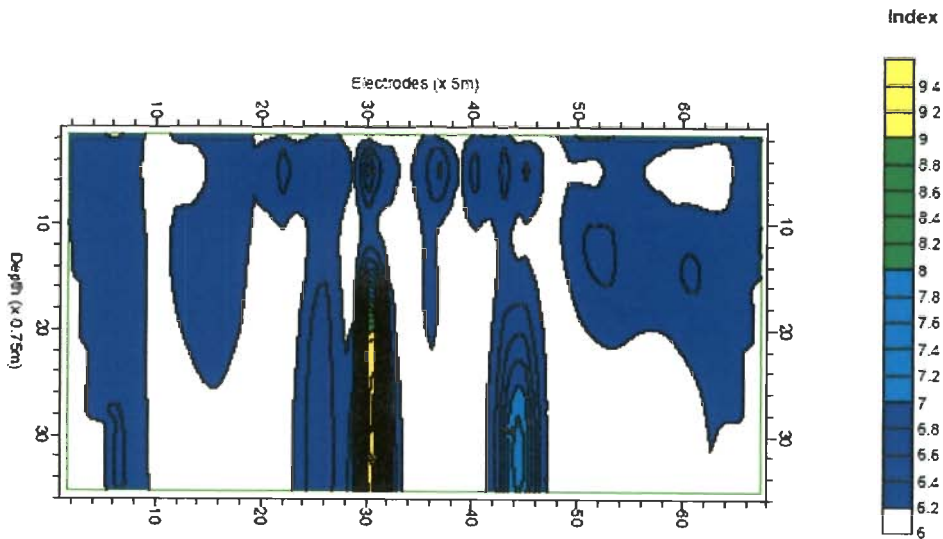


Fig. 8.28 Predicted Terzaghi's Bearing Capacity (Peck et al., 1974) Factor, N_q
Section from Angle of Internal Friction Section Along
Profile A₃-B₃, Bhagawanpur

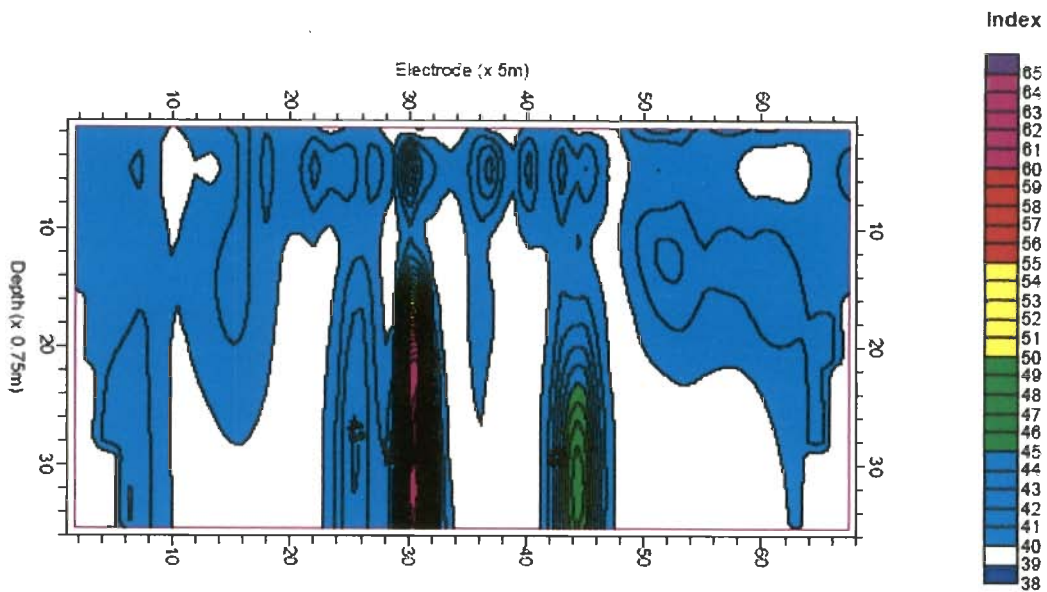


Fig. 8.29 Predicted N_q Factor (Meyerhof, 1953) Section for Driven Piles from Angle of Internal Friction Section Along Profile A₃-B₃, Bhagawanpur

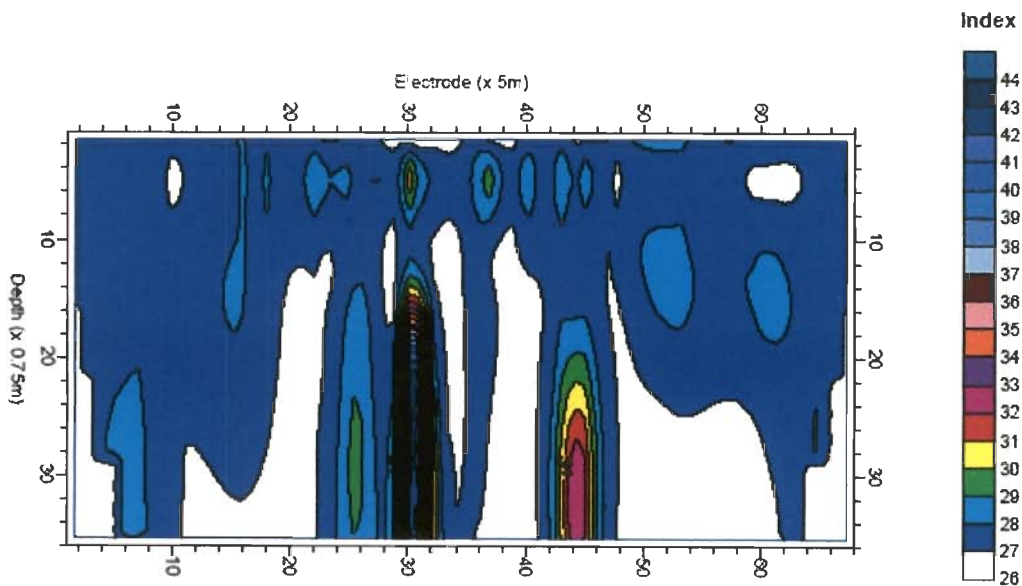


Fig. 8.30 Predicted N_q (Meyerhof, 1953) Factor Section for Bored Piles from Angle of Internal Friction Section Along Profile A₃-B₃, Bhagawanpur

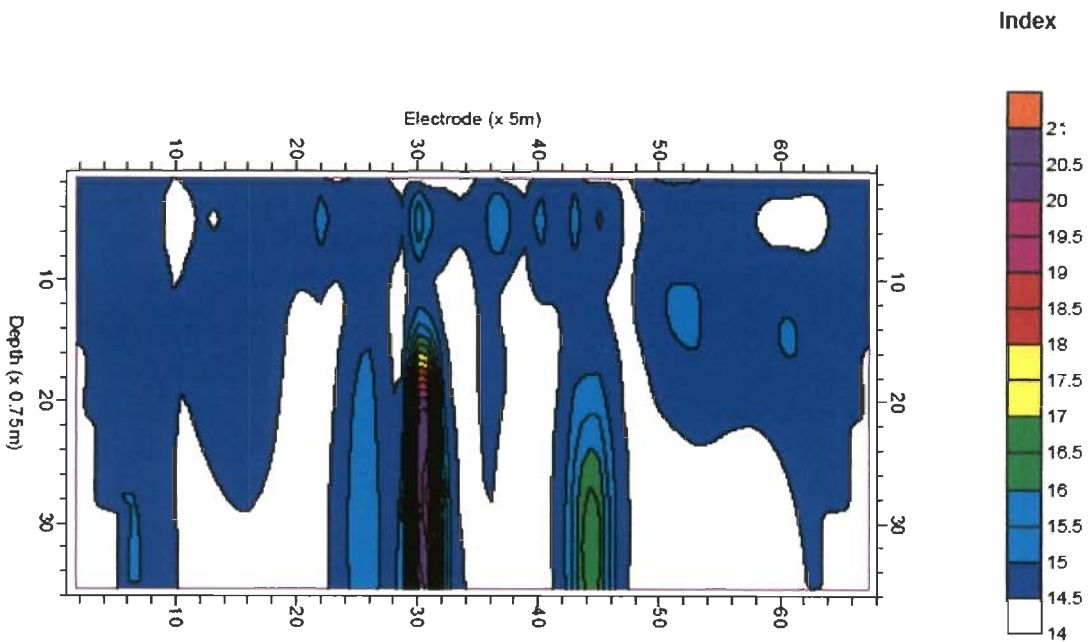


Fig. 8.31 Predicted N_q (Vesic) Factor Section for Bored Piles from Angle of Internal Friction Section Along Profile A_3-B_3 , Bhagawanpur

GEOTECHNICAL CASE STUDIES-IV

9.1 GENERAL

This study region namely the site of proposed construction of a new POL terminal of Bharat Petroleum Corporation Limited (BPCL) at Piyala about 35 km from New Delhi falls in Haryana State, India. It belongs to Delhi Super Group. The methodology detailed in Chapter 5 has been utilized in geotechnical site characterization by using resistivity / IP image data. For geotechnical aspects, the geotechnical report of Civil Engineering Department, IIT Roorkee was consulted.

9.2 SITE LOCATION MAPS

Figure 9.1 illustrates the position location of study region. Broad geology is included in Fig. 9.3, wherein study location, Piyala is mentioned. Different field geoelectric profiles and geotechnical study locations are indicated in Fig. 9.2. The geoelectrical investigations refer to resistivity and IP imaging data acquisition. The profile A₄-B₄ (Fig. 9.2) is considered for further analysis.

9.3 GEOLOGY OF THE STUDY REGION

Our study region falls within Haryana state and it belongs to Holocene era. Table 9.1 provides broad litho-stratigraphy details. Figure 9.3 contains the relevant geological details. Quaternary sediments cover almost whole of Haryana state. It comprises of older fans and piedmont Central Alluvial plains and younger Alluvium unconformably overlies the basement rocks belonging to Delhi supergroup to Siwalik group.

In the area around Delhi, Gurgaon, east of Faridabad and Palwal (Our study region) the basement (Alwar Group) essentially consists of quartzite with limestone and biotite schist. It shows subsurface ridges and deep valleys along N-S direction in the eastern part.

Further, in Delhi area, the boreholes are 35-200 m deep and the bedrock occurs at depths ranging from 32 m to over 200 m. The overlying sediments comprise of sticky and plastic clay with pedogenic kankar granules, fine sandy layers and pieces of quartzite, kaolin and 'Badarpur' type of sand.

In Faridabad - Palwal area (our study region), boreholes are 50-325 m deep with depth of bedrock occurring in depth range 52 to 318.8 m. The sediments consist mainly of clay with bands of fine sand (Thussu, 2006). The thickness of sandy layers increases towards the Yamuna River in the east. Several subsurface ridges and depressions have been inferred on the basis of borehole data east of Faridabad and Delhi.

9.4 GEOELECTRICAL AND GEOTECHNICAL DATA ACQUISITION

Geoelectrical data have been acquired using a micro-processor controlled multi-electrode imaging system of French make (SYSCAL Jr. II of 72 electrode system). The relevant details of resistivity image along chosen profile A₄-B₄ (Fig. 9.2) is included in Fig. 9.4.

The geotechnical data was acquired by Civil Engineering Department, IIT Roorkee which has been used for further analysis.

As per details in Chapters 5 and 6, for generation of regression equations of both formation and geotechnical parameters, a pair of boreholes in the vicinity of geoelectric profile is selected. Both geoelectric image data columns coinciding with projected borehole locations B-7 and B-8 in Fig. 9.2 are correlated with both formation and geotechnical data available at these boreholes. In our present case, electrodes E-12 and EL-33 of profile A₄-B₄ correspond to the projected location of boreholes B-7 and B-8. Figures 9.11a and 9.11b describe the observed SPT data at borehole location B-7 and B-8 respectively. Further analysis is described in the following sections:

9.5 REGRESSION EQUATIONS FOR FORMATION AND SITE GEOTECHNICAL TESTS

As per methodology outlined in Chapter 5 regression equations have been developed for both formation and geotechnical parameters, for Profile A₄-B₄ (Fig. 9.2). For brevity sake, all those details are not included here. Table 9.1 contains all regression equations (sand, clay, lithology, porosity, SPT, DCPT and SCPT) developed for this study region (Profile A₄-B₄ in Fig.9.2).

Figures 6.15a and 6.15b describe the observed DCPT data corresponding to the electrode location EL-18 and EL-25 of profile A₄-B₄. The predicted DCPT on the basis of resistivity is presented in Fig. 9.16.

The observed SCPT data corresponding to the EL-15 and EL-25 have been described in Figs. 9.17a and 9.17b respectively. The prediction of SCPT data on the basis of resistivity has been shown in the Fig. 9.18.

9.6 PREDICTED 2-D SECTIONS OF FORMATION AND SITE GEOTECHNICAL PARAMETERS

As per methodology outlined in Chapter 5, by utilizing the appropriate regression equations that are included in Table 9.1 and Table 4.10, the digital resistivity values (Fig. 9.4a) along Profile A₄-B₄ (Fig. 9.2) are converted to respective formation and field geotechnical sections. All illustrations appear at the end of the chapter and Table 9.2 contains relevant details along with remarks.

Accordingly, Figs. 9.5-9.12 and 9.16-9.18 refer to predicted 2-D sections for sand, clay, lithology, porosity, SPT, DCPT and SCPT. In Figs. 9.13 and 9.14, we compare predicted SPT with observed SPT for boreholes B-7 and B-8.

9.7 PREDICTED 2-D GEOTECHNICAL PARAMETER SECTIONS

By utilizing regression correlation equations developed in Chapter 4 (Ref. Table 4.10), several geotechnical parameter sections have been developed by considering SPT section along Profile A₄-B₄ (Fig. 9.12) as input. Accordingly, Figs. 9.19, 9.22-9.33

respectively contain predicted i) 2-D sections of angle of internal friction, ii) unconfined compressive strength, iii) bearing capacity factors for general shear failure (N_c , N_γ (Vesic) and N_q), iv) ultimate bearing capacity factors (N_c , N_γ and N_q), Terzaghi's bearing capacity (Peck et al., 1974) factors (N_γ and N_q), bored pile factors (N_q (Meyerhof, 1953) and N_q (Vesic)) and driven pile N_q factor (Meyerhof, 1953). In Figs. 9.20-9.21, using regression equations in Table 4.10, 2-D sections of unit weights of soil (dry & saturated) were derived from respective porosity section (Fig. 9.9).

Table 9.1 Inferred Regression Equations Based on Borehole and Geoelectrical Depth Profiles Gathered from Respective Geoelectrical Images at Projected Borehole Position onto Profile A₄-B₄ at Piyala Site, Haryana.

S. No.	Formation Parameter / Geotechnical Parameter	Correlation equation based on RES at B7 (EL - 12) $Y=a_1x^2+a_2x+a_3$	Correlation equation based on RES at B8 (EL - 33) $Y=b_1x^2+b_2x+b_3$	Average Correlation equation based on RES at B7 & B8 $Y=c_1x^2+c_2x+c_3$ [$c_1=av(a_1,b_1)$, $c_2=av(a_2,b_2)$, $c_3=av(a_3,b_3)$]
1	Sand	$a = \{-0.2266, -0.5016, 1.0806\}$ $R2 = 0.5826$	$b = \{-1.6848, 1.0901, 0.6488\}$ $R2 = 0.3731$	$c = \{-0.9557, 0.29425, 0.8647\}$
2	Clay / Shale	$a = \{0.2296, 0.5082, -0.0796\}$ $R2 = 0.5826$	$b = \{1.707, -1.1045, 0.3578\}$ $R2 = 0.3731$	$c = \{0.9683, -0.29815, 0.1319\}$
3	Lithology	$a = \{0.5562, -0.8664, 0.8603\}$ $R2 = 0.4774$	$b = \{0.8611, -1.2356, 0.8003\}$ $R2 = 0.3458$	$c = \{0.70865, -1.051, 0.8303\}$
4	SPT	$a = \{0.8767, -1.0722, 0.666\}$ $R2 = 0.4751$	$b = \{0.5415, -0.8381, 0.6231\}$ $R2 = 0.3432$	$c = \{0.7091, -0.95515, 0.64455\}$
5	DCPT	$a = \{0.482, 0.1319, 0.2691\}$ $R2 = 0.2638$ DCPT 5 at EL-18	$b = \{2.4105, -2.0329, 0.828\}$ $R2 = 0.4873$ DCPT 7 at EL-25	$c = \{1.44625, -0.9505, 0.54855\}$
6	SCPT	$a = \{0.4798, -0.2838, 0.4277\}$ $R2 = 0.4788$ SCPT 4 at EL-15	$b = \{0.1967, 0.6469, 0.1729\}$ $R2 = 0.7785$ SCPT 5 at EL-29	$c = \{0.33825, -0.18155, 0.3003\}$
7	Porosity	$a = \{-0.2266, -0.5016, 1.0806\}$ $R2 = 0.5826$	$b = \{-1.6848, 1.0901, 0.6488\}$ $R2 = 0.3731$	$c = \{-0.9557, 0.29425, 0.8647\}$

Table 9.2 Details of illustrations

S. No.	Formation / Geotechnical Parameter		Fig. No.	Remarks
1	Sand	Resistivity derived	Fig. 9.6	Sand pocket is spotted around 13-16 m depth for a limited width (Electrodes 10-23).
		Geotechnical & Resistivity derived	Fig. 9.7	It seems that the relatively pure sand exist around 13-16 m depth.
2	Clay / Shale	Resistivity derived	Fig. 9.5	Sand pocket is spotted around 13-16 m for a limited width. Shaly sands and clay dominate the subsurface.
		Geotechnical & Resistivity derived	Fig. 9.8	Shaly sands seem to dominate the section.
3	Lithology		Fig. 9.10	Silts and clay in the depth range 7.5-15.0 m of lateral extent 30-75 m overlain by clayey and silty sands. Clayey and silty gravels in the depth range 3-23 m of lateral extent 75-120 m overlain by silty and clayey sands.
4	SPT		Figs. 9.12-9.14	SPT 'N' ranges from 12-26. Relatively low pocket (around N=12) stretching 60m in width is spotted in the depth range 10-19 m. Figures 9.13-9.14 indicate that resistivity derived SPT values are lower than that of observed. So, the predicted SPT values in Fig. 9.12 can be taken as minimum.
5	SCPT		Fig. 9.16	The resolution has improved in comparison to SPT section with broad conclusions remaining intact.
6	DCPT		Fig. 9.18	The resolution has improved in comparison to SPT section with broad conclusions remaining intact.
6	Porosity		Fig. 9.9	This section along with lithology section (Fig. 10) indicates that effective porosity is low.
7	Unit weight of soil	Dry	Fig. 9.20	For major portion it is 15-16 kN/m ³ .
		Saturated	Fig. 9.21	For major portion it is close to 20 kN/m ³ .
8	Angle of internal friction, ϕ		Fig. 9.19	It ranges from 15 – 21°. 2-D inhomogeneity is seen.
9	Unconfined compressive strength, q_u		Fig. 9.22	It ranges from 160-350 kN/m ² .
10	Terzaghi's Bearing Capacity factors (Peck et al. 1974)	N_γ factor	Fig. 9.29	All these bearing capacity factor sections exhibit 2-D variation. Depending on the proposed depth of foundation, the 2-D sections can be transformed into 1-D sections by averaging process. These 1-D sections could of much help in the design of foundations of superstructures.
N_q factor		Fig. 9.30		
11	Bearing capacity factors for general shear failure	N_c factor	Fig. 9.23	
		N_γ (Vesic) factor	Fig. 9.24	
		N_q factor	Fig. 9.25	
12	Ultimate bearing capacity factors	N_c factor	Fig. 9.26	
		N_γ factor	Fig. 9.27	
		N_q factor	Fig. 9.28	
13	Piles	Driven Piles N_q factor (Meyerhof, 1953)	Fig. 9.31	
		Bored Piles N_q factor (Meyerhof, 1953)	Fig. 9.32	
		Bored Piles N_q factor (Vesic, 1953)	Fig. 9.33	

9.8 RESULTS & DISCUSSION

In the present case study, resistivity based prediction of formation and geotechnical parameter profiles are better correlated with the observed ones in comparison to IP derived ones. The methodology adopted herein honors both geoelectrical and geotechnical data. The development of regression equations rests on a pair of boreholes that are projected onto the geoelectrical profile and the resistivity and IP data at those electrode positions. The regression equations are limited to 2nd degree polynomial only as higher order polynomial involves the usual mathematical difficulties as perceived in regional-residual separation for gravity data processing (Dobrin, 1976). Table 9.3 contains all relevant details. Additionally, the followings remarks need to be considered:

- a) The inferred lithology section (Fig. 9.10) clearly outlines the predominance of silty / clayey sand in the subsurface within the probed depth of 24 m.
- b) Except for a small pocket, the predicted porosity section (Fig. 9.9) along profile A₄-B₄ indicates a low porosity variation in the range 5-10 %, which is typical silty / clayey sand.
- c) Resistivity derived porosity section (Fig. 9.9) reveals that porosity varies in the range 35-39 % except for a pocket of low porosity (9-30 %) between electrodes 10-23 at a depth range of 7.5-15 m. Further, porosity based regression equation in Table 4.10 has allowed to predict unit weights of soil (both dry & Saturated) in Figs. 9.20 and 9.21. The dry and saturated unit weights of soil are in the ranges 16-31 & 20-26 kN/m³ except for a small pocket of low values in the range 15-16 and 19.5-20 kN/m³ between electrodes 10-23 at a depth range of 7.5-15 m respectively.
- d) Figures 9.13-9.14 indicate that resistivity derived SPT values are better matched with that of observed. So, the predicted SPT values in Fig. 9.12 can be considered. So, for geotechnical parameter section predictions, the SPT section (Fig. 9.12) derived from resistivity is used. For a major portion of subsurface section (depth up to 24 m) along Profile A₄-B₄ the predicted SPT 'N' (Fig. 9.12) lies in the range 16-26 except for a small pocket of low SPT 'N' (12.5-15) at depth range 7.5-15.0 m between electrodes 10-23.

- e) The predicted DCPT (Fig. 9.16) provides a better resolution with the values ranging from 60-95 up to a depth of 18m excepting for a pocket of high values (100-170) at a depth range of 9.0-12.6 m between electrodes 10-22.
- f) The predicted SCPT (Fig. 9.18) provides a better resolution with the values ranging from 9000-10000 up to a depth of 15 m excepting for a pocket of high values (9400-15000) at a depth range of 7.5-14.5 m between electrodes 10-23.
- g) Unconfined compressive strength, q_u derived from SPT 'N' section is included in Fig. 9.22. Here, q_u ranges from 200-340 kN/m² with a 2-D distribution excepting for a pocket of low values (200-250 kN/m²) at a depth range of 7.5-15.0 m between electrodes 10-23.
- h) Generally, the angle of internal friction, ϕ section (Fig. 9.19) derived from SPT reveals a complex 2-D distribution with 16.2 – 19.2° excepting for a pocket of high values (16.2 – 20.8°) at a depth range of 7.5-14.5 m between electrodes 10-23.
- i) All bearing capacity coefficient sections (Figs. 9.23-9.33), which are derived from angle of internal friction, ϕ section show a 2-D distribution. The traditional 1-D geotechnical models can be developed on their basis. It is expected that such section represents in-situ conditions than those being used in traditional geotechnical practice at the proposed depth of foundation.
- j) The bearing capacity factors based on CPT method is not attempted here. However, earlier outlined procedure for SPT 'N' can easily be extended to CPT method also.
- k) The regression equations included in Table 4.10 have remained constant throughout the study and they are based on current geotechnical literature.
- l) The regression equations listed in Table 9.1 are site-specific and geo-electrical profile specific.
- m) All predicted 2-D geotechnical sections clearly show that 1-D models often resorted to by geotechnical engineers are far from reality and efforts are needed to refine their quality or new procedures need to be evolved. The present effort is geared towards that goal.

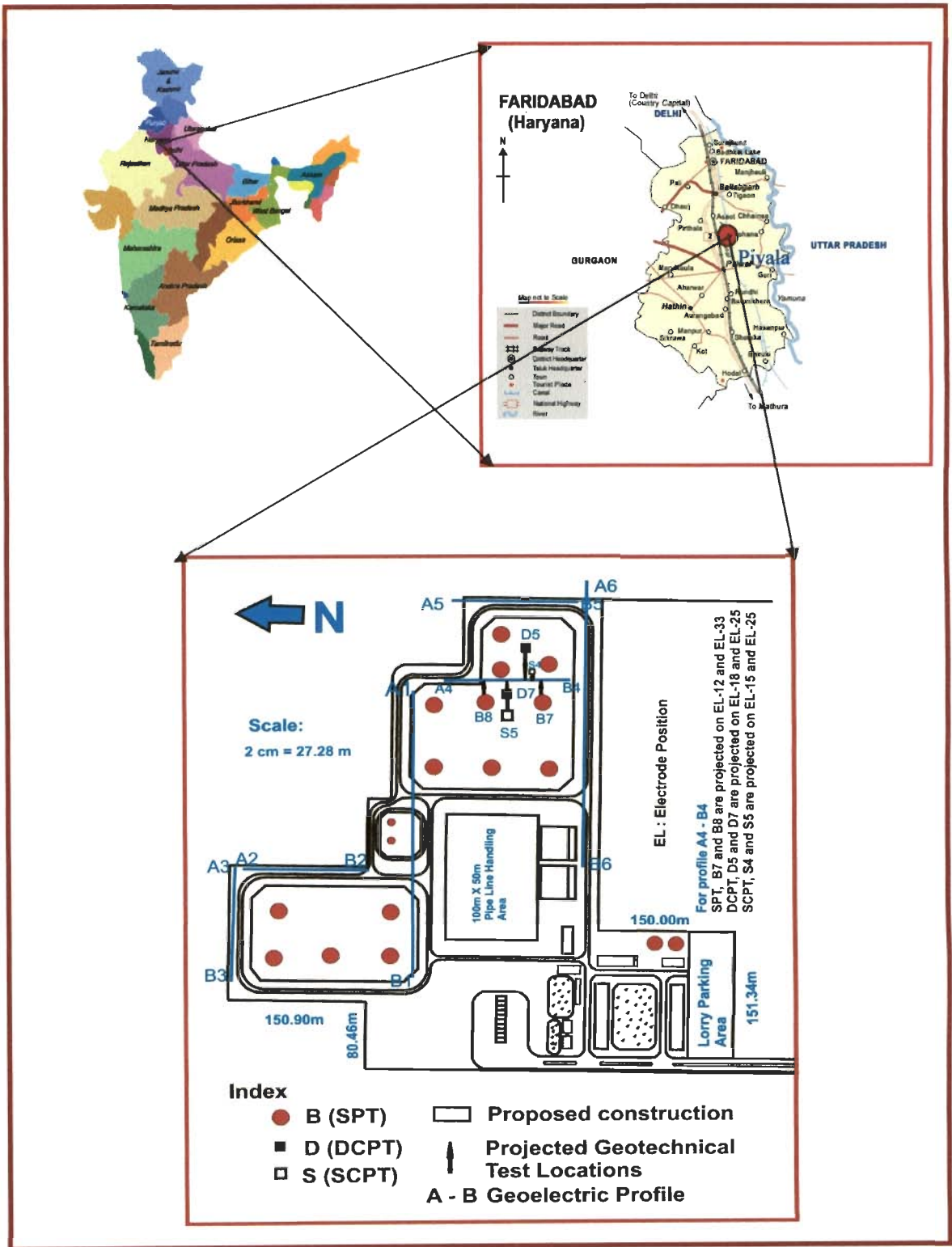


Fig. 9.1 Location Map of Proposed Construction of BPCL at Piyala Site, Haryana, India.

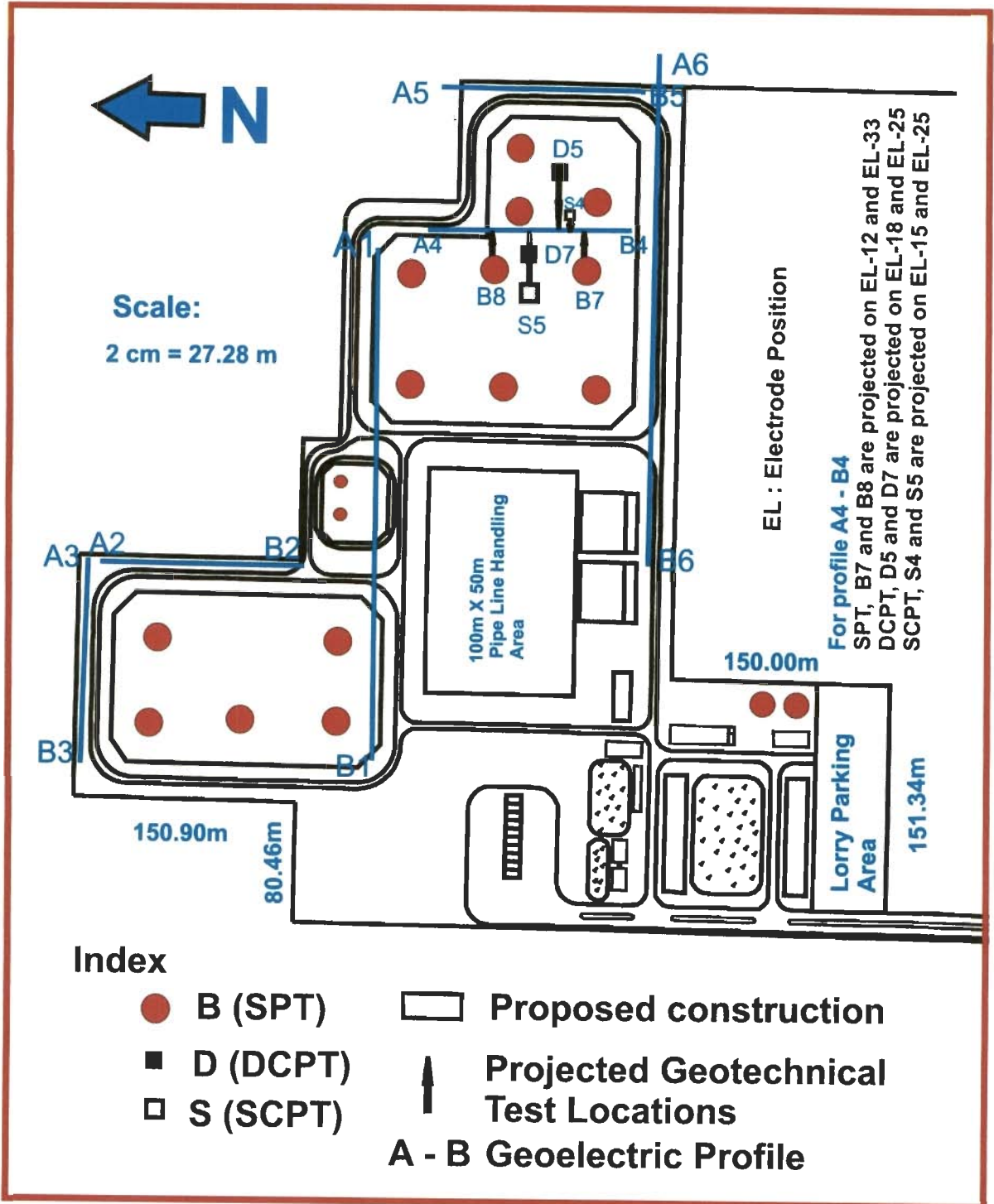


Fig. 9.2 Map Showing the Location of ERT, IPI and Geotechnical Site Investigations

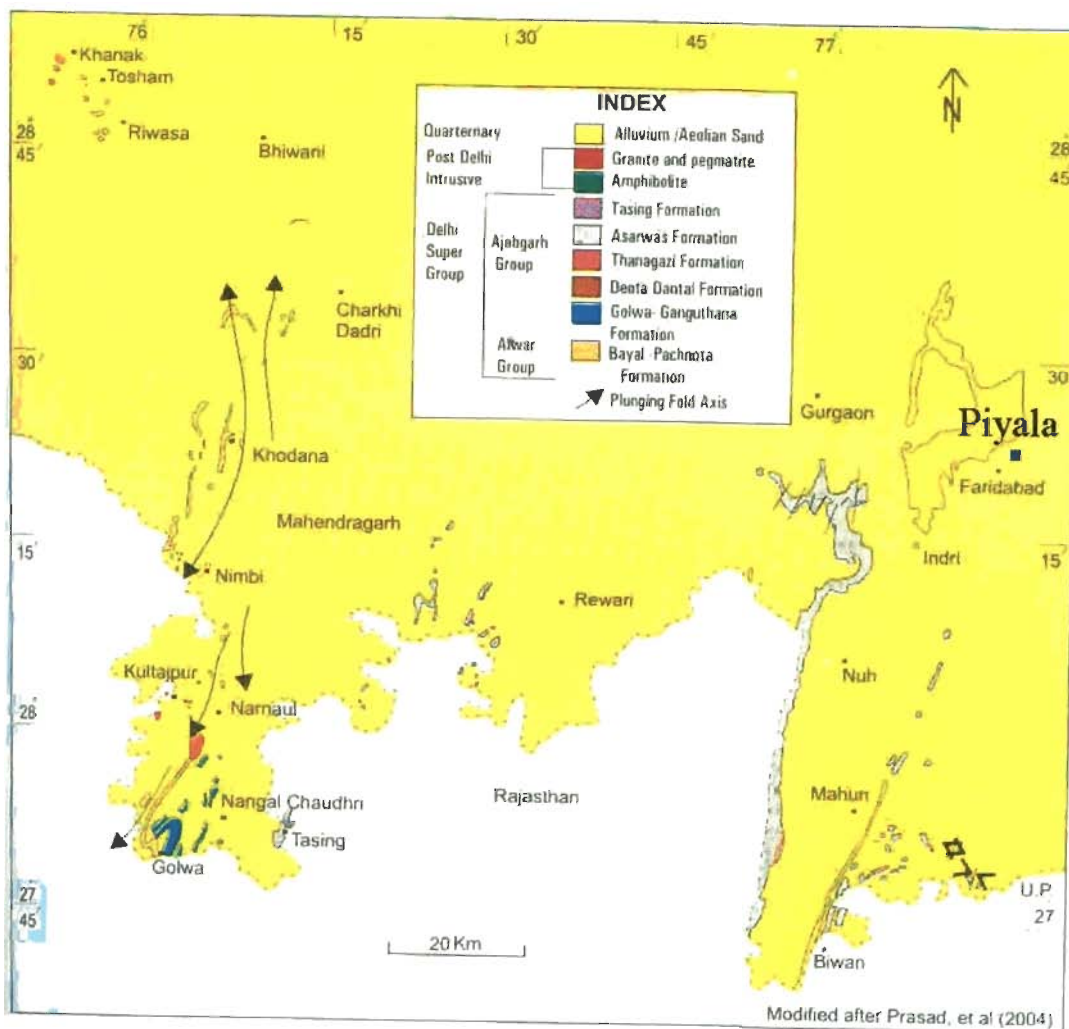


Fig. 9.3 Geological Map of Delhi Supergroup in Haryana Including the Study Region

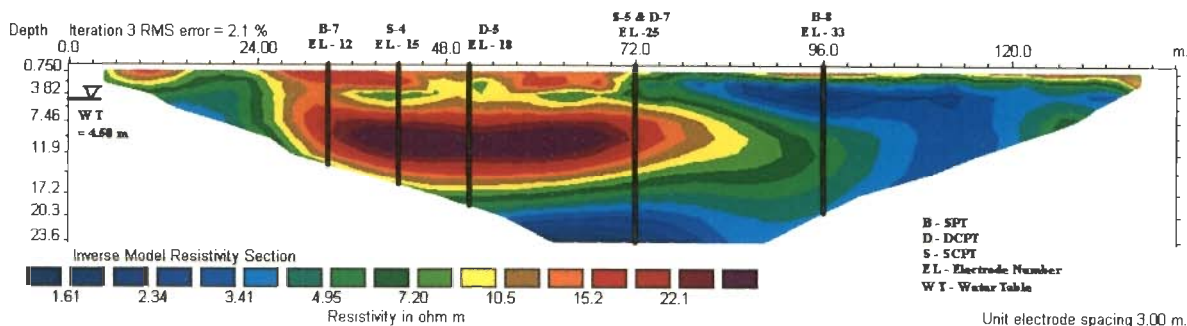


Fig. 9.4 a Resistivity Image (ERT) Along Profile A₄-B₄. The Resistivity (Ω -m) and Depth Scales are Logarithmic

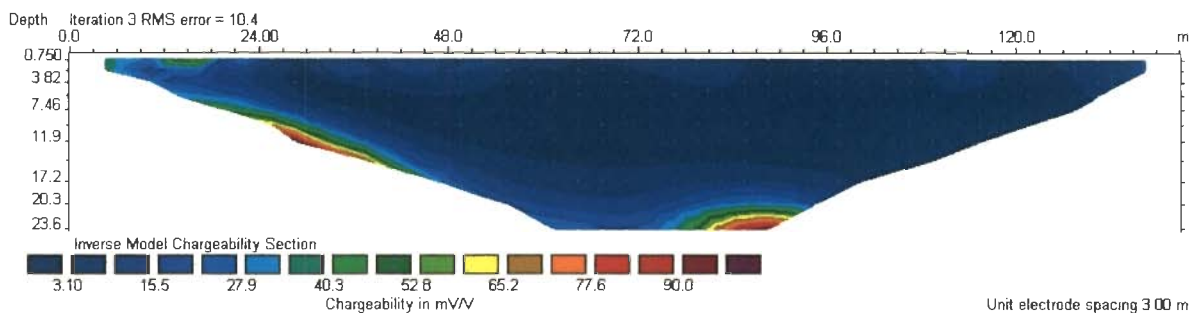


Fig. 9.4 b IP image (IPI) Along Profile A₄-B₄. The Chargeability (m Sec) and Depth Scales are Logarithmic

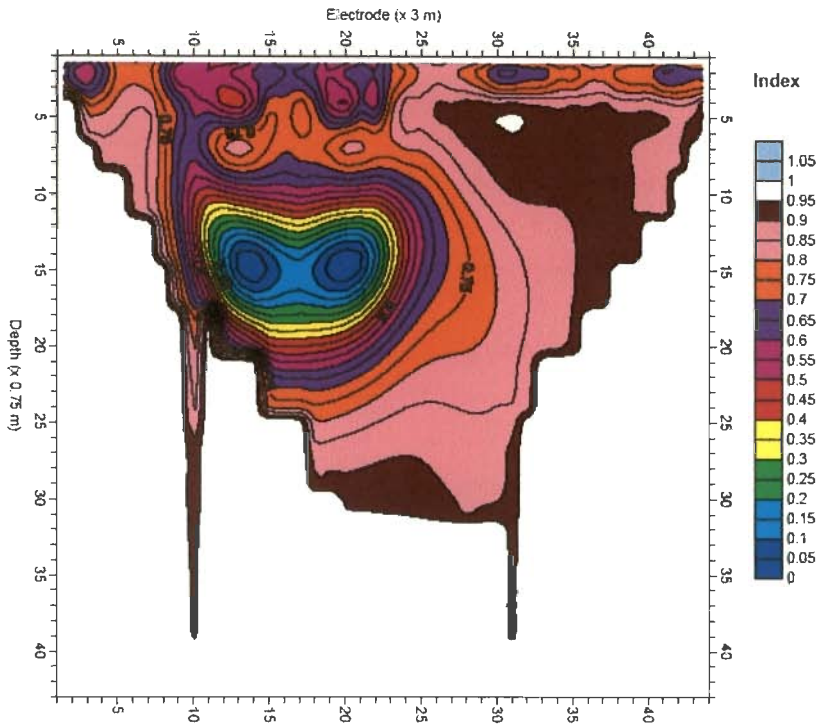


Fig. 9.5 Resistivity Derived Sand (%) Section Along Profile A₄-B₄, Piyala

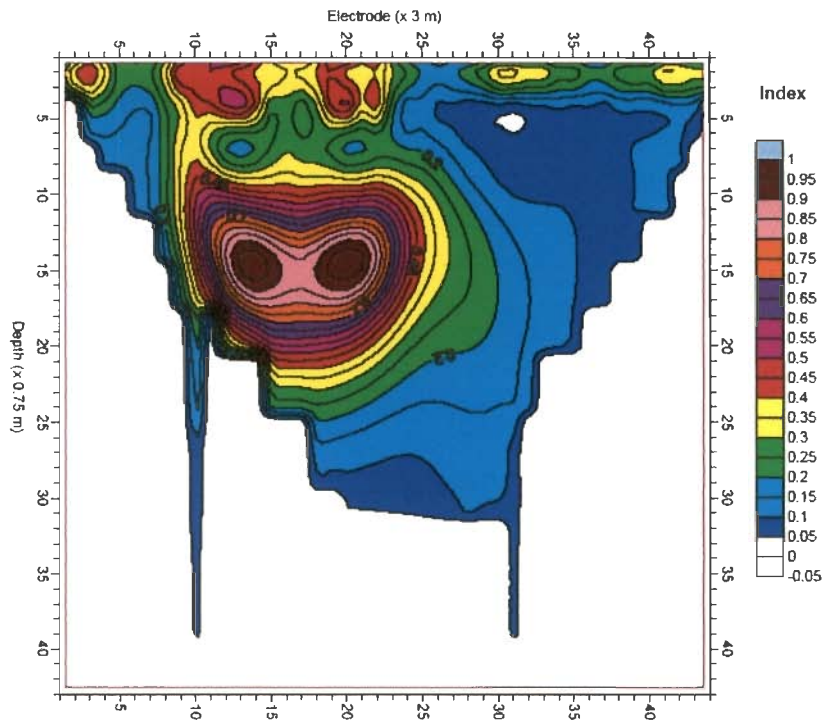


Fig. 9.6 Resistivity Derived Clay (%) Section Along Profile A₄-B₄, Piyala

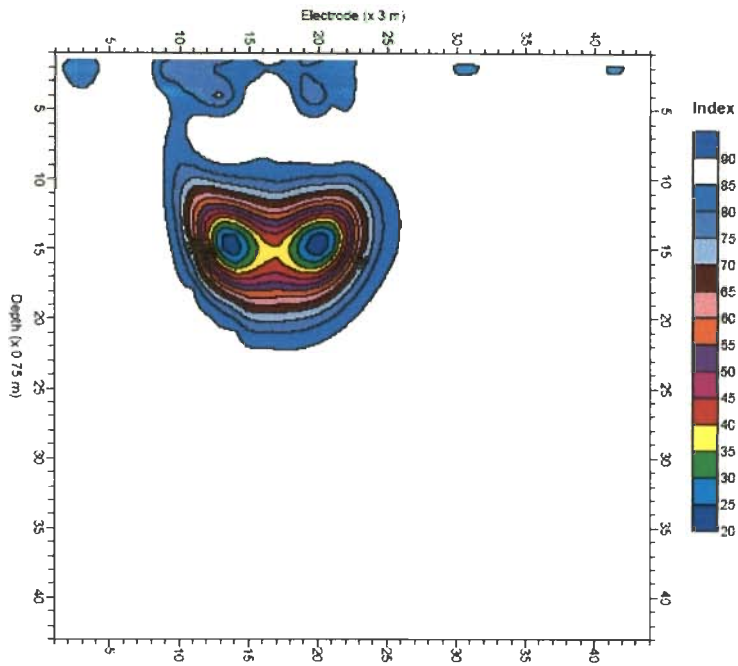


Fig. 9.7 Predicted Sand (%) Section from Geotechnical and Resistivity Data Along Profile A₄-B₄, Piyala

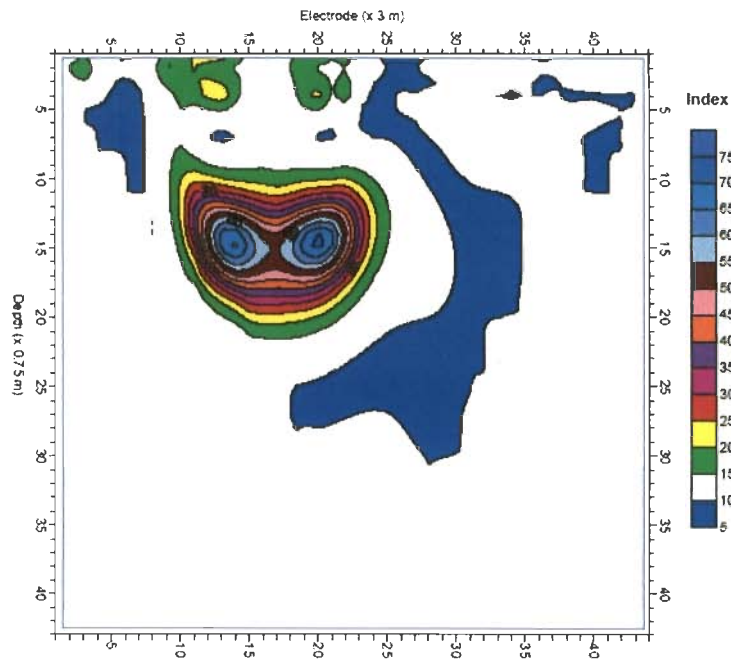


Fig. 9.8 Predicted Clay (%) Section from Geotechnical and Resistivity Data Along Profile A₄-B₄, Piyala

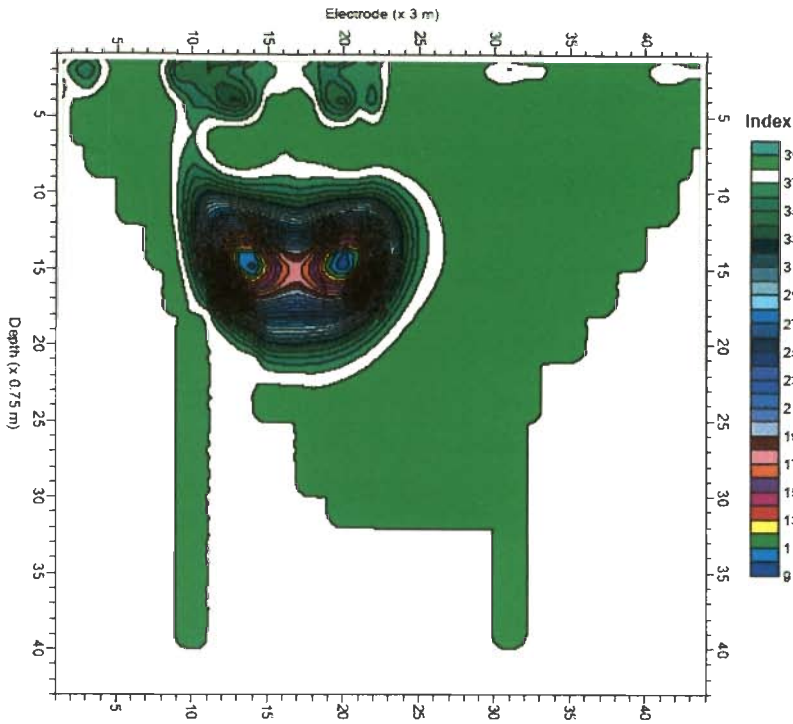


Fig. 9.9 Predicted Porosity (%) Section from Resistivity and Borehole Data Along Profile A₄-B₄, Piyala

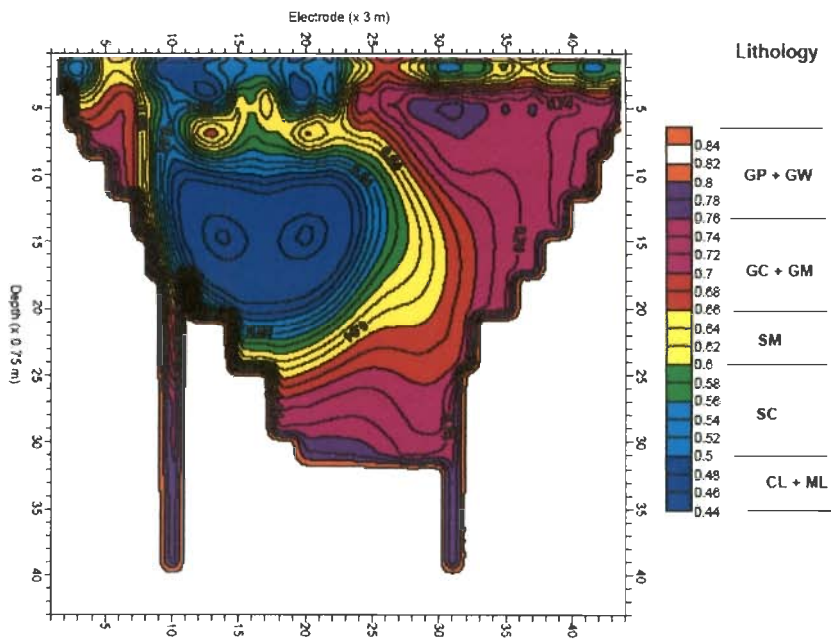
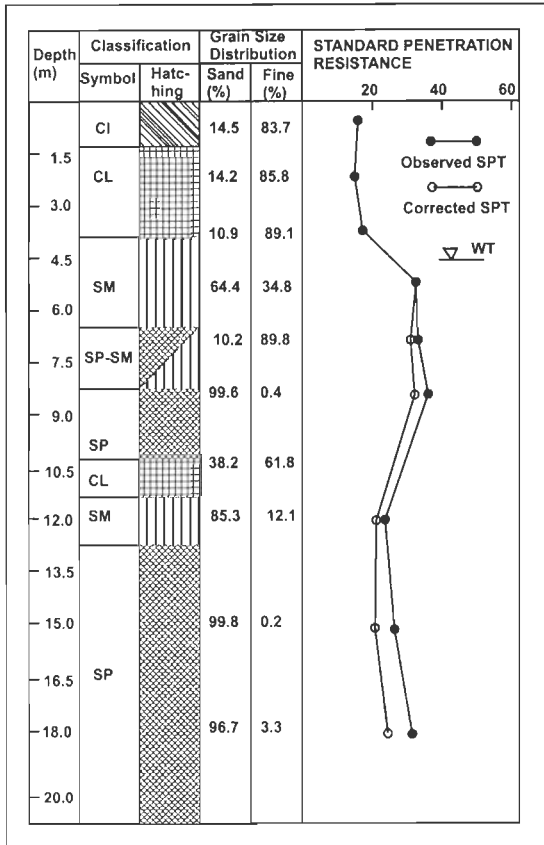
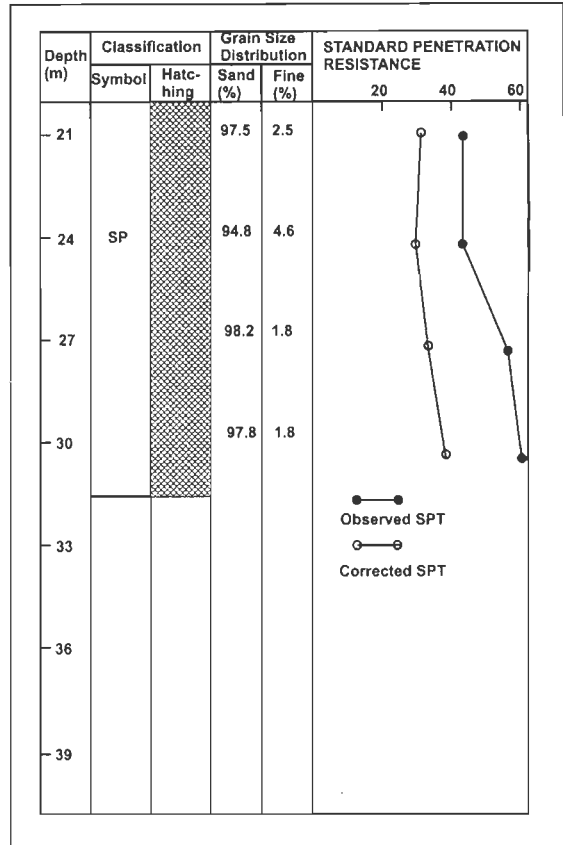


Fig. 9.10 Predicted Lithology Section from Geotechnical and Resistivity Data Along Profile A₄-B₄, Piyala

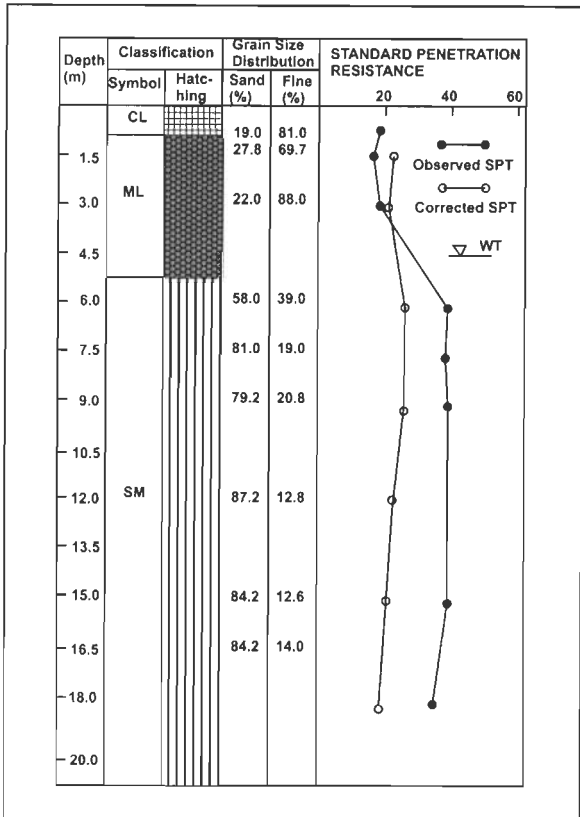


a) Borehole B-7

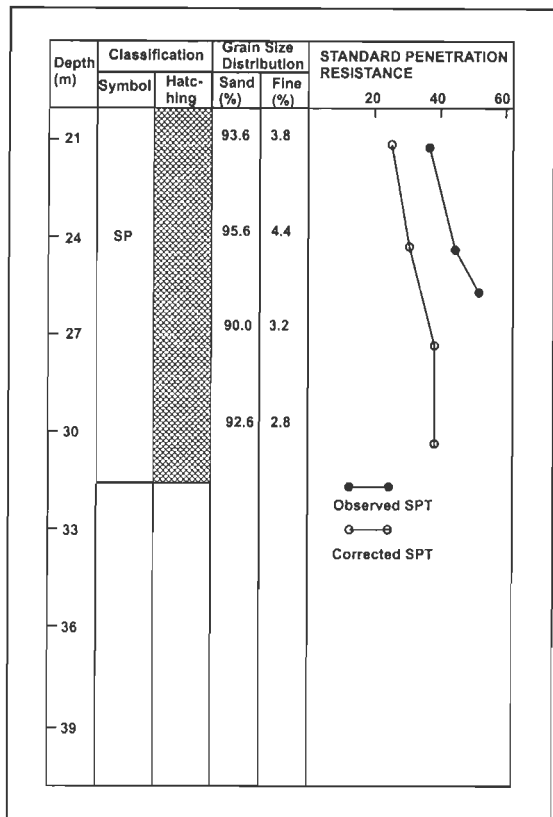


Continue Borehole B-7

Fig. 9.11 a Borehole Data at Location B-7. The Projected Borehole Position Coincides with Electrode, EL-12 of profile A₄-B₄



b) Borehole B-8



Continue Borehole B-8

Fig. 9.11 b Borehole Data at Location B-8. The Projected Borehole Position Coincides with Electrode, EL-33 of profile A₄-B₄

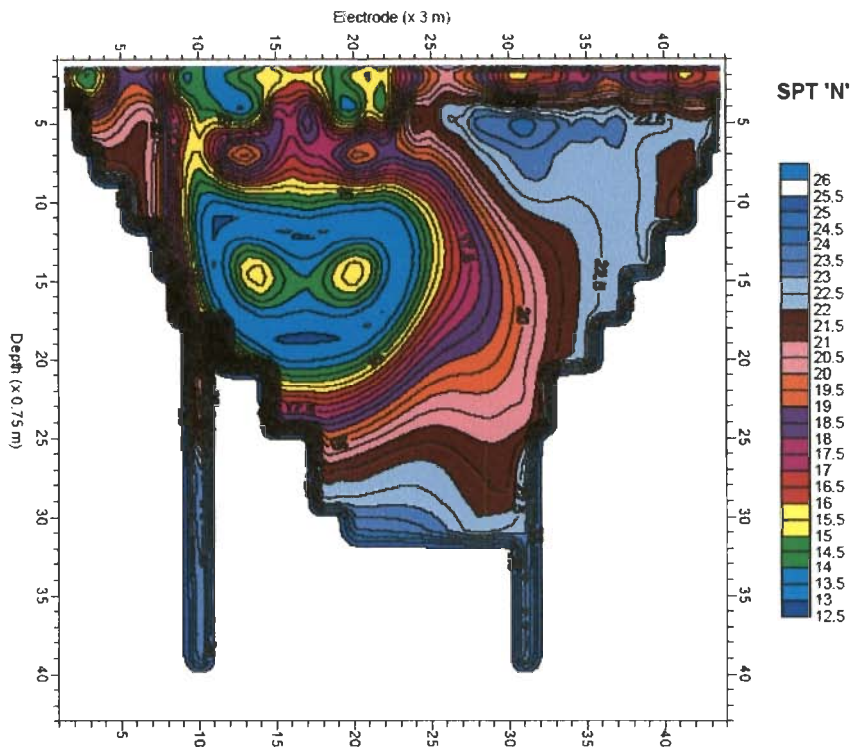


Fig. 9.12 Predicted SPT Section from Resistivity and Borehole Data Along Profile A₄-B₄, Piyala

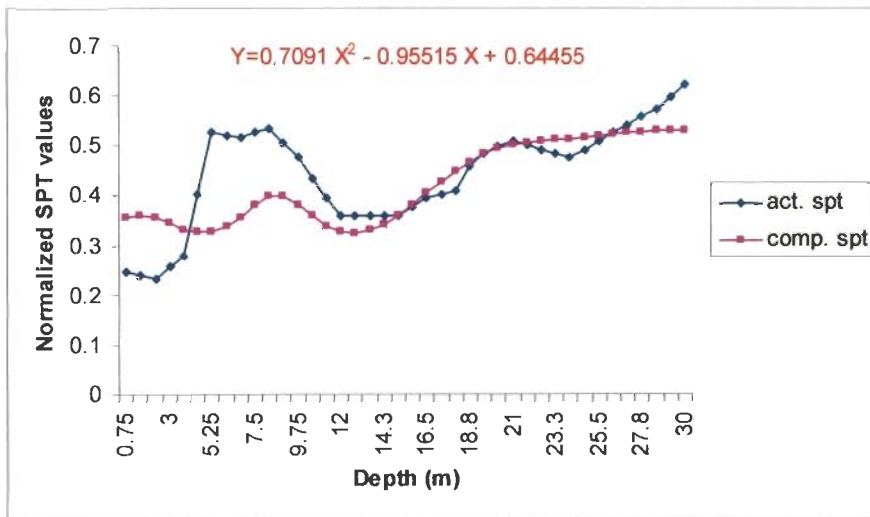


Fig. 9.13 a Comparison of Observed and Predicted SPT 'N' Through Resistivity at Borehole Location- B-7

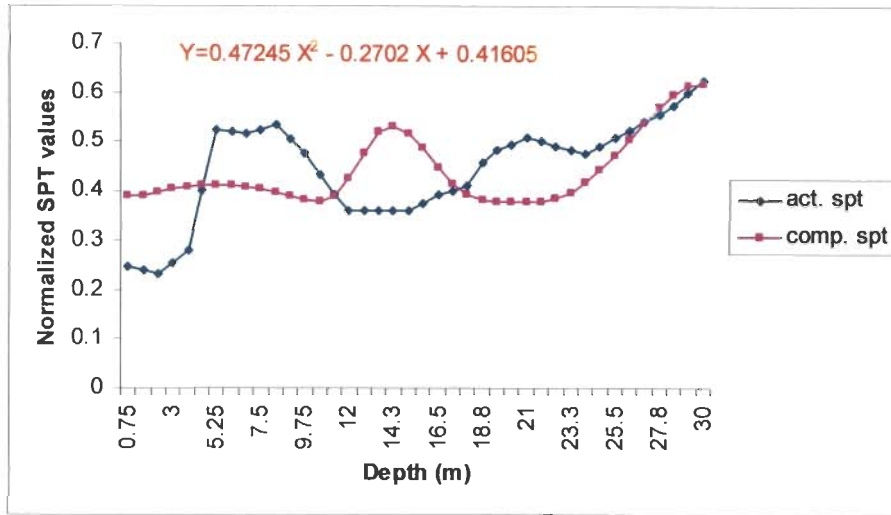


Fig. 9.13 b Comparison of Observed and Predicted SPT ‘N’ Through IP at Borehole Location- B-7

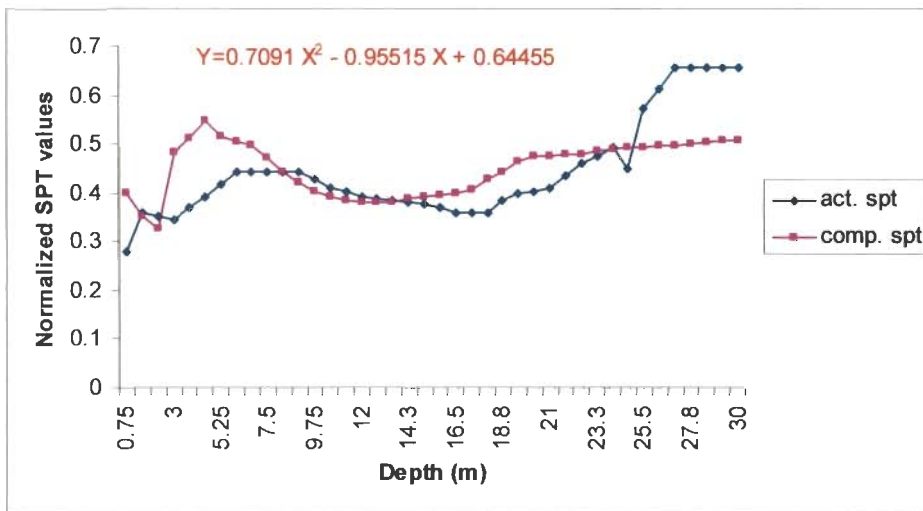


Fig. 9.14 a Comparison of Observed and Predicted SPT ‘N’ Through Resistivity at Borehole Location- B-8

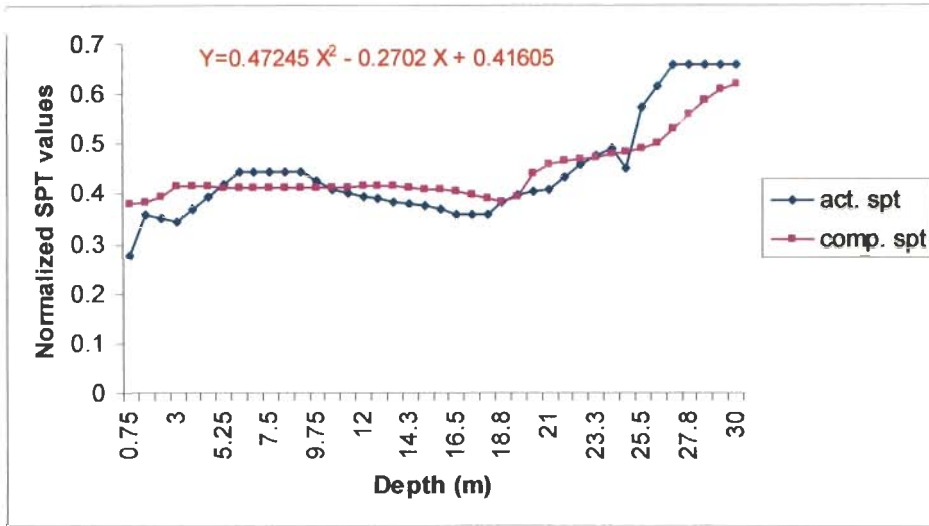


Fig. 9.14 b Comparison of Observed and Predicted SPT ‘N’ Through IP at Borehole location- B-8

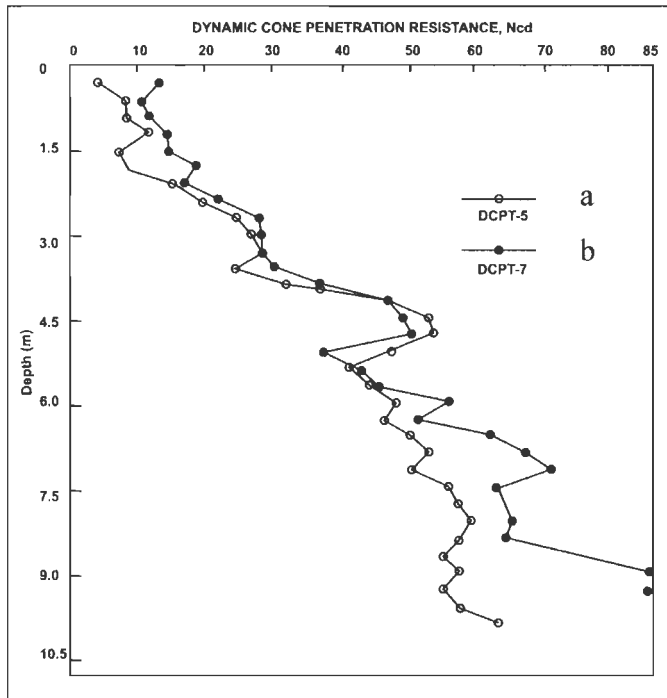


Fig. 9.15 a) DCPT-5 Data. The Corresponding Electrode Position is EL-18 of Profile A₄-B₄

b) DCPT-7 Data. The Corresponding Electrode Position is EL-25 of Profile A₄-B₄

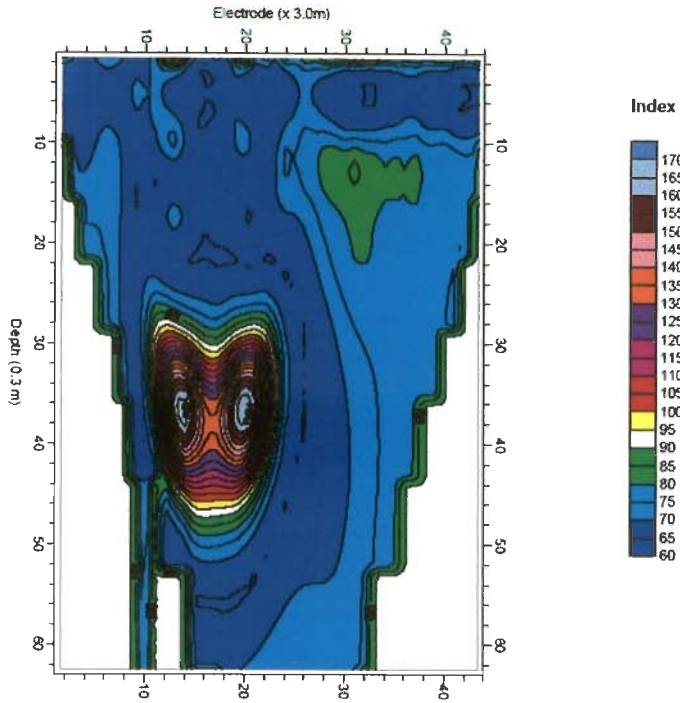


Fig. 9.16 Predicted DCPT Section from Resistivity and Borehole Data Along Profile A₄-B₄, Piyala

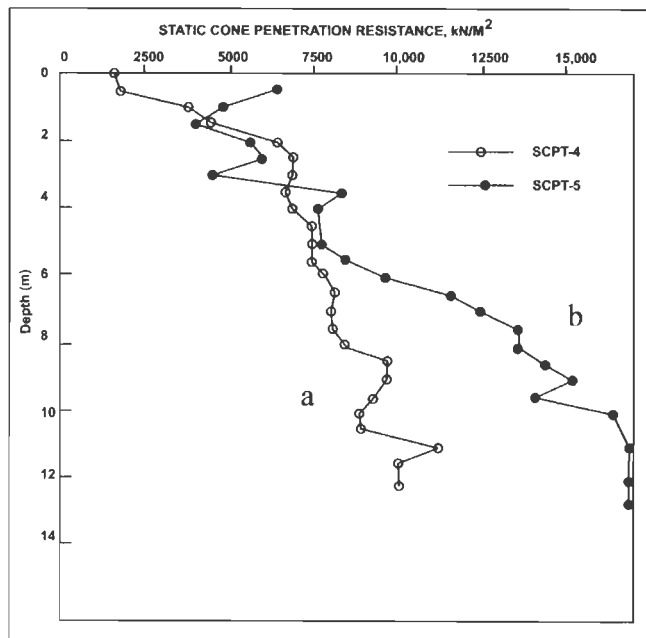


Fig. 9.17 a) SCPT-4 Data. The Corresponding Electrode Position is EL-15 of Profile A₄-B₄
 b) SCPT-5 Data. The Corresponding Electrode Position is EL-25 of Profile A₄-B₄

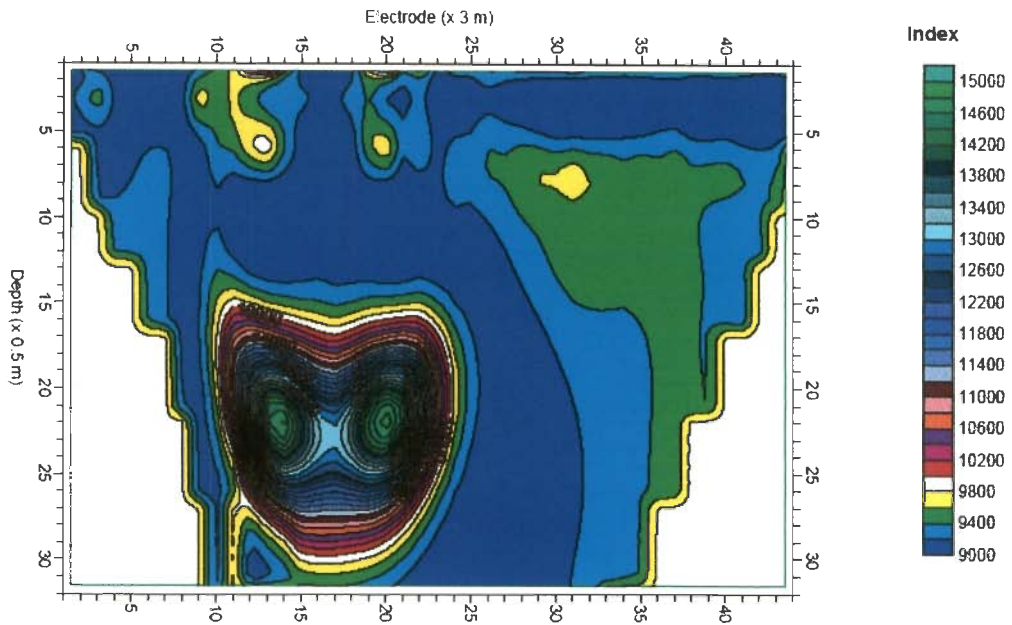


Fig. 9.18 Predicted SCPT Section from Resistivity and Borehole Data Along Profile A₄-B₄ , Piyala

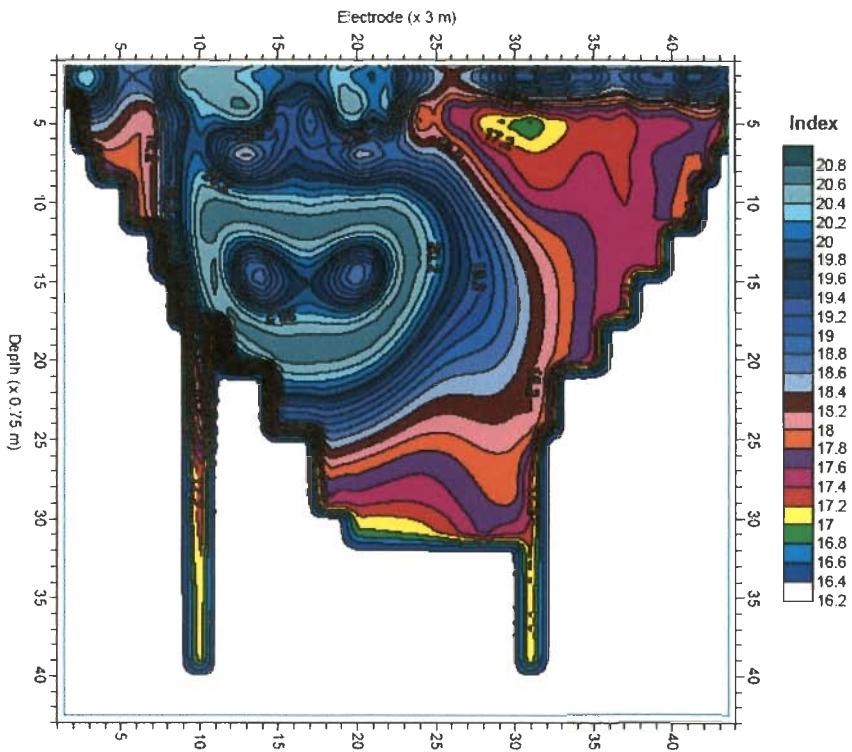


Fig. 9.19 Predicted Internal Friction Angle Section from Synthetic SPT Section Using Resistivity Along Profile A₄-B₄, Piyala

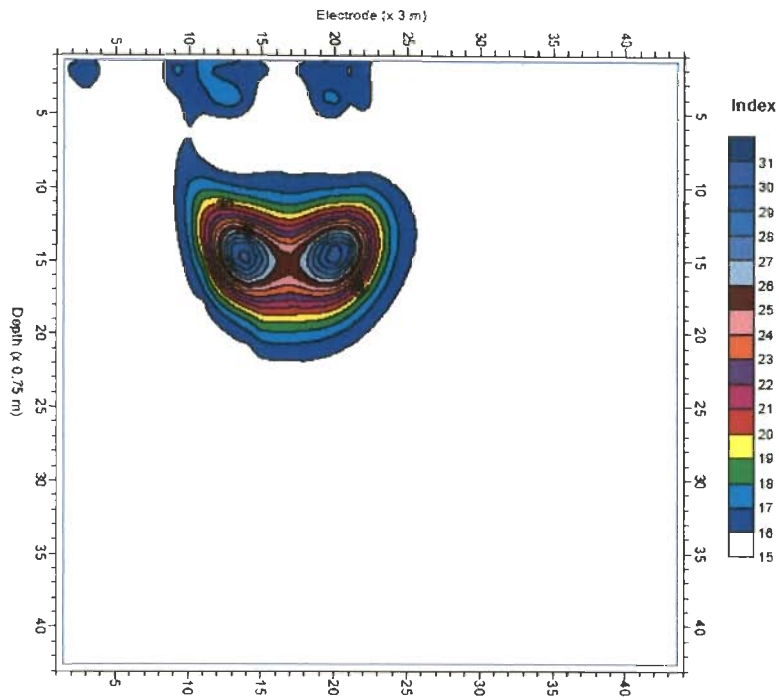


Fig. 9.20 Predicted Unit Weight (Dry) in kN/m^3 from Water Saturation Section Using Resistivity Along Profile A₄-B₄, Piyala

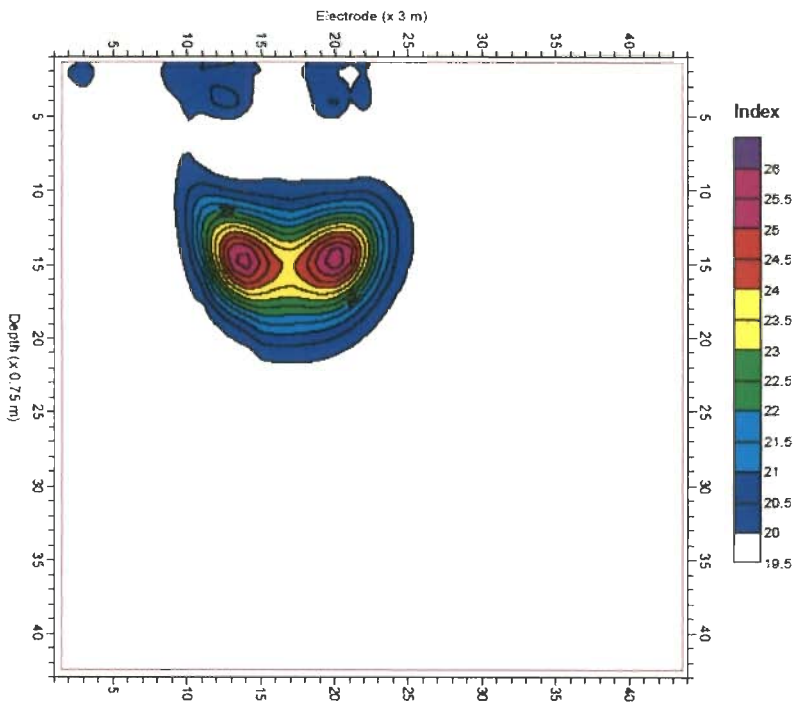


Fig. 9.21 Predicted Unit Weight (Saturated) in kN/m^3 from Water Saturation Section Using Resistivity Along Profile A₄-B₄, Piyala

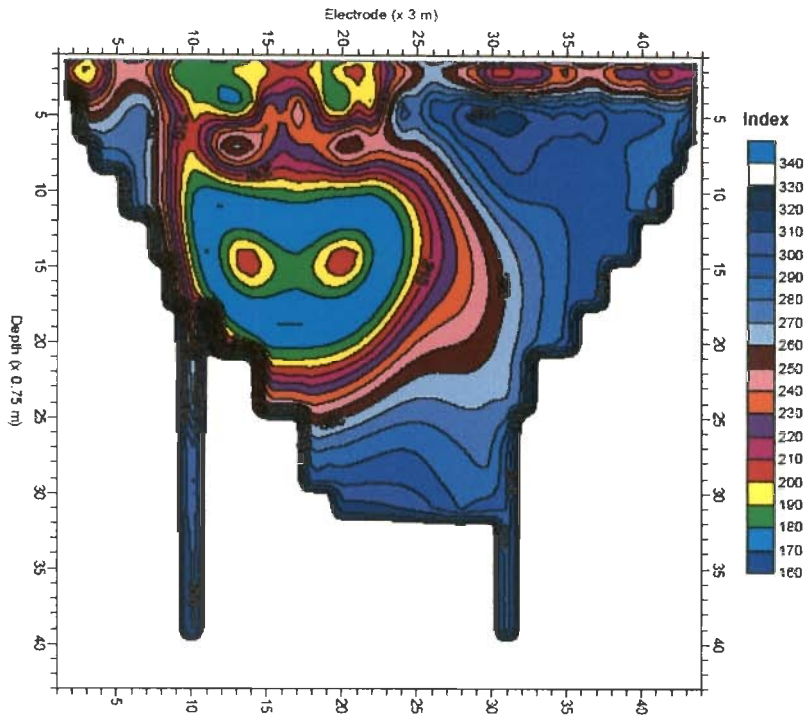


Fig. 9.22 Predicted Unconfined Compressive Strength, q_u from SPT 'N' Section Using Resistivity along Profile A₄-B₄, Piyala

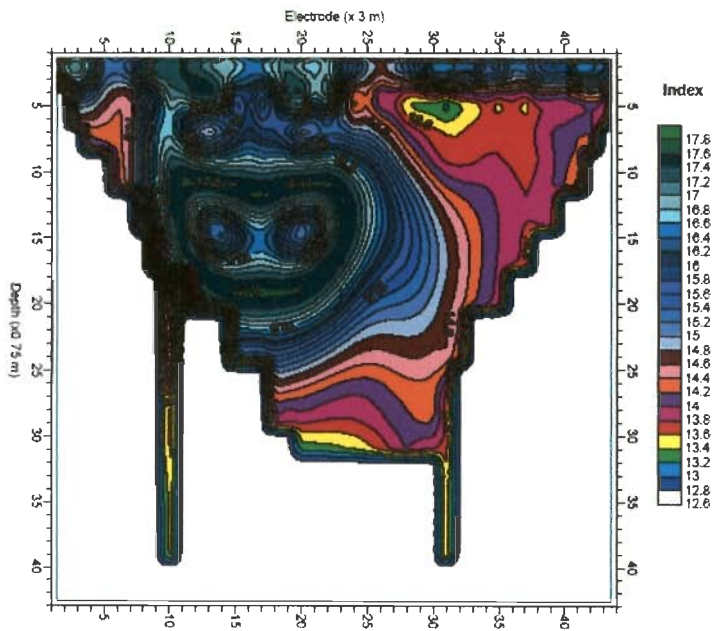


Fig. 9.23 Predicted Bearing Capacity Factor of General Shear Failure, N_c Section from Angle of Internal Friction Section Along Profile A₄-B₄, Piyala

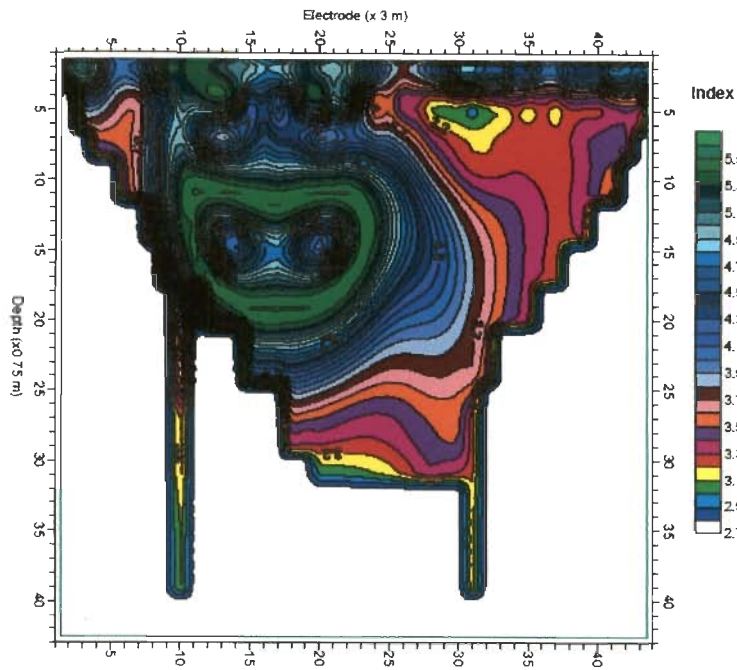


Fig. 9.24 Predicted Bearing Capacity Factor of General Shear Failure, N_γ (Vesic) from Angle of Internal Friction Section Along Profile A₄-B₄, Piyala

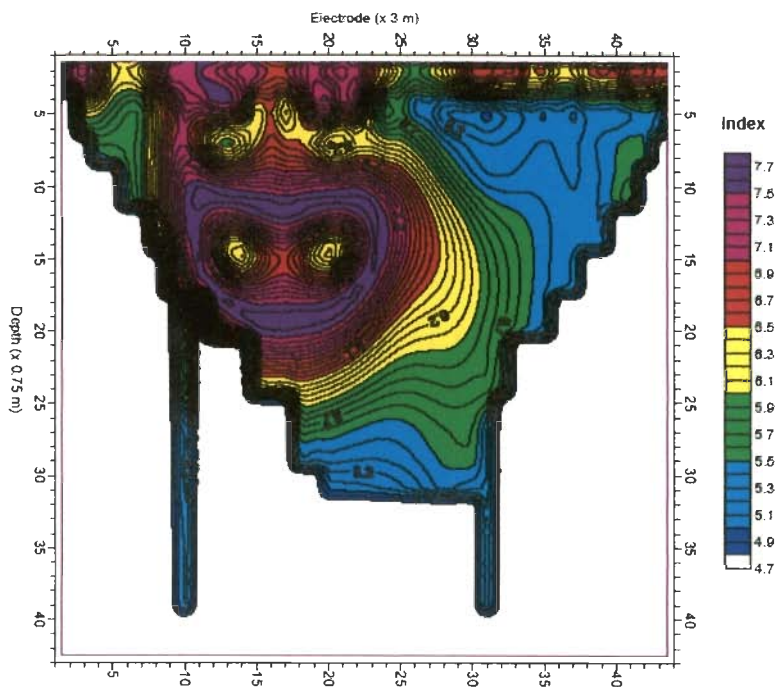


Fig. 9.25 Predicted Bearing Capacity Factor of General Shear Failure N_q , Section from Angle of Internal Friction Section Along Profile A₄-B₄, Piyala

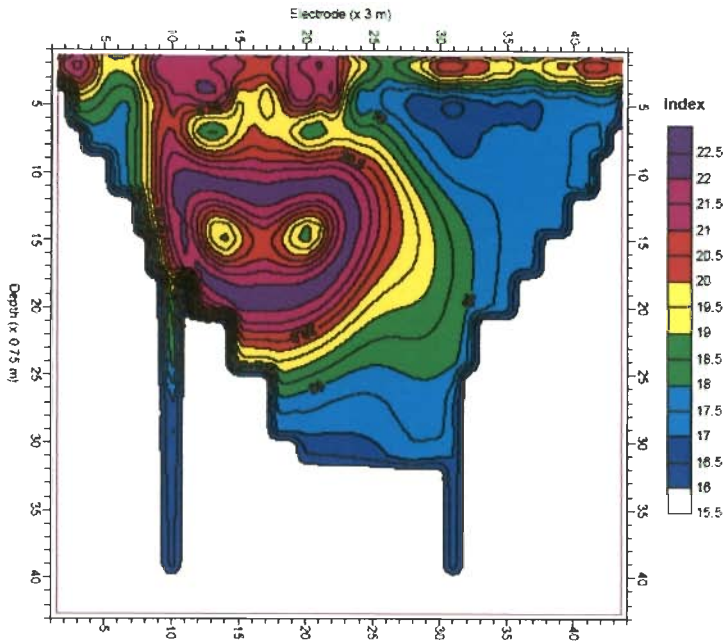


Fig. 9.26 Predicted Ultimate Bearing Capacity Factor N_c Section for Strip Footings from Angle of Internal Friction Section Along Profile A₄-B₄, Piyala

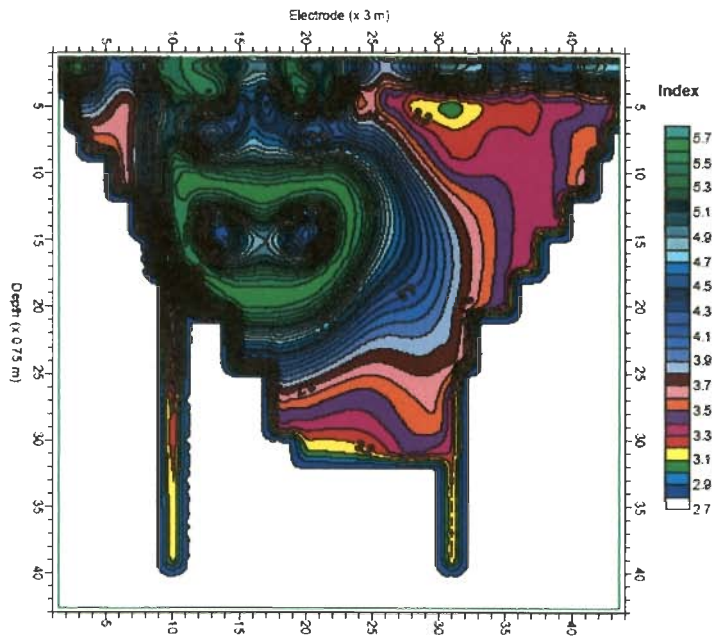


Fig. 9.27 Predicted Ultimate Bearing Capacity Factor, N_γ Section for Strip Footings from Angle of Internal Friction Section Along Profile A₄-B₄, Piyala

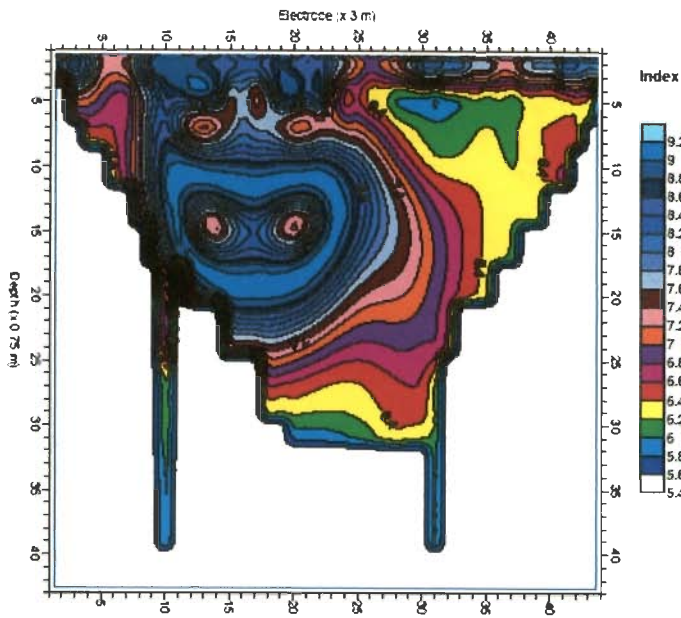


Fig. 9.28 Predicted Ultimate Bearing Capacity Factor, N_q Section for Strip Footings from Angle of Internal Friction Section Along Profile A₄-B₄, Piyala

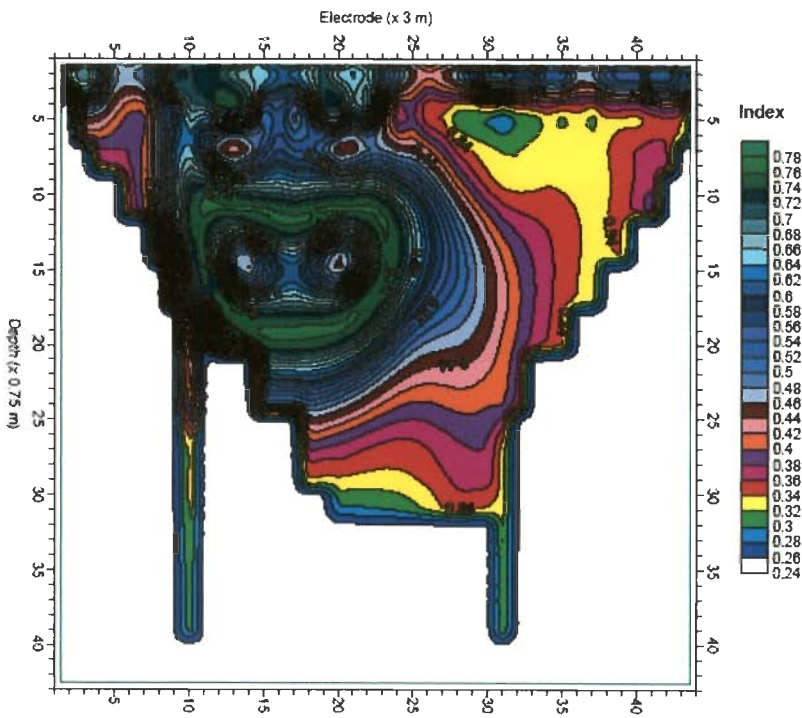


Fig. 9.29 Predicted Terzaghi's Bearing Capacity (Peck et al., 1974) N_γ Factor Section from Angle of Internal Friction Section Along Profile A₄-B₄, Piyala

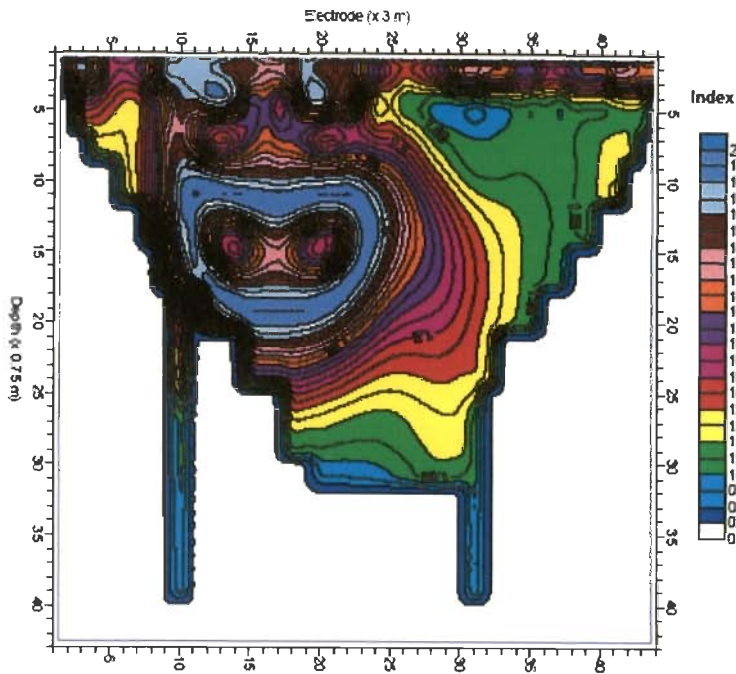


Fig. 9.30 Predicted Terzaghi's Bearing Capacity (Peck et al., 1974) Factor, N_q Section from Angle of Internal Friction Section Along Profile A₄-B₄, Piyala

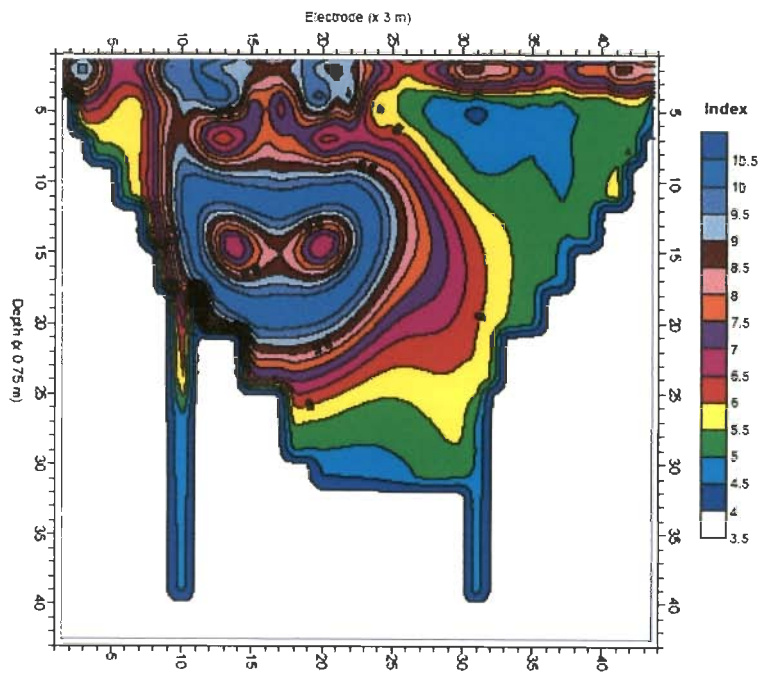


Fig. 9.31 Predicted N_q Factor (Meyerhof, 1953) Section for Driven Piles from Angle of Internal Friction Section Along Profile A₄-B₄, Piyala

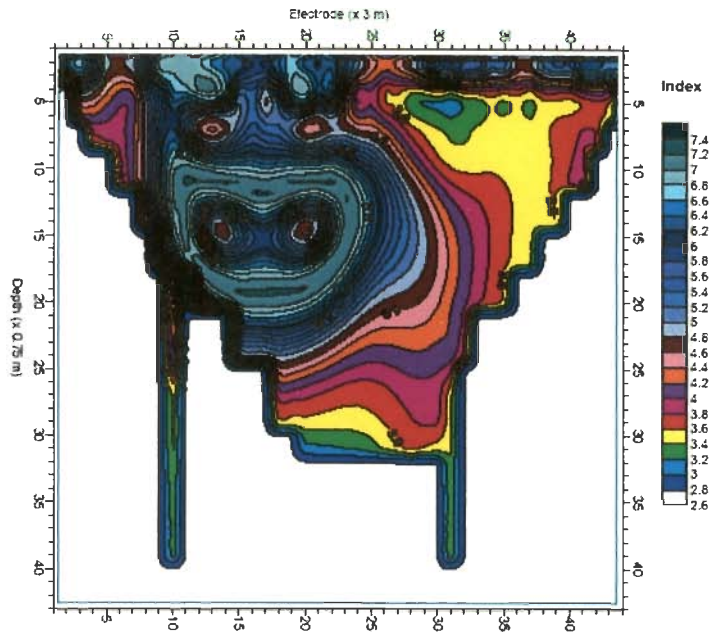


Fig. 9.32 Predicted N_q (Meyerhof, 1953) Factor Section for Bored Piles from Angle of Internal Friction Section Along Profile A₄-B₄, Piyala

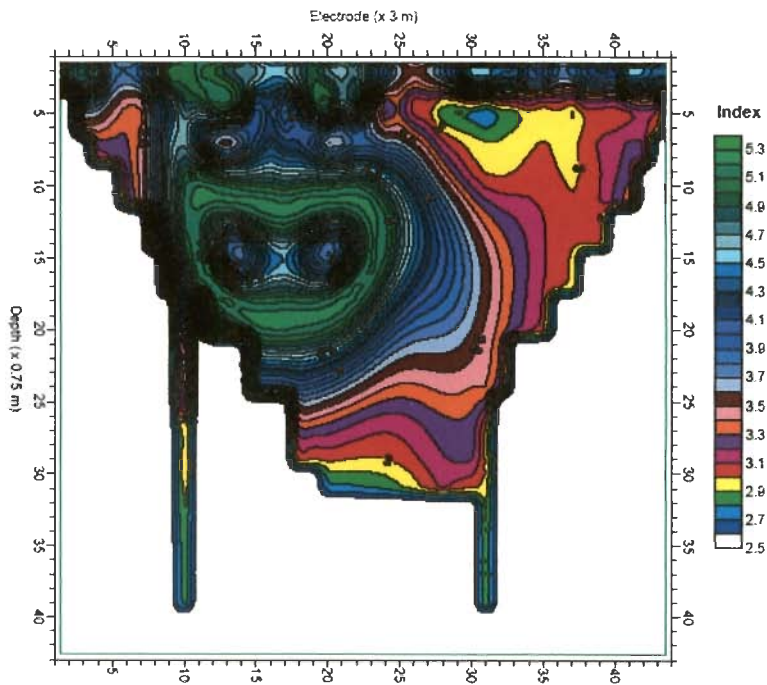


Fig. 9.33 Predicted N_q (Vesic) Factor Section for Bored Piles from Angle of Internal Friction Section Along Profile A₄-B₄, Piyala

SUMMARY AND CONCLUSIONS

10.1 GENERAL

The geotechnical site testing is aimed at assessing the mechanical properties of subsoil. However, the methods are all point-based. By sampling at discrete points, drilling of holes in the ground and in-situ or laboratory testing refer only to a very small proportion of the volume of soil and rock. Geophysical techniques offer the chance to overcome some of the problems inherent in some conventional ground investigation techniques. Ground between boreholes can be checked to see whether ground conditions at the boreholes are representative of them elsewhere. These can help locate cavities, backfilled mine shafts and dissolution features in carbonate rocks. However, Geophysicists have very little idea of the constructional constraints with which civil and construction engineers must work.

By considering the advances in geoelectrical imaging and point geotechnical testing, it is pertinent to develop a procedure for predicting geotechnical parameter sections along different geoelectrical profiles in the study region. The thesis is devoted to this important interface development.

Here, a novel and cost-effective practical methodology has been devised to infer 2-D sections of lithology, formation and geotechnical parameter sections. Proposed methodology has been applied in four case study sites and the results support the efficacy and cost-effectiveness of the approach.

Chapter 5 is totally devoted to methodology and Chapters 6 to 9 deal with four different geotechnical case studies. The results achieved in these case studies demonstrate that the simple 1-D geotechnical parameter sections as being practiced by geotechnical engineers are not tenable in real sense. Rather, the traditional 1-D geotechnical models can be deduced from various 2-D sections generated from combined use of geotechnical tests and 2-D ERT / IP sections through the proposed procedure.

10.2 SUMMARY OF THE WORK DONE

- i) A critical review of literature in Chapter 2 reveals that existing correlations between geophysical properties and formation and geotechnical parameters did not yield any worthwhile procedure to generate formation and geotechnical parameter sections. At best such correlations remained as site-specific qualitative exercises.
- ii) MASW / SASW are surface wave analysis methods that are well recognized methods in geotechnical geophysics discipline. However, no other alternate method from geoelectrical methods has emerged even though the background formation parameters (porosity, water saturation, lithology including clay and sand) affect both geoelectrical and geotechnical field tests. Hence this thesis.
- iii) Chapter 3 is devoted to geoelectrical imaging, where the basic aspects are dealt with. In Chapter 4, relevant geotechnical tests, various empirical tables and curves connected to SPT and bore well tests and various formation and geotechnical parameters have been included. A separate Annexure A details the adopted tables for generation of regression equations. Table 4.10 summarizes the relevant regression equations and relevant illustrations in support of them. Chapter 5 outlines proposed methodology and Chapters 6-9 contain three case studies pertaining to Indo-Gangetic Alluvial Plains and another one belonging to Delhi Super Group of rocks.
- iv) The proposed approach is based on coupling the geoelectrical image (Resistivity / Induced polarization) with at least a pair of geotechnical boreholes and devising a regression equation for each formation and relevant geotechnical parameters.
- v) Regression equations for existing popular empirical tables and plots (Murthy, 2008) between SPT 'N' and different geotechnical parameters have been developed and included in Table 4.10. In such an effort, the relevant material from geotechnical literature is marginally altered occasionally to suit the development of regression equations. Accordingly, Chapter 4 and Appendix A in it contain the relevant details. The indicated procedure is fairly simple and can be extended to include other similar relations / tables etc. in geotechnical literature.

- vi) A method for devising a regression equation on the basis of a pair of geotechnical boreholes projected onto geoelectrical image profiles is developed. This aspect is the cornerstone of the present effort. The procedure is indicated in Chapter 5 and well illustrated in Chapter 6.
- vii) Procedure for formation parameter sections has also been formulated in Chapter 5 and demonstrated in four different case studies pertaining to Chapters 6-9. For correlation purpose, lithological codes have been developed in case of resistivity and IP data sets and Table 5.1 contains the relevant details.
- viii) For both cohesionless and cohesive soils, a procedure for SPT based geotechnical sections is proposed in Chapter 5 and illustrated in Chapters 6-9.
- ix) The choice of proper geoelectrical section (Resistivity / IP / Fictres) for prediction of formation and geotechnical sections is clearly illustrated in Chapter 6 to 9.
- x) Different bearing capacity coefficient sections that were evolved along a selected Profile at each site (Chapters 6-9) can be considered to be in-situ subsurface sections. They provide a unique opportunity to the geotechnical engineer to formulate the traditional 1-D sections in a much more refined and practically effective manner.

10.3 CONCLUSION

- i) Both shallow and deep soil investigation problems can be tackled by the proposed method.
- ii) As resistivity and IP are very much controlled by water saturation, porosity, permeability, sand, clay and rock matrix of near-surface, the respective images have a direct bearing on geotechnical parameters. It may still be premature to mention that the proposed method may even excel the other popular MASW method deployed for a similar purpose.
- iii) Inferred lithology and formation parameter and geotechnical test sections from geoelectric images are both site-specific and profile specific.
- iv) Here, a pair of boreholes in the vicinity of geo-electric profile has been used for arriving at a regression equation. But the procedure remains unaltered if more

boreholes are available for this analysis and in such an event, prediction quality may improve.

- v) A careful scrutiny of the results suggest that geo-electric imaging could be implemented at pre-investigation stage leading to better location of requisite number of boreholes for carrying out conventional geotechnical field tests. Further, the proposed methodology can be utilized in the next stage to infer 2-D image sections of lithology, formation and geotechnical parameters. Such a scheme optimizes the entire site investigation procedures and provides quality information to a geotechnical engineer to refine his models.
- vi) The present methodology is geared towards soil strata only, where conventional geotechnical tests are successful. However, the proposed methodology is very general and it can rope in other scientific inputs also, so that new methodologies can be devised to meet the emerging challenges before a site geotechnical engineer.
- vii) It is envisaged that densification of geoelectrical profiles could lead to a 3-D reconstruction of various formation and geotechnical parameter sections in the study region. But traditional geotechnical tests are still needed for better control.
- viii) The developed procedure in no way replaces the geotechnical site testing; but, their number can be reduced considerably and thus the proposed method can be highly cost-effective.
- ix) It has to be noted that the quality of predicted formation and geotechnical sections are equally guided by the validity of assumed empirical tables, charts and relations gathered from geotechnical literature at a given locality and the underlying basic assumptions and limitations. At best predicted 2-D sections (formation and Geotechnical) could be additional intelligent guess models of subsurface and an experienced geotechnical engineer should weigh them accordingly. Further, the proposed method is of very general nature and it can be a worthwhile exercise to translate geoelectrical depth-wise images into meaningful geotechnical sections by extending to other geotechnical in-situ field tests with relevant empirical tables, graphs and analytical relations.
- x) Here, all predicted geotechnical parameter sections are SPT 'N' based. However, the same procedure can be extended to other point observations including CPT.

- x) It is no exaggeration to mention that as more field experience with our methodology is gained, a cost saving can be gained by appropriate decision making in terms of factor of safety.

10.4 FURTHER PERSPECTIVES

Our methodology needs to be extended to CPT method and also to more variety of geotechnical and hydrological characterizations of subsurface. As soil moisture governs both geotechnical and geoelectrical properties / parameters, it is envisaged that proposed methodology offers a viable alternative to MASW / SASW methods. Further, critical statistical analyses are not attempted in this effort and it needs to be done. But these constitute our future goals.

Table A.1 a Porosity and Unit Weights of Typical Soils in Natural State (Murthy, 2008)

S. No.	Description	Porosity	Unit weight (kN/m ³)	
			Dry, γ_d	Saturated, γ_{sat}
1	Uniform sand, loose	46	14	18.5
2	Uniform sand, Dense	34	17	20.5
3	mixed-grained sand, loose	40	15.6	19.5
4	mixed-grained sand, dense	30	18.2	21.2
5	Glacial till, mixed-grained	20	20.8	22.7
6	soft glacial clay	55	11.9	17.3
7	slightly organic clay	66	9.1	15.5
8	Highly organic clay	75	6.8	14
9	Soft bentonite	84	4.2	12.4

Table A.1 b Relationship between Water Content (%) and Unit Weights (γ_d, γ_{sat}) (After Murthy, 2008)

S. No.	Lithology	Water Sat. (%)	Unit weight (Dry) γ_d	Unit weight (Sat.) γ_{sat}
1	Uniform sand, loose	35	13.24	18
		34	13.47	18.17
2	Uniform sand, loose	32	14	18.5
		30	14.53	18.83
		28	15.07	19.17
3	Mixed grained sand, loose	26	15.6	19.5
4	Mixed grained sand, loose	24	16.07	19.83
5	Soft glacial clay	22	16.53	20.16
6	Uniform sand, dense	20	17	20.5
		18	17.6	20.85
7	Mixed grained sand, dense	16	18.2	21.2
		14	19.07	21.7
		12	19.93	22.2
8	Glacial till, mixed grained	10	20.8	22.7
		8	21.67	23.2
		6	22.53	23.7
		4	23.4	24.2

Table A.2 Unconfined Compressive Strength, q_u versus SPT 'N' for Clay (Murthy, 2008)

N	q_u (kPa)
1	24
3	37
6	75
11.5	150
22.5	300
31	402

Table A.3 Bearing Capacity Factors of Terzaghi for General Shear Failure (Murthy, 2008) versus Angle of Internal Friction, ϕ

Angle of Internal friction, ϕ	Bearing capacity factors		
	N_c	N_q	N_γ
0	5.7	1	0
5	7.3	1.6	0.5
10	9.6	2.7	1.2
15	12.9	4.4	2.5
20	17.7	7.4	5
25	25.1	12.7	9.7
30	37.2	22.5	19.7
35	57.8	41.4	42.4
40	95.7	81.3	100.4
45	172.3	173.3	297.5
50	347.5	415.1	1153

Table A.4 a Terzaghi's Relationship between Internal Angle of Friction, ϕ and SPT 'N' (Murthy, 2008)

S. No.	ϕ	SPT N	Type
1	30.2	10	Medium
2	31.5	15	Medium
3	33	20	Medium
4	36	30	Medium
5	37	35	Dense
6	38.5	40	Dense
7	41	50	Dense
8	42	55	Very Dense
9	43	65	Very Dense
10	44	70	Very Dense

Table A.4 b Terzaghi's Bearing Capacity Factor N_q as a Function of Internal Angle of Friction, ϕ (Murthy, 2008)

S. No.	ϕ	N_q	Type
1	28	7.5	
2	29	10	
3	34	25	Medium
4	35	30	Medium
5	38	57.5	Dense
6	40	80	Dense
7	41.5	100	Dense

Table A.4 c Terzaghi's Bearing Capacity Factor N_γ as a Function of Internal Angle of Friction, ϕ (Murthy, 2008)

S. No.	ϕ	N_γ	Type
1	28	4.8	
2	29	5	
3	32	15	Medium
4	34	25	Medium
5	36	40	Medium
6	38	65	Dense
7	39	80	Dense
8	40	100	Dense
9	41	115	Dense
10	41.1	120	Very Dense

Table A.5 The Relation of ϕ with Different Bearing Capacity Factors, N_c , N_q and N_γ (Vesic) (Murthy, 2008)

S. No	ϕ	N_c	N_q	N_γ (Vesic)
1	0	5.14	1	0
2	5	6.49	1.6	0.4
3	10	8.34	2.5	1.2
4	15	10.97	3.9	2.6
5	20	14.83	6.4	5.4
6	25	20.71	10.7	10.9
7	26	22.25	11.8	12.5
8	28	25.79	14.7	16.7
9	30	30.13	18.4	22.4
10	32	35.47	23.2	30.2
11	34	42.14	29.4	41
12	36	50.55	37.7	56.2
13	38	61.31	48.9	77.9
14	40	72.25	64.1	109.4
15	45	133.73	134.7	271.3
16	50	266.5	318.5	762.84

Table A.6 Bearing Capacity Factors (Murthy, 2008) for Piles (Deep Soil Investigations) versus ϕ

S. No.	ϕ	N_q (Vesic, 1963) Bored piles	ϕ	N_q (Bored piles), Meyerhof(1953)	ϕ	N_q (Driven piles), Meyerhof(1953)
1	25	15	25	25	25	30
2	30	25	27.5	30	28.75	60
3	35	45	28.75	40	36.25	300
4	37.5	80	32.5	80	38.75	600
5	38.75	100	36.25	200	43.75	2000
6	42.5	200	41.25	600		
7	45	300	42.5	1000		
8	48.75	650	45.6	2000		
9	50	1000				

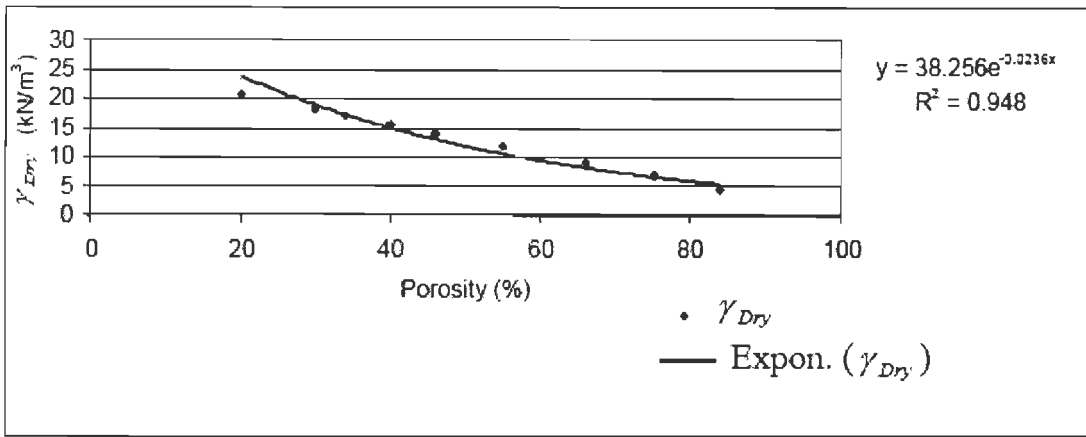


Fig. A.1 a Regression Equation for Porosity versus Unit Weights of Typical Soils (Dry) in Natural State (Murthy, 2008)

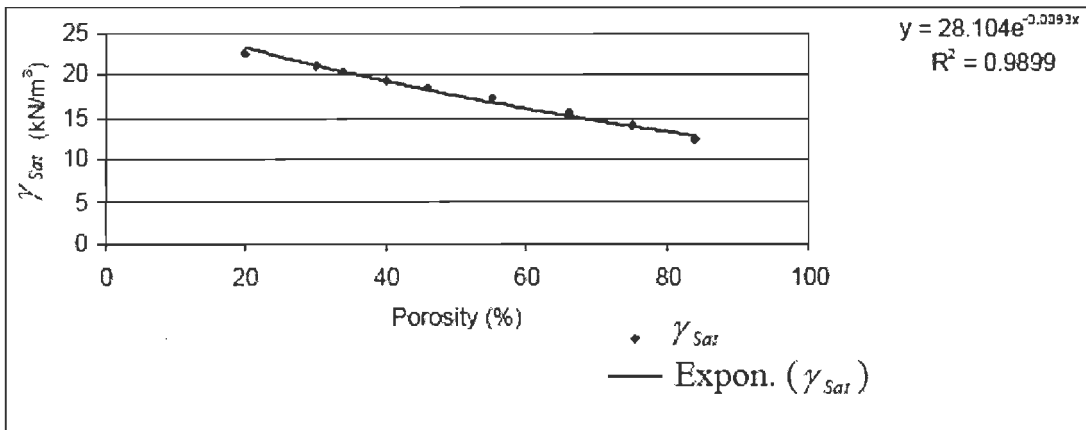


Fig. A.1 b Regression Equation for Porosity versus Unit Weights of Typical Soils (Saturated) in Natural State (Murthy, 2008)

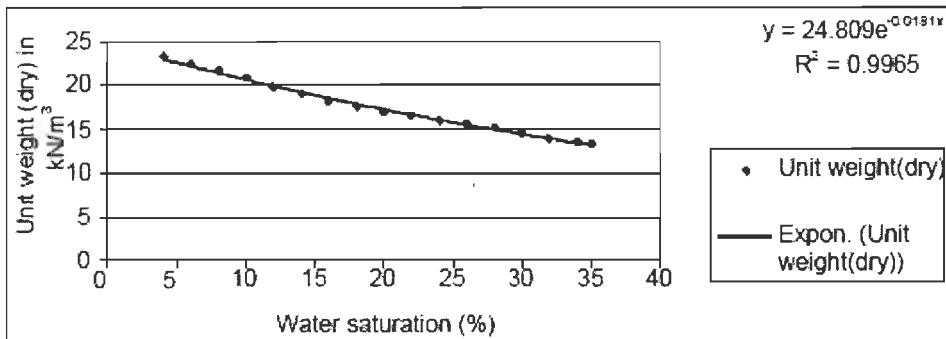


Fig. A.1 c Regression Equation for Water Saturation versus Unit Weights of Typical Soils (Dry) in Natural State (Murthy, 2008)

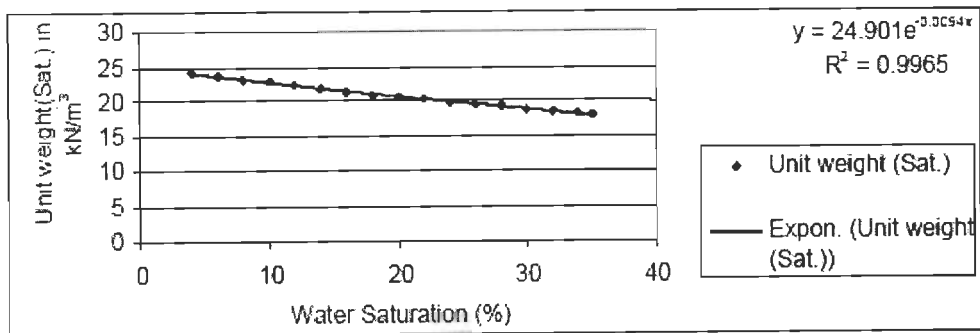


Fig. A.1 d Regression Equation for Porosity versus Unit Weights of Typical Soils (Saturated) in Natural State (Murthy, 2008)

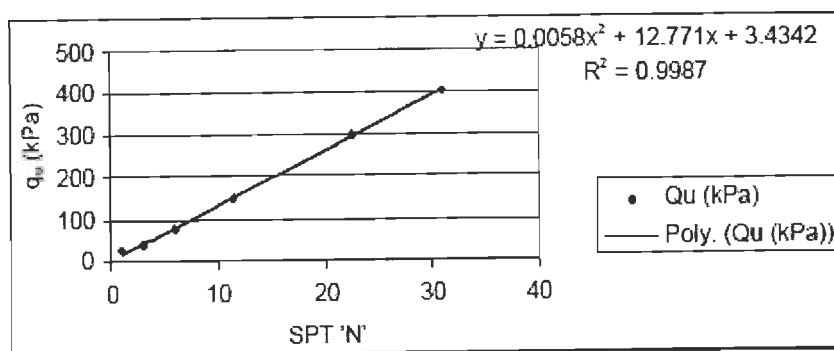


Fig. A.2 Regression Equation for Unconfined Compressive Strength, q_u versus SPT 'N' for Clay (Murthy, 2008)

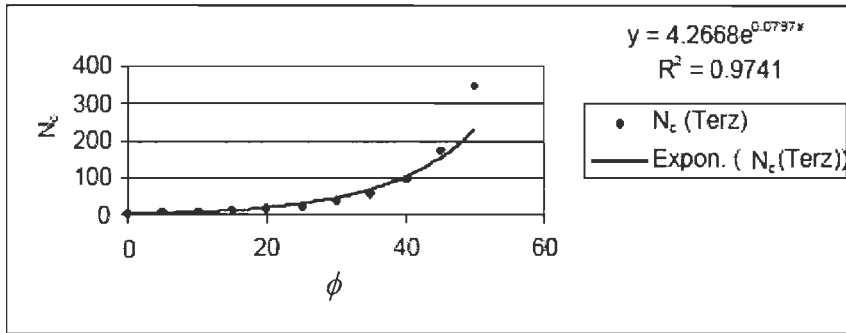


Fig. A.3 a Regression Equation for Bearing Capacity Factor, N_c of Terzaghi for General Shear Failure versus Angle of Internal Friction, ϕ (Murthy, 2008)

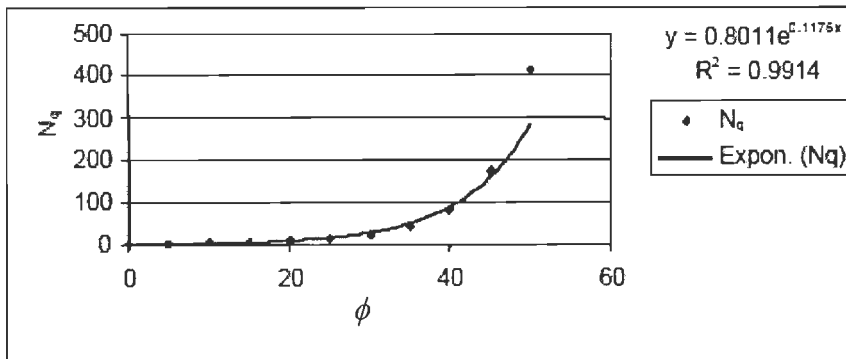


Fig. A.3 b Regression Equation for Bearing Capacity Factor, N_q of Terzaghi for General Shear Failure versus Angle of Internal Friction, ϕ (Murthy, 2008)

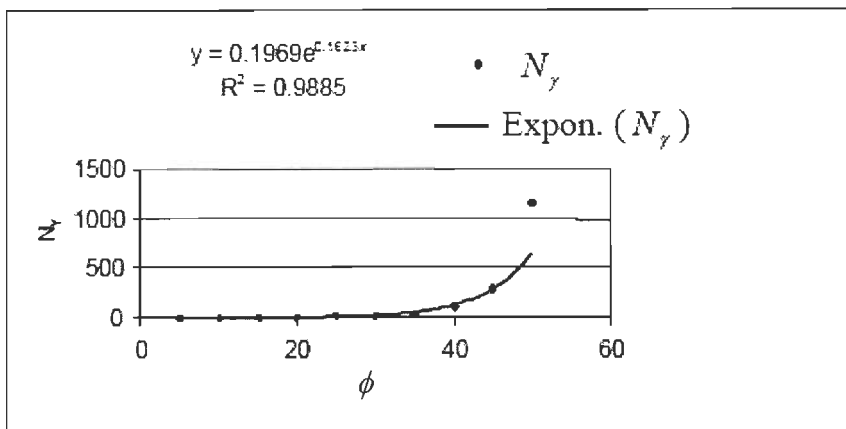


Fig. A.3 c Regression Equation for Bearing Capacity Factor, N_γ of Terzaghi for General Shear Failure versus Angle of Internal Friction, ϕ (Murthy, 2008)

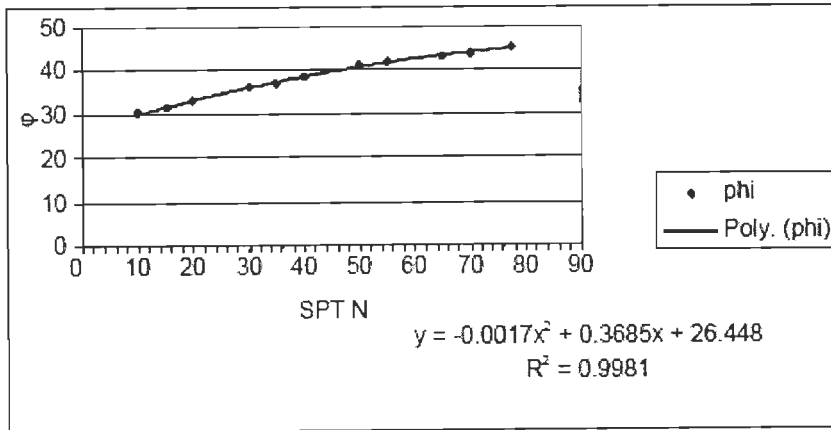


Fig. A.4 a Regression Equation for Terzaghi's Relationship Between Angle of Internal Friction, ϕ and SPT 'N' (Murthy, 2008)

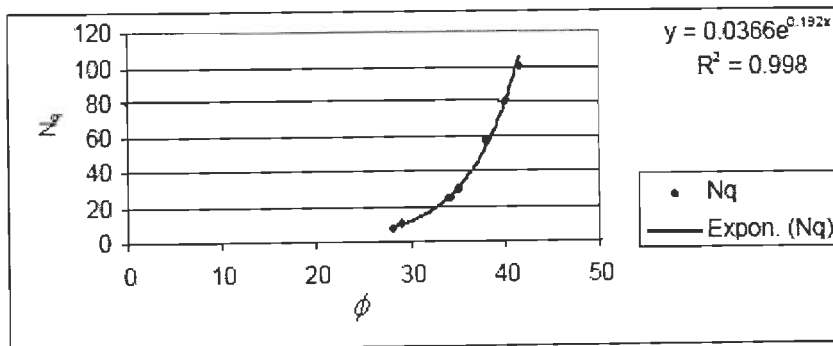


Fig. A.4 b Regression Equation for Terzaghi's Bearing Capacity Factor N_q as a Function of Angle of Internal Friction, ϕ (Murthy, 2008)

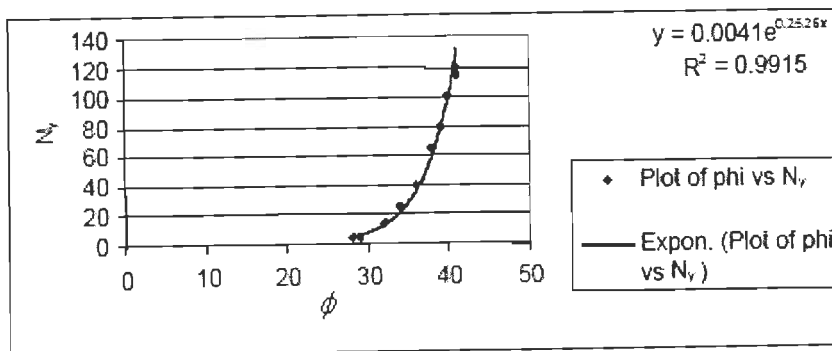


Fig. A.4 c Regression Equation for Terzaghi's Bearing Capacity Factor N_γ as a Function of Angle of Internal Friction, ϕ (Murthy, 2008)

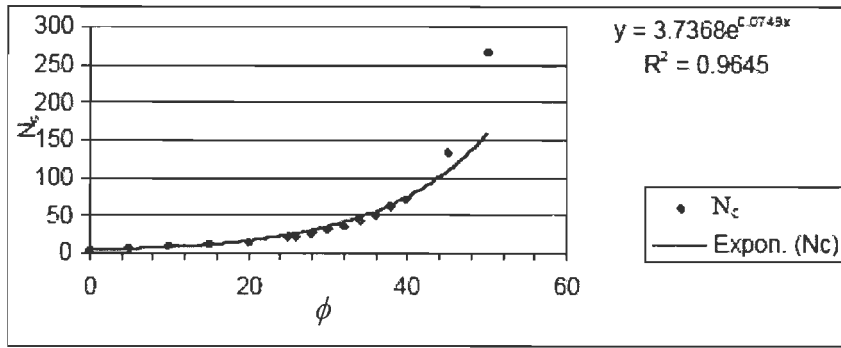


Fig. A.5 a Regression Equation for Bearing Capacity Factor, N_c versus Angle of Internal Friction, ϕ (Murthy, 2008)

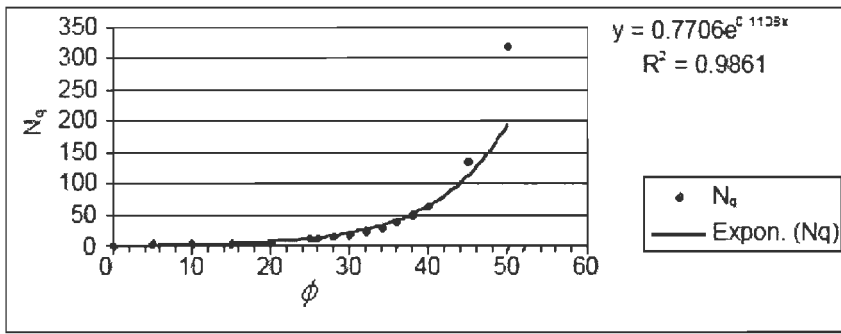


Fig. A.5 b Regression Equation for Bearing Capacity Factor, N_q versus Angle of Internal Friction, ϕ (Murthy, 2008)

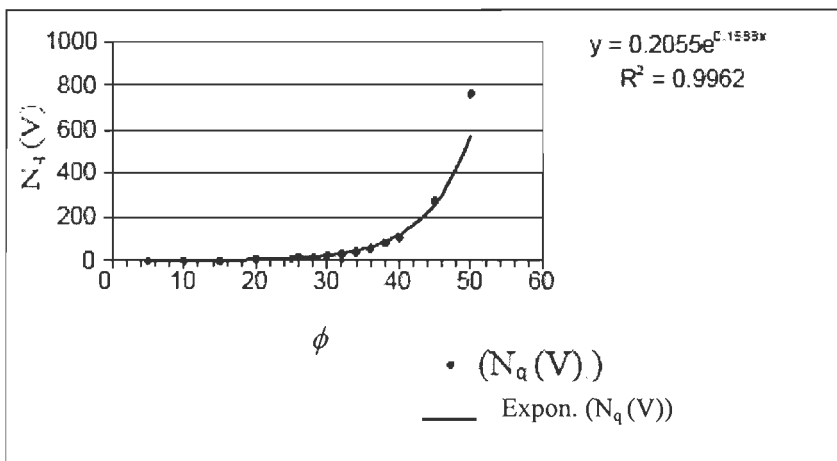


Fig. A.5 c Regression Equation for Bearing Capacity Factor, $N_\gamma(V)$ versus Angle of Internal Friction, ϕ (Murthy, 2008)

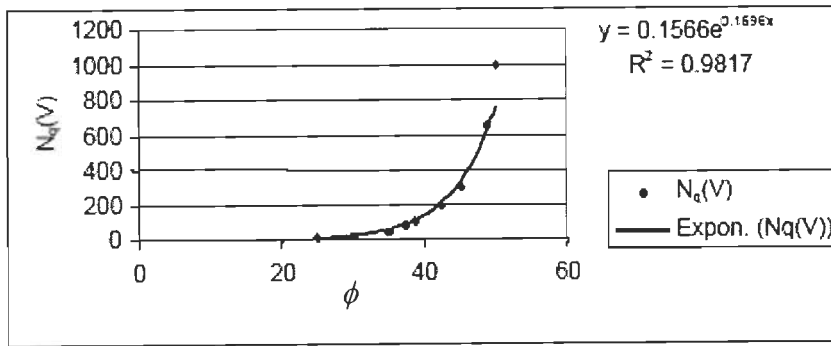


Fig. A.6 a Regression Equation for Bearing Capacity Factor, N_q (Vesic) for Bored Piles (Deep Soil Investigations) versus ϕ (Murthy, 2008)

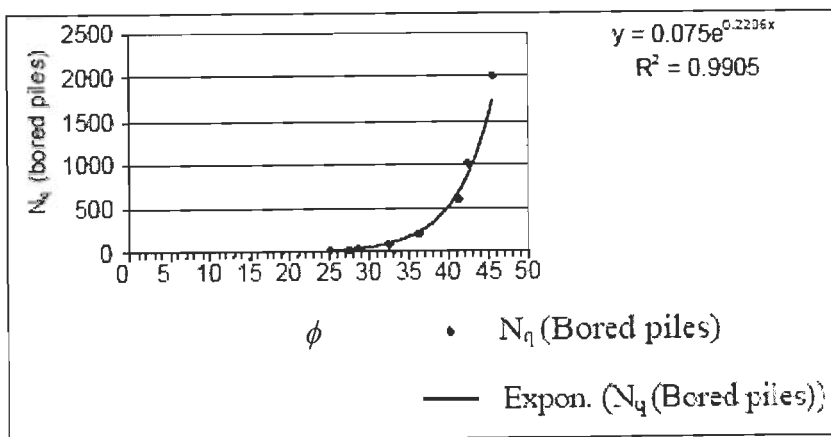


Fig. A.6 b Regression Equation for Bearing Capacity Factor, N_q (Meyerhof, 1953) for Bored Piles (Deep Soil Investigations) versus ϕ (Murthy, 2008)

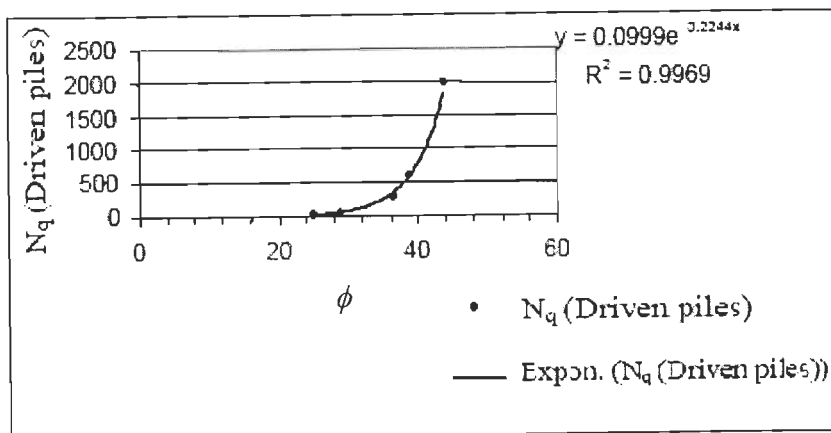


Fig. A.6 c Regression Equation for Bearing Capacity Factor, N_q (Meyerhof, 1953) for Driven Piles (Deep Soil Investigations) versus ϕ (Murthy, 2008)

REFERENCES

- Akca, N., 2003. Correlation of SPT-CPT data from the United Arab Emirates: *Engineering Geology*, 67, 219–231.
- Akintorinwa, O. J., and Adesoji, J. I., 2009. Application of geophysical and geotechnical investigations in engineering site evaluation: *International Journal of Physical Sciences*, 4, 8, 443-454.
- Anbazhagan, P., and Sitharam, T. G., 2008. SPT-N versus shear wave velocity correlation: *A Bulletin of the Indian Geotechnical Society, IGS News, Technical News*, 40, 2, 7p.
- Anbazhagan, P., Sitharam, T. G., and Divya, C., 2006. Site response analyses based on site specific soil properties using geotechnical and geophysical tests: 1st European Conference on Earthquake Engineering and Seismology, Geneva, extended abstract.
- Anderson, N., Thitimakorn, T., Ismail, A., and Hoffman, D., 2007. A comparison of four geophysical methods for determining the shear wave velocity of soils: *Journal of Environmental and Engineering Geosciences*, 13, 1, 11-23.
- Anderson, N., Croxton, N., Hoover, R., and Sirles, P., 2008. Geophysical methods commonly employed for geotechnical site characterization: (<http://onlinepubs.trb.org/onlinepubs/circulars/ec130.pdf>)
- Apparao, A., and Sarma, V. S., 1983. The modified pseudo-depth section as a tool in resistivity and IP prospecting-A case history: *PAGEOPH*, 121, 91-108.
- Apparao, A., Rao, G., T., Sastry, R. S., and Sarma, V. S., 1992. Depth of detection of buried conductive targets with different electrode arrays in resistivity prospecting: *Geophysical Prospecting*, 40, 749-760.
- Barker, R. D., 1989. Depth of investigation of a generalised colinear 4-electrode array: *Geophysics*, 54, 1031-1037.

Braga, A., Malagutti, W., Dourado, J., and Chang, H., 1999. Correlation of electrical resistivity and induced polarization data with geotechnical survey standard penetration test measurements: *Journal of Environmental and Engineering Geophysics*, 4, 123-130.

Brinch Hansen, J., 1961. A general formula for bearing capacity: *Bulletin No 11, Geoteknisk Institute Akademiet for de Tekniske Videuskaber, Copenhagen*, 38-45.

Broyden, C. G., 1972. Quasi-Newton methods, in Murray, W., Ed., *Numerical methods for unconstrained optimization: Academic Press Inc.*, 87-106.

Cardarelli, E., Cercato, M., and Di Filippo, G., 2007. Assessing foundation stability and soil structure interaction through geophysical techniques: a case history in Rome (Italy), *Journal of Near Surface Geophysics*, 5, 2, 141-147.

Cha, M., and Cho, G., 2007. Shear strength estimation of sandy soils using shear wave velocity: *ASTM International Geotechnical Testing Journal*, 30, 6, 12 p.

Cosenza, P., Marmet, E., Rejiba, F., Cui, Y. J., Tabbagh, A., and Charlery, Y., 2006. Correlations between geotechnical and electrical data-A case study at Garchy in France: *Journal of Applied Geophysics* 60, 165-178.

Dahlin, T., 1996. 2D resistivity surveying for environmental and engineering applications: *First Break*, 14, 7, 275-283.

Dahlin, T., 2001. The development of DC resistivity imaging techniques: *Computers and Geosciences*, 27, 1019-1029.

Dahlin, T., and Bernstone, C., 1997. A Roll-along technique for 3D resistivity data acquisition with multi-electrode arrays: *Proc. Symposium on the Application of Geophysics to Engineering and Environmental Problems (SAGEEP)*, 927-935.

Dahlin, T., Leroux, V., and Nissen, J., 2002. Measuring techniques in induced polarization imaging: *Journal of Applied Geophysics*, 50, 279-298.

Dahlin, T., Garin, H., and Palm, M., 2004. Combined resistivity imaging and RCPT for geotechnical pre-investigation: Proceedings Nordic Geotechnical Meeting (NGM), Yastad Sweden, 1-9.

Danzinger, F. A. B., Politano, C. F., and Danzinger, B. R., 1998. CPT-SPT correlations for some Brazilian residual soils: In: Proceedings of the First Int. Conf. on Site Characterization – ISC'98. Atlanta, Vol. 2, Balkema, Rotterdam, 907-912.

Dewaikar, D. M., Varghese, S. P., Sawant, V. A., and Chore, H. S., 2007. Non-linear 3-D finite element analysis of laterally loaded plies incorporating no-tension behavior: Indian Geo-technical Journal, v 37, n 3.

Dewaikar, D. M., Mohapatro, B. G., Sawant, V. A., and Chore, H. S., 2008. Computation of bearing capacity factor N_q -Terzaghi and prandtl mechanisms: Journal of Asian Science and Technology for Development, 25, 2, 227-236.

Dobrin, M. B., 1976. Introduction to geophysical prospecting: Publisher McGraw-Hill, 630p.

Drahor, M. G., Göktürkler, G., Berge, M. A., and Kurtulmus, T. Ö., 2006. Application of electrical resistivity tomography technique for investigation of landslides: a case study from Turkey, Environmental Geology, 50, 147-155.

Durkee, D. B., Rucker, M. L., M.ASCE, Smith, D. E., and Ackerman, A. F., 2006. Role of practical geophysics in in-situ characterization for underground construction in Phoenix: Arizona, Conference Proceeding, 577-588.

Edet, A. E., Oden, M. I., and Efreteui, O. E., 1994. Correlation between cone penetration resistance and standard penetration tests of the coastal plain sands south-eastren Nigeria: Bulletin of the International Association of Engineering Geology, Paris 49, 41-45.

Edwards, L. S., 1977. A modified pseudosection for resistivity and induced-polarization: Geophysics, 42, 1020-1036.

Endres, A. L., and Clement, W. P., 1998. Relating cone penetrometer test information to geophysical data-A case study: Symposium on the Application of Geophysics to Engineering and Environmental Problems, SAGEEP, Chicago, USA, 295p.

Foti, S., 2000. Multistation methods for geotechnical characterisation using surface waves: Ph.D. Thesis, Politecnico di Torino, 229p.

Gallardo, L. A., and Meju, M. A., 2003. Characterization of heterogeneous near-surface materials by joint 2-D inversion of dc resistivity and seismic data: Geophysical Research Letters, 30, 13, 1.1-1.4.

Gautam, P. K., Sastry, R. G., and Mondal, S. K., 2007. The utility of Multi-electrode resistivity data in geotechnical investigations-A case study: 20th Symposium on the Application of Geophysics to Engineering and Environmental Problems (SAGEEP), 731-737.

Gay, D. A., Morgan, F. D., Sogade, J. A., Vichabian, Y., Reppert, P., and Wharton, A. E., 2006a, Investigations of andesitic volcanic debris terrains: Part 1-Geophysical: Geophysics, 71, B1-B8.

Gay, D. A., Morgan, F. D., Vichabian, Y., Sogade, J. A., Reppert, P., and Wharton, A. E., 2006b. Investigations of andesitic volcanic debris terrains: Part 2-Geotechnical. Geophysics, 71, B9-B15.

Giao, P. H., 2001. Some Applications of Engineering and Environmental Geophysics in Geotechnical Engineering: Presentation at Gifu University, Japan.

Giao, P. H., Chung, S. G., Kim, D. Y., and Tanaka, H., 2003. Electrical imaging and laboratory resistivity testing for geotechnical investigation of Pusan clay deposits: Journal of Applied Geophysics, 52 157-75.

Giao, P. H., Kim, J. H., and Chung, S. G., 2002. Application of Engineering Geophysics in Investigation of the Pusan Clays with reference to Reclamation Projects: the European Journal of Environmental and Engineering Geophysics, 7, 3, 201-218.

Ghose, R., and Drijkoningen, G. G., 2000. Interacting soil-physical parameters in the cone penetration process in sand: Scope of integration of seismic to CPT: 6th Meeting of Environmental and Engineering Geophysics, Bochum, Expanded Abstract, vol. EG02.

Ghosh, N., Wadhwa, R. S., and Subbarao, C., 2003. Reliability of empirical relations for estimation of dynamic elastic parameters from insitu compressional wave velocities: Indian national conference on geotechnical engineering for infrastructural development, IIT Roorkee, 1, 25-29.

Golub, G. H., and van Loan, C. F., 1989. Matrix computations: John Hopkins Univ. Press.

Griffiths, D. H., Turnbull, J., and Olayinka, A. I., 1990. Two-dimensional resistivity mapping with a computer-controlled array: *First Break*, 8, 4, 121-129.

Griffiths, D. H., and Barker, R. D., 1993. Two-dimensional resistivity imaging and modeling in areas of complex geology: *Journal of Applied Geophysics*, 29, 211-226.

Hacikoylu, P., Dvorkin, J., and Mavko, G., 2006. Resistivity-velocity transforms revisited: *Leading Edge*, 1006-1009.

Hadidi, R., and Gucunski, N., 2003. Inversion of SASW dispersion curve using numerical simulation: *Proceedings SAGEEP*, 1289p.

Hansen, J. B., 1970. A revised and extended formula for bearing capacity: *Danish Geotechnical Institute Bul. No. 28*, Copenhagen.

Hasancebi, N., and Ulusay, R., 2007. Empirical correlations between shear wave velocity and penetration resistance for ground shaking assessments: *Bulletin of Engineering Geology and the Environment*, 66, 203-213

Hvorslev, M. J., 1949. Surface exploration and sampling of soils for civil engineering purpose, water ways experimental station, engineering foundations, New York.

Inazaki, T., 2006. Relationship between s-wave velocities and geotechnical properties of alluvial sediments: *Proceedings SAGEEP*, 1296p.

Inazaki, T., 1998. Geotechnical use of a shear-wave vibrator: in-situ measurement of nonlinear properties of the ground surface. Proceedings SAGEEP, 471p.

IS: 1498, 1970. Classification and identification of soils for general engineering purposes: Bureau of Indian Standard, New Delhi.

IS: 2131, 1981. Method for standard penetration test for soils.

IS: 6403, 1981. Code of practice for determination of bearing capacity of shallow foundations.

IS: 1888, 1982. Method of load testing.

Iyisan, R., 1996. Correlations between shear wave velocity and in situ penetration test results, Technical Journal of Turkish Chamber of Civil Engineers, 7, 2, 1187-1199.

Jianghai, Xia., Miller, R. D., Park, C. B., Hunter, J. A., and Harris, J. B., 2000. Comparing shear-wave velocity profiles from MASW with borehole measurements in unconsolidated sediments, Fraser River Delta, B. C., Canada: Journal of Environmental and Engineering Geophysics, 5, 3, 1p.

Jianghai, Xia., Miller, R. D., Park, C. B., Hunter, J. A., and Harris, J. B., Ivanov, J., 2002. Comparing shear-wave velocity profiles from multichannel surface wave with borehole measurements: International Journal of Soil Dynamics and Earthquake Engineering, 22, 181-190.

Joh, S. H., 1996. Advances in the data interpretation technique for spectral analysis of surface waves measurements: Ph.D. Thesis. University of Texas, USA. 240p.

Kiberu, J., 2002. Induced polarization and Resistivity measurements on a suite of near surface soil samples and their empirical relationship to selected measured engineering parameters: Thesis, MS, International Institute for Geo-information Science and Earth Observation Enschede, The Netherlands, 137p.

Kim, Dong-Soo., Bang, Eun-Seok., Kim, Jong-Tae., and Seo, Won-Seok., 2006. Evaluation of near subsurface vs distribution map using SPT-Uphole tomography method: 6th International Conference & Exposition on Petroleum Geophysics, Kolkata, India.

Kemna, A., Vanderborght, J., Kulesa, B., and Vereecken, H., 2002. Imaging and characterisation of subsurface solute transport using electrical resistivity tomography (ERT) and equivalent transport models: *Journal of Hydrology*, 267, 125-146.

Kumar, G., 2005. *Geology of Uttar Pradesh and Uttaranchal*: Geological Society of India: 383p.

Loke, M. H., and Barker, R. D., 1995. Least-squares deconvolution of apparent resistivity pseudosections, *Geophysics*, 60, 1682-1690.

Loke, M. H., and Barker, R. D., 1996a. Rapid least-squares inversion of apparent resistivity pseudosections by a quasi-Newton method: *Geophysical Prospecting*, 44, 131-152.

Loke, M. H., and Barker, R. D., 1996b. Practical techniques for 3D resistivity surveys and data inversion: *Geophysical Prospecting*, 44, 499-523.

Loke, M. H., 1999. *Electrical imaging surveys for environmental and engineering studies - A practical guide to 2D and 3D surveys*: 5, Cangkat Minden Lorong 6, Minden Heights, 11700 Penang, Malaysia, 65p.

Loke, M. H., 2002. *Rapid 2D resistivity and IP inversion using the least squares method*, Software manual (<http://www.goelectrical.com/>).

Lontzetidis, K., Raptakis, D., and Pitilakis, K., 1997. Correlation between vs - N (SPT) in Greek soils: *Proceedings of 3rd P.S.G.M, Patra, I*, 419-425.

Luna, R., and Jadi, H., 2000, Determination of dynamic soil properties using geophysical

methods: Proceedings of the First International Conference on the Application of Geophysical and NDT Methodologies to Transportation Facilities and Infrastructure, St. Louis, MO, 15p.

Mackie, R. L., Livelybrooks, D. W., Madden, T. R., and Larsen, J. C., 1997. A magnetotelluric investigation of the San Andreas Fault at Carrizo Plain, California: *Geophysical Research Letter*, 24, 15, 1847-1850.

Marschall, K., Werban, U., Reboulet, E., Linder, S., Hirsch, M., Paasche, H., and Dietrich, P., 2007. Combination of near surface geophysical and geotechnical methods for exploring construction sites: 13th European Meeting of Environmental and Engineering Geophysics, Istanbul, Turkey, 4p.

Matthews, M. C., Hope, V. S., and Clayton, C. R. I., 1996. The use of surface waves in the determination of ground stiffness profiles: *Proc. Instn Civ. Engrs Geotech. Engng* 119, April, 84-95.

Matthews, M. C., Clayton, C. R. I., and Own, Y., 2000. The use of field geophysical techniques to determine geotechnical stiffness parameters: *Proc. Instn Civ. Engrs Geotech. Engng*. January.

McGillivray, P. R., and Oldenburg, D. W., 1990. Methods for calculating Fréchet derivatives and sensitivities for the non-linear inverse problem: A comparative study: *Geophysical Prospecting*, 38, 499-524.

Meju, M. A., Gallardo, L. A., and Mohamed, A. K., 2003. Evidence for correlation of electrical resistivity and seismic velocity in heterogeneous near-surface materials: *Geophysical Research. Letter*, 30, 7, 1373.

Meyerhof, G. G., 1953. The bearing capacity of the foundations under Eccentric and Inclined Loads: 3rd ICSMFE, V 1.

Meyerhof, G. G., 1963. Some recent research on bearing capacity of foundation: CGL Ottawa, V 1.

Meyerhof, G. G., 1956. Penetration tests and bearing capacity of cohesion less soils: JSMFD, ASCE, V 82, SM 1.

Meyerhof, G. G., 1976. Bearing capacity and settlement of pile foundations: Journal of Geotechnical Engineering Division, ASCE, 102, GT3, 197-228.

Mondal, S. K., Sastry, R. G., Gautam, P. K., and Pachauri, A. K., 2008. High resolution 2-D electrical resistivity tomography to characterize active Naitwar Bazar landslide, Garhwal Himalaya, India-A Case Study: Current Science, 94, 7, 871-875.

Mondal, S. K., Sastry, R. G., Gautam, P. K., and Pachauri, A. K., 2007. High resolution resistivity imaging of Naitwar Bazar landslide, Garhwal Himalaya: India. Proc. 20th Symposium on the Application of Geophysics to Engineering and Environmental Problems (SAGEEP), 629-635.

Mondal, S. K., 2009. Geophysical characterization of some active landslides of the Garhwal Himalaya, India: Ph.D. Thesis, Indian Institute of Roorkee, Roorkee, India.

Morey, R. M., 1999. Tomographic site characterization using CPT, ERT and GPR (Unpublished) (www.osti.gov/bridge/servlets/purl/773811-4et2qF/native/773811.pdf).

Morgan, F. D., Gay, D. A., Vichabian, Y., Reppert, P., Wharton, A. E., and Sogade, J. A., 2005. Geophysical and Geotechnical Investigations for Proposed Dominica Airport: Cite abstracts, AGU, 86, 18, Jt. Assem. Suppl.

Murthy, V. N. S., 2008. Soil Mechanics and foundation engineering, CBS Publisher and Distributors, 1043p.

Murthy, V. N. S., 1982. Report on soil investigation for construction of cooling water system, Part II of Farakha Superthermal Power Project, National Thermal Power Corporation, New Delhi.

Oh, S., and Sun, Chang-Guk., 2008. Combined analysis of electrical resistivity and geotechnical SPT blow counts for the safety assessment of fill dam: *Journal of Environmental Geology*, 54, 31-42

Oh, Young-chul., Jeong, Hae-sang., Lee, Young-kyu., and Shona, Howoong., 2003. Safety evaluation of rock-fill dam by seismic (MASW) and resistivity methods: *Proceedings SAGEEP*, 1377p.

Overmeeren, R. A., and Ritsema, I. L., 1988. Continuous vertical electrical sounding: *First Break*, 6, 10, 313-324.

Park, S. K., and Van, G. P., 1991. Inversion of pole-pole data for 3-D resistivity structure beneath arrays of electrodes: *Geophysics*, 56, 951-960.

Park, C. B., Miller, R. D., Ryden, N., Xia, J., and Ianov, J., 2005. Combined use of active and passive surface waves: *Journal of Environmental Engineering Geophysics*, 10, 323-334.

Parkash, B., Kumar, S., Rao, M. S., Giri, S. C., Kumar, C. S., and Gupta, S., 2001. Active tectonics of western Gangetic Plains: In: *DST's Spl. Vol. 2 on seismicity*, Ed., Verma, O.P, Publ. IGC, 141-158.

Peck, R. B., Hanson, W. E., and Thornburn, T. H., 1974. *Foundation engineering*: John Wiley & Sons, Inc., New York, 544p.

Pidlisecky, A., Knight, R., and Haber, E., 2006. Cone-based electrical resistivity tomography: *Geophysics*, 71, 4, G157-G167.

Pazdirek, O., and Blaha, V., 1996. Examples of resistivity imaging using ME-100 resistivity field acquisition system: *EAGE 58th Conference and Technical Exhibition Extended Abstracts*, Amsterdam, P050.

- Pujari, P. R., and Nanoti, M. V., 2006. Integrated Resistivity Imaging and GPR studies to assess groundwater pollution near Landfill site, Nagpur India, Proc. Symposium on the Application of Geophysics to Engineering and Environmental Problems (SAGEEP).
- Pujari, P. R., Pardhi, P., Muduli, P., Harkare, P., and Nanoti, M. V., 2007a. Assessment of pollution near landfill site in Nagpur, India by Resistivity Imaging and GPR: Environmental Monitoring and Assessment, 131, 489-500.
- Ranjan, G., and Rao, A. S. R., 2005. Basic and Applied Soil Mechanics: New Age International (P) Limited, Publishers, New Delhi, India, 762 p.
- Rechtien, R. D., 1996. In-situ liquefaction investigation of liquefaction potential of soils: Report GL-96-1-US Army Corps of Engineer, 46p.
- Robertson, P. K., and Campanella, R. G., 1983a. Interpretation of cone penetration tests- Part I : Sand, Canadian Geotechnical Journal, 20, 4, 718-733.
- Robertson, P. K. and Campanella, R. G., 1983b. Interpretation of cone penetration tests- Part II: Clay, Canadian Geotechnical Journal, 20, 4, 718-745.
- Robertson, P. K., 1990. Soil classification using the cone penetration test, Canadian Geotechnical Journal, 27, 1, 151-158.
- Robertson, P. K., and Campanella, R. G., 1985. Liquefaction potential of sands using the cone penetration test: Journal of Geotechnical Division of ASCE, 22, 3, 298-307.
- Robertson, P. K., Campanella, R. G., and Wightman, A., 1983. SPT-CPT correlations, ASCE, Journal of Geotechnical Engineering 109, 11, 1449-59.
- Roth, M. J. S., Mackey, J. R., Mackey, C., and Nyquist, J. E., 2002. A case study of the reliability of multielectrode earth resistivity testing for geotechnical investigations in karst terrains: Engineering Geology, 65, 225-232.
- Roth, M. J. S., and Nyquist, J. E., 2003. Evaluation of Multi-Electrode Earth Resistivity Testing in Karst,: Geotechnical Testing Journal, ASTM, 26, 167-178.

- Roy, A., and Apparao, A., 1971. Depth of investigation in direct current methods: *Geophysics*, 36, 943-959.
- Sanglerat, G., 1972. *The penetrometer and soil exploration*: Elsevier Publishing Company, Amsterdam. Netherlands.
- Sasaki, Y., 1992. Resolution of resistivity tomography inferred from numerical simulation: *Geophysical Prospecting*, 40, 453-464.
- Sastry, R. G., and Viladkar, M. N., 2004. Role of integrated geophysical studies in defining the rock profile below steep hill slope at the base of an endangered multi-storeyed building in Himachal Pradesh: *Journal Geological Society of India*, 63, 282-290.
- Schlumberger, C., 1920. *Etude sur la prospection electrique du sous-sol*. Gauthier-Villars, Paris, 94p.
- Schnaid, F., and Yu, H. S., 2007. Interpretation of the seismic cone test in granular soils: *Geotechnique*, 57, 3, 265-272.
- Seshunarayana, T., 2006. Multichannel analysis of surface waves-An application to site characterisation, Jabalpur, India: Unpublished Ph.D. Thesis, Centre of Exploration Geophysics, Osmania University, Hyderabad, India.
- Seshunarayana, T., and Sundararajan, N., 2004. Multichannel analysis of surface waves, MASW, for mapping shallow subsurface layers-A case study, Jabalpur, India: Proc. 4th International Conference & Exposition on Petroleum Geophysics, Society of Petroleum Geophysicists, Hyderabad, India.
- Siegel, H. O., 1959. Mathematical formulation of type curves for induced polarization: *Geophysics*, 24, 3, 546-565.
- Sitharam, T. G., Samui, P., and Anbazhagan, P., 2008. Spatial variability of rock depth in Bangalore using geostatistical, neural network and support vector machine models: *Journal of Geotechnical and Geological Engineering*, 26, 503-517.

Skempton, A. W., 1951. The bearing capacity of clays: Proceedings Building Research Congress, V 1.

Slater, L., and Lesmes, D., 2002. IP interpretation in environmental investigations: *Geophysics*, 67, 77-88.

Smith, N. C., and Vozoff, K., 1984. Two-dimensional DC resistivity inversion for dipole-dipole data: *IEEE Transaction on Geoscience & Remote Sensing*, 22, 21-28.

Soupios, P. M., Georgakopoulos, P., Papadopoulos, N., Saltas, V., Andeadakis, A., Vallianatos, F., Sarris, A., and Makris, J. P., 2007a. Use of engineering geophysics to investigate a site for a building foundation: *Journal of Geophysics and Engineering*, 4, 94-103.

Soupios, P. M., Loupasakis, C., and Vallianatos, F., 2008. Reconstructing former urban environments by combining geophysical electrical methods and geotechnical investigations-an example from Chania, Greece: *Journal of Geophysics and Engineering*, 5, 186-194.

Steeple, D. W., 2005. Near-surface geophysics: 75 years of progress: *Leading Edge*, 24 (S1), S82-S85.

Sudha, K., Israil, M., Mittal, S., and Rai, J., 2008. Soil characterization using electrical resistivity tomography and geotechnical investigations: *Journal of Applied Geophysics*, 67, 1, 74-79.

Sumner, J. S., 1976. Principles of induced polarization for geophysical exploration: Elsevier Scientific, Amsterdam, 277p.

Terzaghi, K., 1943. *Theoretical Soil Mechanics*: J. Wiley and Sons, New York, 510p.

Terzaghi, K., and Peck, R. B., 1967. *Soil Mechanics in Engineering Practice*, 2nd ed., John Wiley and Sons, New York.

Thussu, J. L., 2006. Geology of Haryana and Delhi: Geol. Soc. India, Bangalore, 191p.

Tillmann, A., Englert, A., Nyari, Z., Fejes, I., Vanderborcht, J., and Vereecken, H., 2008. Characterization of subsoil heterogeneity, estimation of grain size distribution and hydraulic conductivity at Krauthausen test site using cone penetration test: *Journal of Contaminant Hydrology*, 95, 57-75.

Ulugergerli, E. U., and Uyanik, O., 2006. Statistical correlations between seismic wave velocities and SPT blow counts and the relative density of soils: *Journal of Testing and Evaluation*, 35, 2, 5p.

Ulugergerli, E.U., and Uyanik, O., 2007. Statistical correlations between seismic velocities and SPT blow counts and the relative density of soils: *ASTM Journal of Testing and Evaluation*, 35, 2, 1-5.

Vacquier, V., Holmes, C. R., Kintzinger, P. R., and Lavergne, M., 1957. Prospecting for groundwater by induced electrical polarization: *Geophysics*, 23, 660-687.

Vesic, A. S., 1973. Analysis of ultimate loads of shallow foundations: *JSMFD, ASCE*, V 99, SM 1.

Vesic, A. S., 1974. Bearing capacity of shallow foundations, *Foundation Engineering Hand Book*, Van Nostrand, Reinhold Book, Co., N.Y.

Vipin, K. S., Anbazhagan P., and Sitharam, T. G., 2008. Identification of Liquefaction Susceptible Areas in Bangalore using Probabilistic approach Based on SPT data: *Proceedings of Indian geotechnical Conference Bangalore*, 2, 444-447.

Ward, S. H., Ed., 1990. Geotechnical and environmental geophysics: Investigations in *Geophysics*, 5, 1, Soc. Expl. Geophys, 1-30.

Weiher, B., and Davis, R., 2004. Correlation of Elastic Constants with Penetration Resistance in Sandy Soils: *International Journal of Geomechanics*, 4, 4, 319-329.

Weller, A., Seichter, M., and Kampke, A., 1996. Induced-polarization modelling using complex electrical conductivities: *Geophysical Journal International*, 127, 387-398.

Xu, C., and Butt, S. D., 2006. Evaluation of MASW techniques to image steeply dipping cavities in laterally inhomogeneous terrain: *Journal of Applied Geophysics*, 59, 2, 106-116.

Yoon, H. K., Kim, J. H., Kim, R., and Lee, J. S., 2009. Electrical resistivity and cone tip resistance monitoring by using cone resistivity penetrometer: *Proceedings of the 19th International Offshore and Polar Engineering Conference*, Osaka, Japan.

Zelt, C. A., and Barton, P. J., 1998. Three-dimensional seismic refraction tomography: a comparison of two methods applied to data from the Faeroe Basin. *Journal of Geophysical Research*, 103, 7187-7210.

Zhang, Z., and Tumay, M. T., 1996. Simplification of soil classification charts derived from the cone penetration test: *Geotechnical Testing Journal*, 19, 203-216.

